



Eva Fritzsche, M.Sc., B.Sc.

Optimization and Application of an Optical Carbon Dioxide Sensor for Marine Environments

DOCTORAL THESIS

to achieve the university degree of
Doktorin der technischen Wissenschaften
submitted to
Technischen Universität Graz

Supervisor

Univ.-Prof. Dipl.-Chem. Dr.rer.nat. Ingo Klimant
Institute for Analytical Chemistry and Food Chemistry,

Graz, Oktober 2017

Eidesstattliche Erklärung

Ich erkläre an Eides statt, dass ich die vorliegende Arbeit selbständig verfasst, andere als die angegebenen Quellen/Hilfsmittel nicht benutzt und die den benutzten Quellen wörtlich und inhaltlich entnommenen Stellen als solche kenntlich gemacht habe. Das in TUGRAZonline hochgeladene Textdokument ist mit der vorliegenden Dissertation identisch.

Statutory Declaration

I declare that I have authored this thesis independently, that I have not used other than the declared sources/resources and that I have explicitly indicated all material which has been quoted either literally or by content from sources used. The text document uploaded to TUGRAZ online is identical to the present doctoral thesis.

Datum/Date

Unterschrift/Signature

For my grandmas

Anni and Gertrud (Henryoma)

Zusammenfassung

Sensoren für Sauerstoff, pH und Kohlendioxid sind wichtige Werkzeuge in Forschung und Industrie. Marine Sensoren sind besonders wichtig für die Erforschung der Ozeane und die Bereitstellung großer Datenmengen. Sauerstoffsensoren für die Meeresforschung sind bereits etabliert, elektrochemische und spectrophotometrische pH Sensoren ebenfalls. Kohlendioxid-sensoren hingegen sind eher selten. Eine vielversprechende Technologie zur Messung aller drei Parameter sind Optoden. Dieses Projekt war auf die Entwicklung und Evaluierung einer CO₂-Optode, basierend auf den kürzlich publizierten aza-BODIPY Farbstoffen, ausgerichtet.

Kapitel 1 beschäftigt sich mit der Entwicklung einer langzeit stabilen, mechanisch robusten und sensitiven CO₂-Optode für Meerwasser. Hyflon AD 60 (perfluoriertes Polymer) erhöhte die Stabilität dramatisch, indem es die Vergiftung des Sensors durch Schwefelwasserstoff und andere saure Gase verlangsamt. Der Einsatz dieses Polymers erforderte allerdings einen speziellen Herstellungsprozess des Sensors. Erste Feldtests wurden in der Ostsee im Oktober 2015 durchgeführt. Im zweiten Teil wurde eine intensive Evaluierung und Vergleich des Sensors im pazifischen Ozean for Kalifornien (USA) durchgeführt. Ein vielseitiges, kleines, druckresistentes Gerät wurde mit Sensorfolien für Sauerstoff, pH und Kohlendioxid kombiniert. Die Sensoren wurden mit bereits käuflich erhältlichen Sensoren für den jeweiligen Analyten in verschiedenen Umgebungen (z.B. Aquarium, Flussmündung, offener Ozean) verglichen. Außerdem wurde ein Langzeitstabilitätstest für den entwickelten pH Sensor durchgeführt.

Der Einsatz von perfluorierten Polymeren erhöht die Ansprech- und Erholungszeit des Sensors beträchtlich. Für die Messung von Profilen durch die Wassersäule sind jedoch schnell ansprechende Sensoren essenziell. Der bestehende CO₂ Sensor wurde neu strukturiert. Die Materialauswahl wurde angepasst und die Schichtdicke reduziert, um ein schnelles Ansprechen zu ermöglichen. Der schnell ansprechende Sensor wurde erfolgreich während regelmäßigen Kontrollfahrten eingesetzt, um Profile von bis zu 230 m Tiefe zu messen.

Ein immer größer werdendes Problem sind Sauerstoffminimumzonen in den Weltmeeren. Zum Teil sind sie anoxisch und es kommt zur Produktion von Schwefelwasserstoff durch Bakterien. H₂S hat ähnliche Eigenschaften wie Kohlendioxid, diffundiert ebenfalls in die Optode und verhindert somit eine akkurate Messung der CO₂ Konzentration. Eine Vielzahl von Verbindungen zum Abfangen von Schwefelwasserstoff in Kombination mit Hyflon AD 60 wurde auf ihre Schutzwirkung untersucht. Zinkoxid mit einer hohen spezifischen Oberfläche stellte sich als der vielversprechendste Kandidat heraus.

Abstract

Sensors are indispensable for monitoring purposes in research and industry, especially parameters like carbon dioxide, pH and oxygen. A special case are marine sensors to investigate the ocean and gain large data sets. Oxygen sensors are already established in marine science, pH sensors based on electrochemical and spectrophotometric sensing schemes as well. Carbon dioxide sensors are relatively rare. A promising sensor technique for measuring the three parameters are optodes. This project was focussed on the development and evaluation of an plastic type carbon dioxide optode based on recently presented aza-BODIPY dyes.

Paper 1 deals with the development of a long-term stable, mechanical robust and sensitive carbon dioxide optode for marine applications. The use of Hyflon AD 60 (perfluorinated polymer) enhanced the stability dramatically. Moreover poisoning processes induced by hydrogen sulfide and other acidic gases are decelerated. Due to the use of perfluorinated polymers a special production procedure was developed. First field tests were performed at the Baltic Sea in October 2015.

In the second paper an intensive evaluation and comparison study was done in the Pacific Ocean close to California, USA. A small, versatile and pressure resistant sensor device was developed to measure oxygen, pH and carbon dioxide. The sensor performance of the three optodes were compared with already commercially available sensors for all parameters in different environments (e.g. open ocean, estauries, aquarium, AUV and profiling float). The long-term stability of the pH sensor was although investigated.

The use of perfluorinated polymers enhance the long-term stability, but increase the response and recovery time as well. To allow the measurement of profiles, a fast-responding carbon dioxide optode was developed by redesigning the sensor foil. The selected materials and the layer thicknesses were optimized to obtain a sensor foil responding within 100 s (t_{90}). The redesigned sensor foil was successfully applied for profiling measurements during monitoring cruises in Monterey Bay, California (USA).

An expanding problem in the ocean are oxygen minimum zones. In many cases the water is anoxic and hydrogen sulfide is formed by bacteria. H_2S is an acidic gas and has similar properties like carbon dioxide. Protection of the sensor against hydrogen sulfide is essential to guarantee accurate CO_2 measurements. Several scavenger particles (e.g. metal oxides and organic compounds) in combination with perfluorinated polymers were investigated. Zinc oxide with a high specific surface area was the most promising candidate.

Acknowledgement

Now it is time to say 'thank you'. I want to start with Ingo and Sergey, who give me the chance to do my PhD studies in the highly interesting field of sensor development. Thank you for all the inspiring discussions, the support for going my way and your knowledge shared with me over the last three years.

I want to go on with all the PhD and master students working with me every day. Besides my research, YOU were the reason i came to university with a smile on my face: the bunny and dinosaurs Christoph, Josef E., Shiwen, Martin, Heidi, David F., Silvia, Andi, Berni with the long blond hair, Luki, Philipp, Niki, Birgit, Irene, Max, Tanja and Monika. Thank you for the warm wellcome in the working group, all the funny nights with beer and hot spiced wine, the amazing trips to Dublin and Praque, the funny Business-runs and all the support in the lab and with paper work. We spend so many hours at the university and in the city having fun, you made austria my second home and i hope there will be more hours like that.

My office buddies: Susi, Ulli, Berni (brown hair), Pia, Iris, David P. and Peter. Thank you for creating a funny, relaxed and feel-good atmosphere, all the discussion about everything, the city tour in my first week and everything else.

The centerpiece of the ACFC group: Manuela, Iris W., Eveline, Marion, Anna, Matthias, Lukas T., Alexander, Erika, Torsten, Helmar and Herbert. You are making the system running, without you nothing would work!

The foodchemistry group: Nina, Sigi, Claudia, Barbara S., Barbara P.-Z., Dorothea, Andrea J., Andrea W., Elisabeth and Erich. You were a part of my working day, I never wanted to miss. Thanks for the explanation of gas ordering, the good coffee and milk in the social room, the time during institute events and the amazing food you prepared everytime.

You became more than just colleagues to me and I thank you for all the amazing time and i will come back for a coffee or two!

The colleagues in the 'SenseOcean' project. Thank you all for the productive and motivating annual meetings and the discussions afterwards.

The 'Salme'-crew: Michael, David, Christoph, Jens, Günther and the ship crew. It was a rough trip at the Baltic Sea, but we were still able to get some nice data at times with low wind.

Ken, Josh, Hans, Carol, Marguerite, Tim, Erich and Kristin, you made my time in California relaxed, fruitful and instructive. I never worked at such a nice place and never saw and learned so much about oceanography.

A big special thanks to my family, my mum and dad, my sister, my brothers and grandmas. Thank you for supporting all my crazy ideas, standing behind me and helping me finish my thesis. You made me the person I am. Markus, thank you for giving me strength every day in

last ten months, always making me smile and endless hugs at times when i need them the most.

Jetzt auf deutsch: Ich sag 'Danke'. Mutti, Papa, Mone, Jürgen, Micha und unsere Omas, ich danke euch, dass ihr meine ganzen verrückten Ideen mitmacht, egal ob es mal wieder ein Umzug oder eine Bastelidee ist. Danke, dass ihr immer hinter mir steht und ich mich immer auf euch verlassen kann.

There are many more people, who helped me realizing my PhD studies, the research stay in California and my written thesis. I might have forgot someone in this acknowledgement, so i want to thank everybody, who joined my way in the last three years and three months.

Table of Contents

Zusammenfassung	VII
Abstract	IX
Acknowledgement	XI
1 Theoretical Background	1
1.1 Carbon dioxide in Seawater	2
1.1.1 CO ₂ -Equilibria and Systemparameters	2
1.1.2 Global Carbon System	5
1.1.3 Biogeochemical Processes involving Carbon Dioxide	7
1.1.4 Increasing CO ₂ Content	9
1.1.5 Additional Interacting Parameters	9
1.2 The Ocean – Structure and driving Forces	10
1.2.1 Ocean circulation	10
1.2.2 Layerstructure	12
1.2.3 Special Case – Oxygen Minimum Zone	14
1.3 Sensor Technology in Oceanography	16
1.3.1 Necessity and Benefits	16
1.3.2 Applicationrequirements	16
1.3.3 Fields of Applications	17
1.4 Carbon Dioxide Sensors in Oceanography	21
1.4.1 Sensing Strategies	21
1.4.2 Developed Prototypes	24
1.4.3 Commercially Available CO ₂ -Sensors	26
1.5 Optical Carbon Dioxide Sensors	34
1.5.1 Indicator dyes	34
1.5.2 Measurement principles	36
1.5.3 Sensor foil structure	37
1.5.4 Hardware	38
1.5.5 Poisoning	39
2 Highly sensitive poisoning-resistant optical carbon dioxide sensors for environmental monitoring	41
2.1 Introduction	41
2.2 Materials and Methods	43
2.3 Results and Discussion	47

2.3.1	Measurement principle	47
2.3.2	Support material	48
2.3.3	Effect of protective coating on response times and long-term stability	49
2.3.4	Manufacturing of the luminescent carbon dioxide optode	52
2.3.5	Response and recovery times	53
2.3.6	Sensor calibration	54
2.3.7	Applications	56
2.4	Conclusion	58
	Acknowledgement	58
3	A validation and comparison study of new, compact, versatile optode for oxygen, pH and carbon dioxide in marine environments	59
3.1	Introduction	60
3.2	Methods and Instrumentation	62
3.3	Calibration procedure	65
3.3.1	Oxygen sensor calibration	65
3.3.2	pH sensor calibration	66
3.3.3	Carbon dioxide sensor calibration	67
3.4	Data evaluation	68
3.4.1	Monterey Bay Aquarium-Open Sea Exhibition	68
3.4.2	MLML-Aquaculture facility, seawater intake system	70
3.4.3	MLML-Aquaculture facility, Abalone larvae breeding tank	71
3.4.4	Elkhorn Slough-Mooring buoy LO1	73
3.4.5	Monterey Bay- AUV integration	75
3.4.6	Monterey Bay- Profiling float	76
3.4.7	Elkhorn Slough-pH sensor long-term testing	77
3.5	Summary and discussion	79
3.6	Acknowledgement	80
4	Improved response times of pH and pCO₂ optodes for profiling applications in seawater	81
4.1	Introduction	81
4.2	Materials and Methods	83
4.3	Results and Discussion	87
4.3.1	pH optodes	87
4.3.2	pCO ₂ optodes	89
4.3.3	Application 'Monterey Bay'	94
4.4	Conclusion	95
5	Hydrogen sulfide protection strategies for CO₂ optodes to measure in marine oxygen-minimum zones	97
5.1	Introduction	97
5.2	Materials and Methods	99
5.3	Development steps	101

5.3.1	Material selection	101
5.3.2	Scavenger selection	103
5.3.3	Particle size dependency – Zinc oxide	106
5.3.4	Sensor structure optimization	107
5.4	H ₂ S-protected carbon dioxide sensor	110
5.5	Conclusion	112
	Conclusion and Outlook	114
	References	116
	Appendix A - Photographic images hydrogen sulphide experiments	140
	Appendix B - Curriculum Vitae	140

Chapter 1

Theoretical Background

Scope of the Thesis

The Ocean is a huge water mass with great impact on the earth's climate. Especially anthropogenically produced carbon dioxide is a driving force for changes in the carbonate chemistry in seawater. The ocean is the major sink for CO₂ and so buffers the overall increase. But the uptake is not without consequences; effects like ocean acidification and an increase in the ocean surface temperature occur. For investigating the effects and long-term consequences, the ocean has to be observed with a high temporal and spatial resolution. This is realized by the help of sensor technology and a wide range of oceanic platforms. Parameters like temperature, salinity, oxygen concentration, pH and carbon dioxide are of special interest.

Several important developments were presented in the last decades in the field of sensor technology. Sensors became smaller, lighter, less power consuming and highly reliable. Moreover new mobile oceanic platforms, like glider and profiling floats, were developed and operated worldwide to transport sensors through the harsh ocean. The combination of both enhanced the amount of data available to understand changes in the ocean related to an increased CO₂ concentration.

Carbon dioxide sensors for marine applications are often based on IR-technology. Gas chromatography and the Severinghaus electrode are although suitable for CO₂ determination but are not suitable for seawater. Moreover electrochemical or spectrophotometrical systems are available, but show several drawbacks like a high power consumption, moving parts which are prone to break, waste production during measurements or an insufficient size. These systems cover a wide range of measurable carbon dioxide concentrations, as well as a wide operation temperature. Lately a lot of working groups focussed on optodes ('plastic'-type) to determine the carbon dioxide concentration in seawater. Optodes include an indicator dye and a lipophilic base to determine a pH change generated by carbon dioxide, which diffused through a proton-impermeable polymer. They have the potential to be used for long-term deployments, as well as for fast profiling measurements. This technology is also a good possibility to reliably measure other parameters like dissolved oxygen or pH. A small number of CO₂ optode-prototypes were developed and tested in the last decade.

1.1 Carbon dioxide in Seawater

1.1.1 CO₂-Equilibria and Systemparameters

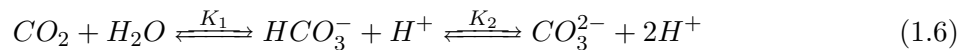
Seawater carbonate chemistry is described by four main species: dissolved carbon dioxide (CO₂(aq)), carbonic acid (H₂CO₃), bicarbonate (HCO₃⁻) and carbonate ions (CO₃²⁻). This species are related by the following equilibria:



The atmosphere-sea exchange (eq. 1.1) with surface waters is rather slow compared to the dissociation and is therefore the limiting step.¹ The concentration of the overall dissolved carbon dioxide can be calculated with the solubility coefficient of carbon dioxide in seawater K_0 and Henry's law. The solubility coefficient is given by²:

$$\ln K_0 = A_1 + A_2(100/T) + A_3 \ln(T/100) + S[B_1 + B_2(T/100) + B_3(T/100)^2] \quad (1.5)$$

where A and B are constants, T the absolute temperature and S the salinity in parts per thousand. After dissolution aqueous carbon dioxide reacts with water to carbonic acid, a second electrical neutral form next to the dissolved CO₂. Since the equilibrium coefficient for the hydration is around 10⁻³, the bulk of the undissociated dissolved carbon dioxide is in the CO₂(aq) form. A distinction between these electrically neutral species is not considered. The sum of CO₂(aq) and H₂CO₃ is denoted by [CO₂] and used for the calculation of dissociation constants for equations 1.3 and 1.4. The formed carbonic acid dissociates to bicarbonate (HCO₃⁻) by losing a proton (eq. 1.3). In the next step a second proton is formed, as well as carbonate ions (CO₃²⁻; eq. 1.4). The use of [CO₂] instead of aqueous CO₂ and carbonic acid simplifies the equilibrium (eq. 1.5) and K₁ and K₂ can be defined as the equilibrium constants for the first and second dissociation step, respectively.³



$$K_1^* = \frac{[HCO_3^-] \cdot [H^+]}{[CO_2]} \quad (1.7)$$

$$K_2^* = \frac{[CO_3^{2-}] \cdot [H^+]}{HCO_3^-} \quad (1.8)$$

The equilibrium constants are temperature, salinity and pressure dependent. Based on the data of Roy et al. 1993 the constants K₁^{*} (eq. 1.9) and K₂^{*} (eq. 1.10) can be calculated for a salinity between 5 and 45 PSS and a temperature between 0 and 45°C. The data were determined in artificial seawater, using pH values in the total hydrogen ion concentration scale.⁴

$$\begin{aligned} \ln K_1^* = 2.83655 - 2307.1266/T - 1.5529413 \ln T - (0.207608410 + 4.0484/T)\sqrt{S} \\ + 0.0846834S - 0.00654208S^{3/2} + \ln(1 - 0.001005S) \end{aligned} \quad (1.9)$$

$$\begin{aligned} \ln K_2^* = -9.226508 - 3351.6106/T - 0.2005743 \ln T - (0.106901773 + 23.9722/T)\sqrt{S} \\ + 0.1130822S - 0.00846934S^{3/2} + \ln(1 - 0.001005S) \end{aligned} \quad (1.10)$$

All species, which describe the carbonate chemistry are in near equilibrium.⁵ The main species present in seawater are bicarbonate ions. In surface waters (pH \sim 8.1) bicarbonate ions are around 90% of the inorganic carbon, 9% carbonate ions and just 1% dissolved carbon dioxide.¹ The aqueous carbonate system can be described by four measurable parameters: total dissolved inorganic carbon (DIC), total alkalinity (TA), fugacity of CO₂ ($f(\text{CO}_2)$) and the total hydrogen ion concentration (pH_T). Additionally parameters like equilibrium constants, temperature, salinity and pressure are indispensable for the description of the carbonate system.

Total dissolved inorganic carbon (DIC, C_T, $\sum \text{CO}_2$ or TCO₂) is defined as the sum of all species formed of dissolved carbon dioxide (eq. 1.6, 1.11).

$$\text{DIC} \equiv \sum \text{CO}_2 = [\text{CO}_2] + [\text{HCO}_3^-] + [\text{CO}_3^{2-}] \quad (1.11)$$

It can be determined by acidifying a seawater sample, generating gaseous CO₂ and measuring the resulting amount of gas.

A second parameter is the *total alkalinity* (TA, A_T). It is most precise described by Dickson 1981: "The total alkalinity of a natural water is thus defined as the number of moles of hydrogen ion equivalent to the excess of proton acceptors (bases formed from weak acids with a dissociation constant $K \leq 10^{-4.5}$, at 25 °C and zero ionic strength) over proton donors (acids with $K \geq 10^{-4.5}$) in one kilogram of sample."⁶ According to Dickson's definition TA can be calculated by the following equation:

$$\begin{aligned} \text{TA} = [\text{HCO}_3^-] + 2[\text{CO}_3^{2-}] + [\text{B}(\text{OH})_4^-] + [\text{OH}^-] + [\text{HPO}_4^{2-}] + 2[\text{PO}_4^{3-}] + [\text{H}_3\text{SiO}_4^-] \\ + [\text{NH}_3] + [\text{HS}^-] - [\text{H}^+]_F - [\text{HSO}_4^-] - [\text{HF}] - [\text{H}_3\text{PO}_4] \end{aligned} \quad (1.12)$$

The total alkalinity of seawater can be determined by an automated closed or open-cell, potentiometric titration with hydrochloric acid.

The *fugacity* of carbon dioxide ($f(\text{CO}_2)$) is the partial pressure corrected for the solubility behaviour in seawater of a non-ideal gas. It can be expressed by the following equation (eq. 1.13)⁷

$$f_{\text{CO}_2} = [\text{CO}_2]/K_0 \quad (1.13)$$

The fourth parameter to fully describe the carbon dioxide chemistry in seawater is the *total hydrogen ion concentration* (pH_T). It is defined by Hansson et al. 1973 as the sum of the free

hydrogen ion concentration and the HSO_4^- concentration⁸:

$$[\text{H}^+] = [\text{H}^+]_F \cdot (1 + S_T/K_s) \quad (1.14)$$

where $[\text{H}^+]_F$ is the free hydrogen ion concentration, S_T total sulfate concentration ($[\text{SO}_4^{2-}] + [\text{HSO}_4^-]$) and K_s acid dissociation constant for HSO_4^- . The most precise measurement is spectrophotometrically by using *m*-cresol purple.

At least two of the previous mentioned CO_2 -related parameters have to be measured for one seawater sample to characterize the carbonate system.⁹ The selected parameters to characterize the carbonate system are depending on the deployment and the facilities to measure the parameters as accurate and precise as possible. A common used and reliable pair of parameters is DIC and pH_T ^{10,11,12}. Considering these two parameter concentrations of CO_2 , HCO_3^- and CO_3^{2-} , as well as the carbonate alkalinity (CA) can be determined (eq. 1.14 - 1.17).

$$[\text{CO}_2] = \text{DIC} / (1 + \frac{K_1^*}{[\text{H}^+]} + \frac{K_1^* K_2^*}{[\text{H}^+]^2}) \quad (1.15)$$

$$[\text{HCO}_3^-] = \text{DIC} / (1 + \frac{[\text{H}^+]}{K_1^*} + \frac{K_2^*}{[\text{H}^+]}) \quad (1.16)$$

$$[\text{CO}_3^{2-}] = \text{DIC} / (1 + \frac{[\text{H}^+]}{K_2^*} + \frac{[\text{H}^+]^2}{K_1^* K_2^*}) \quad (1.17)$$

$$\text{CA} = [\text{HCO}_3^-] + 2[\text{CO}_3^{2-}] \quad (1.18)$$

Moreover DIC and pH_T enable the construction of a Bjerrum plot (fig. 1.1). It is a diagram representing the distribution of dissolved carbon dioxide, bicarbonate und carbonate ions as a function of pH , dissolved inorganic carbon and temperature. The logarithm of the species concentration is plotted against the pH . The curves intersect at two points, which represent the temperature dependent pK -values (pK_1 and pK_2).

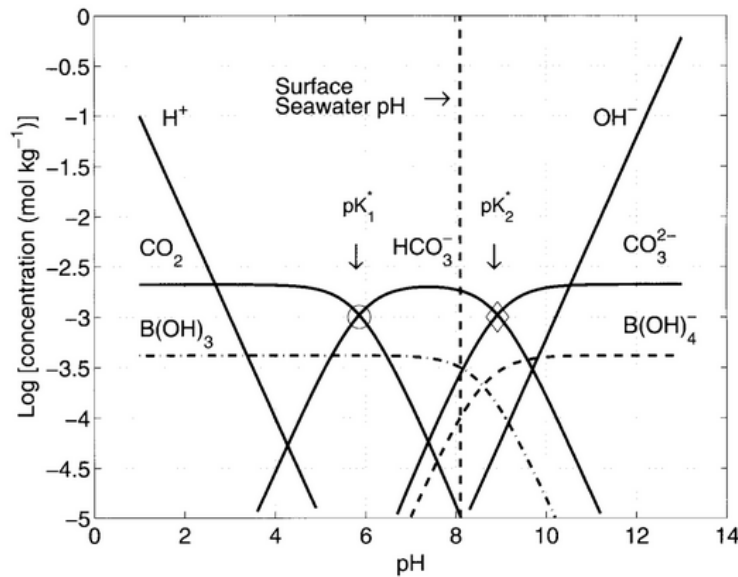


Figure 1.1: Bjerrum plot for carbonic acid, $\text{DIC} = 2.1 \text{ mmol/kg}$, $S = 35 \text{ PSS}$, $T_C = 25 \text{ }^\circ\text{C}$. pK values marked with circle and diamond.¹³

Values at 25°C are 5.86 and 8.92 for pK_1 and pK_2 , respectively. A decrease in temperature, salinity or pressure lead to an increase in the pK -values.

The curve shape for the three carbonate species is dependent on the dissolved inorganic carbon concentration. Whereas the curve shape for H^+ and OH^- are unaffected by DIC. At 25 °C carbonate ions are the dominant species for pH higher than 10.3, bicarbonate for a pH between 6.3 and 10.3 and the neutral carbon dioxide for a pH less than 6.3 (fig. 1.1).¹⁴

In general all combinations of parameters are possible to describe the whole carbonate system. Errors in the sample preparation, the measurement accuracy of the parameter determination and the precision of the dissociation constants K_1 and K_2 (eq. 1.9, 1.10) result in preferred pairs for calculations. There are several studies dealing with the choice of parameters to calculate the carbonate system.^{3 7 11 15 16 17} The measurement and sample preservation of DIC and TA are straightforward and highly reliable reference materials are available. Additionally both parameters are insensitive to temperature and pressure.¹⁸ These factors and the recommendation in 'Guide to best practices for ocean acidification research and data reporting' (Riebesell et al. 2011) make DIC and TA an often used pair of parameters.^{19 20 17} Earlier studies from the 1990ies revealed an underestimation of pCO_2 using DIC and TA to calculate pCO_2 . The problem was minimized by sufficient reference materials for the measurement of both parameters^{15 3 10} The major problem by using the total alkalinity is an uncertainty in titration generated by organic alkalinity, which often occurs in estuarine areas. If TA can not be determined reliably, the use of DIC and pH_T is also sufficient. In this case the critical point is the accuracy of the pH measurement.¹¹ Spectrophotometric measurements of the pH value using *m*-cresol purple are highly accurate and straightforward, but the accuracy depend on the dye purity.¹⁷ Overall the data, obtained through calculations using the aqueous carbonate system, should be compared with caution, because the chosen set of input parameter and equilibrium constants can affect the calculated data set.

Currently there are several programmes supporting the calculation of the carbonate system from any chosen input parameters: CO2SYS by Lewis and Wallace 1998²¹ and the next generation CO2calc²² by Robbins et al. 2010, SEACARB²³ by Lavigne and Gattuso and SWCO2²⁴ by Hunter. They give almost similar results, when inserting the same parameters and equilibrium constants.¹¹

1.1.2 Global Carbon System

The global carbon cycle is a biogeochemical process, which describes fluxes of carbon (carbon dioxide, methane, organic matter, dissolved inorganic carbon, organic compounds, etc.) between the three major reservoirs. Carbon reservoirs are the atmosphere, the ocean, including the marine biota and the terrestrial system, including soils, vegetation and fossil fuels. Whereat the atmosphere transfers carbon between the ocean and the terrestrial system. The rate of exchange between the reservoirs depends on spacial and seasonal patterns.²⁵ Furthermore the exchange is influenced by the human hand through antropogenically produced carbon dioxide. Each reservoir can act as a sink (take up carbon) or source (release carbon) of carbon in the atmosphere. The carbon can be released naturally by respiration, decomposition of organic

matter, volcanic activities or soil emission and antropogenically by forestry, agriculture, cement industry and fossil fuel burning.^{25 26}

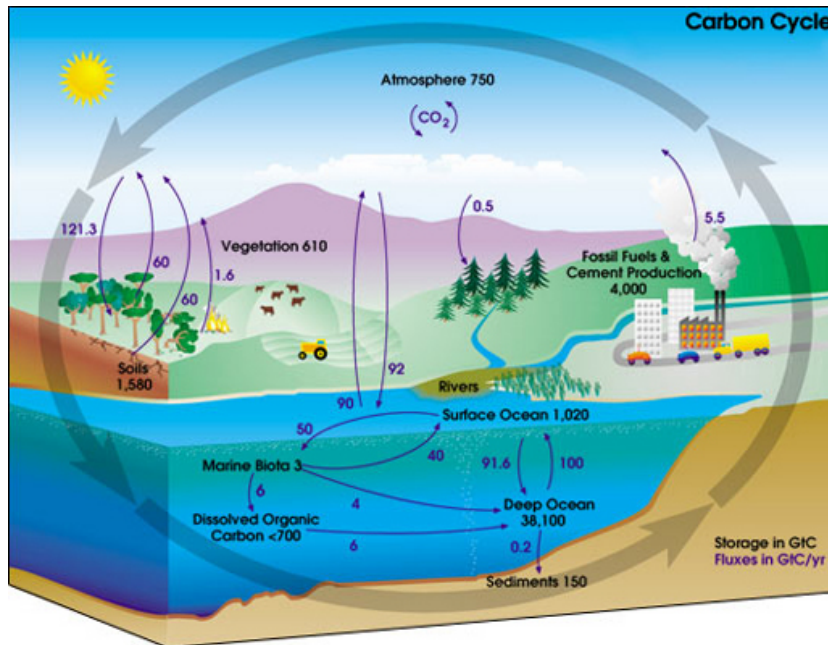


Figure 1.2: Global carbon cycle with stored carbon (gigatons) in black and carbon fluxes in purple (gigatons per year).²⁷

The ocean is the largest reservoir of carbon in the global cycle and stored 38,400 gigatons of carbon²⁶. The reservoir takes up and convert carbon dioxide by three different processes: physical, chemical and biological. The physical process is driven by the equilibration of the partial pressure of carbon dioxide in the atmosphere and the surface ocean water. This exchange is rather rapidly and the effectiveness is determined by the wind over the ocean surface area. The carbon can be further transported into deeper water by vertical mixing. A more effective process to transport carbon in deeper water layers is the so called 'biological pump'. The process starts in the well-mixed ocean surface area, where organisms convert dissolved inorganic carbon into inorganic compounds and organic matter via photosynthesis (primary production). A lot of the manufactured substances sink to deeper water as dead organisms or fecal particles. The organic matter gets remineralized and decomposed by bacteria or decomposed at the ocean floor.²⁵ An additional biological process takes place, the 'carbonate pump'. A variety of plankton species use $\text{Ca}(\text{CO}_3)$ to build up shells, which sink in the deep water and get dissolve again.²⁶ Both processes decrease the amount of DIC in the mixed surface layer and allow further carbon dioxide uptake. Moreover they increase the amount of DIC in the deep ocean. The chemical process includes the whole carbon chemistry described above.

The terrestrial system will be described shortly. The system contains several pools of carbon like the terrestrial biosphere (plants, animals, microorganisms). Via photosynthesis carbon dioxide from the atmosphere gets consumed and stored as organic matter. It is although released to the atmosphere by several respiratory pathways. Without human impact the exchange between the terrestrial system and the atmosphere would be in balance over a decade time scale.²⁵

The *atmosphere* is the smallest reservoir with just 750 gigatons of stored carbon in form of

carbon dioxide, methane and other compounds.²⁸ It represents the connection between the ocean and the terrestrial system. Moreover the atmosphere has a big impact on the world's climate, especially the increasing concentration of carbon dioxide (280 ppm preindustrial to 384 ppm in 2008).²⁹ The impact of several factors, like soil respiration³⁰, agriculture³¹, climate extremes³² or tropical forests³³, on the atmosphere and the whole global carbon cycle were investigated over the last decades.

1.1.3 Biogeochemical Processes involving Carbon Dioxide

Several biogeochemical processes are involved considering carbon dioxide in the ocean. They are driving forces in the global carbon cycle and responsible for the distribution of carbon in the ocean. Biological processes like algae metabolism and the carbonate chemistry have an influence on total alkalinity and dissolved inorganic carbon in seawater. The uptake or release of CO_2 just alter the amount of DIC and let TA unaffected. Moreover the trend in pH can be estimated throughout the diagram (e.g.: CO_2 release \rightarrow reduction of pH). Photosynthesis instead changes TA and DIC at the same time (fig. 1.3).

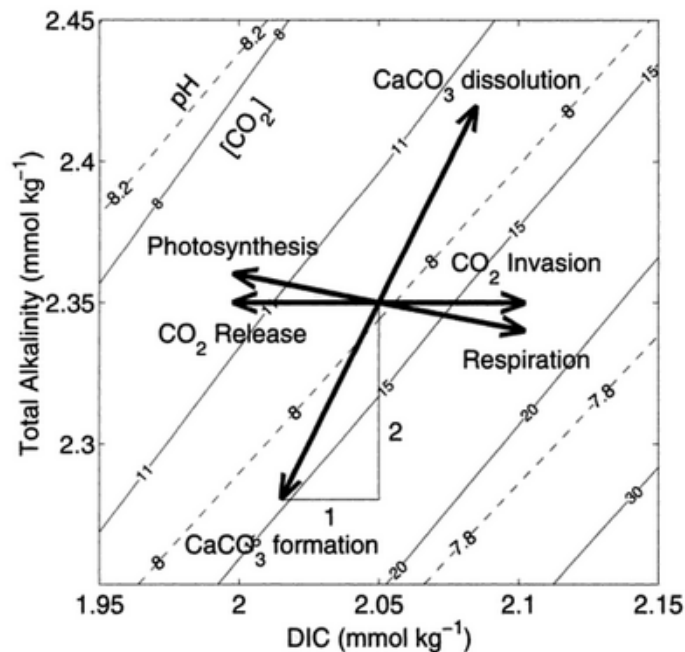


Figure 1.3: Effect of processes on TA and DIC. Dashed and solid lines represent constant values of pH and dissolved carbon dioxide (μM), respectively.¹³

Just a small selection of important processes in the ocean were selected and will be described briefly below. There are more processes going on in the water column and their interactions are highly complex.

Photosynthesis is probably the most known biological process involving carbon dioxide which appears in the ocean. The process converts carbon dioxide into oxygen and organic matter by light. Photosynthesis results in a reduced DIC and a slightly increased TA. The rate of photosynthesis is dependent on illumination. The maximum water depth light can penetrate seawater and microalgae grow, called photic zone, is dependent on optical conditions and vertical turbulent mixing.³⁴ Within that zone net primary production (NPP) occurs. It is defined according to

Field et al. as 'the amount of photosynthetically fixed carbon, available to the first heterotrophic level in an ecosystem'.³⁵ In the ocean NPP is mainly generated by phytoplankton. Moreover it is in direct relation to the plant biomass. Results of satellite-derived measurements in combination with knowledge about the sea surface temperature, solar irradiation and mixed layer depths allow the calculation of the global oceanic NPP of ~ 48 Gt C per year. Approximately a third of the produced organic matter reaches the deeper ocean.³⁶ The highest oceanic primary production can be found in coastal areas and the Northern hemisphere during summer time.

The second biological process dealing with carbon dioxide is the *formation and dissolution of calcium carbonate* (CaCO_3). CaCO_3 can be found in sediments in the deep sea, which derived mostly from pelagic skeletal organisms, as well as in skeletons of calcifying organisms. The chemistry around CaCO_3 influences the global carbon cycle by reducing the carbon dioxide level in the upper ocean ('carbonate pump') and is therefore influenced by the increasing amount of CO_2 in the atmosphere (see section 1.1.4).³⁷ The precipitation of CaCO_3 result in a simultaneous decrease of total alkalinity and dissolved inorganic carbon in a ratio of 2:1. So the carbonate system changes to higher CO_2 levels and a reduced pH.¹³ Calcium carbonate can be formed either by inorganic processes, like cristalization or organic processes, like biogenic calcification in marine calcifiers. The precipitate can either be calcite, aragonite, high-magnesium calcite (> 5 mol % MgCO_3) or amorphous calcium carbonate.³⁸ The two main forms are calcite and aragonite, two polymorphs with a very similar crytal structure. Are double charged ions, like Mg^{2+} , present in the solution, the formation of aragonite is favored.³⁹ The most important parameter for calcification is the calcium carbonate saturation state (Ω_{cal}). The degree of saturation is represented by the ion product of the concentration of calcium and carbonate ions for a certain temperature, salinity and pressure.⁴⁰

$$\Omega_{calc} = [\text{Ca}^{2+}][\text{CO}_3^{2-}]/K_{spcal}^* \quad (1.19)$$

The carbonate concentration primarily determine the level of saturation and is defined through the carbonate system. The major planktonic CaCO_3 production occurs in the upper ocean by three main groups of calcifiers: coccolithophores (calcite shell), foraminifera (calcite shell) and euthecosomatous pteropods (aragonite shell).³⁸

Material forming processes, like photosynthesis (NPP) and shell production, occur mainly in the upper ocean (~ 100 m). A large proportion of the net primary production is respired by metabolic mechanisms in the upper ocean (0-200 m, main reason temperature-dependent bacterial respiration⁴¹). The smaller fraction sinks below the thermocline and get remineralized (200-1000 m). Just a tiny fraction reaches the deep ocean, but remains there for hundreds of years.⁴² The remineralization depth is known as the depth where sinking carbon is decomposed to carbon dioxide. The depth depend on the sinking speed of the particles and the rate of decay, as well as on the temperature, oxygen concentration, particle composition and stratification.⁴³ Decomposition of dissolved organic matter (DOM) in the water column is mainly realized by heterotrophic bacteria. Via intracellular transformations and enzymatic decomposition organic material is converted to nitrogen, phosphorus and inorganic carbon, related to the elemental

composition of the DOM.⁴⁴ Overall remineralization increase the amount of carbon dioxide and nutrients, as well as reduce the oxygen concentration.

1.1.4 Increasing CO₂ Content

Since the industrialization started in the late 18th century, the level of atmospheric carbon dioxide increases continuously.⁴⁵ A large proportion of the antropogenically produced carbon dioxide is taken up by the ocean and stored in the deep sea.⁴⁶ The increasing carbon dioxide concentration in the ocean results in a lowered pH and a change in the carbonate chemistry (see section 1.1.1). A huge number of studies have been made to investigate the impact of a rising CO₂ level to the marine ecosystem. The studies were focussed on global scale variations, as well as the response of marine flora and fauna.

To understand global scale variations in the ocean, changes in the world's climate have to be considered. The most known process is the *greenhouse effect*, caused by the so called greenhouse gases (carbon dioxide CO₂, methane CH₄ and nitrous oxide N₂O).⁴⁷ Normally the earth's surface and the overlying atmosphere absorb solar radiation and re-radiate the energy by infrared and longwave emissions. Gases like carbon dioxide absorb the emitted radiation. Therefore less energy is re-radiated to space and the atmosphere is getting warmer. This difference in energy transfer is called greenhouse effect. But not exclusively greenhouse gases contribute to the effect, water vapour and aerosols are a part of it as well.⁴⁸ Overall the greenhouse effect lead to a higher ocean surface temperature (0.6 °C over the last 100 years). The higher temperature result in an intensified stratification of the ocean with impact on the oxygen concentration, nutrient availability and primary production. Moreover a rising sea level is although a result, induced by thermal expansion and meltwater from terrestrial glaciers and ice sheets. Moreover the temperature affects the rate of animal metabolism and primary production (whole food web).⁴⁹ High levels of pCO₂ changed and will further change pH (0.1 pH unit decrease compared to preindustrial times), dissolved inorganic carbon (DIC), carbonate concentration and saturation state of CaCO₃. A lowered pH cause a higher dissolution rate of calcite shells and minerals, as well as weaker and smaler carbonate skeletal of calcifying organisms, like corals. The combination of a higher temperature and a more acidic pH causes although bleaching of coral reefs.^{50 51}

1.1.5 Additional Interacting Parameters

There are several other parameters affecting the carbonate chemistry and the marine ecosystem in general. The most important parameter are the oxygen, nutrient concentration and their distribution. The oxygen concentration influences the respiration of marine organisms, as well as the remineralization in the deep ocean. The upper ocean layer is in equilibrium with the atmosphere generating a constant level of high oxygen concentration. Furthermore the photosynthesis rate is high due to a high light intensity. Afterwards it gets consumed in sub-surface waters by respiration of sinking organic matter. Additionally oxygen-rich water masses get transported in the ocean water body by circulation. An overall decrease in the ocean oxygen concentration could be observed by several oceanographers. The likely reason is a reduction in ocean circulation and a solubility change due to a higher sea surface temperature. Decreasing

oxygen concentration causes expanding oxygen minimum zones (see section 1.2.3)⁵²

The group of nutrients consist of nitrate, nitrite, phosphate and silicate, as well as their organic counter parts particulate organic carbon, particulate organic nitrogen and particulate organic phosphorus. Nutrients mainly influence the rate of primary production in the eutrophic zone and therefore influence the biological pump dramatically (transport of CO₂ in the deep sea via organic matter). Nutrient sources are upwelling events, bringing nutrient rich water from the deep sea to the upper ocean. Nutrient enrichment occurs via remineralization in the deep sea. The second factor are nutrient rich terrestrial water inputs, in many cases leading to eutrophication. Both factors are influenced by the annual cycle. The Mediterranean Sea for example is characterized by a large annual variability of hydrological structures, from a strong stratification during summer to a homogenisation in the water column in winter times. Due to the winter mixing, algae blooms can occur in spring. Overall the winter mixing determine the initial stock of nutrients and the stratification during the summer lowers the availability of new nutrients significantly. Corresponding to the study of Moutin et al., the surface nutrient concentration is near the detection limit. The deeper in the water column, the higher is the nutrient concentration. Whereas the concentration is relatively constant between 1000 and 3000 m. A maximum in nutrient concentration is mostly related with a minimum in oxygen concentration.⁵³

1.2 The Ocean – Structure and driving Forces

Almost everybody knows 'the Ocean'. It covers around 70% of the world's surface and influences the climate significantly. 97% of the world's water reservoir are united in the ocean, in numbers 1.35 billion cubic kilometers. The average depth is around 3675 m.⁵⁴ The deepest point is the 'Mariana trench' with almost 11,000 m in the western Pacific Ocean.⁵⁵ The mean surface salinity is between 32 and 38 PSS, depending on precipitation and river water influence. Scientists divide the large water body into four major parts: The Pacific, Atlantic, Indian and Arctic. Additionally smaller parts are called sea, gulf or bay.

The Ocean is additionally a big economic factor. The probably biggest segment is the transport of goods via tankers, bulk carriers and container ships. The growth of global trade led to an extension of the global merchant fleet (2009: 53,005 vessels, 31% general cargo ships, 27% tankers, 15% bulk carriers, 13% passenger liners, 9% container ships, 5% others) with a carrying capacity of 1192 million dwt ('death weight tonnage'). For commercial goods just a few principle transport routes are used worldwide. The second segment is fishery. The estimated value of landed fish worldwide was around 90 billion US dollar (2010). The most caught fish 2006 were herings, sardines and anchovies with around 21% of the overall fish caught. The most important nation concerning fishing are China, Peru, Indonesia, USA and Japan. Other economic segments are tourism, resources and renewable energies.⁵⁶

1.2.1 Ocean circulation

Ocean current carries an enormous amount of heat around the world. The water anomaly is the main reason for the characteristics of water, which are necessary for sufficient water circulation

around the world. Saltfree water has his highest density at 4 °C, because water molecules are packed closest together. In solid ice instead, water molecules are further away from each other, leading to a lower density. Furthermore water has besides ammonia the highest heat capacity. It is able to take up a large amount of heat before it boils. Seawater is salty, which shifts the density maximum to -3.8 °C. The freezing point is -1.9 °C for the same water mass. So water with high density is formed till ice formation starts.

There are three main forces abeting the ocean circulation: i) convektion, ii) eddies and iii) wind. The main force is 'convektion'. Depending on salinity and temperature, the density of water changes. Cold and salty water sinks down to great depths. This phenomenon is powerful and can be observed in some polar regions of the North Atlantic. The overall process of density driven movement of huge amounts of water in the polar region is called 'convektion'. The cold and salty surface water sinks down (convektion), salty water from nearby warmer area flows in from south. The warmer water cooles down in the Arctic air and begins to sink down again. Therefore convektion happens continuously. The water masses driven by convektion just sinks down till around 2000 m and settle on denser deep-water from the Antartic. Before the water sinks down, it absorbs a high amount of carbon dioxide and transport it to the deep ocean. Convektion in the polar region, e.g. Labrador and Greenland Sea, is the engine for a worldwide thermohaline (thermo - temperature driven; haline - salinity driven) circulation (fig. 1.4). This phenomenon not only occurs in the North Atlantic reagon, it can be observed in the Artic region as well. The salinity is even higher. Therefore the water sinks till the sea floor and forms the so called Antartic Bottom Water. This water mass flows across the whole ocean floor. The formation of ice promote this effect by increasing the salinity (ice just contains 0.5% salt).⁵⁶ Several studies dealt with the impact of global warming on the convektion process.^{57 58 59} A higher sea surface temperature is expected to decrease the efficiency of convektion.

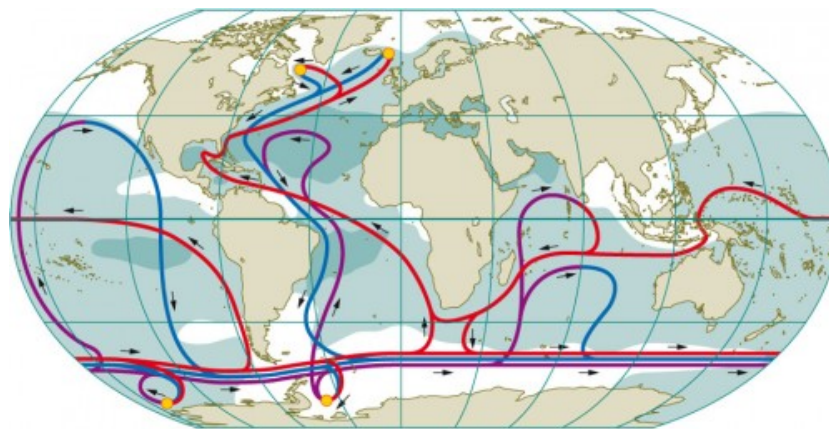


Figure 1.4: Thermohaline circulation of cold saline surface water (blue) downwards and toward south. Warm surface water (red) flows in opposite direction. Yellow points represent convection areas. Dark areas has a high salinity.⁵⁶

The second driving force for ocean circulation are eddies. They are formed, when water flows between regions with high temperature or density differences. These eddies are comparable with low-pressure systems in the atmosphere, but smaller. They can be observed in surface waters as well as in the deep ocean.

The third driving force for ocean circulation are strong winds in combination with the Earth'

rotation (Coriolis force) and the shape of ocean basins. These three influences determine characteristic currents in the sea surface circulation (fig. 1.5). Examples for such currents are the 'Gulf Stream' in the Atlantic Ocean, which is driven by a combination of winds and thermohaline circulation and the Kuroshio in the Pacific Ocean, which gets weaker by depth. Moreover winds are responsible for up- and downwelling of water masses. Especially upwelling processes are interesting, because they transport nutrient rich deep water to the surface, leading to a big fish population.⁵⁶

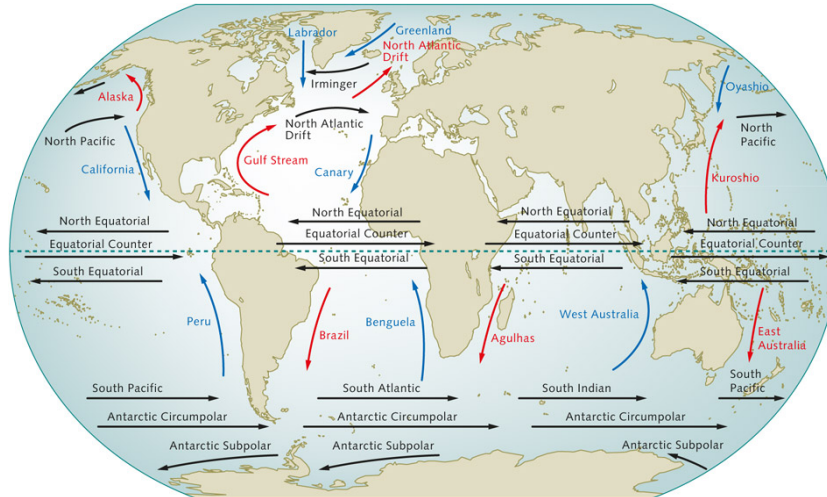


Figure 1.5: Sea surface current worldwide: warm streams in red; cold streams in blue.⁵⁶

1.2.2 Layerstructure

The ocean is mainly divided in three layers depending on the temperature: the surface layer, the pycnocline and the deep zone. A more detailed layer structure depending on light appearance can be seen in figure 1.6. Their shape and size depends on the latitude and annual season. The formation of the layer structure is driven by gravity and density differences depending on temperature and salinity. The epilagic zone is equal with the surface layer. This zone is well mixed by wind and wave and it is penetrated by sunlight. The zone is up to 200 m deep and represents 2% of the ocean volume. The mesopelagic zone is from 200 to 1000 m water depth and includes the pycnocline. The temperature drops very fast, forming a thermocline, which prevent mixing events. The penetrating light is faint (aphotoc). 18% of the ocean water body belong to this zone. Followed by deep water consisting of bathypelagic (till 4000 m), abyssopelagic (till 6000 m) and hadalpelagic zone (till 10,000 m). The temperature in this region is almost constant. Just a few invertebrates live in that region.

The first layer in the ocean starting from the surface is the *mixed surface layer* or *upper ocean*. It is considered to be a quasihomogenous region, where little variations in temperature, salinity and density occur. The mixing and the resulting uniformity is generated by turbulent mixing from wind and the formation of eddies, as well as heat fluxes, resulting in evaporation or the formation of sea ice. The mixed layer depth (MLD) varies annually and interannually. Moreover the layer thickness determines the air-sea exchange rate. The MLD can range from 20 m (summer hemisphere) to more than 500 m (winter hemisphere subpolar latitudes).⁶⁰ In the ocean

mixed layer primary production takes place. Light penetrates the upper few tens of meters and deliver the energy source for the production of biomass. Carbon fixation just take place, when the solar insolation is strong enough. Normally the ocean mixed layer is nutrient-poor and carbon dioxide rich. Nutrient rich water enters the layer by upwelling events, inducing a high rate of primary production. Primary production is an important factor for carbon fixation in the biological pump (section 1.1.2).

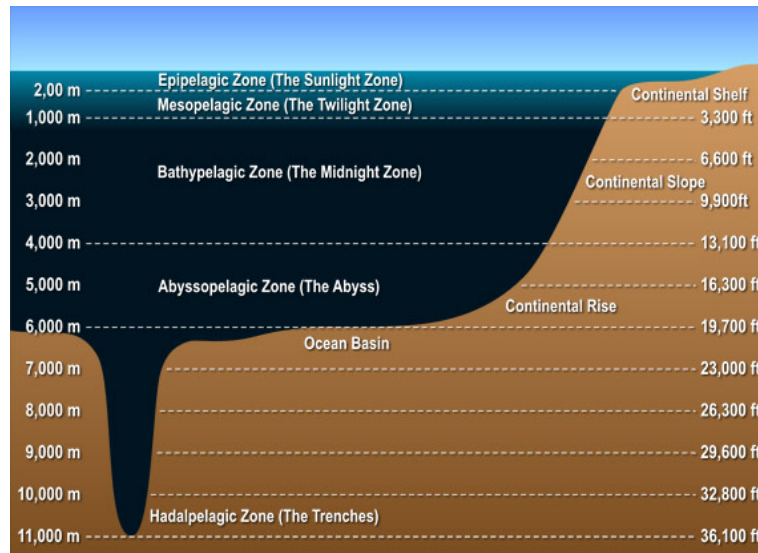


Figure 1.6: Vertical structure of the ocean depending on temperature.⁶¹

The *mesopelagic zone* is characterized by deminished light, increasing hydrostatic pressure and high nutrient concentration, as well as episodic food supply. It is a heterogeneous layer with high gradients in temperature (thermocline) and salinity (halocline). These gradient influence the microbial and metazoan distribution and activity. The mesopelagic layer can also be defined by ongoing processes for the upper and lower depth. The zone begins when light is too low for photosynthesis and ends, when downwelling irradiation is insufficient to effectively capture prey. Furthermore $\sim 90\%$ of annually from the surface exported carbon is respired to carbon dioxide. The zone accomodates a highly divers and active community of bacteria, archaea, protists, viruses and plankton.⁶² The mesopelagic zone includes the pycnocline, which is defined as a rapid change of density, generated by temperature and salinity differences. The pycnocline represents an effective barrier for heat transport and fluxes of organic matter. Fluxes in this layer occur by diffusion and eddies.⁶³ Additionally marine diel migrating biota enhance the flux of organic matter through the pycnocline. They obtain organic carbon by feeding above the pycnocline during nightttime and respire during the day below the pycnocline.⁶⁴ The pycnocline strength is high ($0.04\text{-}0.07\text{ kg/m}^4$) at low latitudes (equator), because of a high surface temperature and getting weaker with increasing latitude ($<0.02\text{ kg/m}^4$). Although the pycnocline depth varies worldwide, from 250 m in the Southeast Pacific Ocean to 60 m in Northwest Pacific Ocean.⁶⁵

The *deep zone* is the largest and highly unknown ecosystem on earth. The deep sea is characterized by permanent darkness, high pressure, low temperatures, carbon scarcity and energy limitation. It accomodates numerous pelagic organisms, which are able to emit light. The biological activity relies on organic matter coming from the sea surface. Downwelling events, triggered

by density changes at the surface during winter cooling or evaporation, result in higher bioluminescence produced by pelagic organisms.⁶⁶ Therefore the deep sea ecosystem is influenced by the primary production in the upper ocean layer. A higher surface temperature for example enhance the stratification of the ocean and alter the respiration rate in the upper ocean, consequently the flux of organic matter in the deep sea is reduced.⁶⁷

1.2.3 Special Case – Oxygen Minimum Zone

Oxygen minimum zones or dead zones are a spreading problem in the world's oceans. The formation of hypoxic zones are driven by high primary production. An enhanced primary production lead to accumulation of organic matter, which is exported to the bottom layer. A high amount of organic matter encourage microbial respiration and consequently a high demand of dissolved oxygen. A high primary production is mainly caused by eutrophication in the coastal zones worldwide, due to a high amount of riverine runoff of nutrients. Hypoxic water contains less than 2 mL O₂/L. Mass mortality occurs when the dissolved oxygen concentration is below 0.5 mL O₂/L. Often hypoxia is going along with semi-enclosed hydrogeomorphology (intensified by water-column stratification), which hinders water exchange. But not only eutrophication induced by human hand, also natural processes can cause high productivity. Coastal upwelling events transport nutrient rich water to the ocean surface layer generating high primary production. Such regions often occur in the eastern Pacific Ocean, south Atlantic Ocean, Arabian Sea and Bay of Bengal. The oxygen minimum zones are persistent in that regions and can be observed between 200 and 1000 m. Eutrophication-induced oxygen minimum zones are generally once per year during summer time after an intensive spring bloom. Moreover in summer stratification is strong and water warm.⁶⁸

Coastal hypoxia is suggested to follow a predictable pattern:

1. increased formation and export of organic matter leading to enhanced microbial growth and respiration, which increase the oxygen demand
2. hypoxia occurs temporary in combination with a high mortality of benthic animals
3. seasonal or periodic hypoxia is observed, as well as boom-and-bust cycle of benthic populations; organic matter and nutrients enriches in the sediment
4. hypoxia exists for years, zones start to expand and level of dissolved oxygen decreases; anoxia occurs and microbial generation of hydrogen sulfide⁶⁸

A low level of dissolved oxygen also affect the marine fauna (e.g. habitat compression). Hypoxia causes a low secondary production and a dramandous decrease of marine fauna in that region. Some animals are able to adapt their energy household to a low oxygen supply. Inhabitants of regions with a persistent low dissolved oxygen level adapt their aerobic metabolism by a lowered oxygen consumption rate or a highly effective oxygen removal from water. Pelagic crustaceans for example remove oxygen more effective via several adaptations: i) enhanced ventilatory ability, ii) enhanced O₂ removal from ventilatory system, iii) enlarged gill surface area, iv) shorter diffusion distances into the blood and v) proteins with higher affinity to oxygen.⁶⁹ Natural occuring oxygen minimum zones are located in the eastern Pacific (37°S till 52°N,

from coast to 180°W), Indian (northern part semi-enclosed by continents) and Atlantic Ocean, according to figure 1.7. They appear due to a relatively high sea surface temperature and consequently a strong stratification. In the gulf of Alaska (fall-winter-spring) and the West Bering Sea (winter) a low oxygen level occur seasonally.

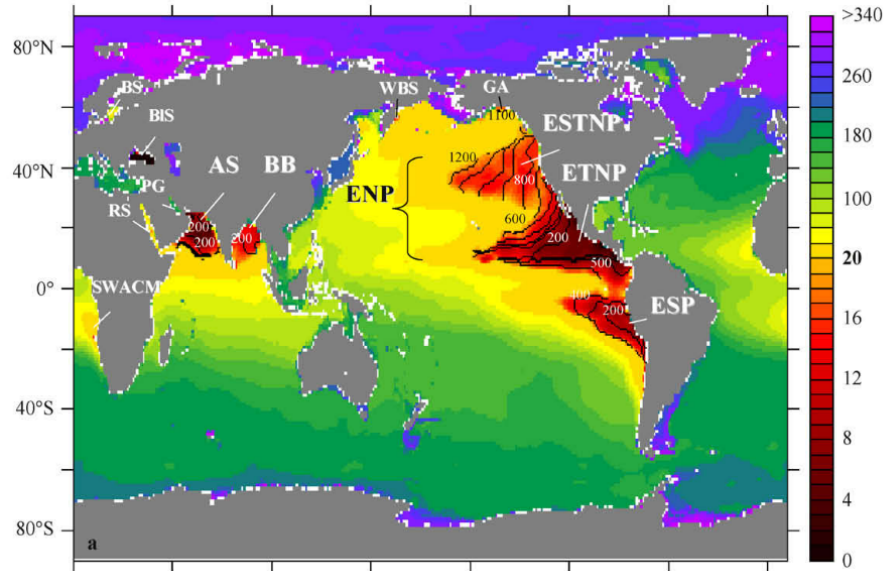


Figure 1.7: Worldwide distribution of oxygen concentration with depth of minimal oxygen concentration indicated by solid lines according to WOA2005 climatology. BS= Baltic Sea, BLS= Black Sea, PG= Persian Gulf , RS= Red Sea, SWACM= southwest African continental margin, AS= Arabian Sea, BB= Bay of Bengal, ENP= Eastern North Pacific, WBS= Western Bering Sea, GA= Gulf of Alaska, ESTNP= eastern subtropical North Pacific, ETNP= eastern tropical North Pacific, ESP= eastern South Pacific.⁷⁰

1.3 Sensor Technology in Oceanography

1.3.1 Necessity and Benefits

Sensor technology became an indispensable tool in oceanography. The ocean is a huge, continuously changing and harsh environment. Ocean circulation is the continuous movement of water masses around the globe, which are not fully understood. The interdependency between the ocean circulation and the climate change is not completely investigated yet. The impact of ocean acidification on flora and fauna is of special interest for research groups all over the world. These are just a few subjects which are currently investigated. For the prediction of adequate models for ocean circulations and climate change, as well as the correct interpretation of flora and fauna response, a large amount of data is necessary. In the last decades data acquisition was limited to ship based measurements, like profiling measurements and taking discrete samples. Especially discrete samples were collected, treated for transport and measured in the lab. Parameter determination in the lab is time-consuming and the sample treatment on the ship is error prone. Moreover the amount of data is limited and the costs for ships and trained staff are very high. In the last decades huge effort was put in the development of sensors and carrier platforms. The combination of a reliable sensor and a long-lasting platform increase the temporal and spatial resolution of ocean data significantly. In some cases a ship measures a profile at a certain station once a year. This is too little to make appropriate statements about ongoing processes. A monitoring buoy for example can be installed and deliver data over a long period, allowing to observe short-term, long-term or annual events. The use of mobile oceanic platforms enable the collection of large data sets through the whole water column. Continuous profiling measurements allow the investigation of the ocean mixed layer. Overall the increased amount of data is used to investigate and model the human impact on the ocean (e.g. offshore installations), marine eutrophication, biodiversity issues, pollution research, animal behaviour studies and food safety issues (e.g. toxic algae).⁷¹ Sensors have to fulfill certain requirements to be used in oceanography.

1.3.2 Application requirements

Several working groups developed and are developing sensor systems for marine applications. Each sensor has to fulfill certain requirements, which have to be considered during development. There are several characteristics an ideal sensor systems generally have to have. The sensor should be:

- selective, highly accurate and precise
- reversible
- sensitive (low limit of detection)
- easy to calibrate and handle
- drift-free (no periodic recalibration necessary, long-term stable)
- fast (ensure real-time measurements)

- robust (sensor chemistry and housing)

Further instrument specifications depend on the area of use and the platform chosen for implementation. For the use in the ocean, factors like power consumption, size, resistance to corrosion (e.g. biofouling) are important. For oceanic applications, the power consumption of the sensor is essential. It limits the duration of the deployment, as well as the versatility of potential platforms for integration. Power efficient sensor components, as well as an intelligent data acquisition (powering down between measurements) are possibilities to reduce power consumption. Another factor is the size and weight of the sensor device. A small size allow the integration into mobile platforms like glider and AUVs. Especially when the sensor is supposed to be attached to animals or implemented in surf boards ('smartfin' project). The sensor should be resistant to corrosion, a special issue is biofouling. It occurs during long-term deployments and deployments in nutrient rich water masses with a high biomass production rate (e.g. estuaries, see section 3.4.7). Marine biota (e.g. algae and barnicles) tend to populate the sensor after a certain time, can cause variations in the sensor response and potentially slows down the response time. Copper materials and the retraction of the sensor surface are successful strategies to avoid biofouling. Furthermore the sensor should be user-friendly. Conditions at sea are harsh, so the handling of the sensor system should be as easy as possible, to minimize sources of errors. A high degree of automatization can simplify the handling dramatically and can enhance the long-term stability by automated frequent self-calibration. Moreover the sensor has to have an appropriate dynamic range to cover all analyte levels, which can appear during the measurement. A special case are areas affected by the tidal cycle, where large variations in all parameters occur. Almost every sensor shows a temperature and salinity dependency, which should be fully characterized in the required range to guarantee accurate data. The sensor has to be sensitive, even in a high saline medium with a wide variety of other compounds with partially the same characteristics as the target molecule. The response time is important especially for profiling applications. Another important factor are the costs for the sensor device itself, but also for installation and maintenance.^{71 72 73} Depending on the area of deployment certain requirements are more important than others.

1.3.3 Fields of Applications

Aquarium

Aquaria differ significantly in size, animal population and water characteristics. An aquarium can be found in many households. Commonly filled with fresh water and a mixture of plants and fish to mimic a natural environment. Huge saltwater aquaria are commonly for research purposes and/or open for public. Famous examples are the Oceanographic in Valencia (Spain), the Georgia Aquarium in Atlanta (USA) and the Monterey Bay Aquarium in California (USA). It is essential to control the water quality to ensure appropriate conditions for the individual animal population. Often used sensors measure temperature, oxygen, pH and turbidity. They should be installed invisible for visitors and at best unreachable for animals. Therefore sensors should be small, long-term stable, accurate and unattractive for fish (e.g. no blinking light), as well as moderately fast to deliver real-time data. The service interval should be long. Power consumption, weight and pressure resistance are no limiting factors.

Aquaculture facilities and fish transport

Water quality monitoring systems are essential in aquaculture facilities. Such facilities getting more and more automated to increase profit. They are typically characterized by a large number of fish in a relatively small water volume. Variations in water quality parameter can cause fish mortality and a high economic loss. Therefore the use of sensors for oxygen, pH, carbon dioxide, salinity, alkalinity and ammonia are of special interest. These parameters directly affect animal health, feed utilization and growth rates. Each parameter should be at the optimum level to ensure a low stress level of the fish, distinct appetite, a high growth rate and a low disease susceptibility. The most important parameter seems to be oxygen, due to the need for fish respiration as well as phytoplankton activity (break down toxic ammonia).⁷⁴ The transport of living fish from aquaculture farm to farm or from the farm to customer is practiced worldwide. The fish is transported in so called wellboats with large storage volumes to transport efficiently. The transport of salmon is closely monitored to ensure fish health: Salmon die from hypoxia at low oxygen concentration, a high carbon dioxide concentration can have sedative effects and a high ammonia gas level increase the mortality rate. Sensors are used to keep the parameters within the limits.⁷⁵

Sensors used in aquaculture facilities and boats are not limited in terms of energy consumption, size or weight. They should have a moderate response time, a high ruggedness and long maintenance interval. Additionally biofouling is a big issue during such deployments.

Brackish water

Brackish water are water masses with a salinity lower than 30 PSS. They commonly appear when seawater meets fresh water. Therefore estuaries are the biggest brackish water masses worldwide (a river end in the sea). A big brackish sea is the Baltic Sea. Due to its hydrographic location, saltwater barely enter the basin and fresh water is continuously delivered by a number of rivers. If estuaries are influenced by the tidal cycle, large and rapid changes in temperature and salinity can occur. Due to the high amount of nutrients transported by river water, estuaries are regions with high biomass production.⁷⁶

These environments are a special challenge for sensor systems. They have to be well characterized for a wide salinity- and temperature range. Moreover sensors have to be fast responding and resistant to biofouling.

Ship deployments

Currently a large number of research vessels (RV; RRS - royal research ship) are used for oceanographic research purposes. They are commonly allotted to research institutes like the RV *'Roger Revelle'* owned by SCRIPPS Institute of Oceanography, the Research ice breaker *'Polarstern'* maintained by the Alfred-Wegener-Institute Helmholtz Centre for Polar and Marine Research, the RRS *'Discovery'* owned by the National Oceanography Centre or the RV *'Elisabeth Mann Borgese'* owned by the Institute for Baltic Sea Research. Almost all research vessels are equipped with a CTD rosette connected to a rope. They are made to measure Conductivity, Temperature and Depth through the whole water column and taking discrete samples at chosen depths for additional lab measurements. Sensors used for profiling applications via a CTD have

to be fast and highly pressure resistant. CTD profiles were measured in the Mariana Trench down to 10877 m with a velocity of around 1 m/s.⁷⁷ Power supply, size and weight are minor issues. Moreover sensor should be unaffected by changing the environment from aqueous phase to gas phase and the other way around. Additionally sensors can be integrated in continuously pumped shipboard systems to measure surface parameters. Such pumped systems are although implemented in commercially used ships like ferries.

Moreover reasearch vessel are sometimes equipped with a *Remotely Operated Vehicle*, short ROV. ROVs are mobile devices connected with the ship and operated by a pilot. They have a continuous power supply, cameras and robotic arms to take samples or to do maintainance (fig. 1.8).



Figure 1.8: From left: Research vessel '*Rachel Carson*' operated by Monterey Bay Aquarium Research Institute (MBARI), CTD rosette with 12 water samplers and the ROV '*Ventana*'.

Monitoring buoys

Monitoring buoys are used to observe certain parameters of the ocean, like temperature, salinity or turbidity over time. They can be drifting or anchored at the sea floor. So called drifting bouys move with ocean current and can be localized via satellite. They mainly consist of a surface float and an underwater drifting drogue connected with a rope. Sensors are attached to the rope or the surface float, which also includes GPS and communication systems. Instead a mooring buoy is located at a certain position. These buoys although consist of an equipped surface float, which is achored via a chain on the sea floor. Sensors can be attached to the chain at certain depths. Also profiling moorings, like the GODESS profiling mooring in the Baltic Sea⁷⁸ were developed. Sensors used at monitoring buoys should be highly long-term stable, to minimize maintainance. Moreover they have to be mechanically robust, especially when used at drifting buoys. Monitoring buoys are not limited to observe geochemical parameters (temperature, salinity, oxygen concentration), they are although used for fish population or whale calls investigations. These buoys are also suitable to measure air quality parameters.

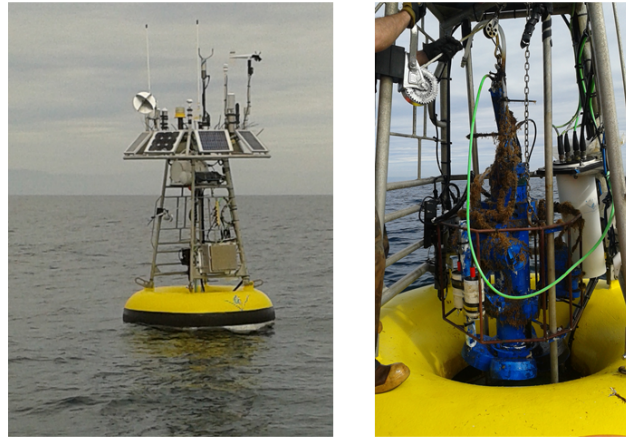


Figure 1.9: Mooring Buoy C1 in the Monterey Bay maintained by MBARI.

Mobile platforms

The group of mobile oceanic platforms is indispensable for *in situ* observations. They act as autonomous carrier for sensors through the whole oceanic water mass. Several platforms for different deployment areas were developed in the last 50 year. The platforms differ in terms of shape, propulsion, working depth, time of deployment and production cost. All presented mobile platforms are unmanned maritime vehicles (UMV). They all include a communication and localisation system to transmit data and the position in almost real-time to a land-based server.

An often used mobile oceanic platform are **wave gliders**. It is an autonomous surface vehicle (ASV) and designed to measure just in the upper ocean (< 10 m). The platform utilizes ocean wave energy for platform propulsion. It consists of a sea-surface float and a submerged glider connected via a tether. The sea surface float has a size of 2 m x 0.6 m on average, is equipped with solar pannels to continually charge the batteries and carries the control electronics, communication systems and sensors. The glider is mostly placed ~ 7 m under water surface and has a size of roughly 2 m x 0.4 m with wings of 1 m. The glider is responsible for the propulsion of the platform independent on the wave direction. The movement is induced by the position of the wings relatively to the float position and exclusively mechanical. Therefore a limitless movement is possible.^{79,80} For this type of mobile platform the sensors have to be small, fast and less prone to biofouling. The power consumption is a secondary issue due to the installed solar panels, as well as the data logging, pressure resistance and in a certain range the weight.

Continuous profiling measurements can be realized by **profiling floats**. They are suitable to measure profiles from the upper 2000 m of ice-free global ocean. The floats drift at a certain depth, in a programmed interval water is pumped in an external bladder. The float ascend to the surface measuring temperature and salinity and dive back to the waiting depth. The horizontal movement of the float is dependent on currents at the waiting depth. The Argo project was launched to develop, deploy and maintain profiling floats all over the world. They are mainly used to investigate the ocean mixed layer.⁸¹ Sensors attached or integrated in a profiling float should be small and lightweight, as well as driftfree and cheap. At the moment around 3800

Argo floats are deployed worldwide.⁸²

The **Autonomous Underwater Vehicle (AUV)** is an often used mobile platform in oceanography. They are programmable, robotic carriers, which move through the ocean without human real-time control by the use of propellers. AUVs are used to obtain huge data sets with high temporal and spatial resolution, as well as detailed seafloor maps in deep water. They are mostly torpedo-shaped, but can have more complex designs allowing special deployments (e.g. slower movement). AUVs typically move with a speed of $1.5\text{--}2.0\text{ m/s}^{-1}$. They are capable to transport a variety of marine instruments like CTDs, cameras, geophysical instruments and other sensors, as well as discrete water samplers. The loading of the AUV determines the altitude and the deployment duration. High energy consuming instruments shorten the deployment.⁸³ Therefore sensors should be low power consuming, pressure resistant and fast.

A special kind of AUV are **glider (Autonomous Underwater Glider, AUG)**. They glide through the water column by changing the buoyancy. The rapid sink and ascend movement is converted in forward motion. Small low power consuming pumps are often used to change the buoyancy. The glider pitch can be adjusted by the center of mass. An energy efficient design of the whole glider allows durations over many months and a range of several thousand kilometers. The cost and size of gliders are often kept moderate, to allow a widespread use and the launch out of small boats.⁸⁴ Even 'Deepglider' are available which can glide down to 6000 m.⁸⁵ Sensors for the use in a glider have to be small, lightweight, low power consuming, driftfree, pressure resistant and relatively fast (response times up to 10 s)



Figure 1.10: Mobile platforms from left a waveglider, a profiling float, an AUV and a glider.⁸⁶

1.4 Carbon Dioxide Sensors in Oceanography

1.4.1 Sensing Strategies

Several sensing strategies for oceanic carbon dioxide were developed in the last decades. But oceanography is not the only field, where carbon dioxide measurements are of special interest. The determination of CO_2 is although important in medicine, biotechnology, chemical industry and meteorology.

Carbon dioxide can be measured *electrochemically* by using a so called 'Severinghaus' electrode. The first pCO_2 electrode was published by J. W. Severinghaus et al. in 1958 for the

analysis of blood. The main component is a pH-electrode surrounded by an aqueous buffer chamber. A thin gas-permeable membrane connects the sample and the inner buffer solution with a known pH. Gaseous carbon dioxide diffuse through the membrane and forms, in combination with water, carbonic acid. Due to the dissociation of carbonic acid, the pH of the buffer solution changes. This pH change can be detected via the pH electrode. The pH electrode voltage is measured relative to the reference electrode.⁸⁷ Such electrodes have response times of 5 - 15 minutes controlled by diffusion and buffer reaction rates.⁸⁸ A more recent method to measure carbon dioxide electrochemically are Ion-Selective Field-Effect Transistor (ISFET) pH sensors. The pH sensor is although combined with a buffer solution and a membrane. In this case the pH change lead to a change in the surface charge of the ISFET. Additionally the strength of the electric field of the transistor alternated relativ to the reference electrode. The pH electrodes are the limiting factor in terms of crosssensitivity, temperature and pressure dependency.⁸⁹ Furthermore the membrane significantly influences the response time as well as the sensitivity of the carbon dioxide sensor.⁹⁰

The probably most often used sensing strategy is *NDIR-spectroscopy*. The non-dispersive infrared spectroscopy (NDIR) is predicated on characteristic molecule vibrations of carbon dioxide. CO₂ is a linear molecule. Due to the symmetry and the electronegativity of oxygen and carbon, the molecule has no dipol moment. But it can change during vibrations of the molecule. Typical vibrations generating a dipol moment change in a three atom molecule are asymmetric stretch and bending vibrations. Both types are IR-active vibrations and can be measured via IR spectroscopy. Characteristic for carbon dioxide are vibrations/bands at 2349 cm⁻¹ (asymmetric) and 546 cm⁻¹ (bending)(fig. 1.11). The symmetric vibration do not induce a dipol moment change and is therefore not IR-active and cannot be seen in the spectrum. The method requires a measurement in the gas phase, because water or water vapour interfere significantly. Therefore an equilibration between the seawater sample and an internal standard gas phase is necessary. The equilibration is realized by an gas-permeable membrane inserted in a flow through equilibrator system. The membrane is mechanically supported to bear up high pressure. The equilibrated gas phase is transfered to the analyzer. On the way to the IR analyzer the gas stream gets temperature controlled. The heater is used to minimize temperature changes and generate more accurate and precise data. Additionally the temperature, pressure and relative humidity is determined within the gas stream to correct the obtained data from the IR-analyzer. The sensor response is non-linear.⁹¹

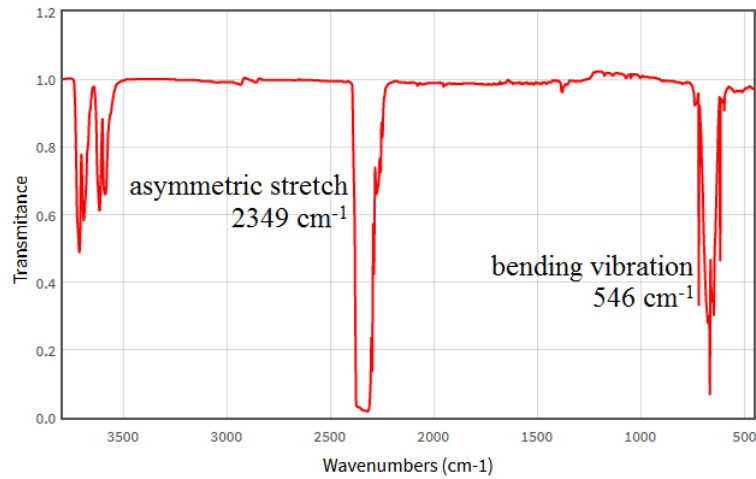


Figure 1.11: IR spectrum of carbon dioxide.⁹²

Another method using the absorption properties of carbon dioxide for light, is the *cavity ring-down spectroscopy (CRDS)*. The system consists of a air-seawater equilibrators, a laser and a high finesse optical cell. The optical cell include two or more mirrors with a reflectance of >99.99% and a photodetector. Light from the laser is inserted in the optical cell via one partially reflecting mirror. The light intensity increases steadily over time and is determined by the photodetector. After a certain light intensity was generated, the laser got switched off rapidly. Afterwards the 'ring-down' measurement is done by determining the light intensity in the cavity. The exponential decay is dependent on the cavity mirrors and the absorption of carbon dioxide at 1603 nm. An analyte-dependent time constant τ can be calculated and converted into the carbon dioxide concentration. Overall the light remains in the cavity for a long time, creating a kilometer long effective path length. This long path length is responsible for a high sensitivity of CRDS devices. An equilibration of an internal gas phase with the seawater sample is necessary prior to determination. The technology is also suitable to measure methane and water in a gas sample.⁹³

A third group of sensing strategies for carbon dioxide in seawater are optical as well, but additionally include an indicator dye. A *wet-chemical spectrophotometric* carbon dioxide measurement is based on the induced pH change corresponding to the CO₂ level. The seawater sample has to be equilibrated with an internal buffer solution of a known pH via a gas-permeable membrane. After diffusion through the membrane the colour of the internal pH-sensitive indicator dye solution changes. The equilibrated indicator solution is transferred to an optical cell and the absorbance is measured spectrophotometrically at three different wavelengths. The three wavelengths are at the absorbance maxima of the protonated and deprotonated form of the indicator dye, as well as at a non-absorbing wavelength to generate a baseline. The indicator solution should be of an equal ionic strength compared to seawater to minimize osmotic pressure across the membrane.⁷² Commonly used indicator dyes are thymol blue^{94 95}, bromothymol blue⁹⁶ and hydroxypyrene-1,3,6-trisulfonic acid (HPTS)⁹⁷. *Optodes* are although based on the CO₂ induced pH change. In the case of optodes the analyte-sensitive indicator dye is embedded in a gas-permeable matrix (sensor foil/spot). Depending on the amount of carbon dioxide, the indicator dye changes its spectral properties. By exciting the sensor spot via a light emitting

diode (LED), the analyte dependent emission can be detected with a photodetector. A more detailed description of optical carbon dioxide sensors is presented in section 1.5.

A more sophisticated strategy to measure carbon dioxide was presented by Liu et al. 2010. The strategy is based on aggregation-induced emission. Hexaphenylsilole is non-fluorescent in solution, but emit light after aggregation. Aggregation of the compound is supported by the restriction of intramolecular movement. Furthermore the restriction is realized by an CO₂-induced increase of viscosity of an ionic liquid.⁹⁸

Sensing strategies for gas phase carbon dioxide sensors are among others based on solid-state gas sensors. Changes in electrical conductivity of a semiconductor induced by adsorption and desorption of carbon dioxide is used for determination, first mentioned 1962.⁹⁹ Several different materials were developed to tune the sensor performance: graphene for ambient conditions and room temperature¹⁰⁰, electrical conducting polymers for room temperature¹⁰¹ or lithium ion conducting electrodes for high temperature¹⁰².

1.4.2 Developed Prototypes

Some sensing strategies showed good potential to be used in sensor devices. Therefore several prototypes and later on commercially available carbon dioxide sensors for the use in seawater were developed. A number of commercially available sensors are described in section 1.4.3. Some prototypes are not commercialized yet. These will be described in this section, with no claim of completeness.

Based on the previously mentioned ISFET-technology a prototype was developed and deployed in the last years. A pH-ISFET was combined with a Cl-ISE as a reference electrode and sealed in a unit, covered with a gas-permeable membrane and filled with a 1.5% NaCl solution. Due to the use of a differential measurement system, potential calibration drifts and thermal sensitivity could be eliminated. Therefore the determined pH change of the NaCl-solution is just induced by carbon dioxide, diffused through the membrane. Special focus was set on the material of the gas-permeable membrane. Often used are PVC-based membranes, which have adhesion problems. A second material is a highly polymerized silicone rubber with additives like lipophilic ionics or plasticizer. Additives were used to lower the high electrical resistance of the membrane. A third material is Teflon AFTM.⁹⁰ A pCO₂-ISFET sensor was integrated in an AUV (REMUS) to investigate a shallow hydrothermal vent. The AUV moved with 2 knots in a depth of 5 m, 10 m and near the bottom. The measurement interval was set to 10 s. Due to no calibration of the sensor before and after the deployment, only raw data were available showing high and low carbon dioxide levels.¹⁰³ Later on the sensor was used to monitor CO₂ leakages from seafloor CO₂ storage facilities. The sensor was characterized to have a response time (t_{90}) less than 60 seconds (3000 m water depth; 1.8°C). The sensor was calibrated prior to deployment and *in situ* recalibrated using depth, temperature, salinity and total alkalinity from bottom water reference samples. The sensor was placed in 10-12 m water depth with 3-5 cm between the sensor and the seafloor. The test were performed over at least 13 days.

A second electrochemical sensor prototype were microelectrodes. Cai et al. presented a microelectrode for carbon dioxide measurements in marine sediments. The pCO₂ microelectrode consisted of an outer pipette and an pH microelectrode (15 µm tip diameter). The very tip was covered with a gas-permeable silicone membrane. Additionally the outer pipette was filled with a 2 mM NaHCO₃ and 0.5 M NaCl solution. The pH microelectrode was placed at the center with a distance to the silicone membrane of 5-30 µm. The tip diameter of the pCO₂ electrode was 100-250 µm. Three Carbon dioxide standards were used for calibration. The response time was 1-3 minutes and the storage life several days up to a week under correct storage conditions.^{104 105}

Moreover several prototypes with an optical indicator dye based sensing strategy were fabricated in the last decades. A prototype of our working group called 'MuFO' (Multiple Fibre Optics) was developed during the european project ECO₂- sub-seabed CO₂ Storage: Impact on Marine Ecosystems. The sensor system consisted of three components: A camera to take pictures of the polished fibre ends, a number of optical fibres (up to 100) guiding excitation and emission light and the sensor foil containing a pH-sensitive indicator dye. The sensor foil is fixed on the tip of the fibre via metal sleeves. The sensor foil itself were prepared of three knife coated layers. The first layer contained the sensing chemistry, the second layer for proton protection and a third layer for optical isolation made of carbon black and silicone rubber. Corresponding to the carbon dioxide level the indicator is protonated or deprotonated, resulting in a different colour recognized by the camera. The pictures were analyzed for the red, green and blue channel, which contain information about the emitted light. The preparation and calibration of the system is very complex and time consuming, as well as the software development. The system was deployed 2013 at Panarea Island (Sicily Italy).¹⁰⁶ Additionally several optode prototypes were developed in the last decade. Prototypes for marine carbon dioxide determination were presented by: Atamanchuk et al. 2014 including a sensor foil from PreSens GmbH^{75 107}, Clarke et al. 2017 using HPTS as the indicator dye⁸⁹, Fritzsche et al. 2017 using aza-BODIPY indicator dyes¹⁰⁸, Schröder et al. 2007 using HPTS as the indicator dye¹⁰⁹ or Nakano and Yoshida 2011 using bromocresol purple¹¹⁰. A more detailed description of the indicator dyes, sensing scheme and hardware can be found in section 1.5. None of the optode is commercialized yet.

EU-Project 'SenseOCEAN'

At the moment a wide variety of sensors to monitor ocean health are available. Additionally several platforms were developed to transport the sensors through a harsh environment. Commonly each sensor requires its own software and is equipped with an individual connector for energy supply and in-time read out. The european project 'SenseOCEAN - Marine Sensors for the 21st Century' brings together 'world leading marine sensor developers to create a highly integrated multifunction and cost-effective in situ marine biogeochemical sensor system' (official project description¹¹¹). The aim of the project was the development of a modulate sensor system consisting of state-of-the-art sensor technology, new developed sensors and an overall data logger and transmitter. During the four year-project-duration several new sensor systems were developed:

- ANESIS: Autonomous Nutrient Electrochemical Sensor *In Situ* → The sensor measures

silicate and phosphate electrochemically. The nutrients first get converted into the corresponding molybdenum complexes, which can be detected in the second step via a gold electrode. The sensors were 25 cm long and 9 cm in diameter with a weight of 2.2 kg in air.

- Multiparameter optical sensor for CDOM, Chlorophyll a and PAHs → It is a multichannel fluorometer, which is suitable to measure coloured dissolved organic matter (CDOM), chlorophyll and polyaromatic hydrocarbons (PAHs) using the same sensor design but determining different emission wavelengths.
- Optodes for marine measurements → Two new optode designs were developed one for deep sea applications and a second stand-alone device with internal logger and battery (max. depth 300 m). The hardware is compatible with sensor foils for oxygen, pH, pCO₂ and NH₃.
- Electrochemical microsensor for carbon dioxide and nitrous oxide → The microsensors are needle-shaped with a tip diameter of around 50 µm. They reductively convert CO₂ and N₂O on a silver cathodes. According to the analyte the structure of the microsensor was adapted.
- Lab on chip chemical sensor for various analytes → A common design was developed to measure pH, nitrate, nitrite, silicate, phosphate, ammonia, iron, total alkalinity and dissolved inorganic carbon. The diversity was realized by changing the necessary reagents.

The complete sensor package including the logger system was deployed several time all over europe. The first field test was done in the Kiel harbour for five days. Up to seven sensors were plugged to the logger system (MODBUS module). Additionally several depth profiles (25 m) in the Kiel fjord were measure. Several more tests and rigorous validation were carried out in e.g. Southampton and the Mediterranean Sea. Overall the project lead to a 'truly integrated and easy to use multi parameter sensor system, which will be available to scientists, industry and regulatory bodies throughout the world.' (final brochure 'SenseOCEAN'¹¹²) Participants of the project were: National Environment Research Council (United Kingdom, coordinator), Aarhus University (Denmark), Alfred Wegener Institute Helmholtz Centre for Polar- and Marine Reasearch (Germany), Chelsea Technologies Group (United Kingdom), CNRS-LEGOS (France), Graz University of Technology (Austria), Max Planck Institute of Marine Microbiology (Germany), nke Instrumentation (France), PyroScience GmbH (Germany), TE Laboratories (Ireland), Unisense A/S (Denmark) and University of Southampton (United Kingdom). Besides the presented project, several others dealing with sensor development were and are funded by the European Union, e.g. ECO₂ (05/2011-04/2015, www.eco2-project.eu), COMMON SENSE (11/2013-02/2017, www.commonsenseproject.eu), SCHEMA (10/2013-09/2017, www.schema-ocean.eu) or SMS (12/2013-08/2017, www.project-sms.eu).

1.4.3 Commercially Available CO₂-Sensors

Some of the invented prototypes were further developed to a commercially available sensor system. A technical comparison of the following systems are presented in this section: SAMI CO₂

from Sunburst Sensors, CONTROS HydroC[®] CO₂ from Kongsberg Maritime Contros GmbH, Seaology[®] pCO₂ monitoring system from BATTELLE, CO₂-ProCVTM from ProOceanus Systems Inc. and Picarro G2201-*i* Analyzer from Picarro Inc. An overview of the relevant sensor characteristics can be found in the table (tab 1.1). A more detailed description of the measurement principle and deployments of each sensor can be found later on. The chosen sensor system are only a brief selection of commercially available carbon dioxide sensors for marine applications based on divers measuring principles. Some sensors use the same measurement principle, but each company modified the basic analyzer to make the sensor more accurate, more reliable, lightweight or otherwise better fitting to customer needs.

SAMI CO₂ from Sunburst Sensors

Statement and promotion of Sunburst Sensors: 'Our pCO₂ and pH sensors are available for your next research project. With improved reliability, durability and user-friendliness, the SAMI supports up to three additional sensors and can be deployed to depths of up to 600 m.'

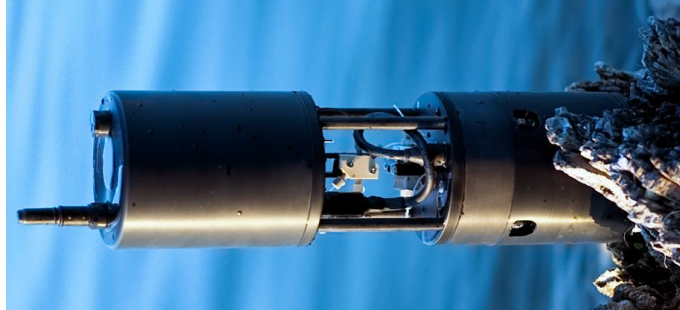


Figure 1.12: SAMI CO₂ carbon dioxide sensor developed by Sunburst Sensors.¹²⁷

The SAMI-CO₂ carbon dioxide sensor is based on the spectrophotometric measurement of a colorimetric pH-indicator dye (bromothymol blue). The sensor consists of a membrane equilibribrator combined with a fiber optic flow cell. The ambient carbon dioxide is connected to the internal indicator solution via a tubular gas-permeable silicone rubber membrane. The CO₂ reaches the internal solution and forms carbonic acid, which dissociates and change the pH of the solution. According to the CO₂-initiated pH change the indicator absorbance varies. The sensor response is calculated from two characteristic wavelengths, which correspond with the absorption maxima of the mono-protonated and deprotonated form of the indicator dye. In the case of bromothymol blue they are at 434 nm (mono-protonated) and 630 nm (deprotonated). By using the ratio of the absorbance, the dependency on operational parameters is eliminated. The necessary indicator solution is pumped in the membrane from a storage bag for each measurement. The constant exchange of the indicator solution lead to more stable carbon dioxide data and a high reproducibility between the sensors. The equilibration of the seawater sample with the internal indicator solution is the time limiting step.¹²⁸

The sensor is suitable for freshwater and seawater applications. Due to the low drift the sensor system is often used for long-term measurements, most likely in combination with air-water flux investigations. The sensor was used by Turk et al. in the northern Adriatic Sea at the buoy Vida (45°32'55.68" N; 13°33'1.89" E) in 2007 and 2008. Sea surface measurements were done to calculate air-sea fluxes. The deployment duration varied between 49 and 149 days. The carbon dioxide concentration varied between 200 and 500 μatm at temperatures of 10 to 25 °C.¹²⁰ Moreover the sensor was used to evaluate CO₂ fluxes of Lake Tännaren (central Sweden) in 2010. It is a fresh water shallow lake with a mean depth of 1.3 m. The sensor was deployed for one year with a measurement interval of 30 minutes.¹²¹

The producer provide no information about a suitable temperature range. However, Turk et al. deployed the sensor in Canada's eastern Arctic (Cumberland Sound). The sensor measured for 22 days in a temperature range between -1 and +1 °C at 32 m water depth.¹²⁹

Table 1.1: Short overview of relevant sensor characteristics of a selection of commercially available carbon dioxide sensors from various producers.

	SAMI CO₂ ¹¹³	CONTROS HydroC ¹¹⁴	Seaology pCO₂ system ^{115,116}	CO₂-ProCV ¹¹⁷	Picarro G2201-i Analyzer ^{118,119}
producer	Sunburst Sensors	Kongsberg Maritime Contros GmbH	Battelle	ProOceanus	Picarro Inc.
principle	spectrophotometric	NDIR spectroscopy	NDIR spectroscopy	NDIR spectroscopy	cavity ring-down spectroscopy
response time	~5 min	t ₆₃ ~ 60 s with SBE 5T pump	full cycle 20 min	t ₆₃ = 50 s	5 min (pumped)
temperature range	-	-2 °C - +35 °C	0 - 40 °C	0 - 30 °C (max. -2 - 40 °C)	-10 - +45 °C
measuring r.	150 - 700 µatm	200 - 1000 µatm	100 - 600 ppm	0 - 600 ppm	100 - 4000 ppm
apployable depth	max. 600 m	standard 2000 m (max. 6000 m)	surface only	600 m (max. 4000 m)	surface only
drift	<1 µatm/6 months	0.15 µatm d ⁻¹	drift correction	drift correction	<0.5%
accuracy	±3 µatm	<1 µatm	<1 µatm	± 0.5%	-
precision	<1 µatm	±0.5%	~ 0.6 µatm	-	<1%
size	550 mm x 152 mm	89 mm x 380 mm	4 parts	380 mm x 100 mm	430 mm x 460 mm x 180 mm
weight [kg]	1.1 in seawater	2.2 in water	74	0 in water	25.4
exemplary deployments	long-term test northern Adriatic Sea ¹²⁰ Lake Tännaren, Sweden ¹²¹	profiling float Cap Verde Islands ¹²² CTD profiling Long Island, USA ¹²³ Cruise Atlantic ⁹¹	NOAA/PMEL carbon program used worldwide ¹²⁴	northeast Atlantic Ocean monitoring position ¹²⁵	meridional transect Atlantic Ocean ¹¹⁹ shallow Arctic Ocean (western Svalbard margib) ¹²⁶

CONTROS HydroC[®] CO₂ from Kongberg Maritime Contros GmbH

The sensor is described by the producer as 'a unique and versatile underwater carbon dioxide sensor for *in-situ* and online measurements of dissolved CO₂' (fig. 1.13).¹¹⁴



Figure 1.13: CONTROS HydroC[®] CO₂ carbon dioxide sensor developed by Kongberg Maritime Contros GmbH.¹¹⁴

The measurement principle used for the HydroC[®] carbon dioxide sensor is based on Infrared-spectroscopy. Dissolved carbon dioxide diffuse through a custom made semi-permeable membrane into an internal gas system. The gas is transferred to the detection chamber and the CO₂ partial pressure is measured via IR absorption spectroscopy. The characteristic vibration at 2349 cm^{-1} is concentration dependent. The measured IR light intensity is converted in an output signal using calibration coefficients and additional data from the gas sensor system. Each sensor is calibrated individually at deployment temperature in a water tank. The standard calibration range is 200 to 1000 μatm . Annual recalibration is recommended by the producer. Moreover the sensor can be adapted for special customer requirements. Optional pumps for a faster response time, anti-fouling heads for conditions with high biofouling pressure, internal logger and an additional battery pack is available.

Due to the power consumption, response time and housing design, a deployment on profiling floats, mooring buoys and at a CTD-rosette is possible. Field applications were published by Fietzek et al., Wallace et al., Fiedler et al. and many more. The chosen deployments are representative examples. Fietzek et al. used the HydroC pCO₂ sensor for a long-term (> 4 weeks) underway shipboard deployment in the North and South Atlantic ocean from Germany to Chile 2010 and in the eastern tropical Atlantic 2011. Data was obtained continuously with an one minute measurement interval between 295 μatm and 430 μatm pCO₂ in a temperature range between 7 and 30°C. The sensor system was monitored the whole time and zeroing every 12 hours with a CO₂ free gas was necessary to compensate drift behaviour. The average difference between obtained sensor value and reference was after drift correction $-0.6 \pm 3\ \mu\text{atm}$.⁹¹ Fiedler et al. used the carbon dioxide sensor to integrate it into a profiling float. The float was launched in the area of the Cao Verden Islands. Zeroing was although necessary during the deployment using CO₂ free air. The profiling float measured profiles between ocean surface and 500 m water depth according to carbon dioxide levels between 350 and 700 μatm . The estimated accuracy was 5 μatm and 10-15 μatm for surface and profile measurements, respectively. The slow response time made the data processing more complicated.¹²² Finally Wallace et al. used the sensor for eutrophication measurements in the Long Island Sound, USA in 2012 and 2013. The carbon dioxide levels were high (500- 2300 μatm). The sensor system was mounted at a CTD and profiling measurements till 40 m water depth were recorded.¹²³ Improvements in terms of response time and drift behaviour were planned.

Seaology[®] pCO₂ monitoring system from BATTELLE

The producer about the sensor: 'The autonomous Battelle Seaology pCO₂ Monitoring System is the first offering in the Battelle Seaology[®] platform of scientific instrumentation. The system was developed as part of a cooperative effort between Battelle, the Monterey Bay Aquarium Research Institute (MBARI) and the National Oceanic and Atmospheric Association (NOAA).'

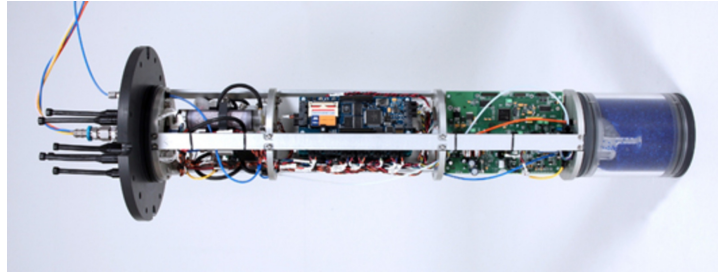


Figure 1.14: Seaology[®] pCO₂ monitoring system developed by BATTELLE.¹¹⁵

This carbon dioxide sensor system consists of four separate waterproofed housings comprising the electronics, battery, transmitter and reference gas (provided by NOAA's Earth System Research Laboratory). The electronic case consists of control and logging panel a LI-COR LI-820 CO₂ gas analyzer, a relative humidity and temperature sensor. The carbon dioxide content is determined by the absorption of IR energy in an optical cell filled with the sample gas. The system uses relative humidity and temperature to determine the CO₂ content of the air equilibrated seawater sample (closed loop, h shaped equilibrator). A reference gas is used to calibrate the LI-COR system before every measurement. The system additionally includes the measurement of an atmospheric sample. A whole cycle with in-situ calibration, atmospheric sample and seawater sample takes 20 minutes. The system is suitable for atmospheric and seawater measurements.¹¹⁶

The monitoring system can easily be integrated at mooring buoys. The NOAA Pacific Marine Environmental Laboratory operated more than 26 monitoring systems around the world. The technology was first developed at the Monterey Bay Aquarium Research Institute in Moss Landing, California. To introduce a global ocean observing system, the PMEL carbon group in cooperation with the inventors made the technology more accurate, more reliable and easier to deploy. The system can operate without maintenance up to a year. A daily summary file is transmitted to PMEL, processed and posted in near-real time. Later the technology was transferred for commercial production to BATTELLE. Dozens of Seaology systems are operated worldwide by the PMEL carbon group and others. The systems are deployed in the Pacific, Atlantic and the Indian Ocean. Deployment sites can be divided in three categories: Open Ocean, Coastal and Coral Reef.¹²⁴

CO₂-ProCVTM from ProOceanus Systems Inc.

ProOceanus about the own product: 'The CO₂-Pro CVTM is a compact, lightweight, plug-n-play pCO₂ sensor that is designed for use on moorings, on profilers, on ships in under-way mode, and in laboratories.'



Figure 1.15: CO₂-ProCVTM carbon dioxide sensor developed by ProOceanus Systems Inc.¹¹⁷

The CO₂-ProCVTM is although based on NDIR spectroscopy. An internal detection loop with an NDIR detector based on a PPSystems SBA-4 CO₂ analyzer, highly modified for the present sensor. The analyzer is connected to a patented equilibrator composed of a PDMS membrane. The gas transfer interface has a tubular design. Therefore the gas stream is surrounded by sample water. The tube is wound with a copper wire to provide biofouling protection. Physical protection is realized by an end-cap. Water gets pumped by a Seabird Electronics 5 m pump past the tube and an equilibrium is accelerated. Depending on the pump rate, the equilibrium can be reached in 2 minutes. The internal gas phase is measured at a controlled optical cell temperature. Additionally parameter like sample temperature, pressure and humidity of the internal gas are determined. Each CO₂-Pro is calibrated between 0 and 600 ppm at a certain optical cell temperature. After starting the system a zero point calibration is carried out for baseline determination.¹³⁰

The sensor can be applied for ocean acidification measurements, long-term monitoring, deep ocean studies, shipboard flow through measurements and coastal zone flux investigations.¹¹⁷ Jiang et al. presented an application study of the described sensor system. It was used in a laboratory tank in comparison with calibrated air-water equilibrator system and they agreed at $-3.0 \pm 4.4 \mu\text{atm}$ over two months. Field applications at a mooring buoy and shipboard underway systems revealed larger differences between reference values and measured carbon dioxide levels. Possible problems, like temperature fluctuations of the detector optical cell and calibration errors were identified and eliminated.¹³⁰ Additionally the sensor system was deployed at the Porcupine Abyssal Plain sustained Observatory operated by the National Oceanography Centre, Southampton. It was used to obtain long-term data (range of months) at a depth of 30 m. The collected data was used to calculate CO₂ fluxes and identify seasonal and inter-annual variations. Carbon dioxide levels ranged from 320 μatm up to 400 μatm (T: 12- 18 °C).¹²⁵

The system is although sold by Turner-designs as the C-Sense carbon dioxide sensor. This sensor was used in section 3 in the aquaculture facility of the Moss Landing Marine Laboratories.¹³¹

Picarro G2201-*i* Analyzer from Picarro Inc.

The producer about the product: 'Pioneering environmental scientists take our CRDS instruments into the harshest conditions to gather and analyze data on the spot.'



Figure 1.16: Picarro G2401 Analyzer carbon dioxide sensor developed by Picarro Inc..¹¹⁸

A very sensitive spectroscopic method is used to analyse the carbon dioxide level in this sensor system: Cavity ringdown spectroscopy (CRDS). This technique measures the absorption of a gaseous phase in the time domain. The main component of the system is a resonant optical cavity with two or more reflective mirrors (reflectivity $\sim 99.999\%$). The cavity is coupled with a narrow bandwidth laser beam. Due to the mirrors the laser light is reflected back and forth in the cavity, leading to a very long effective pathway. The light intensity steadily increases in the cavity. After a certain level is reached, the laser is shut off (continuous wave, *cw*). A small portion of the light is lost during each roundtrip. The loss is measured by photodetectors behind the rear mirror. The detected values are plotted in an intensity-time profile, resulting in a mono-exponential plot. The quality of the ring down cavity can be expressed by the decay constant of the exponential plot. Are absorbers present in the cavity, additional intensity changes are observable. The detected decay time gets shorter, the higher the absorber concentration in the cavity. Prior to analysis the seawater sample has to be equilibrated with an overlaying gas phase and dried thermoelectrically. The method was declared as 'calibration-free'. Only the determination of the isotope ratio required a reference gas standard measurement on a daily basis.¹¹⁹

The sensor developed by Picarro were used for underway shipboard measurements in the Atlantic Ocean and the Arctic Ocean. Becker et al. used the system to measure the fugacity of carbon dioxide in sea surface water during a meridional transect of the Atlantic Ocean between Germany and Chile. The underway flow system was set to 3 L/min. Reference samples were measured by using a NDIR detector. Overall carbon dioxide measurements showed no drift. The mean offset between the reference and the sensor system was $\Delta(\text{fCO}_2) = 0.35 \mu\text{atm} \pm 0.29 \mu\text{atm}$.¹¹⁹ Pohlman et al. implemented the system in research activities around the western Svalbard margin (Arctic Ocean, Spitsbergen). They investigated CO_2 air-sea fluxes. The sea surface temperature varied between 5 and 6 °C, whereas measured CO_2 values were between 250 and 350 μatm . A carbon dioxide uptake rate of $33,000 \pm 7,900 \mu\text{mol m}^{-2} \text{d}^{-1}$ was measured by the help of the Picarro sensor system.

1.5 Optical Carbon Dioxide Sensors

This section is dedicated to optical carbon dioxide sensors, especially optodes. Several optodes were developed and are mentioned briefly in section 1.4. Optode technology is a trendsetting technique. The hardware is relatively cheap, versatile and easy to miniaturize in high unit numbers, as well as often has a low energy consumption. The corresponding sensing chemistry is adaptable for several analytes, do not require wet chemicals and do not produce waste during measurements, as well as depending on the optode do not need frequent recalibration. The combination of analyte-suitable sensing chemistry and fitting hardware allow the independent, long-term deployment in a hostile environment. In the last decades especially carbon dioxide optodes were developed by several working groups to determine the carbonate chemistry in seawater.

Carbon dioxide optodes mainly consist of an analyte-sensitive indicator dye embedded in a analyte-permeable matrix (sensor spot). A LED and a photodetector are used to read out the carbon dioxide dependent response of the sensor spot.

1.5.1 Indicator dyes

The core part of a carbon dioxide optode is the indicator dye. Its properties determine the sensor spot composition, as well as the hardware requirements and at the end the construction plan of the device. Potential indicator dyes for CO₂ optodes should be stable upon immobilization, sensitive enough to measure in the desired range and show a low photo bleaching rate. Actually almost all indicator dyes used in CO₂ optodes are pH-sensitive. So they respond to a pH change induced by the equilibrium between carbon dioxide and water. The pK_a value of the indicator dye mainly determine the dynamic range of the sensor. There are two main groups of indicator dyes used for CO₂ optodes: fluorescent and absorption-based indicator dyes. The presented compounds are a selection of frequently used or lately developed indicator dyes for carbon dioxide.

Fluorescent indicator dyes for carbon dioxide optodes are for example 1-hydroxypyrene-3,6,8-trisulfonate (HPTS) and diketo-pyrrolo-pyrrole (DPP) (fig. 1.17, tab. 1.2). HPTS was frequently the indicator of choice for carbon dioxide optodes, because of the physiological relevant pK_a value, a large Stoke's shift, a high photostability and water-solubility.^{132 133 134 135} The pH-dependent fluorescence of HPTS is induced by the photoinduced proton transfer (PPT). The transfer is based on different pK_a values of the ground and excited state, generated by different electron densities of the molecules. DPP indicator dyes are substituted with different building blocks in R position (fig. 1.17). The groups, e.g. phenol, are used to facilitate a photoinduced electron transfer effect (PET). When adding a phenolic group to the DPP basic structure, fluorescence gets quenched around the pK_a value of the substituent.¹³⁶

Absorption-based indicator dyes for carbon dioxide optodes use the pH-dependent absorption of the compound to determine the CO₂ concentration. Typical examples are (bromo-)thymol blue, *m*-cresol purple representing the group of sulfonephthalein indicators, Sudan red III (1-[4-(Phenylazo)phenylazo]-2-naphthol) or the lately developed group of aza-BODIPY dyes (fig.

1.18, tab.1.3). Normally the indicator dye shows two distinct absorption maxima for the protonated and deprotonated form, which are used in combination with a reference to calculate the pH and consequently the amount of carbon dioxide.

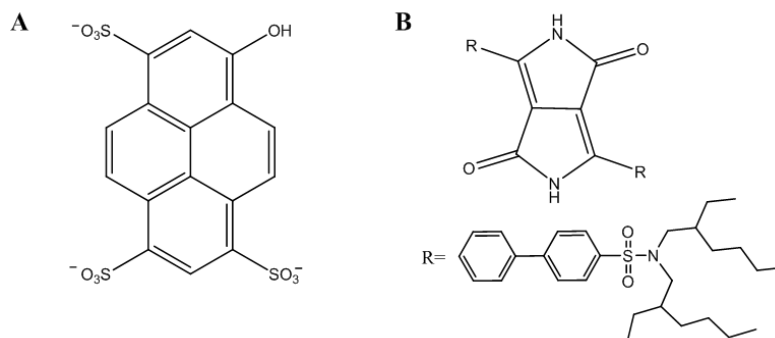


Figure 1.17: Fluorescent indicator dyes for carbon dioxide optodes: A: HPTS, B: DPP

Table 1.2: Properties of fluorescent indicator dyes for carbon dioxide optodes: pK_a value, absorption maxima (λ_{max}), molar absorption coefficient (ϵ) and emission maxima (λ_{em}). n= neutral form; d= deprotonated form; g= ground state; e= excited state.

	HPTS ¹³² (in H ₂ O)	DPP ¹³⁷ (in THF)
pK_a	g: 7.3-8.1; e: 1.4	< 11.8
λ_{abs} [nm]	n: 403; d: 455	n: 497, 533; d: 633
ϵ [$10^{-3} M^{-1} cm^{-1}$]	24.0	n: 50.1 (533 nm); d: 25.6 (633 nm)
λ_{em} [nm]	512	n: 552, 594; d: 673

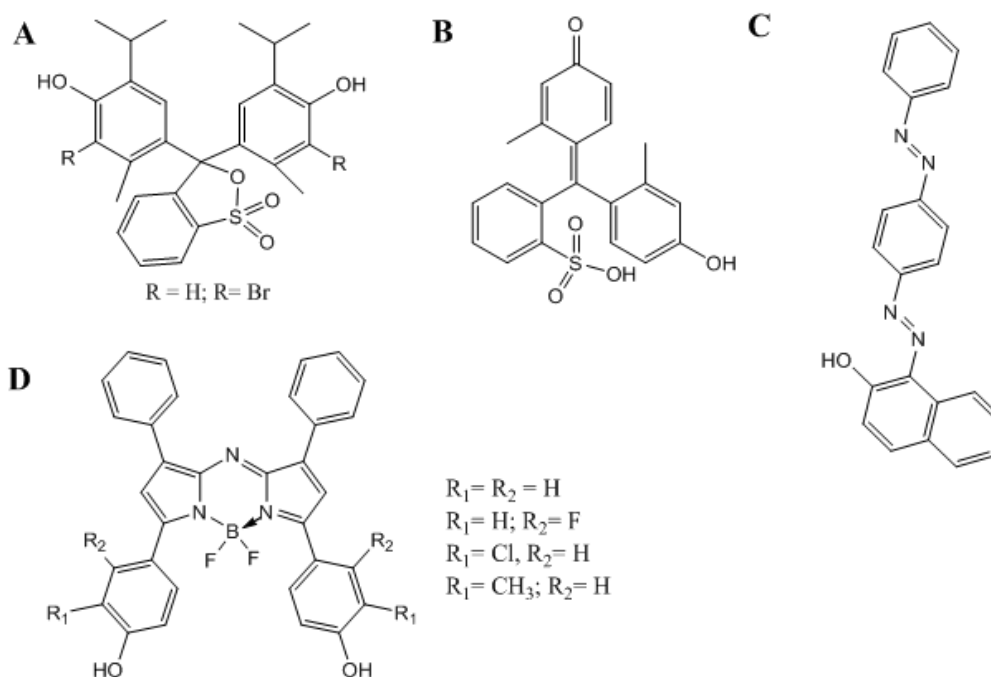


Figure 1.18: Absorption-based indicator dyes for carbon dioxide optodes: A: (bromo-)thymol blue, B: *m*-cresol-purple, C: Sudan red III and D: aza-BODIPYs.

Table 1.3: Properties of non-fluorescent indicator dyes for carbon dioxide optodes: pK_a value, absorption maxima (λ_{max}) and molar absorption coefficient (ϵ in $10^{-3} \text{ M}^{-1} \text{ cm}^{-1}$). n= neutral form; m= mono-anionic form; d= di-anionic form. * in EtOH/aq. buffer (1:1)

	thymol blue ¹³⁸	<i>m</i> -cresol purple ¹³⁸	Sudan red III	aza-BODIPY (R = H)* ¹³⁹
pK_a	8.86	8.28	~ 11.65 ¹⁴⁰	n: 8.18; m: 10.34
λ_{abs} [nm]	n: 590; m: 432	n: 571; m: 428	n: ~ 503 ; m: ~ 590 ¹⁴¹	n: 692; m: 745; d: 805
ϵ	n: 53.0; m: 29.0	n: 40.0; m: 20.0	2.3 ¹⁴²	n: 60; m: 51.3; d: 55.2

1.5.2 Measurement principles

The direct measurement of absorbance or fluorescence intensities to determine the carbon dioxide concentration was preferred for a long time. The intensity based instrumentation revealed some drawbacks: i) emitted or absorbed light is indicator concentration dependent (affected by leaching and photobleaching); ii) interfered by stray light and iii) sensitive to fluctuations of the light source and the photodetector. Therefore a ratiometric approach is more reliable and less interfered.¹⁴³ Two different measurement principles are frequently used to read out the carbon dioxide sensor spot based on different indicators. Depending on the photophysical properties of the indicator dye, the sensor response get detected via *Dual lifetime referencing (DLR)* or the so called *inner filter effect*.

DLR is a unique method to translate an analyte-sensitive fluorescence signal into a phase domain. The translation is realized by immobilizing an inert luminophore with a long lifetime (reference) in combination with an pH indicator with a short lifetime (indicator). The emission spectra of the reference and the absorption spectra of the indicator have to overlap sufficiently.^{141 143} Therefore the use of one excitation source and photodetector is possible. The light source generates a modulated signal with a frequency compatible with the long-lifetime reference. The phase angle of the reference luminophore is constant. In contrast the indicator has a phase angle of zero, induced by the short lifetime. Differences in the CO_2 concentration cause a modification of the modulated fluorescence intensity of the indicator. The change in fluorescence intensity induces a phase shift of the overall luminescence intensity. The CO_2 -dependent luminescence intensity change can be detected by using phase fluorometry.^{135 144} Carbon dioxide optodes using DLR were developed by Burke et al. 2006 using HPTS¹³⁵, by von Bültzingslöwen et al. 2003 based on fluorescence resonance energy transfer (FRET) between a ruthenium polypyridyl complex (reference) and Sudan III¹⁴¹ or Čajlaković et al. 2006 using HPTS as well¹⁴³. Often used reference luminophores are ruthenium complexes.

The inner filter effect read out is mainly used for non-fluorescent colorimetric indicator dyes. The inner filter effect convert the changes in the absorption of an indicator dye into a long-lived luminescence intensity. The sensor foil includes an absorption based indicator, as well as

secondary emitter with a long luminescence lifetime and a broad excitation. Most important the emission spectra of the secondary emitters have to overlap with the absorption spectra of the indicator. The absorption spectra of the indicator depends on the amount of analyte. Therefore the overall luminescence intensity changes with the analyte concentration as well. This measurement principle provides some advantages: It is i) widely useable, ii) not interfered by luminescence quencher and background luminescence and iii) ratiometrically referenced.¹⁴⁵ The inner filter effect was used for carbon dioxide optodes by Schutting et al. 2015¹³⁹ or Pérez de Vargas-Sansalvador et al. 2009¹⁴⁶.

1.5.3 Sensor foil structure

The sensor foil structure is determined by the used indicator dye. Like mentioned before the bulk of indicators for carbon dioxide optodes are pH-sensitive and respond to CO_2 induced pH changes after reacting with water. Therefore a buffer system has to be implemented in the sensor foil. This can be done in basically two ways.

1. The 'Severinghaus'-type sensor spot consists of a polymer matrix with an implemented aqueous buffer. This type is adapted from the Severinghaus electrode presented 1958⁸⁷. The buffer is commonly based on bicarbonate or phosphate ions dissolved in water. Such a wet sensor has a big drawback; Just small changes in the internal buffer solution result in a change in the calibration of the sensor, due to the sensitivity of the indicator to ionic strength. The sensor spot has to be stored under certain conditions in a water/ CO_2 atmosphere. The sensor can dry out during storage under dry conditions or change the ionic strength of the inner buffer solution by storing it in solution. After loss of water a long re-conditioning is necessary.¹³³ They generally have long response times and are dependent on osmotic pressure.

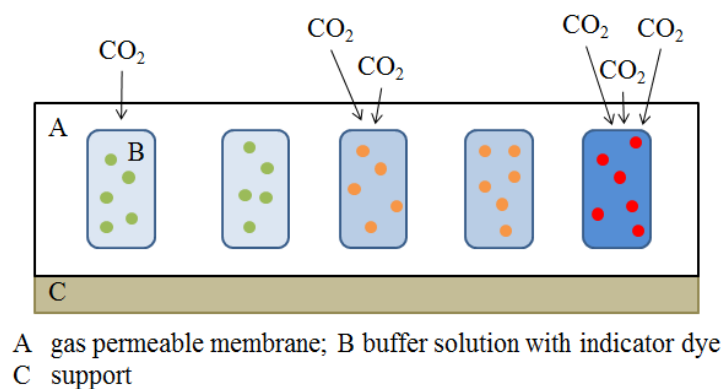


Figure 1.19: Generalised composition of pCO_2 optode based on the 'Severinghaus'-type. Intensified blue represent decreasing pH due to an increase in CO_2 concentration. Indicator response from green to red according to pH change induced by carbon dioxide.

2. The second sensor type is almost non aqueous and referred to as 'plastic'-type sensor, first reported by Mills et al. 1992¹⁴⁷. The indicator dye is transferred into its anionic form by adding an lipophilic quarternary ammonium hydroxide. The indicator/base pair is formed immediately and can be easily dissolved in even hydrophobic polymers (e.g. ethyl

cellulose or silicone rubber). The polymer acts as a proton barrier. It is gas-permeable and the diffusion of CO₂ can be enhanced by the use of a plasticizer. An excess of water is not necessary. They respond in the range of seconds, but are prone to get poisoned by acidic gases, due to a low buffer capacity.¹⁴⁸

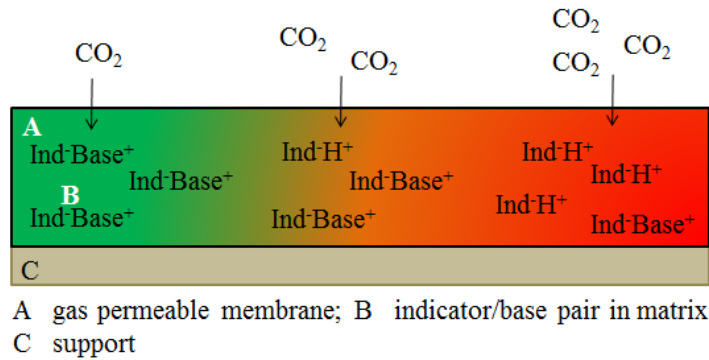


Figure 1.20: Generalised composition of pCO₂ optode based on the 'plastic'-type. Increasing CO₂ concentration from low (green) to high (red).

1.5.4 Hardware

The sensor foil including the 'sensing chemistry' and the necessary read out hardware have to be dovetailed. The main electronic parts are a light source, an optical waveguide and a photodetector. The light source is chosen depending on the selected indicator dye/measurement principle. It has to provide a stable illumination in combination with a lower power consumption at best. Light Emitting Diodes (LEDs) are often the material of choice, due to their size and reliability. Moreover they are available at a variety of wavelengths. Filter can be used to tune the signal-to-noise ratio. Depending on the measurement principle one or more LEDs can be necessary. Another crucial part is the photodetector. They should be highly sensitive and show a fast response time. Several photodetectors are available: photodiodes, avalanche photodiodes and photomultiplier tubes. They differ in sensitivity, size and power consumption.⁸⁹ The arrangement of the main components is almost the same. In some sensors an optical waveguide (plastic or glass fibre) is incorporated. The LED and the photodetector are on the same side of the sensor foil. The sensor foil can be attached to the tip of an optical fibre^{89 108 149}, as well as on a glass window^{75 107} (fig. 1.21). All the components are implemented in pressure resistant housing made of polymer for shallow water applications or titanium for deep sea deployments.

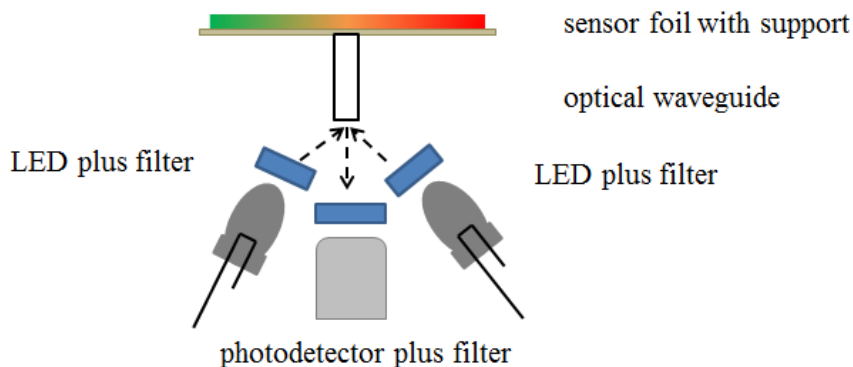


Figure 1.21: Schematic drawing of an optode setup.

1.5.5 Poisoning

Carbon dioxide optodes can get poisoned by other acidic gases like SO_2/SO_3 , NO_x , HCl or H_2S , who diffuse through the gas-permeable membrane. Poisoning processes and cross-sensitivities result in an overestimation of the carbon dioxide level, due to the contribution of the non- CO_2 gas molecules to the overall pH change detected by the sensor. A cross sensitivity is reversible instead of poisoning. Almost every carbon dioxide optode using a pH-indicator is prone to get poisoned. Tests in the lab showed rapid poisoning by hydrochloric acid, acetic acid and SO_2 . Of special interest in oceanography is hydrogen sulfide as a poisoning gas. It often appears in oxygen minimum zones, due to bacterial metabolism (see section 1.2.3). Especially solid-state optodes are susceptible for poisoning, due to their low buffer capacity. Atamanchuk et al. investigated the impact of hydrogen sulfide on carbon dioxide optodes by using an incubating chamber installed at the floor of the Baltic Sea. Inside the chamber H_2S containing water was generated. Compared with CO_2 levels from outside the lander, significantly higher amounts were detected and no recovery was observed in surface waters. It was estimated, that hydrogen sulfide gets oxidized by oxygen inside the sensor foil, forming sulphurous acid.¹⁰⁷ The same effect was observed by Neurauter et al. using a HPTS based CO_2 optode.¹⁵⁰ The poisoning by hydrogen sulfide is independent from the chosen indicator dye.

Strategies for poisoning prevention are rare. Often the use in hydrogen sulfide containing water is not recommended. The use of perfluorinated polymers slow down the poisoning process, due to the low permeability for the gas molecule (see section 2 and 5). So a time-limited deployment is possible. On the other hand poisoning processes limit the shelf life of the sensor dramatically, when stored under not sufficient conditions.

Chapter 2

Highly sensitive poisoning-resistant optical carbon dioxide sensors for environmental monitoring

This Chapter was published in **Analytical Methods**, 2017, DOI: 10.1039/c6ay02949c. It is reproduced by permission of The Royal Society of Chemistry.

Authors: Eva Fritzsche, Pia Gruber, Susanne Schutting, Jan P. Fischer, Martin Strobl, Jens D. Müller, Sergey M. Borisov and Ingo Klimant

*A new optical carbon dioxide sensor for environmental monitoring is presented. It combines a robust and long-term stable sensing material with a compact read-out device. The sensing material relies on a NIR pH indicator immobilized into ethyl cellulose along with a quaternary ammonium base. The perfluorinated polymer Hyflon AD 60 used as a protection layer significantly enhances the long-term and mechanical stability of the sensor foils, as well as the robustness against poisoning gases, e.g. hydrogen sulfide. The sensor can be stored at ambient conditions for more than six weeks, whereas sensors covered with silicone rubber deteriorate within one week under the same conditions. The complete sensor device is applicable after a three-point (re)calibration without a preconditioning step. The carbon dioxide production and consumption of the water plant *Egeria densa* was measured in the laboratory. Furthermore, results of profiling carbon dioxide measurements during a research cruise on the Baltic Sea at water depths up to 225 m are presented.*

2.1 Introduction

Carbon dioxide is an analyte with great impact on the marine ecosystem. Since the industrialization, started in the late 18th century, the atmospheric level of carbon dioxide increased by about 40% due to fossil-fuel burning or deforestation. More than a half of the antropogenically produced CO₂ is taken up by the ocean.⁴⁶ The rising amount of carbon dioxide in seawater

causes a reduction of the pH (ocean acidification) and a lower carbonate saturation in surface waters.¹ The air-sea-exchange is driven by the difference in partial pressure of carbon dioxide. The dissolved CO₂ equilibrates with bicarbonate and carbonate ions. The carbonate system itself is characterized by four measurable parameters: pH, TA (total alkalinity), DIC (dissolved inorganic carbon) and *f*CO₂ (fugacity of carbon dioxide). The complete system is determined when two of these parameters and the equilibrium constants, which are salinity and temperature dependent, are known.³

Common analytical techniques for measuring carbon dioxide in seawater directly are IR spectroscopy, the Severinghaus electrode and optical chemosensors. The sensors based on IR spectroscopy rely on diffusion of the analyte molecules through a gas-permeable membrane into an internal gas chamber and the direct measurement of the absorption of the analyte. The sensors are very robust but show interference by water vapour¹⁵¹, which condensation can present a serious problem. Nevertheless, several IR carbon dioxide sensors have been commercialized for marine applications (CO₂-Pro CVTM, Pro-Oceanus Systems Inc., Canada; HydroC[®] CO₂, Kongsberg Maritime Contros GmbH, Germany).

The Severinghaus electrode shows interferences from electromagnetic fields and is prone to drifts due to osmotic pressure effects.⁸⁷ A similar design was adapted for use of an optical transducer representing a solution of a pH indicator in a bicarbonate buffer. A commercially available sensor for aquatic CO₂ measurements (SAMI CO₂, Sunburst Sensors, LLC, USA) consists mainly of a membrane equilibrator connected to a fiber optic flow cell. The ambient seawater carbon dioxide diffuses through a gas-permeable membrane (silicone rubber) and changes the color of bromothymol blue indicator due to a change in the pH of the buffer.^{96 128 152} However, the device is bulky since the indicator solution has to be renewed for each measurement, which can be particularly critical for long-term trials due to the high volume of the reagent needed and the waste has to be stored or released to the environment. Moreover it has high energy consumption due to pumping and moving parts, which are prone to break. On the other hand, the advantage of the approach includes high resistance to drift due to renewal of the solution. In the last decades optical carbon dioxide chemosensors (optodes) became increasingly popular.^{133 141 153 154} Although several new concepts of optical carbon dioxide sensors have been proposed recently such as using viscosity or polarity-sensitive dyes as transducers^{98 153 155} the so called 'plastic type' sensors remain most popular.^{147 156 157 158 159} These sensors are based on a pH-sensitive indicator dye embedded in a polymer matrix along with a lipophilic quaternary ammonium base. The dye changes its spectral properties according to the degree of protonation induced by carbon dioxide. A wide range of indicators have been reported but only a few show favorable optical properties, high photostability and sensitivity sufficient for measuring accurately at atmospheric levels of CO₂. Fluorescent sensors also require a reference luminophore to obtain reliable results. In most cases an analyte-insensitive reference dye which possesses a different emission spectrum (ratiometric 2-wavelength measurement) or a different luminescence decay time (Dual Lifetime Referencing) is used.^{107 135 143 160} By far, hydroxypyrene trisulfonate (HPTS) has been the most popular fluorescent indicator.^{133 135 161 162} Unfortunately, the brightness, photostability and the sensitivity of these sensors are far from being optimal. Recently reported BF₂-chelated tetraarylazadipyrromethene indicators (aza-BODIPYs) represent a promising alternative.^{139 163 164} These highly photostable dyes absorb and emit in the

near-infrared region of the electromagnetic spectrum which is beneficial due to low levels of autofluorescence and availability of low cost excitation sources and photodetectors. Colorimetric aza-BODIPY indicators were demonstrated to be very promising for the design of carbon dioxide sensors with a tunable dynamic range.¹³⁹

These (and other) promising indicators published recently enable greater flexibility of choice in respect to optical properties, photostability and sensitivity. However, comparably little effort has so far been put into improving the long-term stability of the CO₂ optodes. Low stability of the sensing materials hinders application of this promising technology in oceanography and many other fields.

For example, the optode presented by Atamanchuk et al. 2014 showed sufficient stability only after preconditioning over several months during which the indicator lost most of the original signal.¹⁰⁷ Moreover, the calibration was time consuming and complicated, the sensor has to be stored in an aqueous solution and complete poisoning by hydrogen sulfide ($c_{H_2S} = 175 \mu\text{mol/L}$) was observed within 3 hours. In this contribution we present a chemically and photochemically robust, long-term stable sensing material, based on a highly sensitive di-OH-aza-BODIPY indicator dye. It will be shown that the new sensing material is highly promising for in situ applications in marine biology and oceanography.

2.2 Materials and Methods

Chemicals and materials

Ethyl cellulose (EC49, ethoxyl content 49%), *m*-cresol purple (indicator grade), tetraoctylammonium hydroxide solution (TOAOH, 20% in methanol), sodium sulfate (anhydrous) were received from Sigma-Aldrich. Toluene, potassium carbonate, potassium dihydrogen phosphate (99%, water free) and tetrahydrofuran (THF) were purchased from Carl Roth GmbH + Co. KG. 1H, 1H, 2H, 2H-perfluorooctyldimethylchlorosilane (97%), vinyltrimethylsiloxy-terminated polydimethylsiloxane (viscosity 1000 cSt), methylhydrosiloxanedimethylsiloxane copolymer (25-35 cSt), 1,3,5,7-tetravinyl-1,3,5,7-tetra-methylcyclotetrasiloxane (97%) (delayer) and platinum-divinyltetramethyldisiloxane complex in vinyl terminated polydimethylsiloxane (3-3.5% Pt) (catalyst) were obtained from ABCR GmbH. Hyflon AD 60 was acquired from Solvay GmbH, Teflon AF 1600 from DuPont de Nemours GmbH and Cytop 809 A from AGC Chemicals. Anhydrous ethanol was purchased from Merck. Sodium bicarbonate and cyclohexane were received from VWR. Poly(ethylene naphthalate) (PEN) support Teonex Q51 and poly(ethylene terephthalate) (PET) support Melinex 505 were received from Pütz GmbH + Co. Folien KG. The FireStingO₂ and an oxygen sensor (OXR 230-0, oxygen retractable microsensor) were acquired from PyroScience GmbH. Optical plastic fibres were obtained from Ratioplast-Optoelectronics GmbH. Perfluorodecalin (PFD, 98%; cis and trans, ABCR), was washed with an 1 M aqueous solution of K₂CO₃ prior to use. Synthesis of 4,4'-(5,5-difluoro-1,9-diphenyl-5H-4λ4,5λ4-dipyrrolo-[1,2-c:2',1'-f][1,3,5,2]triazaborinine-3,7-diyl)diphenol (di-OH-aza-BODIPY) and staining of polystyrene-microparticles (PS-particles) with 3,7-bis(4-butoxyphenyl)-5,5-difluoro-1,9-diphenyl-5H-4λ4,5λ4-dipyrrolo-[1,2-c:2',1'-f][1,3,5,2]triazaborinine (di-butoxy-complex) was performed according to Schutting et al. 2015.¹³⁹ Silanized Egyptian Blue was produced analogously

to the literature procedure¹⁴⁵ but using 1*H*, 1*H*, 2*H*, 2*H*-perfluorooctyldimethylchlorosilane instead of trimethylchlorosilane. The engraving pen used was a MICROMOT 50/E with a 2 mm mounted point made of fused aluminium oxide from PROXXON GmbH. The temperature control was performed with a cryostat F12 from Julabo GmbH. The pH was determined with pH meter SevenEasy combined with a pH electrode InLab Routine Pro from METTLER-TOLEDO GmbH.

Preparation of sensor foils

Planar optodes (model system) for dynamic response, poisoning and stability tests

100 mg ethyl cellulose and 1 mg *m*-cresol purple were dissolved in 2.4 g of toluene:ethanol mixture (6:4 w/w). The viscous solution was flushed with carbon dioxide and 100 μ L of tetraoctylammonium hydroxide solution (20% w/w TOAOH in methanol) were added. The 'cocktail' was knife coated onto a PET foil to obtain a sensing film with a thickness of \sim 3 μ m after evaporation of the solvents. The protection layers (thickness \sim 8 μ m) were prepared by coating solutions of the corresponding polymers (100 mg of Teflon AF 1600 or Hyflon AD 60 in 1.9 g PFD or Cytop 809 A solution (9 % wt.) in an unspecified perfluorinated solvent used as received from AGC Chemicals). Silicone rubber was prepared by mixing of 500 μ L vinyl-terminated polydimethylsiloxane, 500 μ L cyclohexane, 20 μ L methylhydrosiloxane-dimethylsiloxane copolymer, 2 μ L delayer and 3.5 μ L catalyst and polymersization of this mixture after coating and evaporation of the solvent. For the stability tests, the thickness of the silicone rubber layer was 13.5 μ m.

Carbon dioxide sensors (di-OH-aza-BODIPY-dye) on a PEN support

A 'cocktail' made of 100 mg ethyl cellulose, 1 mg of di-OH-aza-BODIPY-dye (1% w/w with respect to the polymer) and 1.683 g of a toluene:ethanol mixture (6:4 w/w) was flushed with carbon dioxide. This was followed by the addition of 100 μ L tetraoctylammonium hydroxide solution (20% w/w TOAOH in methanol). 0.75 μ L of this 'cocktail' was pipetted on pre-cut spots (diameter of 5 mm) of a roughened, dust-free PEN support. After evaporation of the solvent, a sensing film with \sim 2 mm in diameter and \sim 14 μ m thickness was obtained. For the second 'cocktail' 50 mg Hyflon AD 60 were dissolved in 0.935 g PFD and 25 mg Egyptian blue powder and 25 mg stained PS-particles were added and dispersed homogenously. 0.75 μ L of the second 'cocktail' were pipetted right on top of the sensing film. The estimated thickness after evaporation of the solvent was \sim 6 μ m. Finally, the sensor spot was covered with a protective layer (thickness of \sim 1.7 μ m) prepared from the solution of 100 mg Hyflon AD 60 in 2.22 g perfluorodecalin (washed with solution of K₂CO₃ prior to use).

Comparison of protection polymers

The response and protective properties of planar optodes with different layers (silicone rubber, Teflon AF 1600, Hyflon AD 60, Cytop 809 A) and *m*-cresol purple as indicator were investigated in 0.1 M phosphate buffer. The absorption measurements were recorded on a Cary 50 UV-Vis spectrophotometer (Varian) at 600 nm. The response and recovery times of the optodes were determined between an air saturated phosphate buffer (0.04 % CO₂ \approx 13.5 μ M) and 10% CO₂ (\approx 3320 μ M) at 23 °C. The protective properties of the polymers were investigated by placing

the planar optode in a closed cuvette and adding 200 μL of 12 M hydrochloric acid to the bottom of the cell. The poisoning experiments with hydrogen sulfide were performed in a constantly stirred cuvette, filled with 0.1 M aqueous phosphate buffer (pH 7.75, S = 35 PSS) equilibrated with the ambient air and 270 μM total sulfide.

Instrumentation

The read-out of the sensors based on the aza-BODIPY indicator was performed with a compact four channel FireStingO₂ reader (PyroScience GmbH, Aachen). The sensors were attached to the distal end of 10 cm-long plastic optical fibres (10 cm). The measurements were performed with the following settings of the FireSting instrument: LED intensity of 30%, an amplification of 400x, a measuring time of 16 ms and a modulation frequency of 2000 Hz. The measuring interval varied between 3 and 10 seconds, corresponding to the experiment and temperature. Field experiments were made with a modified FireStingO₂ reader in a pressure resistant housing provided by PyroScience.

Calibration procedure

For the calibration of the carbon dioxide sensors a 0.1 M phosphate buffer with a pH of 7.7 was used. The sensors were inserted into a temperature-controlled, constantly stirred vessel (Glasfachhandel Ochs, Germany) and connected to the read-out device. To obtain a calibration curve, individual sensors were measured at 8 different pCO₂ levels. A calibration was determined for two temperature ranges: 1) 4- 10°C and 2) 10- 35°C. The rising levels of carbon dioxide were obtained by adding hydrogen bicarbonate solution to the phosphate buffer. The amount of pCO₂ was calculated with the following equation:

$$[CO_2] = \frac{DIC}{\left(1 + \frac{K_1}{[H^+]} + \frac{K_1 \cdot K_2}{[H^+]^2}\right)} \quad (2.1)$$

The equilibrium constants were determined according to Roy et al. 1993.⁴ These constants were suitable for temperatures between 0 and 45°C, as well as for salinities between 5 and 45. For the calculation it was necessary to consider the pH, temperature, salinity, the sample volume and the concentration of the sodium bicarbonate solution. The calibration was acquired for carbon dioxide levels between 3 μM ($\sim 52 \mu\text{atm}$) and 8300 μM ($\sim 145,000 \mu\text{atm}$). Prior to calibration, the phosphate buffer was flushed with nitrogen for several hours until a stable signal was reached. In the next step sodium bicarbonate solution was added and the spots interrogated until a plateau was obtained. This procedure was repeated for each point of the calibration curve. A three-point calibration ($\sim 18 \mu\text{M}$, $\sim 87 \mu\text{M}$, $\sim 10\,000 \mu\text{M}$ T = 8°C) was performed before the *in situ* experiments.

Response and recovery time

The response and recovery times were determined for a low and a high carbon dioxide concentration at five different temperatures (5- 35°C). The sensors were moved from a temperature-controlled, constantly stirred ($\sim 540 \text{ rpm}$) vessel with $\sim 14 \mu\text{M}$ CO₂ to a vessel with $\sim 28 \mu\text{M}$

and back, as well as from a flask with $\sim 70 \mu\text{M}$ CO₂ to one with $\sim 125 \mu\text{M}$ CO₂ and back.

Long-term stability

The long-term stability was investigated in the gas phase and in water using the planar optodes with *m*-cresol purple as an indicator. The poisoning effects of ambient air at different storage conditions were compared. The foils were stored in the darkness to avoid photobleaching and were photographed each day and the absorption spectrum of the indicator was measured every 7 days. The long-term stability of carbon dioxide sensors based on di-OH-aza-BODIPY was investigated in aqueous phosphate buffer (constantly stirred, temperature $\sim 24^\circ\text{C}$), which was equilibrated with ambient air with a measurement interval of 1 h over 35 days.

Applications

The applicability of the new pCO₂ sensing material was investigated in a lab experiment with the water plant *Egeria densa*. The respiration behaviour in the absence and presence of light was measured. The plant, an oxygen sensor, a temperature sensor and a carbon dioxide sensor based on di-OH-aza-BODIPY with a glass support were inserted in a constantly stirred desiccator completely filled up with tap water. The illumination was provided by two halogen lamps (photosynthetic photon flux density $\sim 250 \mu\text{mol} \cdot \text{s}^{-1} \cdot \text{m}^{-2}$). The carbon dioxide sensors were also applied in the research cruise 'PROSID 2014', which took place at the Gulf of Finland and Central Baltic Sea in October 2015. The depth profiles were acquired with a continuous and a stepwise movement of the carrier. The pCO₂ values were calculated only for the stepwise profiles. Two stations were investigated: Gotland deep (TF_ 271, 57.32088°N/ 20.05341°E) and Gulf of Finland (GoF_ 7, 59.56354°N/ 24.88670°E). The sampling depths were chosen to cover large pCO₂ gradients, which were inferred from the hydrographical conditions at each site. The depths were at TF_ 271 20 m, 100 m, 125 m, 200 m, 225 m and at GoF_ 7 20 m, 40 m, 55 m and 70 m. The carbon dioxide sensors were recalibrated during the cruise.

Reference data for the profiling experiments

For the validation of the results obtained from the deployed carbon dioxide sensors discrete water samples were taken manually from Niskin water sampler at both stations. At each depth two samples (250 mL) were taken. The samples were poisoned with saturated mercury chloride (100 μL) right after sampling. For each water probe TA, DIC and pH were determined. The pH was measured spectrophotometrically at 25°C with *m*-cresol purple as indicator dye.¹⁶⁵ DIC was obtained by using the SOMMA system (Single Operator Multi-parameter Metabolic Analyzer) at 15°C .¹⁶⁶ TA of the water probe was determined by an open-cell titration at 20°C .¹⁶⁶ A software (CO2SYS) developed by Lewis and Wallace 1998²¹ was chosen to calculate the partial pressure of carbon dioxide from DIC and pH values.

2.3 Results and Discussion

2.3.1 Measurement principle

The recently reported di-OH-aza-BODIPY indicator dyes¹³⁹ are promising candidates for the measurement of carbon dioxide, especially at low concentrations (below atmospheric level). Particularly the absorption in the near infrared region and the well separated absorption maxima for the mono-anionic and di-anionic forms (fig. 2.1) allows the use of the compact FireSting phase fluorometer for read-out of the sensors. To convert this colorimetric system into a luminescence-based system, the inner-filter effect was used. A two layer system (fig. 2.2) consists of: i) indicator dye and quaternary ammonium base TOAOH embedded in ethyl cellulose (CO₂-sensitive layer) and ii) polymer layer with inert light emitting reference particles (combination of phosphorescent Egyptian Blue¹⁴⁵ microparticles and PS-particles doped with fluorescent pH-insensitive di-butoxy-aza-BODIPY dye). The emission spectra of Egyptian Blue (~max 900 nm) and the fluorescent dye (~max 725 nm) overlap with the absorption maxima of the di- (~max 805 nm) and mono-anionic (~max 745 nm) forms of the di-OH-aza-BODIPY indicator dye, respectively (fig. 2.1). Both the phosphor and the fluorophore are excited by a red LED (620 nm) and the emitted phosphorescence or fluorescence are absorbed by the indicator dye depending on the concentration of carbon dioxide (fig. 2.1, fig. 2.2). Since at 2000 Hz, the luminescence phase shift of the phosphor is 55° and that of the fluorophore is 0°, the change in pCO₂ is converted to the changes in the luminescence phase shift thus enabling ratiometric referenced read-out.

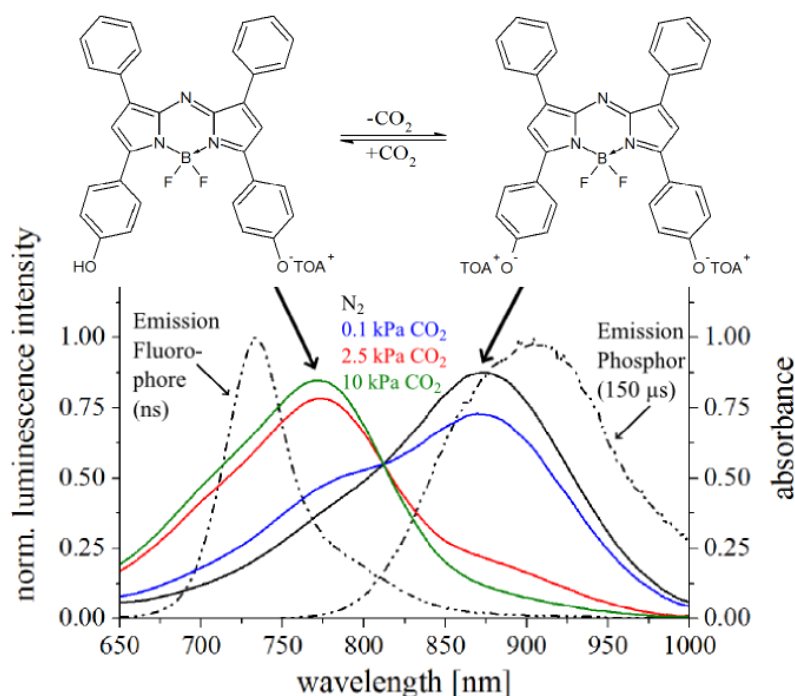


Figure 2.1: Chemical structure and de-/protonation equilibrium in absence and presence of carbon dioxide of pH-sensitive di-OH-aza-BODIPY dye: absorption spectra of the dye at different carbon dioxide concentrations at 25°C and emission spectra ($\lambda_{exc} = 620$ nm) of Egyptian Blue (dashed line; 'Emission Phosphor') and di-butoxy-aza-BODIPY-complex embedded in PS-particles (dashed line: 'Emission Fluorophore').

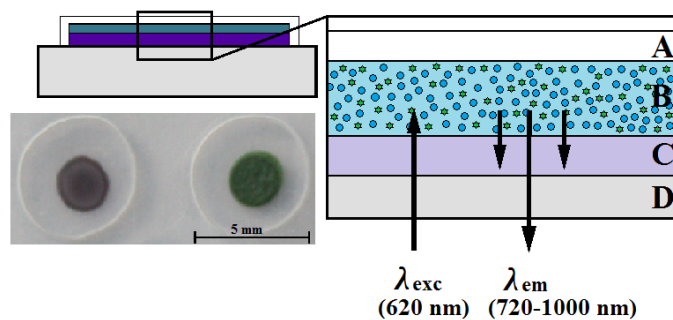


Figure 2.2: Cross section of a carbon dioxide sensor based on the inner-filter effect; A: protection layer; B: inert light emitting layer (reference layer); C: CO₂ sensitive layer (di-OH-aza-BODIPY-complex); D: transparent support (PEN foil). Photographic image shows the sensor spot after coating of the indicator layer (left) and in the final form with all the layers.

2.3.2 Support material

The selection of the support and its pretreatment mainly influence the recovery time and the mechanical robustness of the planar optode. The chosen materials should have a low permeability for carbon dioxide to accelerate the recovery time. A transparent poly(ethylene terephthalate) (PET) foil is frequently a support of choice for optodes. Another promising material is poly(ethylene naphthalate) (PEN), which has similar mechanical properties. Both polymers have similar solubilities for carbon dioxide ($S_0 = 8.3 \pm 2.9 \text{ cm}^3(\text{STP})\text{cm}^{-3}\text{bar}^{-1}$ for isotropic PET; $S_0 = 7.2 \pm 1.2 \text{ cm}^3(\text{STP})\text{cm}^{-3}\text{bar}^{-1}$ for isotropic PEN¹⁶⁷), but mainly differ in their diffusion properties ($D_0 = 0.479 \pm 0.016 \text{ cm}^2\text{s}^{-1}$ for isotropic PET; $D_0 = 0.180 \pm 0.003 \text{ cm}^2\text{s}^{-1}$ for isotropic PEN¹⁶⁷). The lower permeability of PEN for carbon dioxide ($P_0 = 4.0 \pm 1.4 \text{ cm}^3(\text{STP})\text{cm}^{-3}\text{bar}^{-1}\text{cm}^2\text{s}^{-1}$ for isotropic PET; $P_0 = 1.3 \pm 0.2 \text{ cm}^3(\text{STP})\text{cm}^{-3}\text{bar}^{-1}\text{cm}^2\text{s}^{-1}$ for isotropic PEN¹⁶⁷) results in slower diffusion of carbon dioxide accumulated in the support into the sensing foil, which minimizes the impact of the support material on the sensor signal. The surface of the PEN foil was roughened to improve the adhesion between ethyl cellulose and the support. In addition, the foil was cut before the application of the sensor layers to minimize the mechanical forces during the production of the sensor spots. Glass is another promising material for design of sensitive CO₂ optodes due to its high chemical stability and extremely low CO₂ storage capacity. However, the production process, especially the pretreatment of a glass disk, was more time consuming than for a PEN foil. Additionally, we found that a direct contact between the sensitive layer and rough glass surface should be avoided to prevent the reaction between the base and the glass surface. This required deposition of another layer of inert perfluorinated polymer on the glass discs. The complex architecture of the sensing chemistry in combination with the pretreatment of the supporting material (PEN foil) makes manufacturing of individual spots time-consuming, but automatization is certainly possible. Faster spot production is likely to be achieved by using such techniques as inkjet-printing, spray-coating etc..

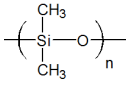
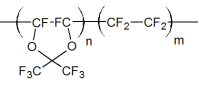
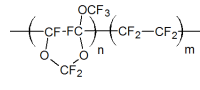
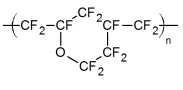
2.3.3 Effect of protective coating on response times and long-term stability

The long-term stability of sensors is an important factor in oceanographic applications. Investigation of the acidification of the ocean requires a stable and robust carbon dioxide sensor. The research of the last years has mostly been focused on the development of new indicators for carbon dioxide sensors whereas the stability of them was often not addressed in detail. The shelf life and long-term applicability of the optical carbon dioxide chemosensors is governed by stability of the indicator, the polymer (which is generally rather good) and the base. The base not only reacts with carbon dioxide but also with other acidic gases present in the environment. The reaction with the gases corresponding to strong acids is irreversible; however, poisoning of the sensor will also be observed with such gases as SO₂ or H₂S, which form strong sulfuric acid upon oxidation. The protective polymer should fulfil the following requirements: (i) be highly permeable for carbon dioxide; (ii) be hydrophobic to avoid interference from protons and other ionic species and (iii) represent a good barrier for acidic gases. Silicone rubber (cross-linked polydimethylsiloxane, PDMS) is often the polymer of choice for protection layers.^{96 150 168 169} It has good mechanical stability and is highly permeable for carbon dioxide¹⁷⁰ but not permeable to protons and other ionic species due to its hydrophobic character. Unfortunately, silicone rubber is also highly permeable for other gases such as SO₂/SO₃, NO_x or H₂S (tab. 2.1) which poisons the base in the CO₂ sensor.

Recently perfluorinated polymers became popular for gas separation applications.^{171 172 173 174 175}¹⁷⁶ Commercially available representatives are Teflon AF (DuPont), Hyflon AD (Solvay Solexis) and Cytop (Asahi Glass). Amorphous perfluorinated polymers are extraordinary thermally and chemically stable, are resistant against common organic solvents, but can be dissolved in perfluorinated solvents to fabricate thin layers. Moreover, they have low permeability for polar and sulphur-containing molecules. Of special interest are the transport properties for hydrogen sulfide, which appears in many marine environments.^{68 177 178} The study of Merkel and Toy (2006)¹⁷⁹ revealed CO₂/H₂S selectivities much larger than 1 for perfluorinated polymers in contrast to silicone rubber (tab. 2.1). The reason for this effect is a low H₂S solubility, caused by unfavourable interactions between the penetrant and the fluorinated polymer. The permeability for carbon dioxide decreases in the following order Teflon AF 1600 > Hyflon AD 60 > Cytop, whereas the selectivity towards H₂S increases. The protective properties of the coatings towards poisoning by acidic gases have been investigated by introducing conc. hydrochloric acid into the cuvette with a planar optode. The poisoning kinetics can be determined via measurement of the absorption of the deprotonated form of *m*-cresol purple since the hydrophobic quaternary ammonium base is converted to the corresponding chloride salt (fig. 2.3C). It is evident that the protective properties of silicone rubber are very poor (tab. 2.1). On the other hand, ~10-fold, 18-fold and 25-fold improvement is observed for Teflon AF 1600, Hyflon AD 60 and Cytop, respectively. The protective properties of the polymers for other acidic gases are likely to be similar to those towards poisoning by HCl. Furthermore, the poisoning process with hydrogen sulfide in presence of oxygen (air saturation) was investigated for each polymer (fig. 2.3D). Silicone rubber showed the least protection, followed by Teflon AF 1600, Hyflon AD 60 and Cytop 809 A. Cytop 809 A showed almost no poisoning even after 5 h of exposure

to H₂S. It should be noted that the chosen total sulfide concentration for the experiment is slightly higher than found in Baltic Sea after a long stagnation period (Godland Sea deep water (200 m): $\sim 200 \mu\text{mol/kg}^{180}$) so that poisoning by H₂S in the in situ experiments is expected to be similar or slower, because of the salt water inflow December 2014.

Table 2.1: Gas permeabilities for polydimethylsiloxane (PDMS) and perfluorinated polymers given in barrer.

	PDMS	Teflon AF 1600	Hyflon AD 60	Cytop
structure				
P _{O₂}	781 ¹⁸¹	340 ¹⁸²	51 ¹⁸²	16 ¹⁷⁵
P _{NH₃}	6552 ¹⁸³	229 ¹⁸³	41 ¹⁸³	-
P _{CO₂}	4400 ¹⁷⁹	680 ¹⁷⁹	124 ¹⁸⁴	17 ¹⁷⁹
P _{H₂S}	6670 ¹⁷⁹	100 ¹⁷⁹	-	0.6 ¹⁷⁹
P _{CO₂/H₂S}	0.66 ¹⁷⁹	6.8 ¹⁷⁹	-	27 ¹⁷⁹

Investigations of the protective properties of these perfluorinated polymers as well as the dynamic response and recovery times were performed with a planar optode based on *m*-cresol purple in ethyl cellulose with TOAOH.¹⁴⁷ This commercially available dye shows a visible colour change (blue-yellow), is characterized in detail and has been extensively used for seawater applications.^{165 185 186 187 188} It represents a good model system for preliminary experiments. The layer of a perfluorinated polymer was coated over the sensing layer. As expected, the response and recovery times increase with decrease in the permeability of the polymer for carbon dioxide (fig. 2.3, tab. 2.2).

Table 2.2: Response, recovery (13.5 μM - 3320 μM CO₂ concentration), times required for complete poisoning with 12 M hydrochloric acid (gas phase, in seconds) and kinetics of poisoning with aqueous hydrogen sulfide (total sulphide: 270 μM) for a planar optode based on *m*-cresol-purple and TOAOH in ethyl cellulose covered by 8 μm thick protection layer of different polymers.

polymer	response time (t ₉₀ , sec)	recovery time (t ₉₀ , s)	time of complete poisoning (HCl)	poisoning after 3 h (%)
silicone rubber	6	93	9	100% (35 min)
Teflon AF 1600	10	139	87	100% (75 min)
Hyflon AD 60	12	180	159	36%
Cytop 809 A	15	208	230	0%

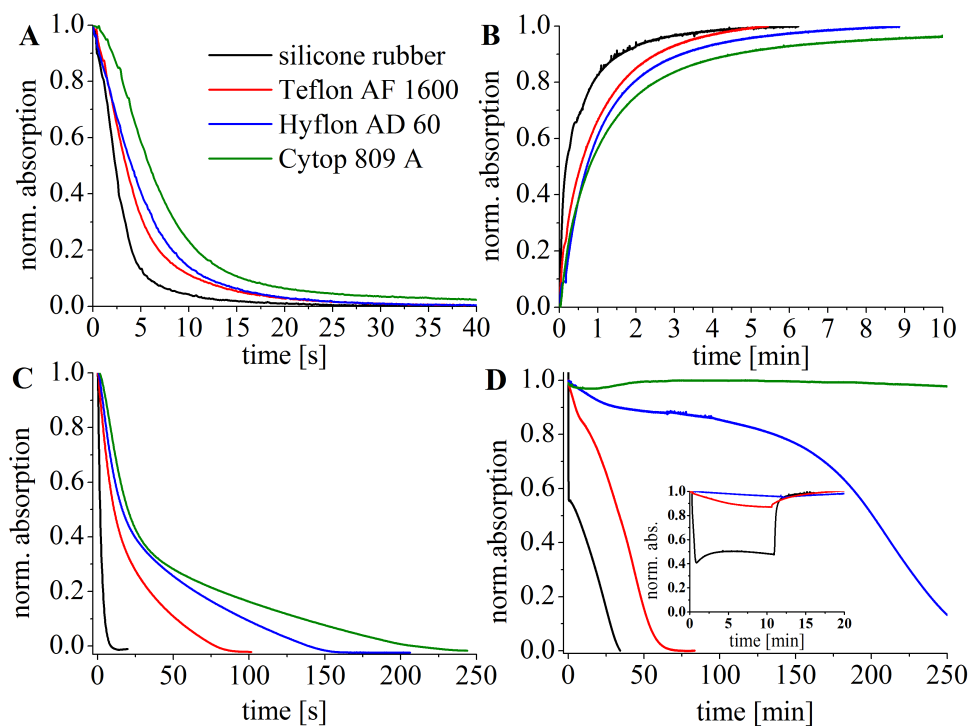


Figure 2.3: Response and poisoning behaviour of a planar optode based on *m*-cresol purple and TOAOH in ethyl cellulose covered with different protective polymers at 25°C in phosphate buffer: A: response times from ambient air saturated phosphate buffer to 3320 µM carbon dioxide; B: recovery times from 3320 µM carbon dioxide to ambient air saturated phosphate buffer; C: kinetics of poisoning caused by hydrochloric acid and D: kinetics of poisoning caused by hydrogen sulfide (270 µM total sulphide; $c_{H_2S} \approx 20$ µM dissolved H₂S) for the four polymer coating and cross-talk to hydrogen sulfide for silicone rubber, Teflon AF 1600 and Hyflon AD 60 (insert).

It should also be considered that H₂S can cause a reversible cross-talk of the sensor due to its acidic properties. In anoxic conditions such cross-talk may be the major error source despite the fact that H₂S is not expected to irreversibly poison the sensor. Indeed, we observed a decrease in the absorption of the deprotonated form of *m*-cresol purple in presence of H₂S which was reversible if the gas was removed promptly. As can be seen, the cross-talk is more pronounced for silicone rubber and almost negligible in case of Cytop 809 A and Hyflon AD, whereas Teflon AF 1600 occupies intermediate position (fig. 2.3D insert). Thus, due to the fact that perfluorinated polymers do not allow fast equilibration of the sensor with H₂S they efficiently reduce the cross-talk to this substance in case of short term exposure. This can be highly beneficial for profiling experiments.

Although Cytop shows the best protective properties, the sensors show significantly longer response and recovery times due to the rather low permeability for carbon dioxide (tab. 2.1, tab. 2.2). Evidently, Cytop coatings will not be suitable for most applications. However, it may be possible to use this perfluorinated polymer as the protection polymer for the systems where the changes in the carbon dioxide concentration are much slower than the response time of the sensor. Compared to Cytop, the permeability of Teflon AF 1600 for carbon dioxide and hydrogen sulfide is 40-fold and 160-fold higher, respectively, which enables much faster response times but also reduces the shelf life and long-term stability due to faster poisoning. Although no literature data are available for permeability of Hyflon AD 60 for hydrogen sulfide,

the poisoning experiments with HCl and especially H₂S showed better protective properties compared to Teflon AF 1600 (fig. 2.3C,D). Therefore, we decided to use this polymer as a protective layer as the best compromise between dynamic response and protective properties, which provide long shelf-life and operational life. Other advantages of Hyflon AD 60 make it even more attractive for sensing applications. The material is resistant to swelling¹⁸⁹ and is highly transparent to light from far UV to near infrared¹⁸². It has high resistance against abrasion or friction and low affinity to dust and other contamination. Additionally, low biofouling on the perfluorinated surface is expected.

The above system (*m*-cresol purple and TOAOH in ethylcellulose) was also used for investigation of the long-term protective properties of Hyflon AD 60 in comparison with silicone rubber. The sensors covered with silicone rubber showed continuous drift if stored at ambient conditions. It lost about 50% of the signal already after 1 week of storage (fig. 2.4C) and was poisoned completely after 1.5 months. On the other hand, the indicator remained deprotonated in the sensors covered with Hyflon AD 60, indicating excellent stability during this period (fig. 2.4B).

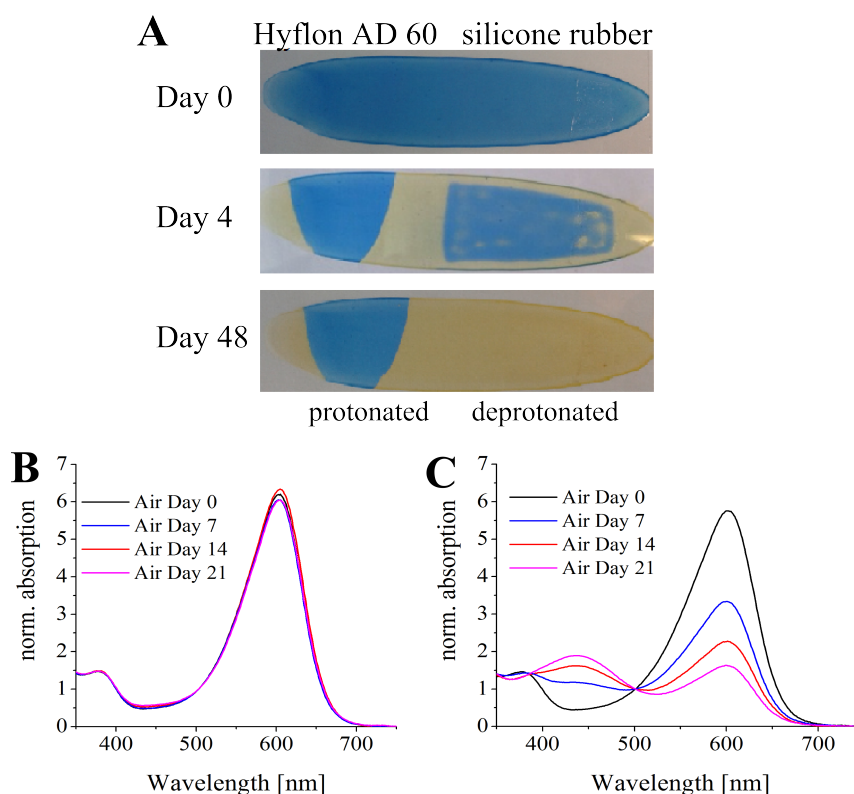


Figure 2.4: Protective properties of silicone rubber and Hyflon AD 60. A: photographic images of the planar optode based on *m*-cresol purple and TOAOH in ethyl cellulose covered with the protective layers; B and C corresponding UV-VIS absorption spectra for the Hyflon AD 60 and silicone rubber, respectively.

2.3.4 Manufacturing of the luminescent carbon dioxide optode

Due to the use of Hyflon AD 60 as polymer for the reference and protection layer, a new design of the sensing material was necessary. The adhesion of the very hydrophobic Hyflon AD 60 on significantly more hydrophilic ethyl cellulose was very weak and the sensor material lacked mechanical stability. For example, the protective layer detached during punching-out of the

sensor spots. Even a reduction of mechanical stress during the spot production by laser cutting was not successful, leading to a separation of the sensor layers after several measurements. Therefore, a new sensor design and manufacturing procedure were developed (fig. 2.2). The sensor 'cocktail' composed of the solution of the dye, TOA OH and ethyl cellulose in an organic solvent was pipetted in the middle of a pre-cut PEN support treated with a sand-paper to improve the adhesion. The sensing layer was covered by the reference layer (luminescent particles dispersed in Hyflon AD 60). Finally, the upper layer of Hyflon AD 60 was introduced, covering both the reference layer on top and the sensing layer on sides and having direct contact to the support material. The advantages of the method include complete protection of the sensing layer from all the sides and absence of mechanical or thermal stress during manufacturing.

To evaluate the long-term stability of the new sensors in aqueous media, three sensor spots were inserted in a constantly stirred vessel with a 0.1 M phosphate buffer (pH 7.9), equilibrated with ambient air over 35 days (fig. 2.5). The sensor spots showed no indication of an intrusion of protons or other poisoning molecules, which would result in increase of the luminescence phase shift, and therefore in overestimation of the carbon dioxide concentration.

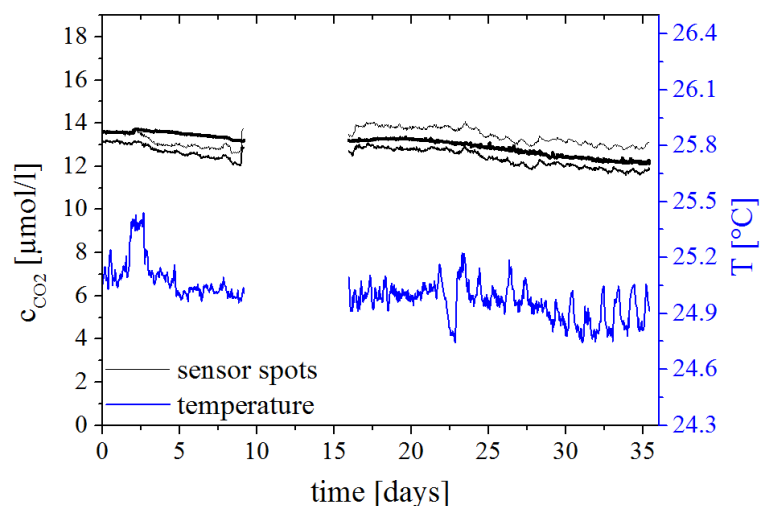


Figure 2.5: Long-term stability of luminescent carbon dioxide sensors based on di-OH-aza-BODIPY dye in a constantly stirred open flask at 23.5–25.5°C; measuring interval 1 h. Measurement interruption between day 10 and day 16 is due to software problems.

2.3.5 Response and recovery times

The response and recovery times of the luminescent carbon dioxide sensor in aqueous phase have been estimated for two relevant concentration ranges (fig. 2.6). The response and recovery times are very similar. They are significantly faster (about 4-fold) in the upper range of CO₂ concentrations (70–125 μM) than in the lower range (14–28 μM). As expected, temperature significantly affects the response time. Whereas the response (particularly at higher concentration range) is sufficiently fast at higher temperatures, it becomes very slow at 4 °C. This is due to the relatively low carbon dioxide permeability of Hyflon AD 60 used in the reference and protective layer. The above limitation of the sensor should be considered when designing profiling experiments. Further optimization of the thicknesses of the reference and protective layers is likely to improve the response times.

The response times of the planar optodes based on *m*-cresol purple (model system) are much faster than of the presented fluorescent carbon dioxide sensor. It can be explained by a higher carbon dioxide concentration gradient (13 μM (ambient air) to 3320 μM (10% CO₂)) and the effect of the reference particles on the permeability of the second layer to carbon dioxide. It is also possible, that the thickness of the reference and protective layers in case of the presented fluorescent sensors in some parts of the spot is significantly higher than estimated due to inhomogeneous evaporation pattern. Thus, optimization of the coating procedure may be beneficial for improving the sensor response. Furthermore, the use of more carbon dioxide-permeable Teflon AF instead of Hyflon AD is also possible. Fiber-optic microsensors are known to respond much faster than the planar sensor spots due to better diffusion of the analyte. Although manufacturing of the microsensors with current inner-filter effect-based 'sensing chemistry' is challenging, the approach is likely to be useful in case of fluorescent dyes.

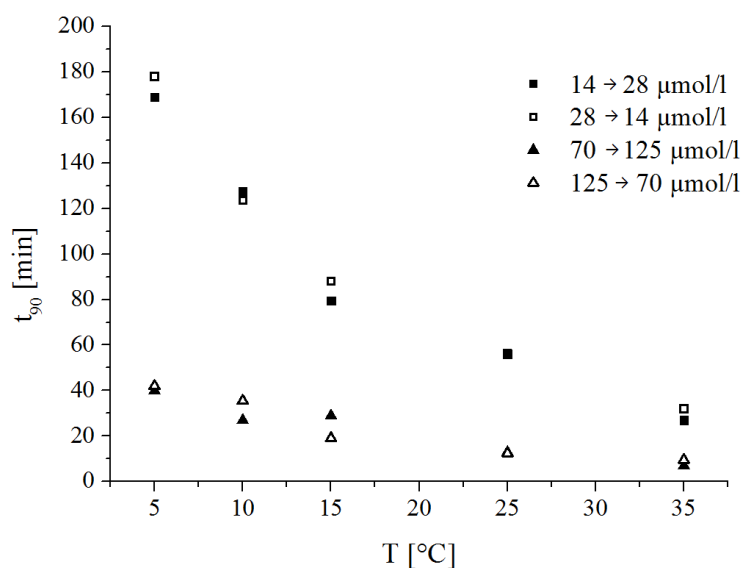


Figure 2.6: Response times (t_{90}) for the luminescent carbon dioxide sensors based on PEN support at two different concentration ranges (lower and upper measuring range) in a constantly stirred solution.

2.3.6 Sensor calibration

Calibration of the sensors in the aqueous phase was performed by addition of sodium hydrogen carbonate solution to 0.1 mol/L phosphate buffer (pH 7.7) to adjust the pCO₂ levels. A non-linear increase in the luminescence phase shift with increasing pCO₂ is observed (fig. 2.7A). The plots of the cotangent of the phase angle against the logarithm of the CO₂ concentration reflect the protonation equilibrium of the indicator. Thus, similarly to optical pH probes, such dependency can be almost ideally described by a sigmoidal function with four parameters ($R^2 > 99.8\%$).

$$y = A2 + \frac{A1 - A2}{(1 + 10^{\frac{x-x0}{dx}})} \quad (2.2)$$

where A1 is the upper plateau, A2 the lower plateau, x0 the inflection point and dx the slope. The response of all optical chemosensors including pCO₂ sensors is temperature-dependent.

Temperature not only affects the permeability of the ethylcellulose for carbon dioxide and the respective pH equilibria but also the luminescence properties of the reference luminophores. This results in a rather complex dependency (fig. 2.7). A pronounced decrease in the sensitivity at higher temperature is evident which is explained by decrease of gas solubility in these conditions. Thus, the sigmoidal function was extended by the temperature coefficients ($A1_t$, $A2_t$, $x0_t$, dx_t) to perform a three-dimensional fit of the data (fig. 2.7). The resulting equation, which was used to obtain the calibration area was:

$$\cot(dphi) = (A2 + A2_t \cdot (T - 20)) + \frac{(A1 + A1_t \cdot (T - 20)) - (A2 + A2_t \cdot (T - 20))}{(1 + 10^{\frac{\log(CO2) - (x0 + x0_t \cdot (T - 20))}{dx + dx_t \cdot (T - 20)}})} \quad (2.3)$$

To minimize the degree of freedom and to simplify the recalibration, all temperature coefficients and the values for $x0$ and dx were fixed. The parameters were set at $A1_t = -0.016541$, $A2_t = 0.0069325$, $x0_t = 0.037465$, $dx_t = -0.040605$, $x0 = 0.953701$, $dx = 1.445015$ for the temperature range between 17°C and 35°C.

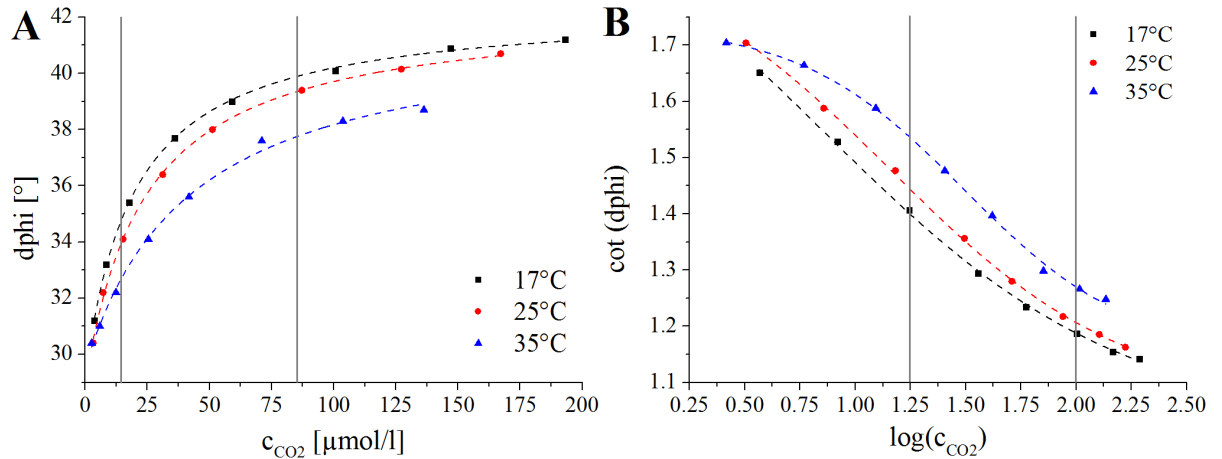


Figure 2.7: A: Calibration plots for luminescent carbon dioxide sensors for the range between 0 and 175 μM CO₂; B: Logarithmic plot of the experimental data and respective fit according to sigmoidal equation (dashed lines). Vertical lines (dark gray) representing recalibration points (18 μM , 84 μM).

It should be noted that each sensor is slightly different due to variation in the thickness of the sensing layer and variation in the thickness of the reference layer as well as in the ratio of phosphorescent and fluorescent reference particles. Therefore the $\cot(dphi)$ values for each sensor spot are not identical, whereas the slope and the inflection point of the sigmoidal function are equal but temperature dependent. Throughout a three-point calibration, right before the application, the calibration area can be adjusted by shifting it to higher or lower $\cot(dphi)$ values. The chosen concentrations of carbon dioxide are at the beginning and the end of the linear part of the calibration curve (18 μM ambient air ($\log(c_{CO_2}) = 1.25$), 84 μM ($\log(c_{CO_2}) = 2.0$); $T \approx 8^\circ\text{C}$) and at the plateau at the end achieved by using carbonized mineral water ($\log(c_{CO_2}) = 4.25$).

2.3.7 Applications

The applicability of the new carbon dioxide sensors was tested by measuring the respiration behaviour of *Egeria densa*. *E. densa* are water plants originally common in Brazil, Argentina and Uruguay with a high rate of growth under ideal conditions.¹⁹⁰ The plant, an oxygen optode, the new carbon dioxide sensor spot placed on a distal end of an optical fibre, as well as the temperature probe were inserted in a desiccator filled with tap water (fig. 2.8A). The plant was illuminated with two halogen lamps for one to two hours (photosynthetic photon flux density $\sim 250 \mu\text{mol} \cdot \text{s}^{-1} \cdot \text{m}^{-2}$). The darkness periods varied between 90 minutes and two hours. The production and consumption of carbon dioxide during dark and light periods, respectively, is clearly visible (fig. 2.8B). Oxygen dynamics mimics that of carbon dioxide but with an opposite trend: oxygen consumption is observed due to respiration during the dark period and oxygen production due to photosynthesis during the illumination period.

The absolute consumption of oxygen is higher than the measured production of carbon dioxide (normally 1:1 ratio). Since we used un-buffered tap water, the produced carbon dioxide is partly transformed into bicarbonate, which was not measured.

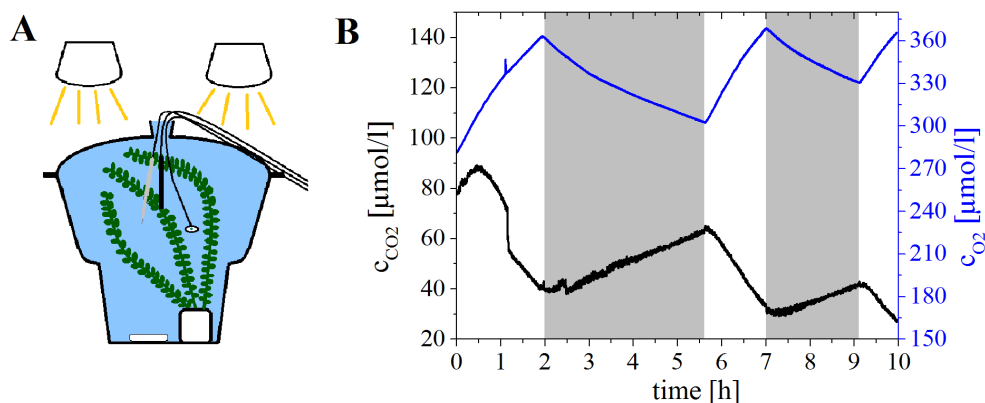


Figure 2.8: A: Scheme of the experimental set up of the investigation of the respiration behaviour of an *Egeria densa*; B: Carbon dioxide and oxygen dynamics of *Egeria densa* in a desiccator filled with tap water (constant stirring) during illumination with halogen lamps (white zone) and darkness (grey zone); $T = 21.3^\circ\text{C} - 27.4^\circ\text{C}$.

The sensing device was further applied for in situ carbon dioxide monitoring during the research trip 'PROSID2014' in the Gotland deep (TF_ 271) and the Gulf of Finland (GoF_ 7). Due to the long response time of the sensor, stepwise profiles were measured. The CTD-rosette was held on a certain depth for 45-105 minutes. A stable signal was observed before the next depth was reached. The pCO_2 was calculated by using A1 and A2 parameters obtained from the three-point (re-)calibration. The obtained data correspond well to the estimated behaviour of the carbon dioxide concentration based on the previously measured dissolved oxygen concentrations (fig. 2.9A). The upper layer ($\sim 40 \text{ m}$) was mixed very well because of the weather conditions and was equilibrated with the atmosphere. This was followed by a pronounced increase of pCO_2 below the halocline (from $13 \mu\text{M}$ to $135 \mu\text{M}$), which can be found permanently in the Baltic Sea.^{191 192} Due to the saltwater inflow in December 2014¹⁹³ a slight decrease of CO_2 was expected at 200 m depth. This could be observed by the reference measurements and the oxygen profile. The predicted amounts of carbon dioxide could be confirmed with the new sensor device

at both stations.

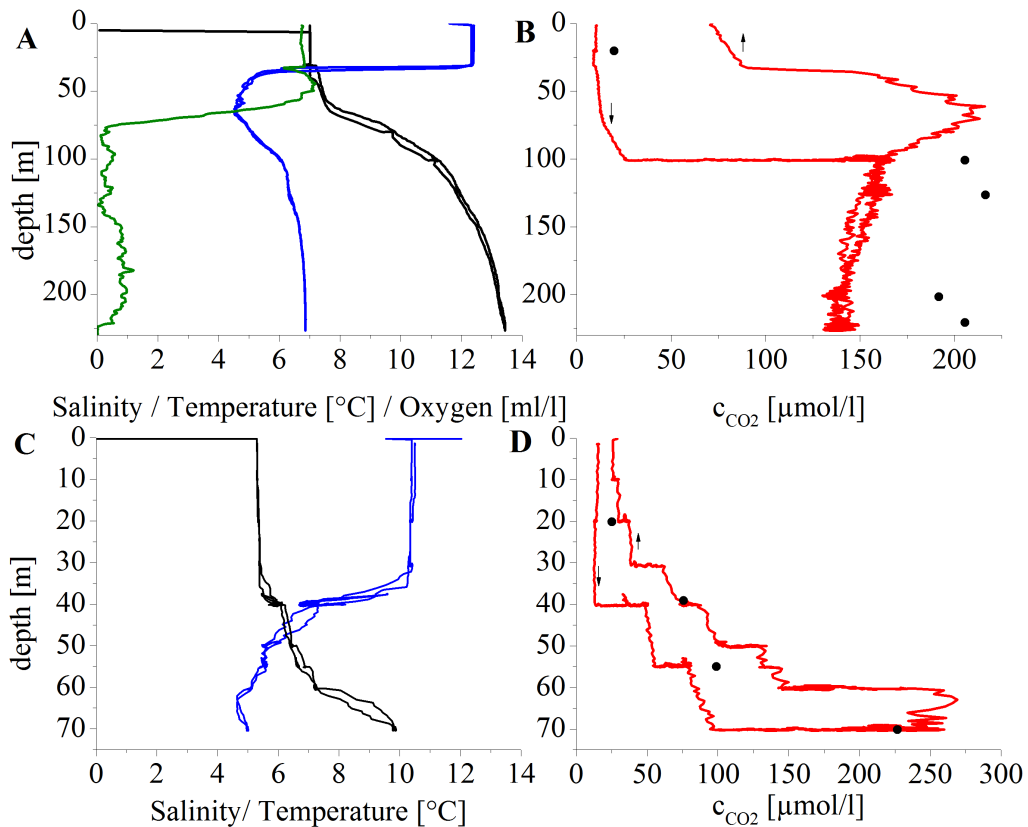


Figure 2.9: Salinity (black), temperature (blue), oxygen (green) and CO₂ profiles (red) obtained during the 'PROSID 2014' cruise in October 2015. A, B: Gotland deep (TF_ 271, 57.32088 lat/ 20.05341 lon); C, D: Gulf of Finland (GoF_ 7, 59.56354 lat/ 24.88670 lon). Black dots indicate the data from the reference photometric measurement.

The measured pCO₂ was verified by using the reference samples taken at the corresponding depths. Due to the use of Hyflon AD 60 as the polymer for the reference and protection layer and low temperatures during the experiment, the response times are very long. This leads to three main problems: i) the recalibration at in the environment expected temperatures is time consuming (up to 6 hours), ii) the measurement of the profile takes several hours, during which the research vessel has to stay at almost the same position and iii) the long response time is responsible for hysteresis, which is clearly observed during the fast profiling. For instance, hysteresis for the depths from 0 to 100 m (station TF_ 271, fig 2.9B) is very distinct due to the fact that the CTD-rosette was heaved continuously back to the surface because of the weather conditions. A longer equilibration time is required to achieve a stable signal for more precise measurements which was hardly possible within the limited time available during the test. For comparison, at station GoF_ 7 it was possible to extend the time for measuring the profile and heaving the CTD-rosette (10 min for every 10 m). The observed hysteresis was much smaller (fig. 2.9D). The values measured with the new carbon dioxide sensor for the Gotland deep (TF_ 271) were often lower than those obtained in the reference method for discrete probes (~ 25% relative error). The likely reason for this deviation is an offset in calibration, due to very long response times of the sensor at the low temperatures and low carbon dioxide concentrations. The data obtained at GoF_ 7 are in a good agreement with the reference data. The measured

profile in the Gulf of Finland shows an increase of the carbon dioxide concentration between 20 and 70 m, in which the main rise was measured between 55 and 70 m water depth. The reference measurements are in the range between the data obtained during lowering and heaving of the CTD-rosette. This indicates that a longer equilibration time is necessary to generate more accurate data. Therefore, optimization of the sensor design aiming at reduction of the response time will be indispensable for profiling applications.

2.4 Conclusion

We presented the quantification of carbon dioxide in marine environment with a highly sensitive, mechanically and (photo-) chemically robust sensing material, which is compatible to the phase fluorimeters from PyroScience GmbH. The new sensor spots based on a colorimetric indicator and inner-filter effect read-out feature a multi-layer architecture which is necessary to ensure high long term and mechanical stability. The use of a protective layer made of the perfluorinated polymer Hyflon AD 60 dramatically enhances the resistance against poisoning dramatically compared to commonly used silicone rubber. Importantly to applications in conditions with low oxygen, partial protection against hydrogen sulfide can be realized with this type of polymer. The trade-off is a much longer response time, particularly at low carbon dioxide concentrations and at low temperatures. This significantly complicates the sensor calibration and profiling in situ. Preparation of thinner layers via carefully controlled layer deposition is likely to improve the response times. Furthermore the use of a different perfluorinated polymer with a higher permeability for carbon dioxide (Teflon AF) is another possibility to improve the response and recovery times. By the use of additional long term field tests more data can be obtained to reveal possible interferences or limitations, like biofouling.

Acknowledgement

Financial support by the European Union FP7 Project SenseOCEAN- Marine Sensors for the 21st century (Grant Agreement Number 614141) is gratefully acknowledged. The research cruise 'PROSID 2014' has received funding from the European Union Seventh Framework Programme (FP7/2007-2013) EUROFLEETS 2 (Grant Agreement number 312762). Dr. Michael Naumann (field cruise leader), Dr. David Meyer (organizer), Dr. Urmas Lips (MSI Tallinn) and the research vessel crew are thanked for their assistance.

Chapter 3

A validation and comparison study of new, compact, versatile optode for oxygen, pH and carbon dioxide in marine environments

This Chapter was prepared for submission to 'Environmental Science and Technology'.

Authors: Eva Fritzsche, Christoph Staudinger, Jan P. Fischer, Roland Thar, Hans W. Janasch, Joshua N. Plant, Marguerite Blum, Gene Massion, Hans Thomas, Jon Hoech, Kenneth S. Johnson, Sergey M. Borisov, Ingo Klimant

Continuous monitoring of dissolved oxygen, pH and carbon dioxide are of great importance in oceanography. Sensors are the optimal tools for in situ measurements from mobile platforms, like Autonomous Underwater Vehicles (AUVs) or Argo profiling floats, and for shipboard deployments. A validation study of small, versatile, easy-to-use, stand-alone optodes is presented. Each analyte can be read out with identical optoelectronics. Several deployments were performed to evaluate the applicability of the sensors. The deployments varied in terms of duration (profiling, long-term monitoring 5 days to 8 weeks) and environmental conditions (salinity: 6-33 PSS; temperature: 9-25 °C). We successfully used a set of sensors at a mooring buoy, in an aquaculture facility and in the Monterey Bay Aquarium Open Sea Exhibition. We also integrated sensors in an AUV and a profiling float. Moreover, the performance of the optodes was evaluated in comparison with already commercially available sensors for dissolved oxygen (Aanderaa Data Instruments AS, Sea-Bird Scientific, OxyGuard®), pH (Hach®, Satlantic) and carbon dioxide (Turner design). The data collected by our optodes and the commercially available sensors are in very good agreement. The new, compact sensor device in combination with sensor foils (pO₂, pH, pCO₂) proved to be excellently suitable for most applications in oceanography.

3.1 Introduction

Sensor technology represents a very important tool in oceanography. The ocean influences the world's climate significantly and is affected by the human hand. The growing human population and increasing industrial activity results in increasing pollution, ocean acidification^{49 194} and expanding oxygen minimum zones.¹⁹⁵ To survey the dimension of changes in ocean chemistry and the impact on the marine ecosystem, in situ observations with sensors are indispensable. The marine environment is challenging to study, due to the dramatic size of the ocean, the hostile conditions and heterogeneous, turbulent water masses, which are hard to reach. As a consequence, the ocean is highly undersampled. Missing spatial and temporal coverage with data prevents the development and test of hypotheses and models.^{196 197}

Sensors in combination with a variety of oceanic platforms, like moorings, Autonomous Underwater Vehicles (AUVs), gliders and autonomous Argo floats can minimize the problem of undersampling by continuous or semi-continuous in situ measurements. In order to be useful for oceanography, apart from a well characterized performance (accuracy, precision, response time) the sensors have to fulfill the following requirements: (i) have low production cost; (ii) have low power consumption and enable long-term autonomous operation; (iii) have small size for easy handling and integration on different platforms; (iv) be robust against pressure and temperature changes, as well as biofouling.¹⁹⁸ Aiming to address these requirements, a number of different prototypes were developed in the last decades to measure dissolved oxygen^{199 200 201 202}, pH^{203 204 205 206} and dissolved carbon dioxide^{91 108 207 208 107} in the ocean.

Most promising prototypes for the measurement of dissolved oxygen in seawater were commercialized and are frequently used in oceanography.^{51 108 209 210} Many commercially available dissolved oxygen sensors are based on the conventional electrochemical Clark electrode. In this sensor type, oxygen has to diffuse through a gas-permeable membrane to be reduced at the cathode, which results in a measurable electrical current. Clark electrodes are prone to drift, very sensitive to salinity and temperature and consume oxygen.²¹¹ Improvements were made to commercialize electrochemical oxygen sensors. Sea-Bird Scientific developed the SBE 43 oxygen sensor^{212 213} and OxyGuard® the OxyGuard 840 oxygen probe.²¹⁴ In the last decades oxygen optodes were developed and commercialized. They are a promising alternative to conventional electrochemical oxygen sensors. The fundamental principle is based on luminescence quenching of a transition metal complex by molecular oxygen. Commercially available optodes for marine applications are among others: 'Optode 4330' (previous '3850') from Aanderaa Data Instruments²¹⁵ and the Fast Optical Oxygen Sensor from Sea & Sun Marine Tech²¹⁶.

Highly accurate and precise pH sensors for marine applications are of special interest, due to the ongoing problem of ocean acidification. Several types of sensors for the *in situ* measurement of pH were already developed. They include electrochemical, potentiometric, photometric and fibre-optic-based instruments. The electrochemical approach to measure pH is based on glass electrodes or Ion Selective Field Effect Transistors (ISFET). A number of electrochemical pH sensors are on the market for example: pH sensors from Hach® using the differential

electrode measurement technique, leading to better accuracy and greater reliability (often used in aquarium)²¹⁷ or the ISFET-type SeaFETTM Ocean pH sensor from Satlantic/Sea-Bird Scientific modified to obtain accurate long-term measurements.^{203 218 219 220} Highly accurate and precise pH values can be obtained by spectrophotometric measurements. pH dependent change of the absorption spectrum of *m*-cresol purple serves as an analytical parameter^{165 188} and is often used to determine reference pH values in the lab. To allow for *in situ* application flow-through sensors based on this sensor scheme were developed.^{221 222} However, they are bulky and require a reagent and waste reservoir apart from pumps and fluidics. Optodes for measuring pH in the marine environment rely on immobilized fluorescent (and more rarely colorimetric) pH indicators and therefore can overcome the disadvantages of the spectrophotometric fluidic sensors. The pH optodes are in the development stage and not commercialized yet. Several prototypes were developed and tested in the last years. Clarke et al. 2015²²³ presented a sensor based on a sensor foil from PreSens GmbH which was used on a cruise in the Southern Ocean. Staudinger et al. 2017 (submitted)¹⁴⁹ described a sensor based on aza-BODIPY dyes covalently coupled to a polymer matrix and successfully tested in the Baltic Sea.

Sensors for dissolved carbon dioxide gained special interest in the last decade as recently reviewed by Clarke et al. 2017.⁸⁹ Promising and already commercially available sensors for dissolved carbon dioxide are based on non-dispersive IR-spectroscopy (NDIR).^{91 116 207} This technique uses the characteristic band of gaseous carbon dioxide generated by the absorption of infrared radiation. NDIR based pCO_2 sensors are widely used for shipboard measurements. They provide highly accurate and precise dissolved carbon dioxide data sets, but they are typically big, require recalibration to guarantee long-term measurements and have a high power consumption. There are a few commercially available NDIR carbon dioxide sensors, for example: Seaology[®] pCO_2 monitoring system by BATTELLE^{116 207}, CONTROS HydroC[®] CO_2 by Kongsberg Maritime Contros GmbH^{91 114}, CO_2 -Pro CVTM by Pro-Oceanus Systems Inc.¹¹⁷ and C-SenseTM by Turner-designs¹³¹. Optodes are a promising sensing technology for *in situ* measurements of dissolved carbon dioxide in the marine environment. Several optode prototypes were developed and successfully deployed during the last years, but none of them is fully commercialized yet. Examples of optode prototypes for marine applications are presented by Atamanchuk et al. 2014, produced by Aanderaa Data Instruments AS using a sensor foil obtained from PreSens^{75 107}, by Clarke et al. 2017 using HPTS as a carbon dioxide sensitive indicator⁸⁹ and Fritzsche et al. 2017 using di-OH-aza-BODIPY indicator dyes and hardware developed by PyroScience GmbH^{108 139}.

For each of the mentioned analytes, sensors based on optodes are a trendsetting technology. The core piece of an optode is an analyte-sensitive dye embedded in an analyte-permeable matrix (called sensor foil). The photophysical properties of the indicator (absorbance, luminescence intensity or decay time etc.) depend on the analyte concentration. Compact set-ups with lower power consumption use Light Emitting Diodes (LEDs) as an excitation source and photodiodes as photodetectors. The chosen indicator determines the sensor foil structure, composition and the type of signal change. Optodes provide a large number of advantages like: small size, low power consumption, easy and low-cost manufacturing, absence of moving parts, no need

of reference gases, fast response time, predictable temperature response and absence of analyte consumption allowing multiple measurements in small sample volumes.²²⁴ Moreover, optodes provide the unique possibility to use the same hardware for more than one analyte, providing that the spectral properties of indicators are similar. However, to the best of our knowledge, virtually all of the described sensors are dedicated to the measurement of a single analyte. The sensor system recently presented by Thomas et al. 2017⁷⁵ represents a notable exception since it is suitable for measurement of two analytes (carbon dioxide and ammonia).

Recently we developed luminescent sensor foils for oxygen, pH and carbon dioxide, which are all excitable with a red 625 nm LED¹⁴⁹. The oxygen optode relies on a platinum(II)benzoporphyrin and luminescence decay time read-out.^{202 225 226} The pH sensor scheme uses a fluorescent aza-BODIPY dye embedded into a hydrogel.^{164 227} Finally, the carbon dioxide sensor relies on a colorimetric aza-BODIPY dye with the inner filter effect read-out allowing to convert the absorption changes into a referenced ratiometric response.^{108 139} All the sensors are based on near infrared dyes which minimize potential interferences from autofluorescence and ambient light and reduces power consumption. Since the special properties of these sensing materials are similar, the same hardware can be used for all the analytes. The detailed characteristics of the optode system and early stage applications were recently presented by Staudinger et al. 2017.¹⁴⁹ In this study we present the more detailed evaluation of the developed set of sensors, the integration in a number of marine platforms and monitoring systems, as well as a validation with already commercially available sensors. We will show that the versatility of the optode system simplifies its integration into oceanic platforms like monitoring buoys, AUVs and profiling floats.

3.2 Methods and Instrumentation

Optodes for oxygen, pH and carbon dioxide

The oxygen sensor foil was obtained from PyroScience GmbH (Aachen, Germany) and is based a platinum(II) benzoporphyrin entrapped in a polymer matrix with the measurement range between 0.1 % and 250 % air saturation.

The pH sensor foil was prepared according to literature (material 'pH 2').¹⁴⁹ Briefly a fluorescent aza-BODIPY indicator dye^{164 227} was covalently coupled to polyacrylmorpholine-co-hydroxyethylacryl-amide, which was further crosslinked by a polyisocyanate crosslinker (Desmodur N75 MPA/X) in presence of a catalyst (dibutyltindilaureat in THF). The reference layer, composed of Egyptian Blue in poly(ethyleneterephthalate), was coated on the backside of the sensor support.

The carbon dioxide sensor foil was produced analogously to the literature procedure¹⁰⁸ with several modifications. First Fomblin Y[®] was added to all Hyflon[®] AD-based compositions (30 % w/w in respect to Hyflon[®] AD 60) to enhance the layer flexibility. Additionally an optical isolation was added between the inert light emitting layer and the protection layer (fig. 3.1). It consisted of two layers based on Hyflon[®] AD 60. The first layer was prepared by coating a 'cocktail' containing 50 mg Hyflon[®] AD 60, 15 mg Fomblin[®] Y, 30 mg ultrafine titanium oxide

(P170, Kemira) and 1300 mg of perfluorodecalin, which was washed prior to use with aqueous 1 M potassium carbonate solution. The second layer was prepared by coating the solution of the same composition as above but using 50 mg of carbon black instead of titanium dioxide. In both cases the 'cocktails' were stirred until the particles were fully suspended.

The read-out device was provided by PyroScience GmbH. It is described previously in detail¹⁴⁹ and is suitable for each of the above described sensor foils. Optoelectronic unit, an internal logger and a rechargeable battery are placed in a POM (polyoxymethylene) housing which is equipped with a pressure stable optical feed-through, resistance thermometer and SubConn connector (fig. 3.2). A PMMA (polymethylmethacrylate) cap with an appropriate sensing material is screwed onto the optical feed-through. The device has small dimensions (length 30 cm with dummy plug, $\varnothing 8$ cm), is lightweight (1 kg in air and ~ 150 g in water) and is optimized for low power consumption allowing for autonomous long-term logging for over 1 year (measurement each 30 s). An flow-through cell was designed and 3D printed at the MBARI (fig. 3.2B). It can be conveniently mounted onto the device with M6 screws. The connectors (fig. 3.2B white parts) are 1.3 cm in diameter and can be easily connected to the tubing of flow-through systems. The flow-through chamber had a volume of around 10 cm^3 and was designed to enclose the temperature sensor and the sensor cap. The cell was made to integrate the optode in an AUV or the monitoring system of the aquaculture facility.

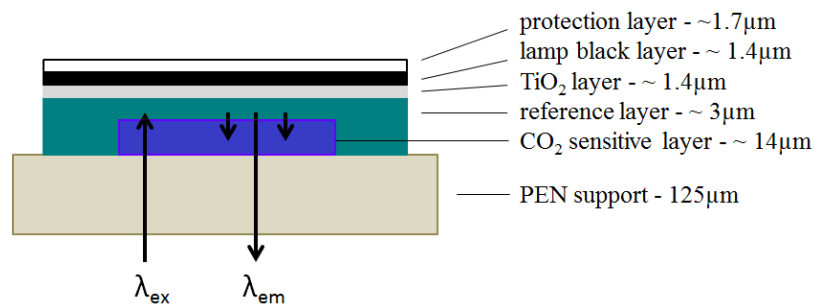


Figure 3.1: Schematic drawing of the applied carbon dioxide sensor foil, containing optical isolation. Approximate layer thicknesses are included.

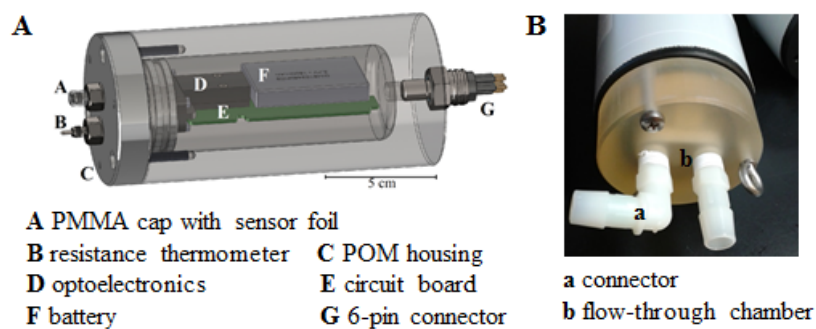


Figure 3.2: 3 dimensional schematic drawing of the read-out device and B: photographic image with mounted flow-through cell.

Commercially available used sensor systems

Characteristic parameters, like temperature, depth and conductivity (to calculate salinity) were measured with several types of CTD systems from Sea-Bird Scientific (e.g. SBE 19, SBE 41+), selected corresponding to the special requirements of each individual deployment. Conductivity and temperature were used to calculate the salinity.^{228 229} Several commercially available sensor systems were used to compare the data obtained with the described sensor system. For each analyte at least one sensor based on different sensor schemes was chosen. For oxygen the 'Optode 4531' from Aanderaa Data Instruments AS was deployed next to our sensor. Similarly the Optode 4531 uses the lifetime-based luminescence quenching principle for the determination of dissolved oxygen.²¹⁵ A SBE 43 Sea-Bird Scientific oxygen sensor based on a membrane polarographic oxygen detector²¹³ and an OxyGuard 840 (OxyGuard[®]) based on a membrane covered galvanic cell²¹⁴ were also available for comparison studies.

A SeaFET Ocean pH sensor from Satlantic/Sea-Bird Scientific was chosen for an additional deployment in the same experiments. The sensor is an Ion Sensitive Field Effect Transistor (ISFET) that determines the pH with two different reference electrodes.^{203 219 220} A second pH sensor was obtained from Hach[®]: GLI Encapsulated LCP (Liquid Crystal Polymer) Differential pH Sensor with internal preamplifier and glass electrode, 5-wire (10 ft. cable), Hach Cat # 6028P0. The sensor measures the pH electrochemically with help of three electrodes.²¹⁷

Carbon dioxide was additionally determined with a C-Sense[™] in situ $p\text{CO}_2$ sensor from Turner-designs. The sensor includes a gaseous CO_2 -permeable membrane, which separates the water sample from a gas filled chamber. The content of carbon dioxide in the chamber is measured by a non-dispersive infrared detector.¹³¹

Reference data

The validation of the obtained sensor data was realized by taking discrete water samples during each deployment. Three samples were taken and prepared for the corresponding method of analysis. Oxygen samples (120 mL) were prepared for a Winkler titration by adding 1 mL manganese(II) chloride solution and 1 mL alkaline sodium iodide solution directly after sampling. The titration was performed at room temperature. pH samples (250 mL) were spiked with 60 μL saturated mercury chloride right after sampling. The pH was determined spectrophotometrically at 25 °C using *m*-cresol-purple as the indicator dye.¹⁸⁸ DIC samples (250 mL) were poisoned with 60 μL saturated mercury chloride and measured with a LI-7000 $\text{CO}_2/\text{H}_2\text{O}$ Gas analyzer (LI-COR[®]) at 25 °C.²³⁰ The CO2SYS software developed by Lewis and Wallace 1998²¹ was used to calculate the carbon dioxide concentration from DIC and pH.

3.3 Calibration procedure

3.3.1 Oxygen sensor calibration

The sensing material for oxygen is based on luminescence quenching of a highly luminescent NIR platinum(II) benzoporphyrin complex embedded in a polymeric matrix. The Stern-Volmer plot describes the decrease of luminescence intensity I and lifetime τ corresponding to the oxygen partial pressure. Since a non-linear Stern-Volmer plot can be observed during calibration, it is assumed, that the indicator complex is embedded in two different environments ('two side model').^{225 231}

$$\frac{I}{I_0} = \frac{\tau}{\tau_0} = \frac{f}{1 + K_{SV}[O_2]} + 1 - f \quad (3.1)$$

where I_0 and τ_0 are the luminescence intensity and lifetime in absence of oxygen, f is the fraction of the total emission and K_{SV} the Stern-Volmer constant for the first site. Moreover, the luminescence quenching is temperature-dependent, which can be compensated by temperature coefficients for τ and K_{SV} (fig. 3.3). Each oxygen sensor has to be recalibrated before and optionally after the deployment for fine adjustment of τ_0 and K_{SV} . A two point calibration at a constant temperature with help of oxygen-free water and air-equilibrated water is sufficient for this purpose. The temperature coefficient is assumed to be constant for all the sensors. The anoxic solution was an aqueous 5 % wt. solution of sodium sulfite containing trace- amount of cobalt(II) chloride (~ 0.001 - 0.01 % wt.). Air-equilibrated water was prepared by a repeated shaking of a water bottle. Preparation of this solution requires particular attention since insufficient air equilibration leads to an overestimation of the oxygen concentration during the measurement. Oversaturation is also possible if the solution is equilibrated with air at lower temperatures than those used for calibration. Therefore, alternative calibration with air and 100 % humidity may be more reliable.

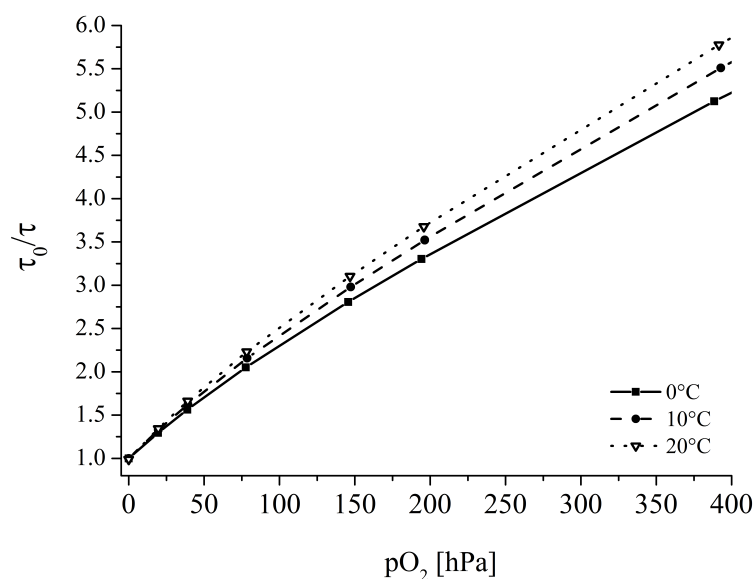


Figure 3.3: Calibration curves of the oxygen sensor material for temperatures between 0 °C and 20 °C. The data were fitted according to the Stern-Volmer equation from the 2-site model.

3.3.2 pH sensor calibration

The calibration of the pH sensing material was performed by adjusting different pH values in artificial seawater with 10 mM of MES, MOPS, TRIS and CHES as buffer substances, by addition of 0.72 M HCl and NaOH. The pH-values were checked with a pH-electrode which was in turn calibrated against spectrophotometric measurements with *m*-cresol purple as indicator dye. Calibration curves were recorded at 0, 2.5, 5, 7.5, 10, 12.5, 15, 17.5, 20, 22.5 and 25 °C and fitted with a Boltzmann sigmoid which was expanded with temperature coefficients for the *top*, *bottom* and *v50* parameters (fig.3.4).

$$\cot(dphi) = \frac{bottom \cdot (1 + bottom_t \cdot (T - 20)) + top \cdot (1 + top_t \cdot (T - 20)) - (bottom \cdot (1 + bottom_t \cdot (T - 20)))}{1 + 10^{\frac{pH - v50 + v50_t \cdot (T - 20)}{slope}}} \quad (3.2)$$

In this equation *bottom* and *top* are the lower and upper limit of the calibration curve, respectively and *top_t* and *bottom_t* are their linear temperature coefficients. *pH* is the pH-value, *v50* the point of inflection and *slope* describes the slope of the curve. *V50_t* is the linear temperature coefficient of the point of inflection. The obtained coefficients are: *bottom_t* = -0.005639, *v50_t* = -0.01122, *slope* = 1.158, *v50* = 8.053 and *top_t* = 0.00026.

Prior to the measurements all deployed sensing materials were recalibrated at 2-points. Due to slight variations in film thickness and composition of the sensing material (ratio of the indicator dye to reference) every sensor is slightly different and the *top* and *bottom* coefficients have to be adjusted. All other parameters and the temperature coefficients are, however, not affected and are assumed constant. The calibrations were done by the addition of Bis-Tris/HCl (pH 7.42 at 20 °C) and Tris/HCl (pH 8.35 at 20 °C) to seawater and the obtained pH-value of the calibration buffers was measured spectrophotometrically. The salinity dependency of the sensor signal is almost negligible for salinities above 20 PSS.

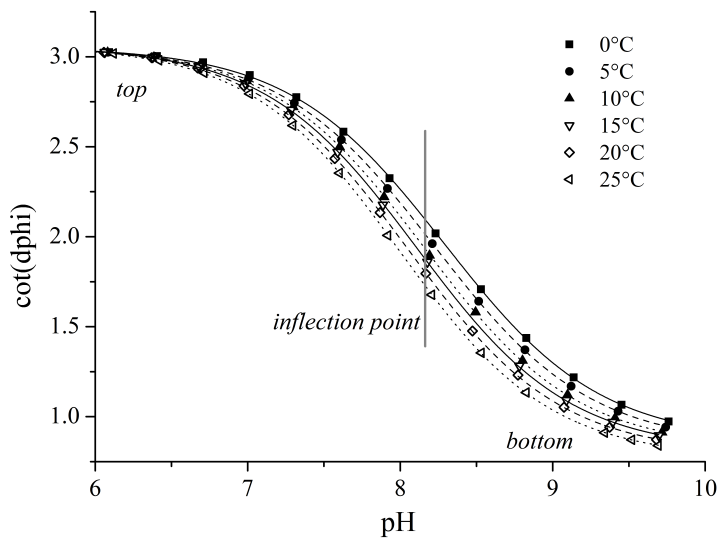


Figure 3.4: Recorded calibration curves of the pH sensor material between 0 and 25 °C at 35 PSS. Only every second calibration curve is depicted. The calibration points were fitted with a Boltzmann sigmoid.

3.3.3 Carbon dioxide sensor calibration

The calibration of the carbon dioxide sensors was performed in a 0.1 M phosphate buffer (pH 7.7) by adding sodium bicarbonate solution to generate increasing levels of CO_2 . The increasing carbon dioxide levels result in a non-linear increase of the measured luminescence phase shift. By plotting the cotangent of the phase angle against the logarithm of the CO_2 concentration an almost ideal fit of the data can be realized by a sigmoidal function with four parameters (fig. 3.5; $R^2 > 0.9980$), equally to pH calibration.

$$\cot(dphi) = bottom + \frac{top - bottom}{1 + 10^{\frac{\log(cCO_2) - v50}{slope}}} \quad (3.3)$$

where *top* is the upper limit, *bottom* the lower limit and *v50* the inflection point (fig. 3.5). The response of optical chemosensors is always temperature-dependent. This dependency can be compensated for adding temperature coefficients to the sigmoidal equation. The following set of parameters for the further developed carbon dioxide sensing material were set at $top_t = 0.02787$, $bottom_t = -0.0044$, $v50 = 1.7429$, $v50_t = 0.01329$, $slope = 1.18156$ and $slope_t = 0.01037$. A more detailed explanation of the calibration procedure can be found in Fritzsche et al. 2017.¹⁰⁸

Due to the production process (variation in the thickness of the sensing layer and reference layer; as well as variations in ratio between reference particles¹⁰⁸), each sensor is slightly different. So it is necessary to recalibrate the sensor right before the deployment. To individually determine the parameters *top* and *bottom* for each sensor, we chose three points at relevant CO_2 levels for recalibration. This recalibration procedure was done before every deployment. The first two points were set at CO_2 level at the beginning and end of the linear region of the sigmoidal curve ($\sim 13 \mu M$ and $\sim 120 \mu M$, fig. 3.5 grey dashed lines). Sparkling water was used for the third recalibration point (supersaturation). It almost represents the value for the parameter *bottom*. Unfortunately this recalibration procedure resulted in underestimated carbon dioxide levels. The most likely reasons for the underestimation of the values on the one hand likely to originate from preparation of CO_2 -free phosphate buffer. A CO_2 -free buffer is hardly reached in reality, but this condition is assumed for the calculations. On the other hand the values for the parameter *top* were too small, resulting in lower calculated carbon dioxide concentrations in the application relevant range between $10 \mu M$ and $100 \mu M$. To calculate the correct actual carbon dioxide concentrations in the performed deployments reference samples were taken to accurately determine the parameter *top* and *bottom*.

To overcome the mentioned problems in the calibration, a new user friendly and less error prone calibration procedure is proposed for correct adjustment of the parameters during the recalibration. The new procedure was developed after the deployments and is a suggestion for future deployments. Reference samples are expected to be not necessary for the adjustment of the parameters. Red vertical lines (fig. 3.5) represent new chosen recalibration points. The first recalibration point was set at $15.2 \mu M$ ($387 \mu atm$; $15 \text{ }^\circ C$; 33 PSS). The preparation of the calibration buffer consists of stirring/shaking seawater with a known salinity overnight till the seawater is fully equilibrated with air. For the second calibration point a carbon dioxide concentration of $47.3 \mu M$ ($15 \text{ }^\circ C$) was chosen. It represents the inflection point of the sigmoidal function ($v50 = 1.7429$). The necessary calibration buffer can be produced by preparing a salt

mixture consisting of sodium chloride, potassium dihydrogen carbonate and sodium hydrogen phosphate to create a phosphate buffer with a pH of 8.04 by adding air-equilibrated deionized water. At the end we kept the last calibration point, created with mineral water. It is the most stable and least error prone calibration point. The new procedure does not shorten the time needed for the recalibration. A stable signal is still essential for a correct adjustment of the parameters.

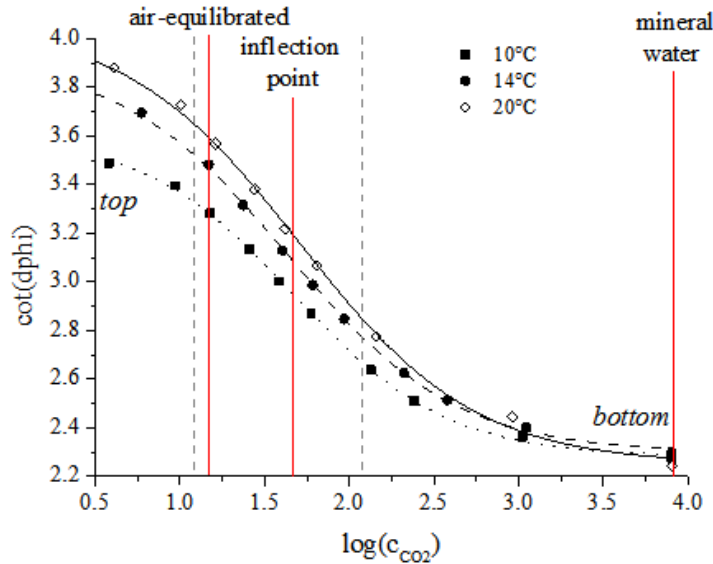


Figure 3.5: Logarithmic calibration plots for four different temperatures between 0 and 8000 μM CO_2 . Lines indicate a fit according to a sigmoidal equation. Dashed gray lines represent former recalibration points (13 μM ; 120 μM ; 8000 μM) and continuous red lines represent new recalibration points.

3.4 Data evaluation

3.4.1 Monterey Bay Aquarium-Open Sea Exhibition

The optode sensors were tested in the Monterey Bay Aquarium in Monterey, California. The Open Sea Exhibition was chosen to install the sensors, due to a relatively stable temperature. The egg-shaped tank (4,500,000 L) has a 24 m broad glass window, contains no plants, a high amount of fish and is continuously monitored. Furthermore, it was possible to compare the performance of the developed optodes with already commercially available sensors under semi-controlled conditions. The fish population during the deployment consisted of 11 dolphin fish (*Coryphaena hippurus*), seven pacific bonito (*Sarda chiliensis*), $\sim 20,000$ sardines (*Sardinops sagax*), five pacific mackerel (*Scomber japonicas*), ten yellow tail (*Seriola lalandi*), six yellowfin tuna (*Thunnus*), 2 green sea turtles (*Chelonia mydas*), one scalloped hammerhead shark (*Sphyrna lewini*) and two pelagic sting rays (*Dasyatis violacea*). The high number of marine animals suggests high variations in dissolved oxygen, pH and carbon dioxide due to metabolism. Sea water was pumped into the tank from the Monterey Bay. The salinity was assumed to be stable and set to 33.48 PSS. The optodes were installed close to the outtake of the sea water on the left side of the exhibition tank, whereas the commercial monitoring sensors were located

close to the intake of the sea water on the right side of the exhibition tank. The monitoring sensor package consisted of an OxyGuard 840 oxygen sensor (OxyGuard[®]) and an electrochemical pH sensor from Hach[®]. The distance between the two sensor packages can result in differences in the two data sets. The optode package position was chosen corresponding to the guidelines of the Aquarium. Reference samples were taken three times (April 5th 5 pm; April 7th 4:30 pm; April 11th 4 pm GMT) close to the sea water outtake. Feeding times were each day 6 pm GMT (11 am Pacific time, PT). The measurement interval was set to 10 minutes for the optodes, 5 minutes for the OxyGuard 840 and undefined for the Hach pH sensor.

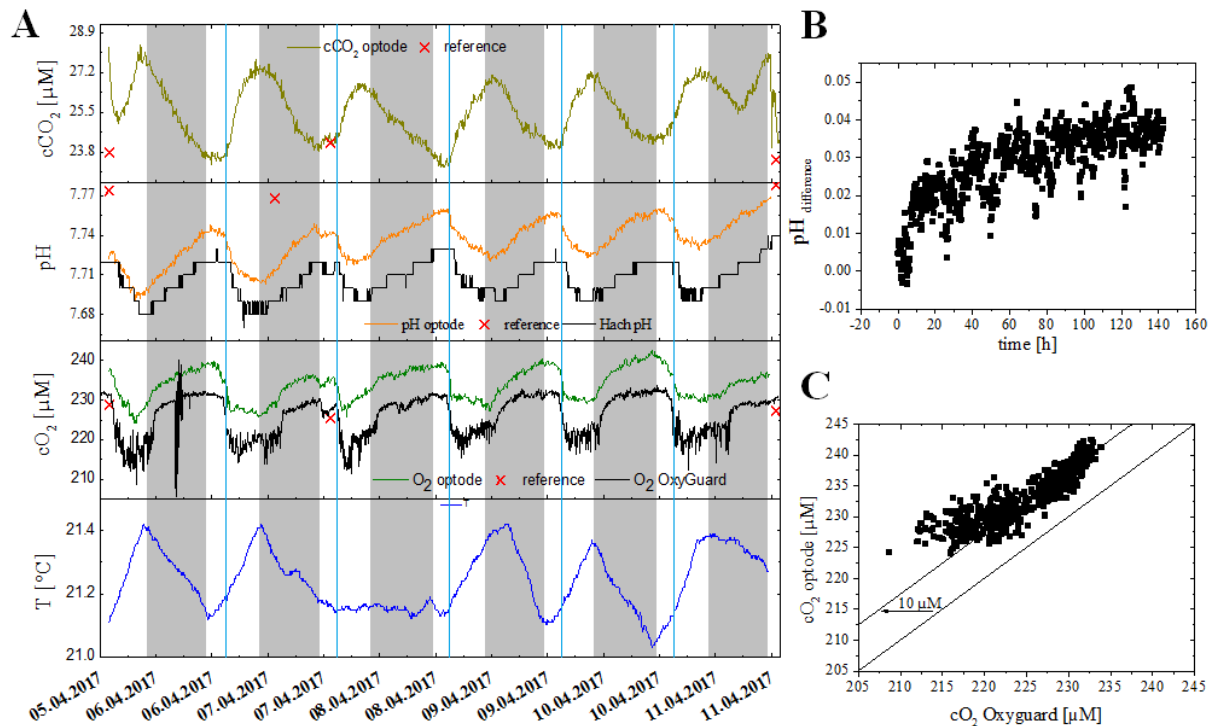


Figure 3.6: Optode CO_2 (dark yellow), pH (orange), Hach pH sensor (black), optode oxygen (green), OxyGuard840 oxygen sensor (black) and temperature (blue) data obtained with different kind of sensors in the Open Sea Exhibition, Monterey Bay Aquarium. Red crosses are reference values determined in the lab. Marked in grey night times (6 pm-7 am PT). Bright blue vertical lines represent feeding times. B: Differences in the pH measured by the electrode and the optode over deployment time. C: Cross correlated oxygen data.

The sensor data sets are in a reasonable correlation to each other (fig. 3.6A). High drops in dissolved oxygen and increases in pH and pCO_2 , induced by the fish metabolism (clearly visible after times of feeding marked in bright blue fig. 3.6A) occur during the day (unshaded sections fig. 3.6A) as water is recirculated. Oxygen increases during the night as Monterey Bay water is circulated into the tank. The carbon dioxide sensor showed no sign of poisoning by other acidic gases. The first reference point was taken right after the installation. Due to the long response time of the carbon dioxide sensor the equilibrium for the first reference point was not reached. Therefore, the second reference sample (April 7th 2017 4:30 pm GMT) was used to adjust the carbon dioxide concentration.

As can be seen, the pH optode and the Hach pH sensor show excellent correlation. Much better resolution of the optode is evident. The data produced by both sensors slightly deviate from the reference values (0.055 and 0.023 pH units for the Hach sensor and optode, respec-

tively). The deviation between the pH sensors increases slightly over time from 0.02 pH units at the beginning to 0.035 pH units at the end of the experiment (fig. 3.6B). The optode pH data are in reasonable accordance with the carbon dioxide data.

The dissolved oxygen dynamics obtained by two different sensing techniques (optical and electrochemical) are generally in good agreement. Interestingly, the readings provided by the electrochemical sensor are very noisy in the lower range of oxygen concentrations (210-220 μM ; 94-96 % air.sat), which might be due to electromagnetic interferences of unknown origin. In contrast, the noise is low in case of the optode and may represent minor fluctuations in DO detected by the optode. The deviation to the reference measurements are 4 % and 1 % for the optode and the OxyGuard840, respectively. It may also result from the calibration: as was discussed above, insufficient saturation of the calibration solution with air would result in overestimation of the DO concentration. Therefore, calibration in gas phase at 100 % humidity and constant temperature may be a better option in future. The almost constant offset of 10 μM between the optode and the electrochemical sensor, except for the regions with high noise, support the explanation of an insufficient calibration (fig. 3.6C).

3.4.2 MLML-Aquaculture facility, seawater intake system

For another deployment the monitoring flow system of the seawater intake in an aquaculture facility, Abalone farm (Haliotis; approximate size: 1.5-3 cm) was chosen. Here, sensors for and $p\text{CO}_2$ were already installed to control the water quality. The installed sensors were a SBE 19 CTD (Sea-Bird Scientific), an Optode 3835 for oxygen (Aanderaa Data Instruments AS) and a C-Sense $p\text{CO}_2$ sensor (Turner design) for carbon dioxide. The optodes were placed in line with these sensors. A flow through cell (fig. 3.2B) was designed and 3D printed for this deployment. The flow rate was set manually to 1-1.5 l/min. Reference samples were taken two times (March 29th 11:55 pm; April 3rd 22:15 pm GMT). The measurement interval for all sensors was set to 5 minutes. The temperature (fig. 3.7) and salinity (data not shown) showed only minor fluctuations.

The obtained data from the optodes are in an excellent agreement with the data of the commercially available sensors for $p\text{CO}_2$ (fig. 3.7C) and oxygen (fig. 3.7D). Moreover, the reference measurements correspond well with all installed sensors. Notably, the uncorrected data from the $p\text{CO}_2$ optode showed a lag time of 31 minutes due to the rather slow response time induced by the used perfluorinated polymers.¹⁰⁸ Correction for this delay (shift by -31 min) completely eliminated this discrepancy. The dissolved CO_2 concentrations measured by the optode and the C-Sense sensor vary in the upper (50-55 μM) and lower region (20-25 μM), but this deviation does not exceed 16 % of the measured value (fig. 3.7C). Both oxygen optodes show excellent correlation except for the period from April 1st 2017 to April 2nd 2017 where deviation up to 20 % at low DO concentrations is observed (fig. 3.7D). The reason for this phenomenon is not clear.

Unfortunately, the pH sensor of the water control system was not available during the measurement period so that only the data provided by the optode were collected. The obtained pH values varied strongly between 7.6 and 8.0, which fits well to the strong fluctuations in carbon

dioxide concentration. Notably, the reference point measurements confirmed both a rather low pH / high CO_2 and a rather high pH / low CO_2 value. Overall, the correlation between all three optodes was excellent. The data reveal high signal changes almost every 12 hours corresponding to the times of low tide in the Monterey Bay (fig. 3.7B).

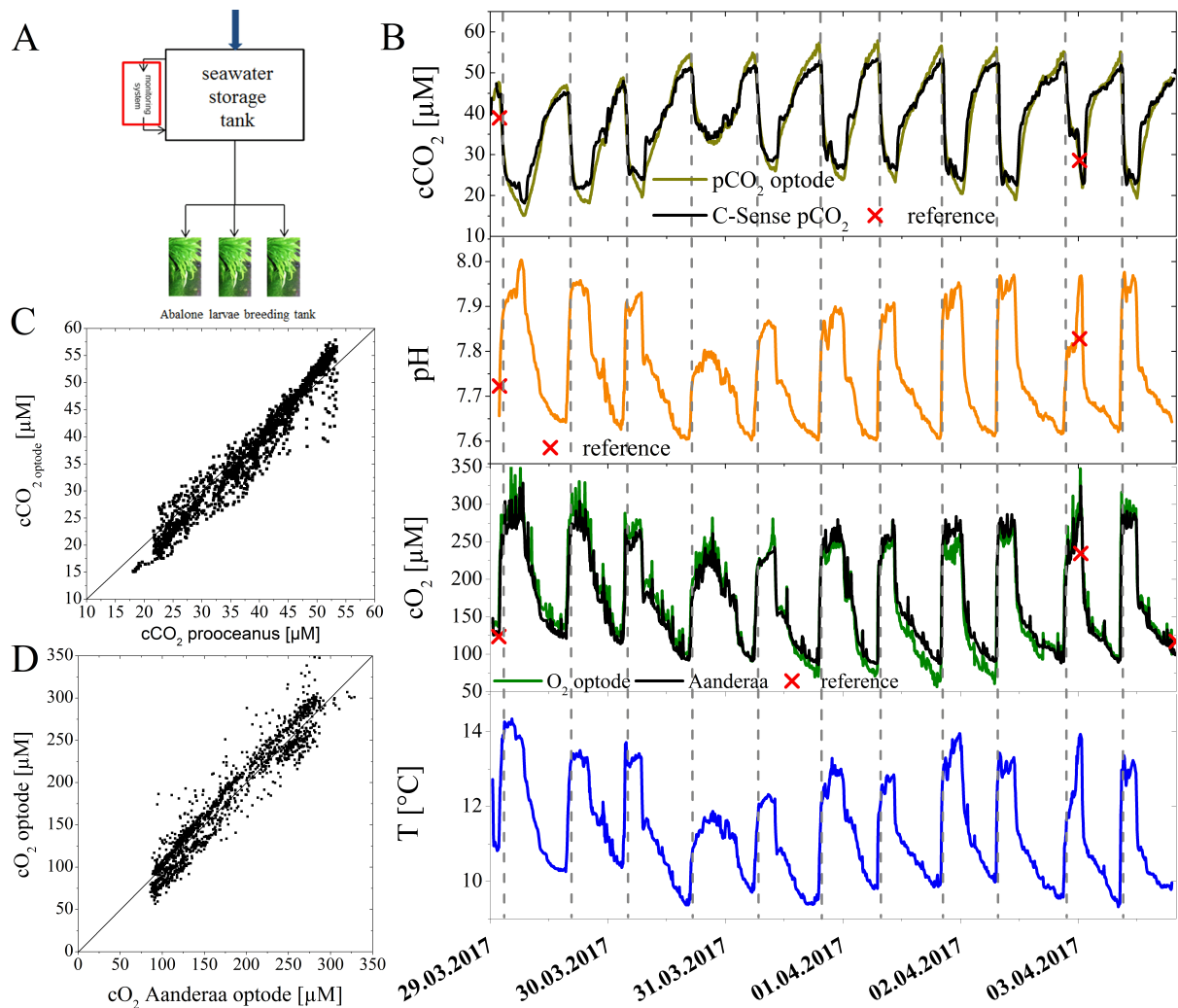


Figure 3.7: Scheme of the Abalone larvae breeding tank seawater supply. Sensor position marked with red box. B: CO_2 optode (dark yellow), C-Sense CO_2 sensor (black), pH optode (orange), developed oxygen optode (green), Aanderaa oxygen optode (black) and temperature (blue) data obtained in the Abalone farm seawater intake monitoring flow system. Red crosses are reference values determined in the lab. Vertical dashed grey lines mark times of low tide. C: Cross correlated CO_2 data. D: Cross correlated oxygen data.

3.4.3 MLML-Aquaculture facility, Abalone larvae breeding tank

The applicability of the developed sensors for oxygen, pH and carbon dioxide was tested by measuring the conditions in a breeding tank of Abalone larvae (*Haliotis*; approximate size: 1.5-3 cm), figure 3.8B. The tank had a volume of $4.5 m^3$ (1.2 m x 1.2 m x 3 m). It was continuously flushed with air, the water was renewed with fresh sea water of the Monterey Bay and the tank was exposed to direct sunlight. The water contained a high mass of different algae species to feed the Abalone larvae. The sensors were placed directly under the water surface for 5 days and were set to measure every 2 minutes.

The recorded data for oxygen, pH and carbon dioxide reveal a day/night cycle induced by algae metabolism (fig. 3.8B). An increase in the oxygen concentration goes along with a decrease in the CO_2 concentration, as well as with an increase in pH. The dynamics during days with a high amount of sunlight (i.e. high intensity of ambient light, which is also measured by the optode, fig. 3.8B), can be clearly distinguished from that during cloudy days by the consumption of carbon dioxide, which is in direct relation to the photosynthetic activity of the algae. Moreover, a slight increase of oxygen and pH, as well as a slight decrease of the carbon dioxide concentration in the sea water can be observed over the 5 days of measurement. The metabolism of the Abalone larvae is negligible. Biofouling protection was not considered necessary for this deployment, due to the short deployment time.

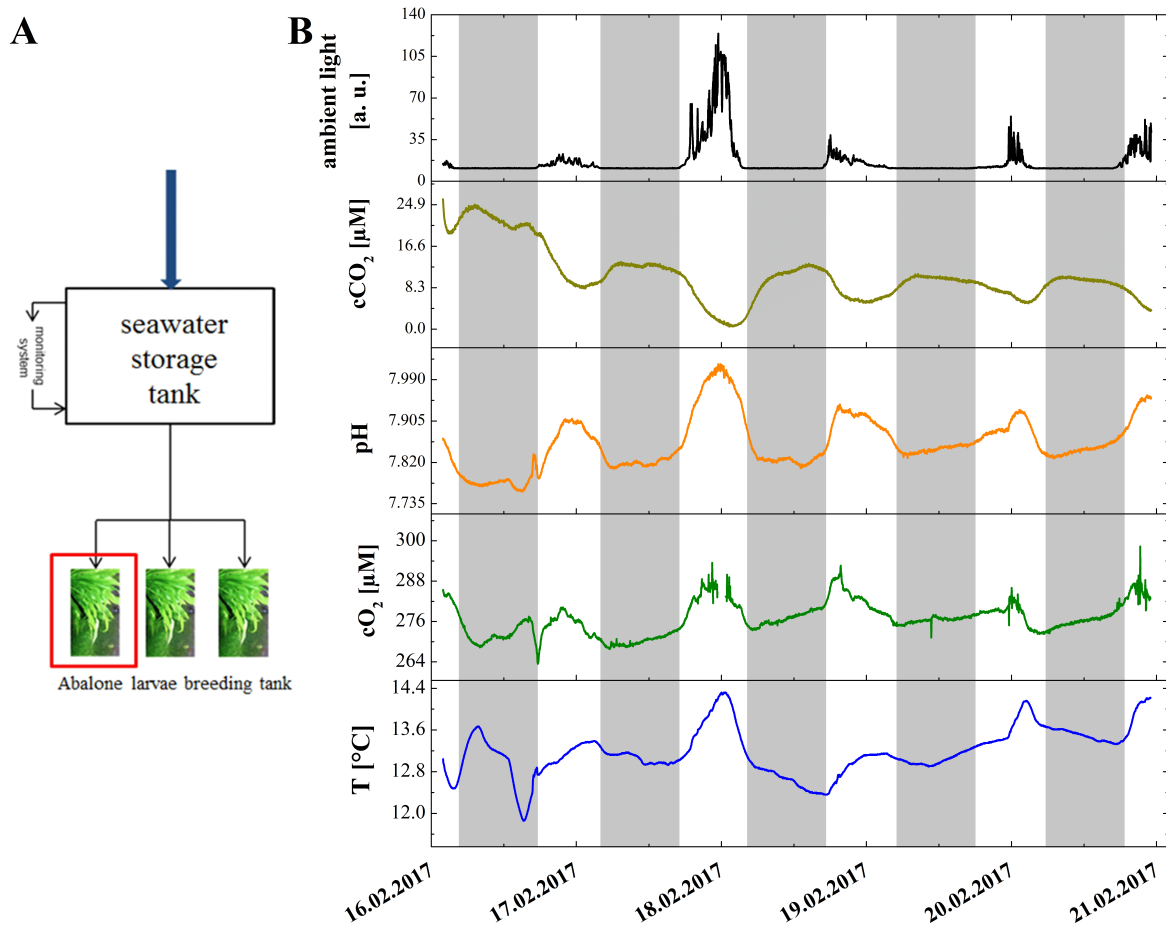


Figure 3.8: A: Scheme of the Abalone larvae breeding tank seawater supply. Sensor position marked with red box. B: Ambient light (black), cCO_2 (dark yellow), pH (orange), oxygen (green) and temperature (blue) data obtained with the developed set of sensors in an Abalone larvae breeding tank exposed to direct sunlight (white and grey zones day and night time, respectively). The time was set to Greenwich Mean Time (GMT, PT +9). Oxygen measurement interruption due to air bubbles on the sensor foil.

3.4.4 Elkhorn Slough-Mooring buoy LO1

This deployment was set in a highly dynamic environment, which represents a special challenge for sensors. The set of optodes was deployed at a mooring buoy in Elkhorn Slough, a national estuarine research reserve next to Moss Landing, California. The buoy located $36 + 48'45''N$ and $121 + 46'29''W$, was initially deployed October 2003 and is operated by MBARI. A detailed description of the buoy can be found in Jannasch et al. 2008.²²⁹ The sensors were placed one meter below water surface at a bracket in a vertical row. The water in the Elkhorn Slough is influenced by the tidal cycle and a high amount of nutrients from the inland. We expected a high variation in temperature, salinity and all three measured parameters. The mooring buoy was already equipped with the following sensors at 1 m water depth (measurement interval 1 hour): SBE 16+ CTD system from SeaBird Scientific, an optode 4531 oxygen sensor from Aanderaa Data Instruments AS, a SeaFET pH sensor from Satlantic and an SUNA nitrate sensor from Satlantic. The measurement interval of the optodes was set to 5 minutes. Reference samples were taken at February 23th between 6:45 pm GMT and 11 pm GMT every 30 minutes to capture the change of the dissolved oxygen, pH and carbon dioxide at the time of low tide (2 pm). Biofouling protection was not necessary, because of the short time of deployment.

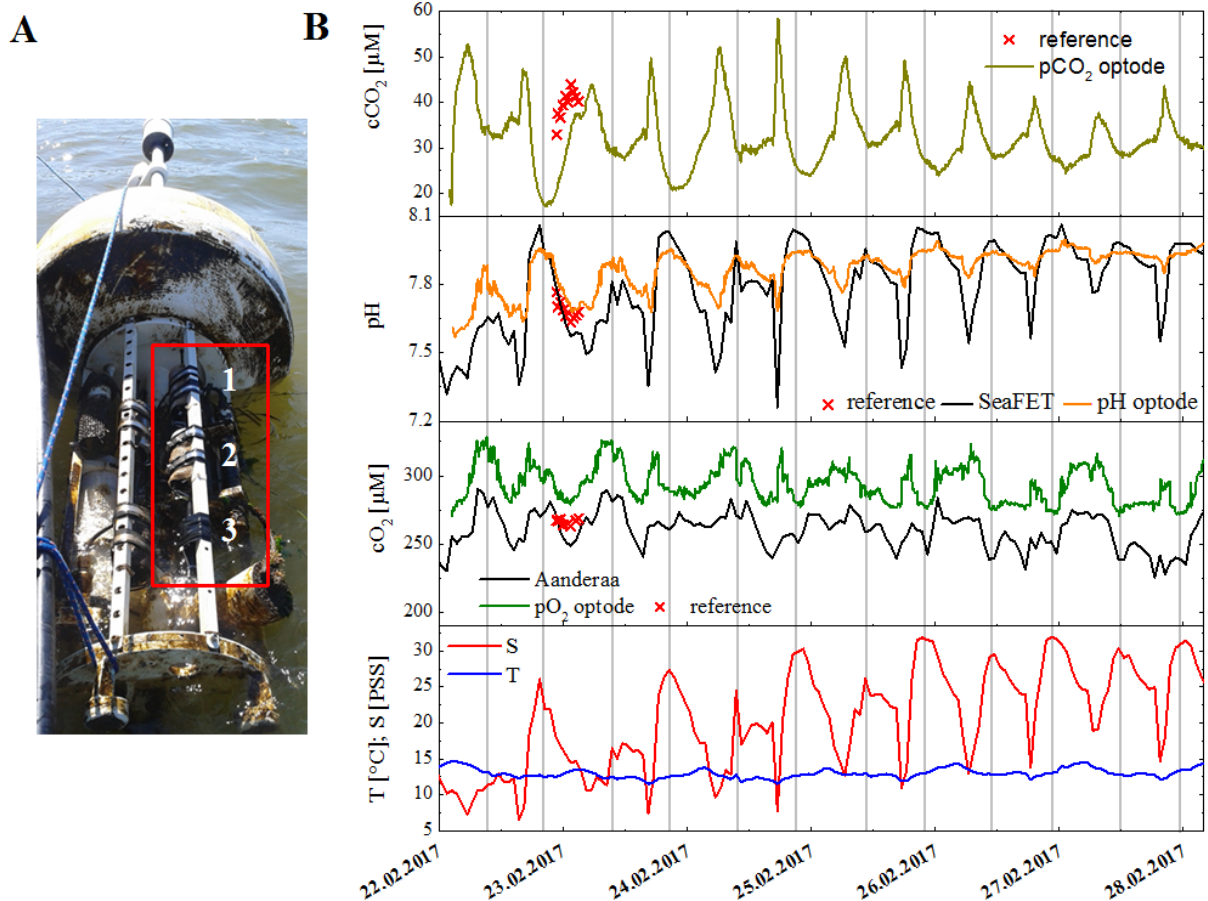


Figure 3.9: A: Photographic image of the mooring buoy LO1 with the attached sensor package. B: Optode CO_2 (dark yellow), pH (orange), SeaFET pH sensor (black), optode oxygen (green), Aanderaa oxygen optode (black) and temperature (blue) and salinity (red) trace obtained with different kind of sensors at the LO1 mooring buoy in Elkhorn Slough, Moss Landing. Red crosses are reference values determined in the lab. Times of high tide were marked with vertical dashed lines.

The correlation of the deployed optodes for oxygen, pH and carbon dioxide was remarkable even in a continuously changing environment (fig. 3.9B). The carbon dioxide data reveal a decrease in variations and a slight decrease of the overall concentration over the 6 days deployment. The reference points are 4 hours shifted to earlier times, which can be explained by differences in water depths for both measurements. Whereas the carbon dioxide sensor was installed at the end of the bracket in 1 m water depth, the reference samples were taken at the water surface. During the tidal cycle the water mass movement starts at the surface and is tardy, which explain the above shift.

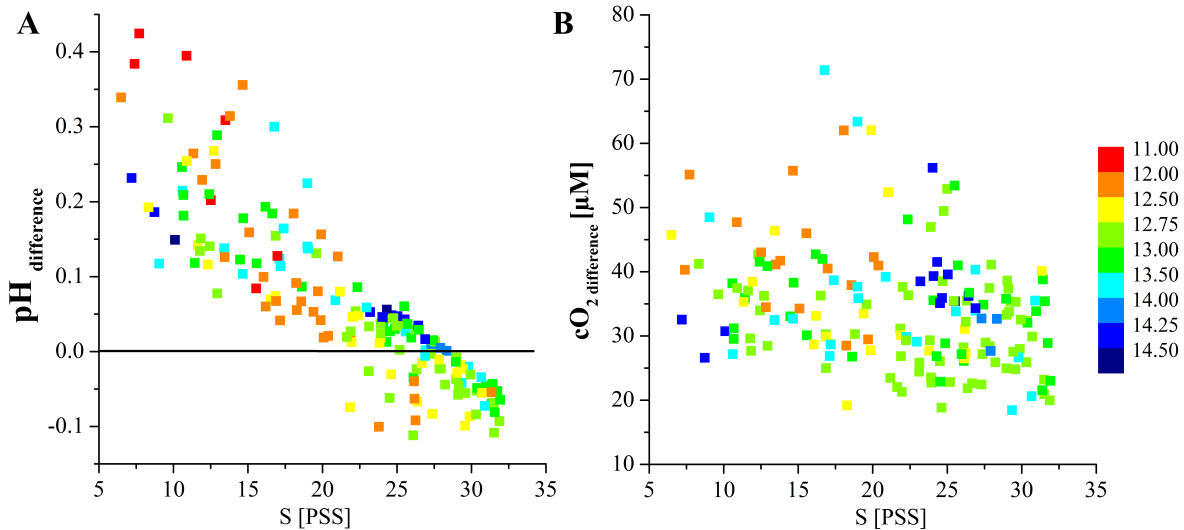


Figure 3.10: Effect of salinity on pH differences ($pH_{optode} - pH_{SeaFET}$) (A) and cO_2 differences ($cO_{2optode} - cO_{2Aanderaa}$) (B) depending on the temperature (color coded) at LO1 mooring buoy in Elkhorn Slough.

The pH data of both sensors are in a good accordance with the spectrophotometrically determined reference values. The deviation is less than 0.9% and 1.2% for the developed optode and the SeaFET pH sensor respectively. Driven by the carbon dioxide concentration the pH variations decrease during the time of deployment and a slight increase in pH is also observable. This increase was 0.21 units and 0.29 units for the developed optode and the SeaFET pH sensor, respectively (smoothed data used). The comparison of the two pH data sets reveals a strong difference in the measured pH changes during the tidal cycle (optode max. 0.28 units; SeaFET: max. 0.78 units). pH differences between the optode and the SeaFET sensor reveal a clear salinity dependency (fig. 10A). At salinities higher than 25 PSS variations in the differences between the pH values are almost consistent. Salinities below 20 PSS result in high and inconsistent pH differences, particularly at salinities between 6 and 10 PSS. Therefore further salinity correction might be necessary for deployments in estuaries with salinity values below 20 PSS. Investigations dealing with salinity compensations were done for both sensors.^{149 203 232 233} Calculated pH values using the CO2SYS program, inserting the total alkalinity (estimated from the salinity) and measured pCO_2 concentrations, were between the two data sets. In contrast to the salinity effect temperature appears not to affect the differences in the pH readings (Fig. 3.10A).

The comparison of the two oxygen data sets shows a satisfactory agreement in the trend, each

change in the oxygen concentration could be found at the same time in both data sets. The data of the developed optode shows fine variations in DO concentrations, which is due to a shorter measurement interval. Moreover the values of the developed optode are shifted to higher values of in average $34 \mu\text{M} \pm 9.3 \mu\text{M}$ with no observable temperature or salinity dependency (fig. 3.10B). A presumable reason is a not-optimal calibration of the sensor at air-saturated conditions. The DO concentrations measured by both optodes differ from the reference values, obtained by Winkler titration, by 6% at maximum. Whereas the values for the developed optode appear to be overestimated for the reason described above, the data obtained by the reference sensor seem to be underestimated. An adjustment of both data sets reveals a slight drift to lower oxygen value of the Aanderaa oxygen optode, which can just partly be explained by a decrease of dissolved oxygen in the water. Fouling of the sensor foil with oxygen consuming algae could be a more likely reason for the observed drift.²¹⁵

3.4.5 Monterey Bay- AUV integration

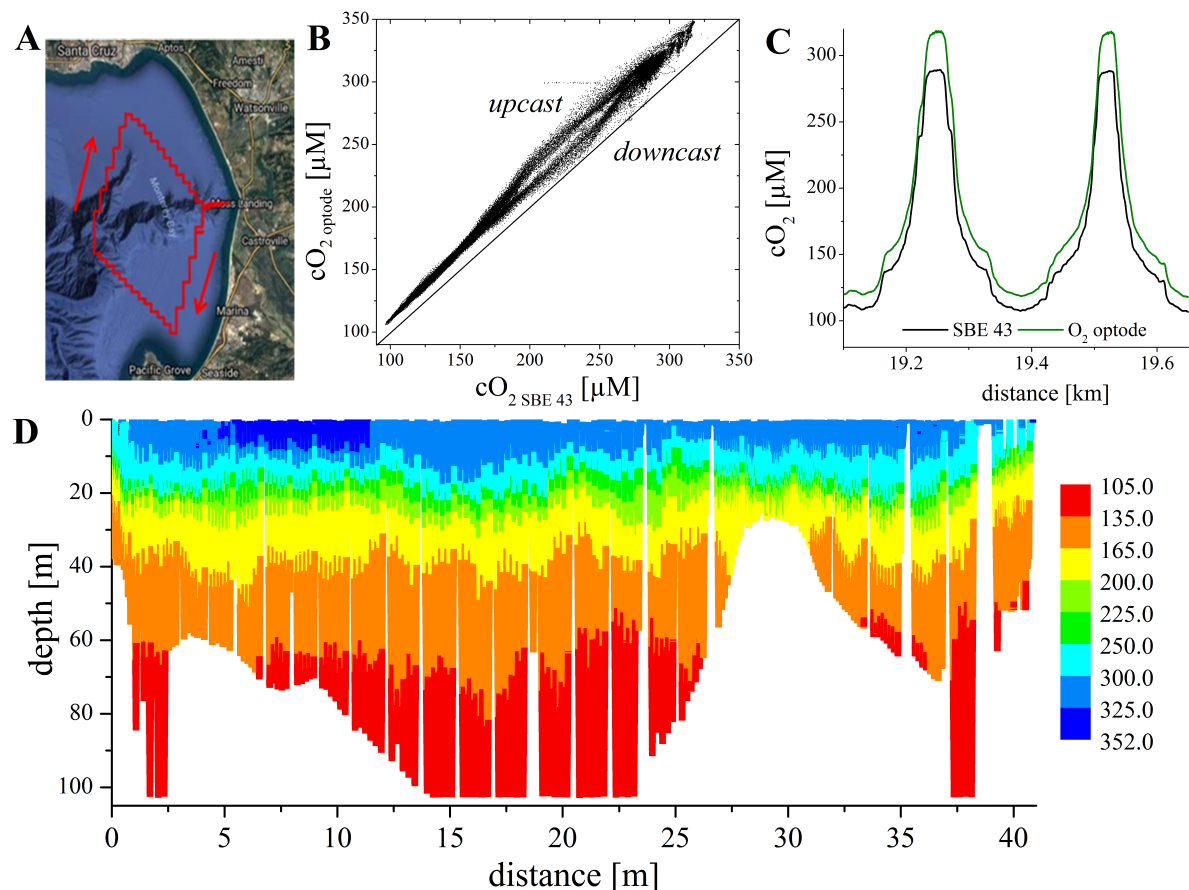


Figure 3.11: A: AUV turn in the Monterey Bay starting at the MBARI, picture generated with GPS Visualizer; B: Cross correlated oxygen data obtained during an AUV turn at March 9th 2017. C: Oxygen data obtained by an SBE 43 sensor (black) and oxygen optode (green). D: Oxygen depth profiles in μM (color coded) collected with the developed oxygen optode in the Monterey Bay.

The oxygen optode was integrated in an AUV as well. The sensor was placed in the front of the vehicle and connected to a pump system using a flow-through cell. The deployed AUV was a

910 Marc Dorado class, 2.5 m long and 0.5 m in diameter. The duration of the test was set to 24 hours with a motion speed of 0.5 m/s. It moved between the water surface and 100 m water depth (fig. 3.11A) and was equipped with a SBE CTD system and a SBE 43 Sea-Bird Scientific oxygen sensor. Due to the continuous movement of the AUV, the measurement interval was set to one second for each sensor. The vehicle was dropped close to Moss Landing in the Monterey Bay and measured more than 150 profiles (fig. 3.11D). No reference samples were taken during the deployment.

The developed oxygen optode showed a highly pleasing performance in terms of device size and response time. The continuous movement of the AUV in combination with the fast response time leads to well resolved DO depth profiles of the Monterey Bay. The comparison with the routinely installed SBE 43 oxygen sensor (Sea-Bird Scientific) revealed a shift of around 10 % to higher dissolved oxygen concentrations of the optode oxygen data. The most likely reason is insufficient air saturation during calibration of the oxygen optode, but it might also be due to the calibration of the oxygen electrode. Moreover the cross correlated oxygen data shown in figure 3.11 B revealed a difference in the response times of the sensors. The oxygen optode seems to have a longer recovery time than the electrochemical SBE 43 oxygen sensor. A likely reason is the storage of oxygen in the support material, which gets released slowly during recovery (in this deployment equal with upcast).

3.4.6 Monterey Bay- Profiling float

A second integration on an autonomous platform for oceanographic applications was done with a prototype of a profiling float developed at the MBARI. The float weights around 40 kg in air and has an adjustable weight in water. By changing the overall volume of the float and keeping the mass constant it was possible to regulate the depth of the float.²³⁴ The platform velocity was set to 0.2 m/s during the deployment. The float was programmed to park at 100 m for 3 hours (anchors if it hits the bottom for 3 hours), to measure a profile and to again park at 100 m. Furthermore, the already integrated sensors were programmed to measure every 30 minutes during the parking, through the ascend process every 5 meters from the full depth to 20 meters and every 2 m from 20 m to the surface. Only the data of the ascend process (upcast) was logged, to minimize the necessary data storage and transmitted data volume. The float was equipped with a GPS system, a SBE 41+ CTD system from Sea-Bird Scientific and an Optode 4330 from Aanderaa Data Instruments AS. The integration of the optodes for dissolved oxygen and pH was realized by a customized bracket made of 6061-T6 aluminium. The measurement interval of the optodes was set to one second. Due to a slow response time, the carbon dioxide sensor was not applied. No reference samples were taken during the test deployment.

Overall the profiling float measured 24 profiles in 5 days. Figure 3.12 B shows the profiles number 1, 12 and 24. The profiles reveal a drastic change in the water masses between 10 and 30 m water depth, which can be confirmed by the AUV data (section 3.4.5). In contrast the last profile showed no distinguishable water masses, but an overall trend within the whole measured water column. The profiling float was in constant weather-driven movement. Therefore the up-

and downcasts are not necessarily performed at the same location, which makes a statement about hysteresis complicated. In the case of the 12th profile, the temperature indicates almost no change in the position between the measured up- and downcast. The oxygen and pH data obtained by the developed optodes are very similar for both casts and confirm that the response of both optodes is sufficiently fast for profiling applications. The DO values obtained with the presented optode are always higher than the values measured by the Aanderaa oxygen optode ($\sim 13\%$ in average). The most likely reason is again offset in calibration of our optode. It should also be mentioned that the collected data volume of the presented optodes is very high (33.000 KB each). This is not an issue if the data are downloaded manually, but a measurement program with times of inactivity would be necessary if data transmission is intended.

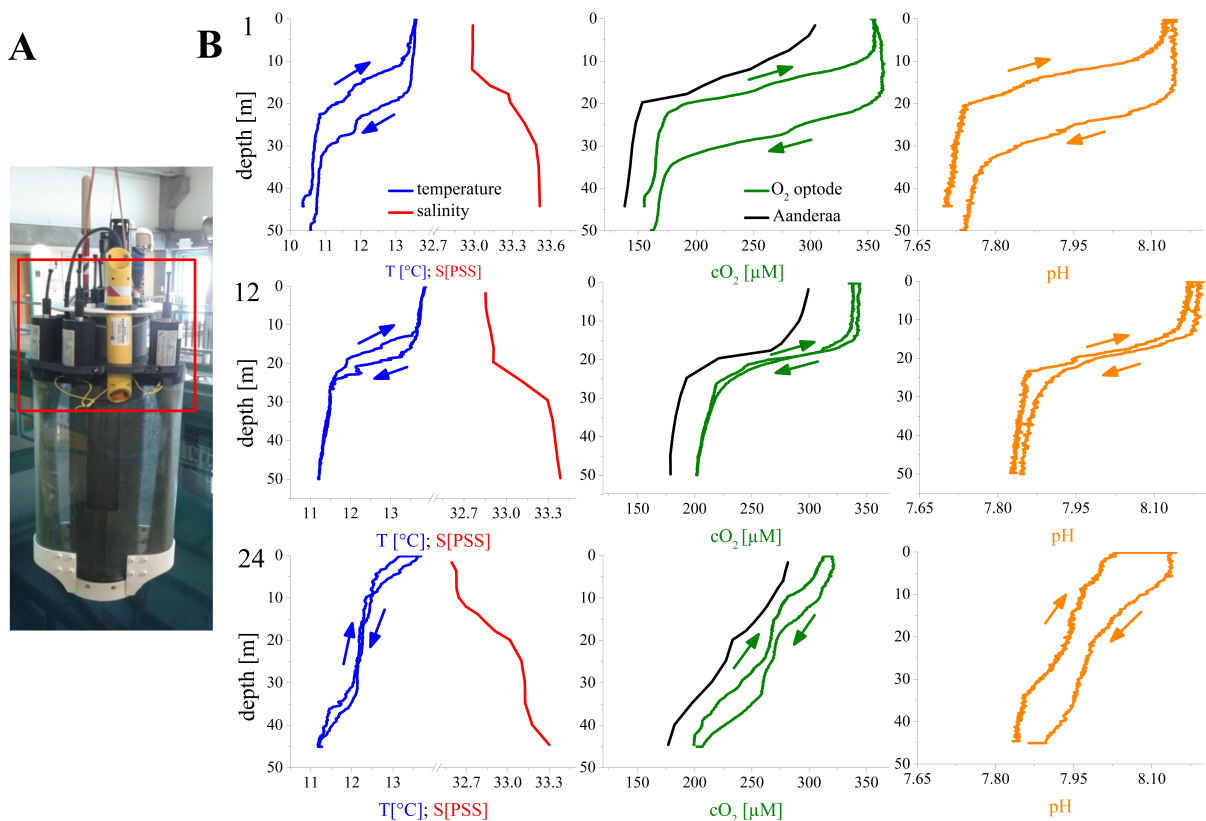


Figure 3.12: A: Photograph of the profiling float before deployment. Sensor location marked with a red box. B: Temperature (blue), salinity (red), optode oxygen (green), Aanderaa oxygen optode (black) and optode pH (orange) data obtained during a profiling float turn in March 2017 in the northern Monterey Bay. First line represents the first profile, the second line the 12th profile measured at day three and the third line the last profile (day five).

3.4.7 Elkhorn Slough-pH sensor long-term testing

So far we presented exclusively optode tests shorter than one week. Another interesting characteristic of a sensor/optode is the long-term stability. According to the specifications of the oxygen sensor foil producer (PyroScience GmbH) it is suitable for at least 10,000,000 data points.²³⁵ The long-term stability of the used carbon dioxide sensor foil was already tested over 35 days in laboratory conditions (Fritzsche et al. 2017¹⁰⁸). The minor modifications of the foil composition were not considered to influence the stability. A relatively short-term stability test for the developed pH sensor was performed at the earlier described mooring buoy in the Elkhorn

Slough (section 3.4.4). However, the pH optode has neither being tested over a longer period of time, nor in the highly dynamic environment with high risk of biofouling. These conditions were met by the test in a National Estuarine Research Reserve in central California. The water mass was influenced by the tidal cycle (annual tidal range maximum: 2.5 m). The salinity can change heavily, especially after heavy rainfall events. The nutrient concentration was high, due to extensive agriculture in the watershed, particularly lettuce and strawberries. The estuary was moderately to highly eutrophobic resulting in microalgal mats.²³⁶ The test for the pH optode took 8 weeks from February 6th 2017 to April 2nd 2017. Biofouling protection was indispensable for this test. It was realized via copper guards made of a 100 % copper net integrated in a plastic frame (fig. 3.13A). The measurement interval was set to ten minutes. For this deployment an in situ 2-point recalibration was used (February 23rd 10 pm; March 16th 11:30 pm GMT).

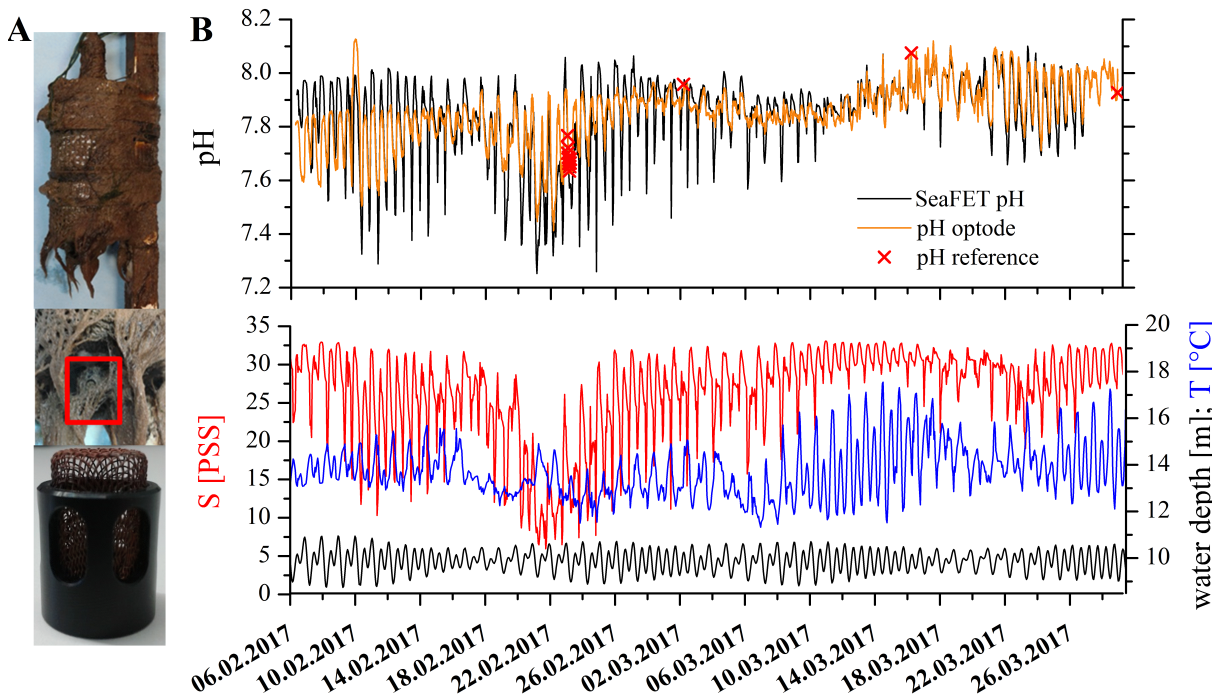


Figure 3.13: A: Photographic image of the sensors after 8 weeks of deployment in a highly biological active environment. Location of the copper guard against biofouling (enlarged image below) is marked with red box. B: Optode pH (orange), SeaFET pH (black), temperature (blue), salinity (red) and water depth (black) data measured during the long-term stability test of the developed pH optode. Reference samples are marked with red crosses.

During the deployment the salinity varied dramatically from 6 PSS up to 33 PSS. Such variations reflect the predominance of seawater at times of high tide and of water from the inlands, which mix up with seawater at low tides. Especially times with a high amount of rain in the catchment area of the estuary lead to a very low measured salinity at the mooring buoy (fig. 3.13B: February 18th to February 26th). Moreover river water carries a lot of nutrients, resulting in a high rate of algae growth at the sensors and the buoy itself. The copper guard provided a sufficient protection for the sensor foil (fig. 3.13B). The optode pH data showed no direct sign of drift caused by biofouling. Overall the pH values correspond with the variations induced by the tidal cycle. The recorded water depths maxima correspond with the phases of the moon (new moon: February 26th and March 27th; full moon: February 10th and March 12th). The

variations in salinity and pH were higher in February than in March. This observation can be explained by the high amount of rain throughout February (average February: 6.6 mm; average March: 1.8 mm).²³⁷

The optode pH data are generally in a good agreement with the SeaFET pH data. Similarly to the short term test at LO1 (Elkhorn Slough), the salinity is an important factor in the comparison. The larger data set reveals a mean difference between the data sets for a salinity > 25 PSS of -0.027 ± 0.059 , 20-25 PSS of 0.03 ± 0.063 and below 20 PSS of 0.155 ± 0.106 . Overall the salinity is an important factor measuring the pH for both sensor systems. The temperature did not affect the pH differences significantly, which indicates an adequate temperature correction. As can be seen, the salinity changes are much smaller from 12th to 28th of March, and both the optode and the SeaFET show very similar results. Overall, the optode is found to be excellently suitable for measurements in highly variable conditions and strong biofouling providing that the copper guard is additionally used.

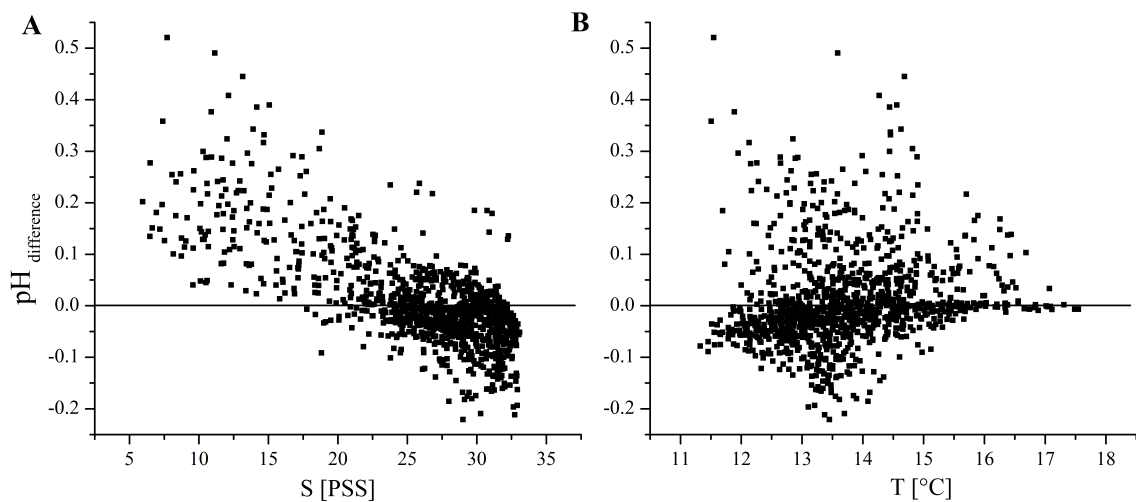


Figure 3.14: Effect of salinity (A) and temperature (B) on the pH differences ($pH_{optode} - pH_{SeaFET}$) from February 14th to March 26th.

3.5 Summary and discussion

We presented a validation and integration study of a new, small, versatile and easy-to-use sensor for dissolved oxygen, pH and dissolved carbon dioxide measurements in marine environments. The sensors were used to monitor algae metabolism in an aquaculture facility, as well as fish metabolism the open sea exhibition in the Monterey Bay Aquarium. In both cases the day/night cycles were recorded and special events like feeding times and times of high sun light were observable. The sensors were installed in a monitoring flow path at an aquaculture facility to ensure the quality of seawater. The tidal cycle is clearly recognizable in all three parameters. Even in a highly dynamic environment the sensors showed satisfactory performance. During all deployments the optodes for the three parameters were in good correlation. An increase in dissolved carbon dioxide leads in a decrease of the pH and in most cases a decrease in dissolved oxygen. We also successfully integrated the pO_2 sensor in an AUV travelling with a velocity of 0.5 m/s. The response time of the sensor was fast enough to measure highly resolved oxygen

profiles of the water column till 100 m. The integration of a $p\text{O}_2$ and pH sensor in a profiling float showed the applicability in case of a continuously moving platform, as well. Moreover the data obtained with the developed sensors were compared to the data delivered by commercially available sensors based on various sensing schemes for all three parameters. This comparison revealed a good agreement with a deviation of maximum 13 %, 1.2 % and 16 % for dissolved oxygen, pH and carbon dioxide, respectively. The crucial point of each sensor usage is the recalibration right before the deployment. An inadequate recalibration leads to incorrect values of the calculated variable parameters and consequently to the deviation in calculated $p\text{O}_2$, pH or $p\text{CO}_2$. Therefore, we developed a more simple recalibration and calculation procedure for the pH and dissolved carbon dioxide sensors. Unfortunately, the dissolved oxygen values obtained by the optode at conditions near air saturation or above this value appear to be overestimated in most cases. This deviation can be explained by lower than 100% air saturation of the second calibration solution. Here, more robust calibration procedure (e.g. in gas phase and 100% humidity) is desirable for future measurements. Moreover we investigated the long-term stability of the pH sensor in a highly dynamic environment (Elkhorn Slough) over 8 weeks. Absence of drift confirmed high stability of the sensing materials and efficiency of the chosen biofouling protection strategy (copper guard).

3.6 Acknowledgement

Financial support by the European Union FP7 Project SenseOCEAN-Marine Sensors for the 21st century (Grant Agreement Number 614141) and the Graz University of Technology (Research Abroad fellowship) is gratefully acknowledged. Deployments on platforms at MBARI were supported by the David and Lucile Packard Foundation. Measurements in the Moss Landing Marine Laboratories (aquaculture facility) were realized by the help of Jason Adelaars.

Chapter 4

Improved response times of pH and pCO₂ optodes for profiling applications in seawater

This chapter was prepared for submission to the 'Journal of Atmospheric and Oceanic Technology'.

Authors: Eva Fritzsche, Christoph Staudinger, Timea Hegediš, J. Timothy Pennington, Marguerite Blum, Jan P. Fischer, Kenneth S. Johnson, Sergey M. Borisov, Ingo Klimant

Profiling measurements are often performed during monitoring programs. Sensors used for this purpose have to have a fast response time to minimize the time needed for one profile. Fast responding temperature, salinity and oxygen sensors have been established so far. In this work, we investigated the effect of different parameters on the response times of already existing sensing materials for pH and carbon dioxide. Selected materials, sensor composition and layer thickness were optimized to match the response time requirements. The redesigned pH sensor with a response time (t_{90}) of 4 s at 4 °C was successfully applied at 'Boknis-Eck' (54.5 °N, 10.0 °E), Baltic Sea. The optimized carbon dioxide sensor with a response time (t_{90}) of 100 s at 20 °C and a shelf life of at least 6 weeks was used to measure stepwise profiles in the Monterey Bay (36.798 °N, -121.848 °E), Pacific Ocean, with a waiting time of 90 s at each depth. The deviation between optode data and reference values was less than 7% (lower than 40 m water depth). Moreover a set of optodes for oxygen, pH and carbon dioxide was successfully applied to measure a depth profile in the Monterey Bay, Pacific Ocean.

4.1 Introduction

Oceanic monitoring activities require complex and expensive equipment, infrastructure and logistics like ships, autonomous platforms and monitoring bouys. Currently 784 marine stations, 3 800 Argo floats and 325 research vessels are distributed worldwide.⁸² They investigate the

physics and biogeochemistry of the marine environment by measuring basic parameters like temperature, salinity, oxygen and nutrients. Based on these data hypothesis and models are created and validated. To test and evaluate the created models additional data like pH and carbon dioxide would be highly beneficial. Models are necessary to understand biogeochemical cycles, atmosphere-ocean interactions (uptake and release of CO_2) and ocean acidification. Data is collected by taking discrete samples and their measurement in the lab. In the last decades sensors for long-term measurements of pH^{203 238 239} and carbon dioxide^{207 108 117 131 91} were developed for the use in monitoring systems. Additionally sensors for integration in Argo floats and Autonomous Underwater Vehicles (AUVs) and for profiling measurements are of special interest. The response time of the sensor is the limiting factor. In the case of oxygen determination fast responding sensors are on the market and used frequently on ships and AUVs.^{240 241 242 243} The majority of the commercially available sensors for pH and carbon dioxide show an adequate long-term stability, but an insufficient response time for profiling applications. Some fast-responding prototypes were developed for pH and carbon dioxide. The SeaFETTM pH sensor based on an Ion Selective Field Effect Transistor (ISFET) shows fast response and recovery times of 7.6 s and 8.1 s, respectively. The sensor is able to measure in a pH range from 6.5 to 9.0 with an initial accuracy of 0.02 pH units. The overall dimensions are 54.9 cm length and 11.4 cm in diameter with a maximum application depth of 50 m.²⁴⁴ Microfluidic automated systems, using thymol blue and phenol red as pH indicator dyes, were used at a rosette to measure profiles with a sample interval of 2 s. Such systems include pumps, produce waste and they are limited by the volume of the indicator solution.^{245 246} pH optodes represent an alternative technique. It has the potential to be very fast with response times of about 1 s. These response times are not achieved in the marine environment so far. Clarke et al. recently presented an optode for oceanic pH measurements based on an immobilized fluorescence indicator for a pH range of 7.6 to 8.2. The sensor is well characterized for temperature and salinity deviations and show a response time of 50 s at 25 °C.²²³

Prototypes for carbon dioxide sensors were mostly developed for profiling measurements in sea water sediments.^{150 247 248} A fast-responding CO_2 microelectrode was presented by de Beer et al. 1997. The sensor had a response time (t_{90}) of around 10 s and a detection limit $< 3 \mu\text{M}$. It is suitable for the investigation of biological processes, like respiration or photosynthesis. The microelectrode could be used for 24 hours, but showed drift and should be recalibrated every 2 hours.²⁴⁷ An often used technique to measure carbon dioxide in seawater is infrared spectroscopy. Several sensor systems were developed, based on a pumped air-water equilibrator and a non-dispersive IR detector. The response time of this sensortype is determined by the time needed for equilibration and is in the range of 70 s to 103 s for different pump systems (t_{63} at 20 °C).⁹¹ Furthermore, a fiber-optic microsensor (optode) was published by Neurauter et al. 2000 based on 8-hydroxypyrene-1,3,6-trisulfonate (HPTS) as the CO_2 -indicator dye. The optode was 10 μm in diameter, had a response time of around 40 s and could be stored for several days. Due to the limited photostability of HPTS, stable signals could just be obtained over 24 hours.¹⁵⁰ Fritzsche et al. recently presented a carbon dioxide optode with an excellent long-term stability due to the use of a protective layer made of a perfluorinated polymer. The implementation of the protective layer negatively affected the response time particularly at low temperatures.¹⁰⁸

In this contribution we present an adapted pH optode with an improved response time achieved by optimizing the layer structure and a redesigned carbon dioxide optode with an optimized response time obtained by adjusting the material selection, the sensor composition and layer thickness. The developed optodes were successfully used for marine profiling applications in the Baltic Sea and the Pacific Ocean.

4.2 Materials and Methods

Chemicals

1H,1H,2H,2H-Perfluorooctyldimethylchlorosilane(97 %), vinyl dimethylsiloxy-terminated polydimethylsiloxane (viscosity 1000 cSt), methylhydrosiloxane-dimethylsiloxane copolymer (25 - 35 cSt), 1,3,5,7-tetravinyl-1,3,5,7-tetramethylcyclotetrasiloxane (97 %) (delayer) and platinum-divinyl-tetramethyl-disiloxane complex in vinyl terminated polydimethylsiloxane (3-3.5 % Pt) (catalyst) and dibutyltindilaurate were acquired from ABCR GmbH. Ethyl cellulose (EC49, ethoxyl content 49 %) and tetraoctylammonium hydroxide solution 20 % in methanol (TOAOH)), acryloylmorpholine and hydroxyethylacrylamide were obtained from Sigma Aldrich. Sodium bicarbonate, sodium hydroxide and sodium chloride were purchased from VWR. Hydrochloric acid and all components of the used pH calibration buffers were received from Carl ROTH GmbH & Co. KG. Anhydrous ethanol and potassium dihydrogen phosphate (99 %, water free) were acquired from Merck. BCl_3 in dichloromethane (1 M) was received from TCI GmbH and Desmodur N75 MPA/X crosslinker from Covestro AG. Toluene and sodium hydrogen phosphate were received from Carl Roth GmbH. Teonex Q51 a poly(ethylene naphthalate) (PEN) support was purchased from Pütz GmbH + Co. Folien KG. Optical fibres were received from Ratioplast-Optoelectronics and the FireStingO2 from Pyro Science GmbH. The synthesis of 4,4'-(5,5-difluoro-1,9-diphenyl-5H-4 λ ⁴,5 λ ⁴-dipyrrolo-[1,2-c:2',1'-f][1,3,5,2]triazaborinine-3,7-diyl)diphenol (di-OH-aza-BODIPY) indicator dye and staining of polystyrene-microparticles (PS-particles) with 3,7-bis(4-butoxyphenol)-5,5-difluoro-1,9-diphenyl-5H-4 λ ⁴,5 λ ⁴-dipyrrolo-[1,2-c:2',1'-f][1,3,5,2]triazaborinine (di-butoxy-complex) were performed according to Schutting et al. 2015.¹³⁹ 4-(7-(4-butoxyphenyl)-5,5-difluoro-1,9-diphenyl-5H-4 λ ⁴,5 λ ⁴-dipyrrolo[1,2-c:2',1'-f][1,3,5,2]triazaborinin-3-yl)phenol (butoxy-OH-aza-BODIPY) was prepared according to literature procedures.^{164,227} Preparation of silanized Egyptian Blue was performed analogously to Borisov et al. 2013 but using 1H, 1H, 2H, 2H-perfluorooctyldimethylchlorosilane instead of trimethylchlorosilane.¹⁴⁵ The sensor devices were developed and produced by Pyro Science GmbH and are described in Staudinger et al. 2017 (submitted).¹⁴⁹

Layer thickness determination

The layer thickness determination was performed with an inductive digital comparator 'Extramess 2000' (serial number: 41110036) from Mahr equipped with Millitron 1240 and caliper 'Messtaster 1340' for thicknesses higher than 10 μm .

Layer thicknesses lower than 10 μm were determined by absorption measurements. The measurements were executed with a Cary 50 Bio UV-Visible spectrophotometer obtained from

Varian. The absorption was used to calculate the layer thickness by using Lambert-Beer law and the molar absorption coefficients for di-OH-aza-BODIPY complex reported by Schutting et al. 2015.¹³⁹

Response time measurements

Response times of the pH sensor materials were determined by alternately submerging the sensor material in TRIS buffer with pH 7.75 and 8.25 and ionic strength of 720 mM. The sensor material was fixed to the distal end of an optical fiber with help of a metal ferrule and read-out with a FireSting from Pyro Science with a measurement frequency of 10 Hz. The measurements were conducted at room temperature.

Response and recovery times (t_{90}) were determined for an application-relevant range between 10 μM and 40 μM dissolved CO_2 . This range represents the linear region of the response curve of the developed carbon dioxide sensor. The temperature was mainly set to 20 °C and additionally response and recovery times for 10 °C and 30 °C were determined. The sensors were alternately inserted into temperature-controlled, constantly-stirred (~ 460 rpm) vessels with 10 μM and 40 μM $p\text{CO}_2$ in a 0.1 M phosphate buffer (pH 8.04). The CO_2 levels were adjusted by adding sodium bicarbonate solution. Each measurement was done in triplicates with three different sensor spots. The same set up was used to perform a long-term stability test.

Sensor foil preparation

The pH sensing material was prepared by coupling BCl_3 -activated acetyl-protected BF_2 chelate of [5-(4-hydroxyphenyl)-3-phenyl-1H-pyrrol-2-yl]-[5-(4-butoxyphenyl)-3-phenylpyrrol-2-ylidene]amine to the polyacryloylmorpholine-co-hydroxyethylacrylamide polymer.²²⁷ 50 mg of this polymer were dissolved in 50 μL DMSO and 400 μL THF. Then 1.5 μL Desmodur N75 MPA/X crosslinker and 1.5 μL of a 10% stock solution of dibutyltindilaureate in THF as catalyst were added. This 'cocktail' was knife coated on a 125 μm poly(ethylene terephthalate) support with either a 25 μm spacer (2.5 μm dry film thickness) or a 200 μm spacer (20 μm dry film thickness) and cross-linked for 1.5 hours at 60 °C. The reference layers were prepared by dispersing 20 mg Egyptian Blue in 1 mL of a 15% solution of poly(ethylene terephthalate) in 35 v% hexafluoroisopropanol:chloroform mixture (35:65 v/v). These dispersions were knife coated with a 25 μm and 76 μm spacer on the backside of the sensor supports for the 2.5 μm and 20 μm sensor films, respectively. For both sensing materials, the protecting group of the pH sensitive functionality was cleaved by submerging the sensor foils in 0.01 M sodium hydroxide solution for 30 minutes. 5 mm spots were stamped out of the sensing film and glued onto the sensing caps with the pH-sensitive layer facing outside.

For preparation of the CO_2 sensors, a 'cocktail' made of 3 mg di-OH-aza-BODIPY-dye (4% in respect to polymer), 75 mg ethyl cellulose and 1800 mg ethanol:toluene mixture (4:6 w/w) was flushed with pure carbon dioxide, followed by the addition of 90 μL of tetraoctylammonium hydroxide solution (20% w/w in methanol). The cocktail was knife coated onto a PEN support to obtain a sensing film of 0.8 μm thickness after evaporation of the solvents. The reference layer (inert light emitting layer) consisted of a four component silicone rubber. It was prepared

by mixing 42 mg Egyptian Blue, 32 mg dye-stained PS-particles, 200 μL vinyl-terminated polydimethylsiloxane, 400 μL cyclohexane, 8 μL methylhydrosiloxane-dimethylsiloxane copolymer, 0.8 μL retarder and 1.4 μL catalyst. After coating, polymerization and evaporation of the solvent, a reference layer of 27 μm was obtained. To systematically investigate the impact of the layer thickness on response and recovery time, different spacer were used. Finally spots (5 mm diameter) were punched out and glued on a PMMA (polymethylmethacrylate) cap, suitable for the sensor device.

Calibration procedure

The sensor materials were characterized in artificial seawater at salinity 10 with 20 mM of TRIS (tris(hydroxymethyl)aminomethane) and 20 mM of BIS-TRIS (bis(2-hydroxyethyl)amino-tris(hydroxymethyl)methane) as buffer substances. pH values between 5.8 and 9 were set by the addition of 0.42 M hydrochloric acid and 0.42 M sodium hydroxide in steps of 0.3 pH units. Chosen temperatures were 4, 6, 8, 10, 12 and 15 $^\circ\text{C}$ (fig. 4.1). No visible hysteresis was observed during calibration. The set pH values were measured with a pH electrode calibrated against spectrophotometric measurements²⁴⁹ and pH values were calculated according to Liu et al.¹⁸⁸.

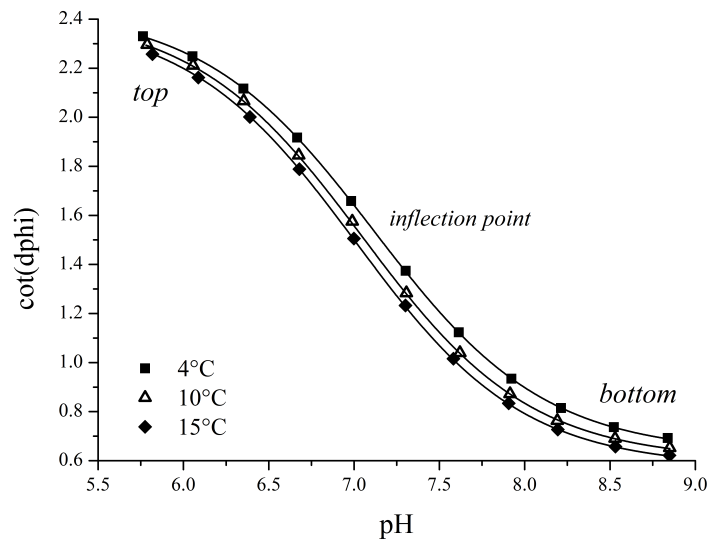


Figure 4.1: Sigmoidal calibration curves for a fast responding pH sensor material at 4, 10 and 15 $^\circ\text{C}$. Continuous lines represent sigmoidal fit.

The obtained calibration points were fitted with a Boltzmann sigmoid, which was extended with temperature coefficients for the top, bottom and $v50$ values:

$$\text{cot}(dphi) = \text{bottom} \cdot (1 + B_t \cdot (T - 20)) + \frac{(\text{top} \cdot (1 + T_t \cdot (T - 20)) - (\text{bottom} \cdot (1 + B_t \cdot (T - 20))))}{(1 + 10^{\frac{\text{pH} - (v50 \cdot (1 + v50_t \cdot (T - 20)))}{\text{slope}}})} \quad (4.1)$$

where bottom is the lower limit of the calibration, T is the temperature in $^\circ\text{C}$, top is the upper limit of the calibration, pH is the pH value, $v50$ is the point of inflection (fig. 4.1), slope describes the slope in the point of inflection and B_t , T_t and $v50_t$ are the linear temperature coefficients of the bottom, top and $v50$ coefficients, respectively.

Prior to deployments pH optodes were re-calibrated with two calibration buffers based on TRIS and BIS-TRIS. This re-calibration was conducted to determine the top and bottom parameter of the calibration equation. The buffers were prepared for the in-field calibration of the pH-optodes based on a recipe for artificial seawater.¹⁶⁶ The buffers for the deployment in Kiel were adjusted to salinity 20 and had a buffer capacity of 80 mM. For the deployment in California artificial seawater with salinity 35 and 80 mM buffer capacity was used. TRIS/TRIS*HCl in a ratio of 1:3 and BIS-TRIS/BIS-TRIS*HCl in a ratio of 3:1 were selected as buffer components. The exact pH and temperature dependence of the calibration buffers was measured spectrophotometrically with *m*-cresol-purple at temperatures between 3 and 15 °C. The equation from Liu et al.¹⁸⁸ was used for the calculation of the pH in total scale.

The factory calibration for the carbon dioxide optodes was performed as described in Fritzsche et al. 2017¹⁰⁸ by adding certain amounts of sodium bicarbonate solution to a 0.1 M phosphate buffer (pH 7.9) to adjust increasing CO_2 levels. 5 different CO_2 levels and 3 different temperatures were used to generate a calibration equation. By plotting the cotangent of the phase angle over the logarithm of the CO_2 concentration, a sigmoidal fit could be applied (fig. 4.2). To reduce the degrees of freedom the following parameter were fixed to the following values: $v_{50} = 1.5820$ and $\text{slope} = 1.8792$.

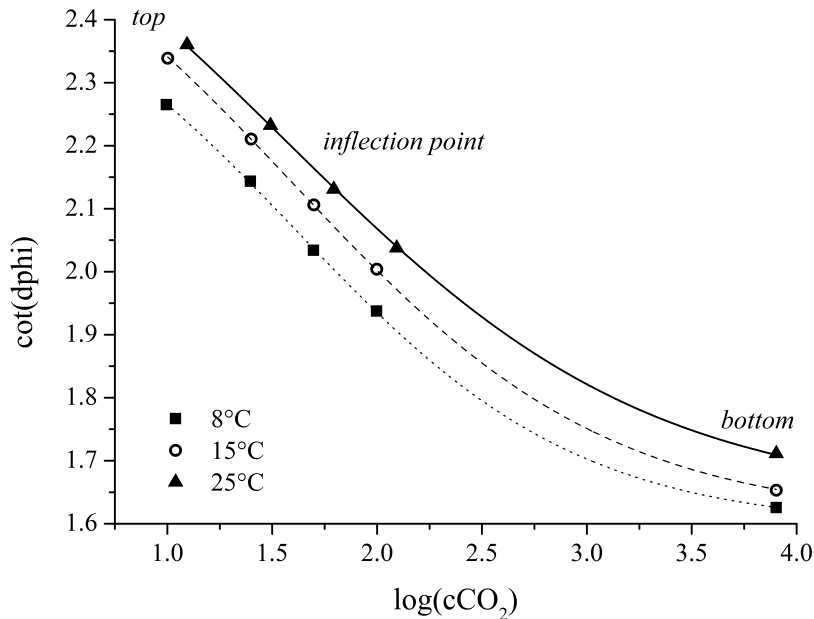


Figure 4.2: Logarithmic calibration plots for luminescent fast-responding carbon dioxide sensor for the range between 0 and 8000 μM CO_2 at 8 °C, 15 °C and 25 °C. Continuous lines represent sigmoidal fit.

The signal of the carbon dioxide optode is temperature dependent. Therefore compensation is necessary, which was realized by inserting temperature coefficients to the calibration equation. The extension leads to the following equation:

$$\text{cot}(d\phi) = \text{bottom} + \frac{(\text{top} + \text{top}_t \cdot (T - 20)) - \text{bottom}}{\left(1 + 10^{\frac{\log(c\text{CO}_2) - (v_{50} + v_{50,t} \cdot (T - 20))}{\text{slope} + \text{slope}_t \cdot (T - 20)}}\right)} \quad (4.2)$$

Since the temperature coefficient for bottom was negligible small, it was set to 0. Temperature coefficients were determined for the parameters top, v50 and slope: top_ t = 0.01419, v50_ t = -0,00289, slope_ t = 0,02675. For recalibration *in situ* measurements were used. Two reference values were chosen to adjust the parameters top and bottom for the individual sensor.

Reference measurements

Discrete reference samples were taken manually from a Niskin water sampler for each profile. Each sample was taken three times and treated corresponding to the measurement methods. Oxygen reference samples were spiked with the reagents for the following Winkler titration (1 mL manganese(II) chloride solution, 1 mL alkaline sodium iodine solution). pH reference samples (250 mL) were poisoned with saturated mercury chloride solution (60 μL) right after sampling. The pH was determined in the lab spectrophotometrically (25 °C, using *m*-cresol purple).¹⁸⁸ A third sample was poisoned as well and the DIC was determined by a LI-7000 CO₂/H₂O Gas Analyzer (LI-COR®) at 25 °C.[?] The carbon dioxide concentration was calculated from DIC and pH using the CO2SYS software (Lewis and Wallace 1998²¹).

Profiling Applications

The suitability for profiling measurements in the ocean was investigated at two application sites. The fast-responding pH sensors were tested several times at 'Boknis-Eck' (54.5 °N, 10.0 °E), located at the entrance of Eckernförde Bay in the southwest Baltic Sea. The profiles were measured till 25 m water depth with a continuously (velocity: 0.12 m/s) and stepwise (30 s waiting time/m) movement of the CTD-rosette.

At the second application site fast-responding oxygen, pH and carbon dioxide sensors were used. The measurements took place at the Monterey Bay station C1, California (36.798 °N, -121.848 °E) with a minimum water depth of 115 m. A stepwise movement of the carrier was necessary. 12 depths were chosen to wait for 90 seconds and to take reference samples during the upcast: 1 m, 5 m, 8 m, 20 m, 30 m, 40 m, 60 m, 80 m, 100 m, 150 m, 200 m, 225 m. The biggest gradient for each analyte was expected between 40 m and 110 m.

4.3 Results and Discussion

4.3.1 pH optodes

The deployed pH sensor material is based on an aza-BODIPY indicator dye immobilized in a water-swallowable polymer matrix. Aza-BODIPY dyes have many favorable properties. They are very photostable, have good molar absorption coefficients and good quantum yields.^{164 227} The selected indicator dyes are highly fluorescent when protonated and completely quenched when deprotonated. They can be modified easily to tune their pK_a value and thereby their dynamic range or to introduce linker groups for covalent attachment. Furthermore, they absorb in the red part of the electromagnetic spectrum and emit in the near infrared. Therefore, already existing measurement equipment for read-out of benzoporphyrin-based oxygen sensors can be used. Because unreferenced, purely intensity based measurements are unreliable (e.g.

due to fluctuations of the excitation source), the dual lifetime referencing (DLR) scheme is used for referenced read out of the pH sensor materials.^{144 164 227} Therefore, a layer containing the inorganic phosphor Egyptian Blue was added to the sensor structure. This phosphor is excitable with red light and emits in the near infrared with a luminescence lifetime of approximately $107\ \mu\text{s}$ ¹⁴⁵ and its emission is not influenced by pH. While the luminescence lifetime of the aza-BODIPY indicator dye is in the nanoseconds range and causes a phase shift of 0° , Egyptian blue has a phase shift of approximately 60° when excited at a frequency of 2 kHz. In the DLR scheme the overall phase shift is determined by the ratio of fluorescence to phosphorescence. High fluorescence intensity (low pH) of the pH indicator in the referenced sensor corresponds to low phase shift and low fluorescence intensity (high pH) corresponds to high phase shift. Thereby referenced readout of the pH sensor material is achieved.

Response time optimization

For most stationary applications a response time of multiple seconds is sufficient. In these applications high signal-to-noise ratio and good resolution are much more important than fast response times. Moreover, an optical isolation may be necessary to enable measurements in direct sunlight. However, high signal-to-noise ratios are obtained by increasing the layer thickness and optical isolation layers further increase the overall thickness of the sensing membrane and therefore the response time of the sensor. In order to obtain sensor materials suitable for profiling applications we reduced the layer thickness of the membranes and omitted an optical isolation layer. The latter is not necessary since the sensors are pointed downward and are protected from direct sunlight. Moreover, a water layer of only 1 m acts already as a very efficient filter for NIR light (corresponding to the detection channel of the read-out device) making the risk of saturation of the photodetector with daylight almost negligible. As can be seen from figure 4.3, reducing the thickness of the sensor materials from $20\ \mu\text{m}$ to $2.5\ \mu\text{m}$, improving the response time (t_{90}) at 4°C from 14 s to 4 s. It is also possible that the response time for the $2.5\ \mu\text{m}$ layers is even faster due to some time needed for transfer of the sensor between beakers with different buffers. However, the reduced signal intensity due to the thinner sensing layer also leads to increased noise in the measured pH value.

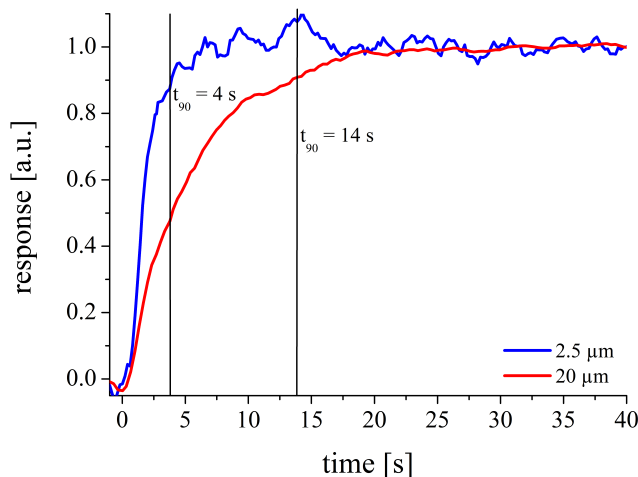


Figure 4.3: Response time of the pH sensing material at 4°C between pH 7.75 and pH 8.25.

Suitability of the new material for profiling applications was tested at the measurement site 'Boknis Eck' in the Kiel fjord which shows extremely steep pH gradients of about 1 pH unit over only 25 m. Due to these conditions the profiling speed was reduced and stops of 30 s were introduced every meter. As can be seen in figure 4.4 the standard pH-sensor material (thick sensing layer and optical isolation layer) was not able to adequately record this profile showing strong hysteresis between up- and downcasts. On the contrary, the new fast sensor material is sufficient to resolve both up and downcast without strong hysteresis. Small deviations might be caused by not completely identical water masses during up- and downcasts which is reflected by small hysteresis visible in temperature and salinity measurements (fig. 4.4). Further improvement of the sensor response is likely to be possible via optimization of the sensor geometry (convex surface), which was a flat sensor spot in both cases.

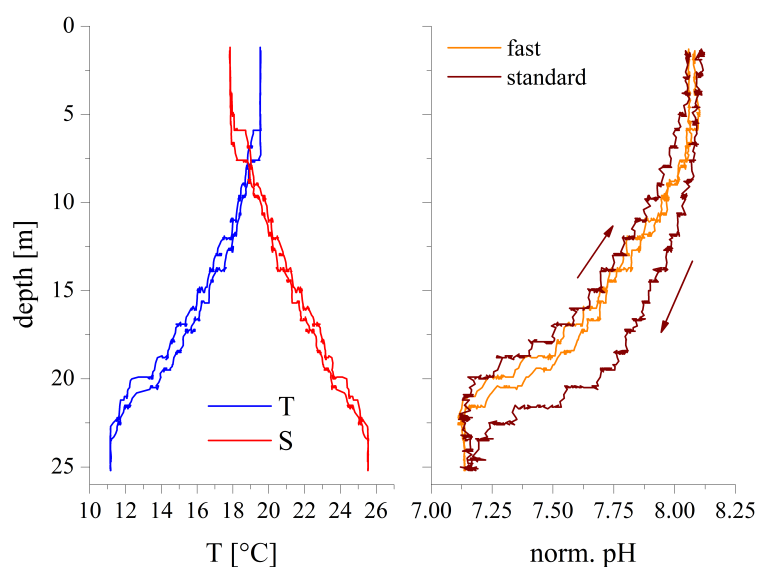


Figure 4.4: Profile recorded at 'Boknis Eck', Kiel (GPS: 54.5 °N, 10.0 °E). Temperature, salinity and normalized pH-profiles from two sensor materials are depicted. The profile was recorded with 30 s stops every meter and with 0.12 m/s speed. Overall the measurement of the profile with up and downcast required approximately 30 minutes. The pH-data was acquired with a frequency of 1 Hz.

4.3.2 $p\text{CO}_2$ optodes

So called 'plastic' $p\text{CO}_2$ optodes rely on use of pH indicators immobilized in a hydrophobic polymer (most commonly ethyl cellulose) along with a lipophilic organic base (most commonly quaternary ammonium hydroxide). A proton-impermeable protective layer is essential for the stability of the pH-indicator-based CO_2 sensor. The recently presented carbon dioxide optodes¹⁰⁸ provided a dramatically improved long-term stability compared to previously reported sensors. The high stability was achieved by making use of (i) new chemically and photochemically stable aza-BODIPY complexes¹⁰⁸ as indicator dyes and (ii) perfluorinated polymers efficiently protecting the lipophilic base of the sensing material from reaction with acidic gases. Importantly, the aza-BODIPY colorimetric indicator dye shows absorption and fluorescence intensity spectra in the NIR region, a high molar absorption coefficient enables read-out via inner filter effect.

This read-out is realized by the addition of pH-insensitive Egyptian Blue and di-butoxy-aza-BODIPY (embedded in polystyrene microparticles) into the protective layer. The light emitted by phosphorescent Egyptian Blue is mainly absorbed by the di-anionic (low $p\text{CO}_2$) form of the indicator whereas the emission of the fluorescent di-butoxy-aza-BODIPY is mainly attenuated by the mono-anionic (high $p\text{CO}_2$) form of the indicator. Although this referencing scheme is not fully identical to the DLR method, it also enables analyte-dependent phase shift measurements. We decided to use the above mentioned advantages of the aza-BODIPY dye class and the already established read-out system to develop a fast-responding carbon dioxide sensor. The main characteristics determining the response time of such optodes are the materials used in the sensing and protective layer, as well as the thickness of them.

Selection of materials

The material selection, not only significantly influences the response and recovery time, but also the technology of sensor spot manufacturing, due to different adhesion of the polymers affecting the mechanical stability of the sensor. The previously reported carbon dioxide optode (fig. 4.5A) consisted of three layer: a CO_2 sensitive layer, an inert light emitting layer (reference layer) and a protection layer. The CO_2 sensitive layer is based on ethyl cellulose, a frequently used polymer for sensor preparation.^{148 150 157 250 251 252} It allows the production of mechanically robust thin layers, is transparent, shows no autofluorescence, is hydrophobic enough to ensure physical immobilization of the indicator dye without aggregation. But at the same time, ethyl cellulose is not too hydrophobic to prevent formation of protons in presence of carbon dioxide. The reference and protection layers were prepared of Hyflon AD 60, a perfluorinated polymer with a high selectivity for carbon dioxide in comparison to other acidic gases like hydrogen sulfide. Thus it efficiently prevents diffusion of acidic gases into the sensing layer and therefore poisoning of the sensor ensuring long shelf life and operational stability. Unfortunately, permeability of Hyflon AD 60 for carbon dioxide is relatively low (145 barrer¹⁸⁹, tab. 4.1) which results in high response and recovery times (80 and 90 min, respectively at 15 °C for change between 14 and 28 μM dissolved CO_2). Moreover, due to poor adhesion of the perfluorinated polymer on ethyl cellulose a time-consuming, production process with relatively low yield was necessary. It included pre-cutting of the support, pipetting of the 'cocktail' for the CO_2 sensitive layer and knife coating of the reference layer.

PDMS (silicone rubber) has a ~ 30 times higher CO_2 permeability than Hyflon AD 60 (tab. 4.1) and therefore can enable a significant reduction of the response and recovery times if used as matrix for dispersion of the reference particles. Moreover, silicon rubber is proton impermeable, has high chemical stability and is biocompatible, which makes it a popular matrix for optodes.^{170 253 254 255} Silicone rubber shows high elasticity and good adhesion on ethyl cellulose, which ensures high mechanical stability of the sensing material. In respect to carbon dioxide sensing, the trade-off is the high gas-permeability for other gases such as H_2S , SO_2/SO_3 or NO_x , which irreversibly poison the sensor. The cross-section of the modified CO_2 sensor is shown in figure 4.5B. The poly(ethylene naphthalate) (PEN) support was directly coated with the ethyl cellulose-based sensing layer which was in turn covered with the silicone rubber layer performing dual function of a hydrophobic gas-permeable barrier and a matrix for reference particles. The

protection layer used in the established carbon dioxide sensor was omitted.

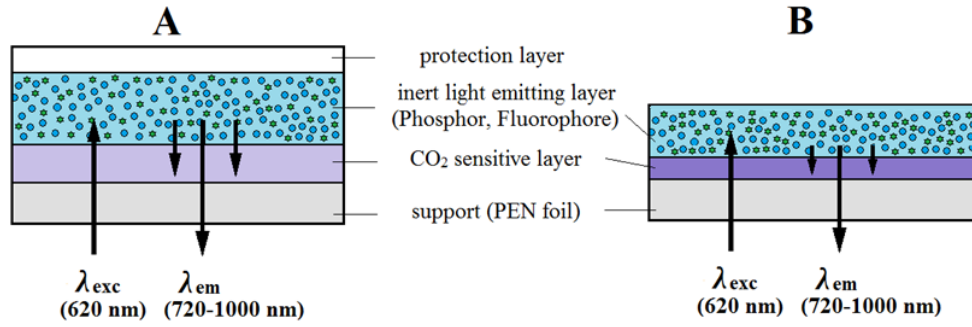


Figure 4.5: Cross section of the long-term stable carbon dioxide sensor (A)¹⁰⁸ and the new fast-responding carbon dioxide sensor (B).

Table 4.1: Diffusivity (D), Solubility (S) and Permeability (P) for PDMS (silicone rubber), ethyl cellulose (EC49) and Hyflon AD 60. * 1 barrer = $10^{-10} \text{ cm}^3(\text{STP})/\text{cm}^2 \text{ s cmHg}$.

	PDMS	ethyl cellulose ²⁵⁶	Hyflon AD 60 ¹⁸⁹
D_{CO_2} [$10^6 \text{ cm}^2/\text{s}$]	25.2 ¹⁷⁴	0.56	0.748
S_{CO_2} [$\text{cm}^3(\text{STP})/\text{cm}^3\text{atm}$]	1500 ¹⁷⁹	1.50	1.45
P_{CO_2} [barrer]*	4400 ¹⁷⁹	113	145

Thickness of the CO_2 sensitive layer

Since the indicator dye is responsible for modulation of luminescence of the secondary emitters, sufficient absorbance of the dye must be guaranteed. Therefore, dye concentration in the sensing layer and the thickness are equally important. The dye concentration in respect to the polymer was set to 4% w/w, because at higher concentrations the indicator dye tends to aggregate. Further, the thickness of the sensing layer was systematically varied (tab. 4.2). As expected, the absorbance A (but not the amount of the absorbed light, $1-10^{-A}$) is proportional to the thickness of the sensing layer. Higher absorbance result in better modulation of the luminescence emitted by the secondary emitters and therefore in better resolution. At the same time, signal intensity decreases with higher layer thickness and the response and recovery times increase almost linearly (tab. 4.2, fig. 4.6). The main reason for increase in the response and recovery time is the moderate permeability of ethyl cellulose for carbon dioxide (tab. 4.1) and the slowly established equilibrium between carbon dioxide and carbonic acid.²⁵⁷

The sensor with the 1 μm -thick sensing layer was selected for further investigations due to best compromise between resolution, signal intensity, response and recovery times. Temperature dependency of the response and recovery times for this material was investigated (fig. 4.6C). As expected, response and recovery of the sensor are significantly shorter at high temperatures (~ 6 -fold between 10 and 30 $^\circ\text{C}$). Interestingly, the response and recovery times become almost identical at 30 $^\circ\text{C}$.

Table 4.2: Absorbance at 772 nm in a gas phase of 100% CO_2 , signal intensity and resolution of the fast-responding carbon dioxide sensor with different layer thicknesses of the CO_2 -sensitive layer made of ethyl cellulose (EC49). * calculated from the sensor response in the linear region of the calibration curve (10 μM - 40 μM CO_2) and the phase shift noise of 0.01° . ** only reference layer

layer thickness [μm]	absorbance	signal intensity [a.u.]	resolution [μM]*	response time [s]
0 **	0	163	-	-
0.6	0.284	117	0.3	105
0.8	0.371	75	0.18	148
1	0.455	84	0.16	148
1.2	0.574	68	0.09	210
1.7	0.793	49	0.08	223
2.7	1.238	61	0.07	314

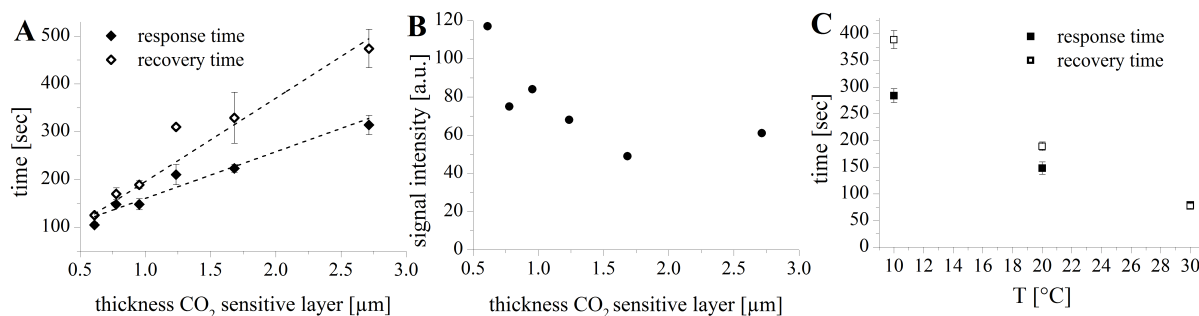


Figure 4.6: Response and recovery times at 20°C (10 μM to 40 μM dissolved carbon dioxide) (A) and signal intensity (B) as a function of the thickness of the ethyl cellulose layer. Response and recovery time as a function of temperature for the sensor with 0.95 μm -thick sensing layer (C). Dashed lines represent linear fit of the response and recovery time data.

Thickness of the reference layer

The thickness of the CO_2 -sensitive layer made of ethyl cellulose was kept at $\sim 0.8 \mu\text{m}$ and the thickness of the reference layer was systematically varied. 26% wt. of reference particles in respect to the polymer were used since the higher amount was found to result in more brittle layers. The thickness varied between $\sim 12 \mu\text{m}$ and $\sim 70 \mu\text{m}$. Interestingly, the response times for all the sensor foils were at around 125 s with no observable dependency on the layer thickness (fig. 4.7A). On the other hand, the recovery times increased significantly with the thickness of the silicone rubber layer. This can be explained by high solubility of carbon dioxide in silicone rubber (tab. 4.1) and therefore its accumulation in this layer. The thicker the layer the longer is the time required to remove the analyte from the polymer. As expected, increasing the layer thickness and therefore the overall amount of the particles enhances the luminescence intensity and signal-to-noise ratio. However, the effect is barely noticeable above 50 μm thicknesses. As a compromise between the response time, the recovery time and the signal intensity, the thickness of $\sim 27 \mu\text{m}$ -thick reference layer was chosen. The temperature dependency investigated for this material is similar to that obtained previously (fig. 4.6C).

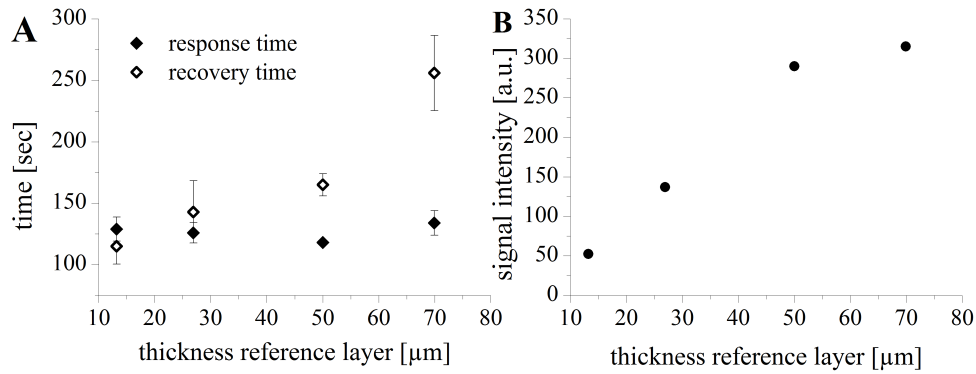


Figure 4.7: Response and recovery times (10 μM to 40 μM dissolved carbon dioxide) (A) and signal intensity (B) as a function of the reference layer thickness (silicone rubber) at 20 $^{\circ}\text{C}$.

Long-term stability

The sensor with a $\sim 0.8 \mu\text{m}$ -thick CO_2 -sensitive layer and a $\sim 27 \mu\text{m}$ -thick reference layer was chosen for further investigations and the deployment due to the best compromise between response time, recovery time and the sensor performance. Previously we showed that the high permeability of silicone rubber for acidic gases results in poisoning of the CO_2 -sensitive layer (dye/base ion pair). The operational stability test was set to mimic an average profiling cycle on a ship. The carbon dioxide level was increased to 40 μM and decreased to 10 μM to imitate a profiling measurement. Afterwards the CO_2 concentration was kept at 10 μM for 90 minutes and the experiment was repeated three times.

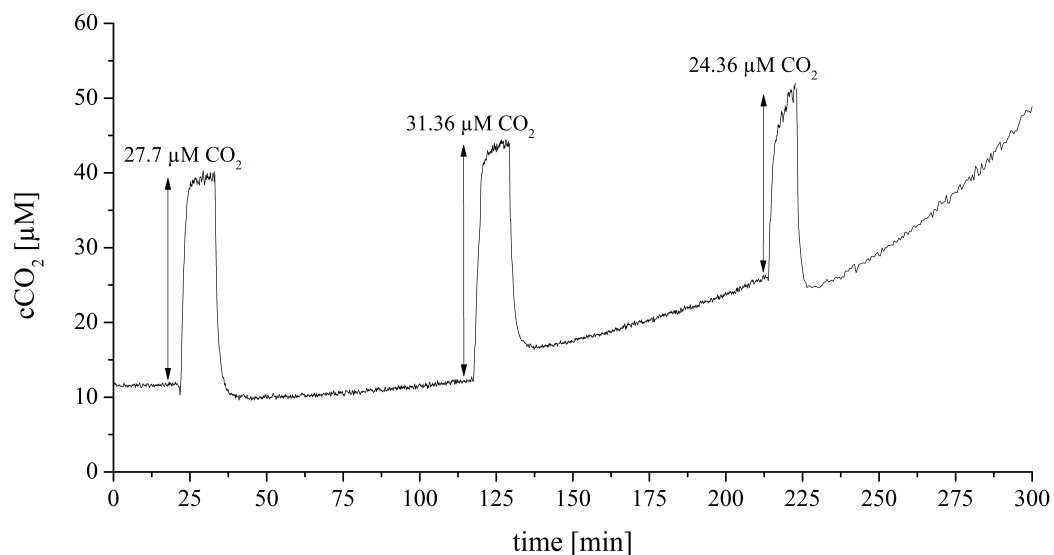


Figure 4.8: Stability test in phosphate buffer with CO_2 level 10 μM at 20 $^{\circ}\text{C}$ over 5 hours. Profiling measurements were simulated by changing carbon dioxide level to 40 μM CO_2 and back.

The stability test confirmed fast poisoning of the sensor (fig. 4.8). Poisoning resulted in increase of the calculated carbon dioxide concentration. The sensor was fully reversible within the first cycle. The response during the second cycle was still satisfactory, the observed slight drift is compensated by an *in situ* recalibration. Afterwards a pronounced drift was observed. Therefore, it is recommended to exchange the sensor cap after 1-2 profiles depending on the waiting time between the profiles. The sensor cap should be kept wet between two measurements to avoid a large drift in the calibration. Fortunately, the sensor caps can be manufactured in large amounts from a single sensing foil and thus can be viewed as disposable tools.

The shelf life of the sensor was not systematically investigated. However, the sensors were fully functional after 6 weeks storage in refrigerator (4 °C) under 100% CO_2 atmosphere. In these conditions no other acidic vapors are present, which excludes poisoning. Previous experiments with sensors based on silicone rubber protective layer indicated full functionality of the sensors after 6 months storage at -18 °C and 100% CO_2 .

4.3.3 Application 'Monterey Bay'

A set of fast-responding sensors for oxygen, pH and carbon dioxide was applied to measure depth profiles at the Monterey Bay station C1 (36.798 °N, -121.848 °E). The oxygen and pH sensor were calibrated before the deployment. The carbon dioxide sensor was calibrated *in situ*, so reference values were used to adjust necessary calibration parameters. The response time of the carbon dioxide sensor was ~ 110 s (10 μM -40 μM cCO_2) for the conditions during the application. Therefore, a stepwise profiling was still necessary. The ship time per day is limited, so the waiting time should be as short as possible. The waiting time at each depth was set to 60 seconds for the first deployment (February 8th, fig. 4.9A).

Oxygen values obtained by the optode are in good agreement with the reference values obtained by Winkler titration. The oxygen data deviate by less than 4% and no hysteresis is observed. The data obtained with the fast-responding carbon dioxide sensor showed a clear hysteresis. The reference values were in a good accordance at water depths between 0 m and 40 m. The values for water depths between 40 m and 220 m are located in the hysteresis (fig. 4.9A). This observation indicated a too short waiting time for each depth. Based on this observation the waiting for the next profile was set to 90 seconds (March 7th fig 4.9B). The second profile was measured down to 110 m water depth. Again, the oxygen data are in very good agreement with the reference values. The same is observable for the pH profile during the upcast. The CO_2 values measured after 90 seconds at the same depth are in a good accordance with the reference values. The values deviate by less than 7% at water depths between 30 m and 110 m. The values between 30 m and the water surface, where the water is well mixed and in equilibrium with the air, differ significantly. The likely reason was small changes in the carbon dioxide concentration between the consecutive reference points, which lead to a longer response time.¹⁵⁰ Therefore the waiting time should be extended in that region.

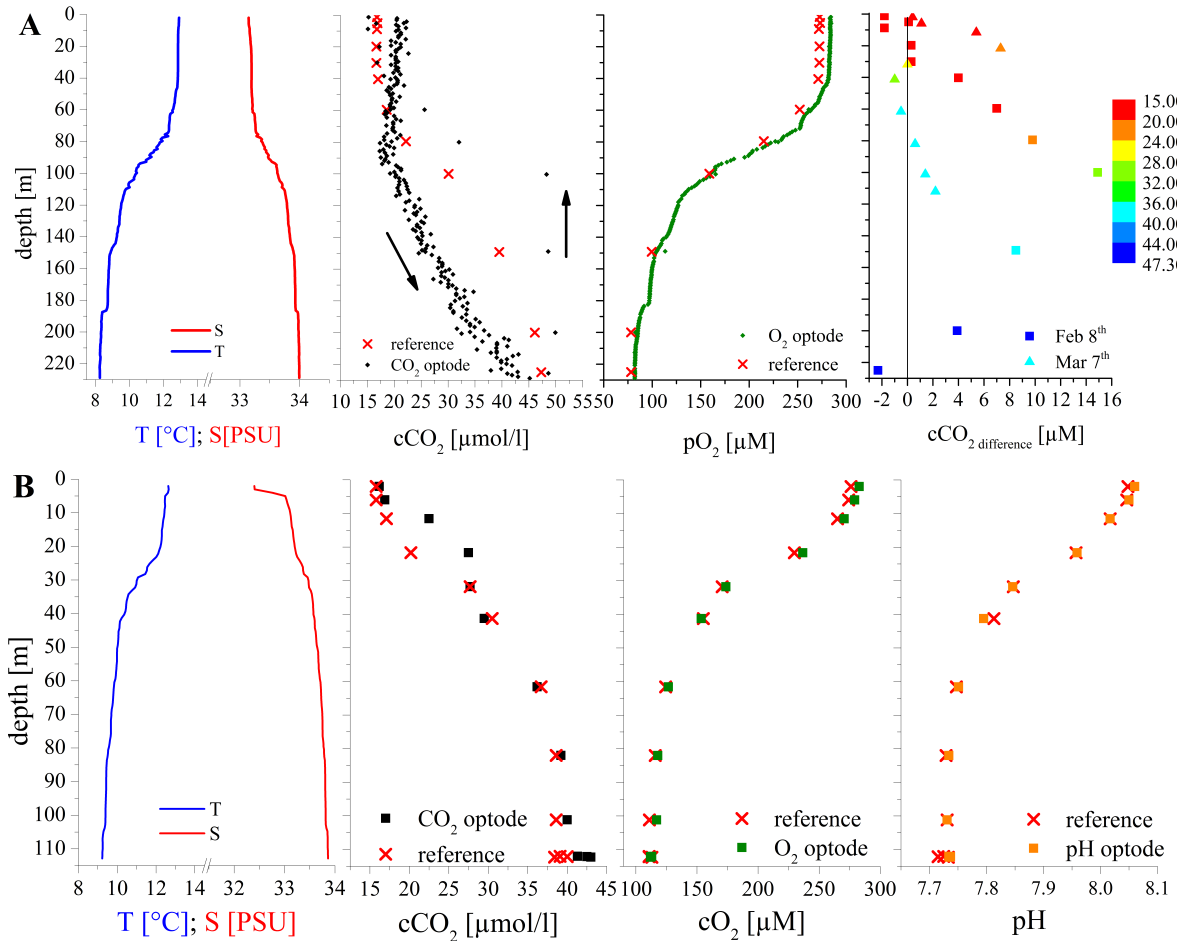


Figure 4.9: Depth profiles Monterey Bay station C1 (36.798 °N, -121.848 °E) for carbon dioxide and oxygen measured at February 8th with waiting time 60 seconds at each depth (above, A) and March 7th waiting time 90 seconds at each depth (bottom, B). Temperature and salinity obtained with a Sea-Bird Scientific SBE 9 CTD-system. $c\text{CO}_2$ differences ($c\text{CO}_{2\text{optode}} - c\text{CO}_{2\text{reference}}$) are shown for February 8th (quad) and March 7th (triangle) depending on the depth and the CO_2 concentration (color coded) in μM .

4.4 Conclusion

We presented fast-responding optodes for pH and carbon dioxide in seawater, which are suitable for profiling measurements. The response time of the pH sensor was successfully decreased by a reduction of the sensing layer thickness. It was possible to reduce the response time (t_{90}) from 14s to 4s at 4 °C. However, a relatively slow profiling speed is still necessary. The reduction of the response time of the carbon dioxide optode was more complex; both the thickness of the sensing layer as well as the reference layer had to be adjusted. We were able to reduce the response time (t_{90}) from 70 min to 100s at 20 °C. Profiling measurements were successfully performed, but still had to be stepwise. The speed and waiting time is important to avoid hysteresis. Even faster sensors would be desirable particularly at low temperatures, but are hard to make due to necessary time for diffusion and equilibrium adjustment, as well as the solubility of carbon dioxide in the polymer. Poisoning of the sensor is an important factor. The presented carbon dioxide sensor gets poisoned rather fast, but can be produced in high unit numbers. Current sensors are a compromise to provide a sufficient sensor performance. The use

of microsensors or a special spot design might be a way for further improvement.

Acknowledgement

Financial support by the European Union FP7 Project SenseOCEAN-Marine Sensors for the 21st century (Grant Agreement Number 614141) and the Graz University of Technology (Research Abroad fellowship) is gratefully acknowledged. We thank the crews of the RV 'Rachel Carson' operated by the Monterey Bay Aquarium Research Institute and of the RV 'Littorina' operated by the GEOMAR for supporting the profiling measurements. Additionally, we want to acknowledge the support of the working group of E. Achterberg at the GEOMAR in Kiel.

Chapter 5

Hydrogen sulfide protection strategies for CO₂ optodes to measure in marine oxygen-minimum zones

5.1 Introduction

Oxygen-minimum zones (OMZ) are an expanding problem in the world's oceans.^{195 258 259} They are described as oxygen-starving regions and depending on the literature are defined as water masses with an oxygen level $< 60 \mu\text{mol/L}$ ²⁵⁹, $< 20 \mu\text{mol/L}$ ⁷⁰ or $< 10 \mu\text{mol/L}$ ¹⁹⁵. Oxygen minimum zones appear when the oxygen demand, generated by the degradation of organic matter exceed the availability in insufficient ventilated water masses (see section 1.2.3). They are often found in the oceans: the tropical North and South Pacific Ocean (30°N - 15°S; 70°W - 180°E), the tropical South Atlantic Ocean (8° - 14°S; 4° - 12°E)¹⁹⁵, the Arabian Sea, the Bay of Bengal²⁶⁰, the Baltic Sea⁶⁸, the Black Sea²⁶¹, the Gulf of Mexico²⁶² and many more. An increasing temperature of the ocean result in an decrease of oxygen solubility and an intensified stratification, which promote the formation of oxygen minimum zones. The lack of oxygen in oxygen minimum zones also lead to the formation of toxic hydrogen sulfide. The formation of H₂S is considered to take place in the sediment and the water column. In areas with a low oxygen level down to oxygen-free, the sediments are often anoxic as well. In anoxic sediments the degradation of organic carbon is supposed to be realized mostly by the reduction of microbial sulfate to elemental sulfur and hydrogen sulfide. The toxic hydrogen sulfide is released in large quantities to the bottom waters.^{263 264} A second source of hydrogen sulfide is the reduction of sulfate in the water column by pelagic organisms. The ratio of each process to the overall hydrogen sulfide production varies for each oxygen minimum zone. The amount of hydrogen sulfide varies corresponding to the annual cycle or other events like salt water inflows in case of the Baltic Sea. H₂S concentrations were detected at the Peruvian coast (4.2 μM at 48 m)²⁶⁴, near the Namibian coast (40.7 μM total sulfide in bottom waters)²⁶⁵ or in the Black Sea ($\sim 400 \mu\text{M}$ at 1500 m)¹⁷⁷.

The monitoring of hydrogen sulfide containing water masses is of great interest, especially in terms of oxygen and carbon dioxide long-term measurements. The measurement of each analyte in this area has some challenges. The oxygen concentration is below 1-2 μM . Therefore sensors for ultra-low oxygen concentrations are necessary, which are not interfered by H₂S. Revsbach et al. developed the STOX O₂ sensor with an detection limit of 1-10 nM O₂ based on an electrochemical sensor scheme.^{199 266} An second ultra-sensitive oxygen sensor was developed by Larsen et al. 2016.²⁶⁷ The sensor is based on luminescence quenching (luminophore: palladium(II)-benzoporphyrin) with a detection limit of 5 nM. Carbon dioxide optodes are sensitive to H₂S as well, due to the similar chemical properties.^{107 108} Most optodes are based on a gas-permeable membrane and a pH-sensitive indicator. The indicator changes its spectral properties according to the pH change induced by carbon dioxide. If hydrogen sulfide diffusing through the membrane as well, the pH gets changed additionally and the carbon dioxide concentration will be overestimated. To eliminate the cross sensitivity and prevent potential poisoning processes, sensor protection strategies are necessary to provide accurate data even in oxygen minimum zones.

The removal of hydrogen sulfide was intensively investigated for oil and gas industries. They developed techniques and defined potential compounds to effectively remove H₂S from drilling fluids and gas streams. The term 'sulfide scavenger' was defined as any chemical, which react with one or more sulfide species to convert them into a neutral form. An effective scavenger (i) delivers an irreversible, rapid, complete and predictable chemical reaction, (ii) should be cheap and available in a large scale and (iii) the reaction product should be non-hazardous.²⁶⁸ For the treatment of drilling fluids and muds two scavenger are widely used: zinc-containing compounds, like ZnO or ZnCO₃ and iron oxide (Fe₂O₃, commercial name: *ironite sponge*).²⁶⁹ These compounds are although used in gas streams, especially zinc oxide.²⁷⁰ Other techniques for hydrogen sulfide interception from various media are based on organic compounds, like 1,3,5-tris (2-hydroxyethyl)-1,3,5-triazinane (triazin)^{271 272} or 2,2',2'',2'''-(Ethane-1,2-diyl)dinitrilo)tetraacetic acid (EDTA)²⁷³. Additionally removal of hydrogen sulfide using biological processes were investigated in the last decades. Oyarzún et al. described a method for biofiltration using *Thiobacillus thioparus*. *T. thioparus* is a sulfur-oxidizing bacteria, which was inoculated in a filter. The biofilter reached a 100% efficiency having a 355 ppm H₂S gas stream with an air flow rate of 0.03 m³/h. The removal efficiency decreased with increasing flow rate.²⁷⁴ Several more techniques using biofilters were investigated.^{275 276 277} A second possibility to intercept H₂S are bioreactors. Two types of bacteria are used in bioreactors: chemotroph and photoautotroph. Chemotroph bacteria use inorganic carbon as a cell material source and hydrogen sulfide for chemical energy. Phototroph bacteria uses light as their energy source, like green sulfur bacteria (e.g. *Chlorobium limicola*). Both types of bacteria can be used in various reactor types, like gas-fed batch reactor, continuous-flow reactors, phototube reactors or bioscrubbers.²⁷⁸ Some of the mentioned scavenger/strategies can be adapted for the use in sensor technology.

We present the development of a new hydrogen sulfide scavenger structure for a carbon dioxide optode to enable accurate, long-term measurements in H₂S-containing water masses.

5.2 Materials and Methods

Chemicals and Materials

Ethyl cellulose (EC49, ethoxyl content 49%), *m*-cresol purple (indicator grade), tetraoctylammonium hydroxide solution (TOAOH, 20% in methanol), Fomblin[®] Y, zinc oxide (ZnO, <100 nm, <50 nm), charcoal, copper(I)oxide (Cu₂O), copper(II)oxide (CuO, <50 nm), manganese(IV)oxide (MnO₂), silver nanopowder (Ag nano, <100 nm), iron(III)oxide (Fe₂O₃, <50 nm), silvertrifluoromethanesulfonate (Ag-triflate) and sodium sulfate (anhydrous) were received from Sigma-Aldrich. Toluene, Kieselgur[®], sodium hydrosulfide (NaHS·xH₂O) and potassium carbonate were obtained from Carl Roth GmbH +Co. KG. Hyflon[®] AD 60 was aquired from Solvay GmbH and poly(ethylene terephthalate) (PET) support Melinex 505 from Pütz GmbH + Co. Folien KG. Perfluorodecalin (PFD, 98%; cis and trans, ABCR) was washed with a 1 M aqueous solution of K₂CO₃ prior to use. Ethanolamine were obtained from Fluka and formaldehyde, silver(I)oxide (Ag₂O), lead(II)oxide (PbO) and lead(IV)oxide (Pb₂O) from Merck KGaA. 1H,1H,2H,2H-Perfluorooctyldimethylchlorosilane (97%), vinyl dimethyl-siloxyterminated polydimethylsiloxane (viscosity 1000 cSt), methylhydrosiloxane-dimethylsiloxane co-polymer (25-35 cSt), 1,3,5,7-tetravinyl-1,3,5,7-tetramethylcyclotetrasiloxane (97%) (delayer), platinum-divinyltetra-methylidisiloxane complex in vinyl terminated polydimethylsiloxane (3-3.5% Pt) (catalyst) and zinc oxide (<300 nm) were obtained from ABCR GmbH. Trisopor[®] was received from VitraBio GmbH and dicopper carbonate dihydroxide (CuCO₃ · Cu(OH)₂) from Fischer Chemicals AG. Synthesis of 4,4'-(5,5-difluoro-1,9-diphenyl-5H-4λ⁴,5λ⁴-dipyrrolo-[1,2-c:2',1'-f][1,3,5,2]triazaborinine-3,7-diyl)diphenol (di-OH-aza-BODIPY) and staining of polystyrene-microparticles (PS-particles) with 3,7-bis(4-butoxyphenyl)-5,5-difluoro-1,9-diphenyl-5H-4λ⁴,5λ⁴-dipyrrolo-[1,2-c:2',1'-f][1,3,5,2] triazaborinine (di-butoxy-complex) was performed according to Schutting et al. 2015.¹³⁹ Silanized Egyptian Blue was produced analogously to the literature procedure¹⁴⁵ but using 1H, 1H, 2H, 2H-perfluorooctyldimethylchlorosilane instead of trimethylchlorosilane.

Sensor foil preparation

A 'cocktail' prepared of 1 mg *m*-cresol purple (1% w/w in respect to polymer), 100 mg ethyl cellulose (5% w/w in respect to solvent), 760 mg ethanol and 1140 mg toluene was flushed with pure carbon dioxide. Afterwards 100 µL TOA OH in methanol were added. The cocktail was knife coated on a dustfree PET support (125 µm thickness), resulting in a 3.3 µm thick layer after evaporation of the solvent.

The scavenger containing cocktail consisted of 1 g of Hyflon[®] AD 60 solution (5% w/w in PFD, washed prior to use), 50 mg scavenger (varied) and 300 mg Fomblin[®] Y solution (5% w/w in PFD). The cocktail was knife coated to obtain a 2 µm dry thick layer. To make meaningful photographs an additional layer was inserted. A titanium oxide containing white layer consisting of 1 g Hyflon[®] AD 60 solution (5% w/w in PFD), 50 mg TiO₂ and 300 mg Fomblin[®] Y solution (5% w/w in PFD) was knife coated with a 3 Mil knife. At the end a pure Hyflon[®] AD 60 layer (1 g 5% Hyflon[®] AD 60 solution in PFD + 300 mg 5% Fomblin[®] solution in PFD) was used

to cover the whole sensing chemistry with a 2 μm thick layer.

The silicone rubber layer was prepared by mixing 150 mg ZnO particles (<100 μm), 150 μL vinyl-terminated polydimethylsiloxane, 300 μL cyclohexane, 6 μL methylhydrosiloxane-dimethylsiloxane co-polymer, 0.6 μL delayer and 1.4 μL catalyst and polymerization of this mixture after coating and evaporation of the solvent.

Protected carbon dioxide sensor foil preparation

A 'cocktail' made of 100 mg ethyl cellulose, 1 mg of di-OH-aza-BODIPY-dye (1% w/w with respect to the polymer) and 1.683 g of a toluene:ethanol mixture (6:4 w/w) was flushed with carbon dioxide. This was followed by the addition of 100 μL TOA OH solution (20% w/w in methanol). The 'cocktail' was knife coated two times to obtain an ethyl cellulose layer with a thickness of ~2.2 μm after evaporation of the solvent. A silicone mixture consisting of 150 μL vinyl-terminated polydimethylsiloxane, 300 μL cyclohexane, 6 μL methylhydrosiloxane-dimethylsiloxane co-polymer, 0.6 μL delayer and 1.4 μL catalyst was prepared and particles (i) 42 mg Egyptian Blue and 32 mg PS-particles [reference layer] ii) 150 mg ZnO <100 μm [scavenger layer] iii) 130 mg ZnO <100 μm, 42 mg Egyptian Blue and 32 mg PS-particles [mixed]) were suspended homogeneously in the mixture. After knife coating and polymerization of the silicone rubber layer with i) 25 μm ii) 35 μm and iii) 60 μm thickness were obtained. Finally the sensor foil was covered with a 2 μm thick pure Hyflon AD 60 solution in PFD (5% w/w).

H₂S atmosphere generation

Hydrogen sulfide was generated by adding 75 μL diluted phosphoric acid to 18 mg sodium hydrosulfide (HNaS·xH₂O) in a 2.4 L dessiccator. A 0.1% H₂S atmosphere in room air was produced. It is equivalent (even more) to the hydrogen sulfide content in the Gotland Basin (Baltic Sea) after a long stagnation period (Gotland Sea deep water (200 m): ~ 200 μmol/kg¹⁸⁰). The sensor foils were inserted in a dessiccator with a reference sample without any scavenger particles. Photographs were made depending on the experiment every hour.

Synthesis of 1,3,5-tris(2-hydroxy-ethyl)-1,3,5-triazinane

A mixture of 9.03 g ethanolamine (147.5 mmol) and 1.2 g ethanol (26.1 mmol) were stirred for 15 minutes at room temperature. The mixture was cooled with a water/ice mixture and 11.0 g aqueous formaldehyd (37%, 147.5 mmol) were added dropwise. Afterwards the reaction mixture was stirred for 2 hours at room temperature. Finally the reaction mixture was distilled under reduced pressure at 60 °C and analyzed by ¹H-NMR spectroscopy in CDCl₃.

¹H-NMR (300MHz, CDCl₃): δ 2.62 (t, N-CH₂-CH₂-OH), 3.48 (br. s, N-CH₂-N), 3.65 (t, N-CH₂-CH₂-OH).²⁷⁹

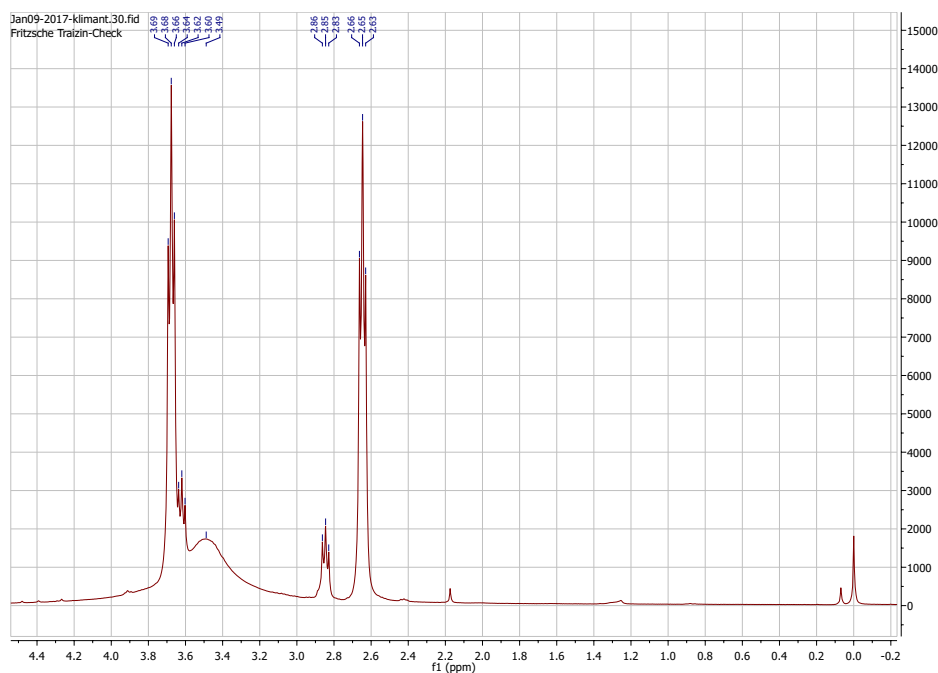
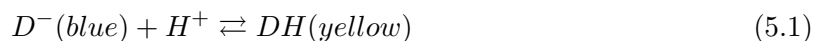


Figure 5.1: ¹H-NMR of 1,3,5-tris(2-hydroxy-ethyl)-1,3,5-triazinane in CDCl₃.

5.3 Development steps

5.3.1 Material selection

The sensor foils used in the investigation are based on *m*-cresol purple, an CO₂ sensitive indicator dye. The dye was embedded in ethyl cellulose and formed an acid-base pair with TOA OH. The deprotonated form of the dye was blue. *M*-cresol purple is rather insensitive to carbon dioxide, so no change was observed with the naked eye after exposure of the foil to room air. The sensor foil turned yellow according to the degree of protonation. In the case of the performed experiments the protonation was generated by hydrogen sulfide, which diffused through the polymers covering the CO₂-sensitive layer.



To protect the indicator/base pair, a diffusion barrier covered the layer prepared of ethyl cellulose. The chosen polymer should have a low permeability for hydrogen sulfide and a high selectivity for carbon dioxide over other poisoning gases, including H₂S. Additionally the polymer should have appropriate photophysical properties, should be mechanically stable and easy to handle. Very promising candidates are perfluorinated polymers. They have a lower permeability for hydrogen sulfide, compared to other often used polymers in sensor production, like silicone rubber^{170 253 254 255} and polystyrol^{280 281 282}(tab. 5.1). A direct comparison of the hydrogen sulfide protection properties can be found in figure 5.2.

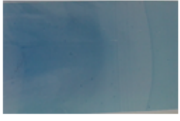






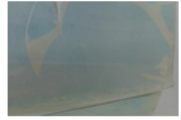


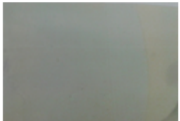

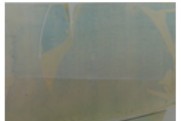


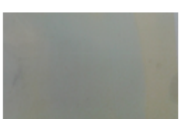
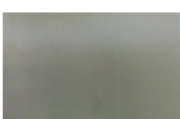

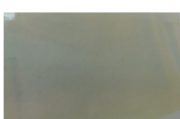
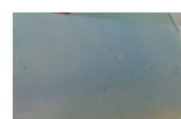


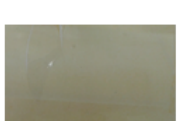

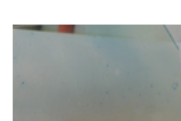
time [h]	ethyl cellulose	silicone rubber	polystyrene	Teflon AF 1400	Hyflon AD 60
0					
0.75					
1.1					
1.75					
2.75					

Figure 5.2: Direct comparison of protection properties against hydrogen sulfide for the following polymers: ethyl cellulose, silicone rubber, polystyrene, Teflon AF 1400 and Hyflon AD 60. The experiment was performed in the gas phase containing oxygen and H₂S at room temperature.

Table 5.1: Permeability for hydrogen sulfide and selectivity for carbon dioxide of silicone rubber, polystyrol, Teflon AF 1400 and Hyflon AD 60. All values are given in barrer.

	ethyl cellulose	silicone rubber ¹⁷⁹	polystyrol	Teflon AF 1400 ¹⁷⁹	Hyflon AD 60 ¹⁸⁴
P_{CO_2}	113 ²⁵⁶	4400	12.4 ²⁸³	680	124
P_{H_2S}	1200 (0°C) ²⁸⁴	6670	-	100	-
P_{CO_2}/P_{H_2S}	0.09	0.66	-	6.8	-

Hyflon AD 60 was chosen as the material for the diffusion barrier, to reduce the amount of hydrogen sulfide getting in the sensor. The matching photophysical properties and the easy handling, as well as the expected low permeability for H₂S and the potential to disperse particles were the main reasons. Moreover the response times are supposed to be slow, but still acceptable for long-term applications.¹⁰⁸ The layer made of the perfluorinated polymer was just the first protection. To fully secure the indicator/base pair, a reservoir of scavenger particles was investigated. Hydrogen sulfide was expected to react irreversibly at the surface of the particles

and do not further diffuse into the sensor foil. This represent just a time-limited protection, but still allows the measurement of carbon dioxide in marine oxygen-minimum and oxygen-free zones.

5.3.2 Scavenger selection

Potential scavenger should not interact with carbon dioxide, should be homogenously suspendable in Hyflon AD 60, commercially available and most important should not influence the sensor performance. Additionally they should react with hydrogen sulfide even at low temperatures. Moreover a white color is beneficial to enlarge the signal intensity of the final sensor. For preliminary tests a serie of scavenger particles were chosen, according to different reaction schemes:

1. reversible adsorption – hydrogen sulfide adsorp at particle surface and stick in the scavenger layer
2. irreversible formation of sulfides – metal- or organometalocompounds react with H₂ to form corresponding metalsulfides
3. oxidation – oxidation to sulfate via manganese(IV)oxide
4. irreversible reaction with organic compounds – often used in gas treatment

The adsorption of poisoning molecules is a typical approach in many medical applications.^{285 286 287 288} (Activated)Charcoal is known to adsorp a broad range of compounds on its surface.²⁸⁹ The adsorption of hydrogen sulfide on charcoal was investigated at high temperature²⁹⁰ and in the gas phase^{291 292 293}. Due to the high specific surface area, the potential to adsorb molecules should be sufficiently high. Moreover charcoal is relatively cheap and the black color act as an optical isolation. The second strategy includes a wide variety of metalcompounds. The compounds were chosen consulting their solubility constants of the corresponding metalsulfide (tab. 5.2). The smaller the value of the constant, the more insolluble is the salt. Consequential the salt is more stable and has a high affinity to form during a reaction. Moreover the environmental compatibility should be kept in mind. Therefore mercury was not investigated.

According to table 5.2, iron, copper, silver, zinc and lead were chosen. The associated oxides were selected, due to the formation of water instead of acids during the reaction with hydrogen sulfide. Acids would interact with the indicator/base pair in the CO₂ sensitive layer and falsify the sensor response or even poison the sensor. Water do not interrupt the sensor response. In the case of silver, even an organometallic compound (silvertrifluoromethansulfonate) was investigated. During the reaction formed trifluoromethansulfuric acid is not supposed to migrate. Another special scavenger is lead(IV)oxide. It has the potential to intercept two hydrogen sulfide molecules per one oxide molecule. Overall the following metal compounds were chosen: Cu₂O, CuO, ZnO, Ag₂O, CuCO₃ · Cu(OH)₂, Fe₂O₃, PbO, Pb₂O and Ag-triflate.

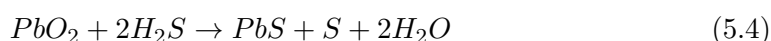
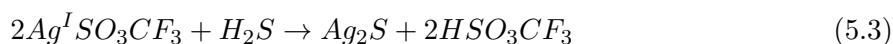
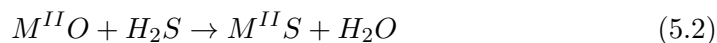
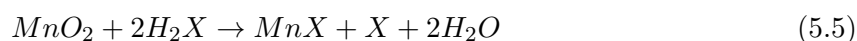


Table 5.2: Solubility constants of different metalsulfides at 25°C.

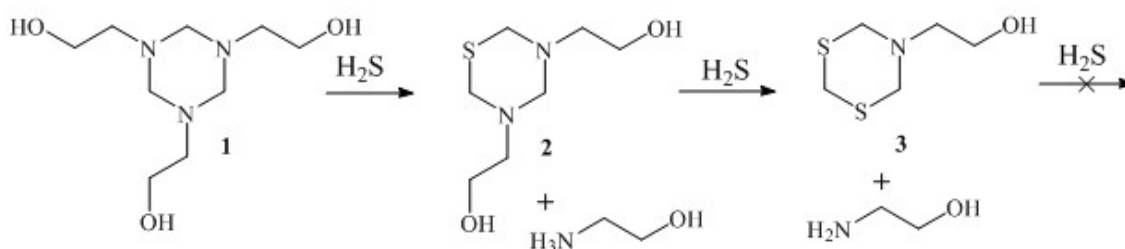
metalsulfide	formula	K _{sp}	choice
iron(II)sulfide	FeS	$8 \cdot 10^{-19}$	✓
copper(I)sulfide	Cu ₂ S	$2.5 \cdot 10^{-48}$	✓
copper(II)sulfide	CuS	$8 \cdot 10^{-37}$	✓
manganese(II)sulfide	MnS	$2.5 \cdot 10^{-13}$	X
nickel(II)sulfide	NiS	$1.3 \cdot 10^{-25}$	X
mercury(II)sulfide	HgS	$1.6 \cdot 10^{-52}$	X
silversulfide	Ag ₂ S	$6 \cdot 10^{-51}$	✓
zincsulfide	ZnS	$2 \cdot 10^{-25}$	✓
lead(II)sulfide	PbS	$3 \cdot 10^{-29}$	✓

The third approach includes the oxidation of sulfide to elemental sulfur or sulfate. An often used oxidizing agent is manganese(IV)oxide (MnO₂, pyrolusite).^{294 295}



For this reaction hydrogen sulfide has to dissociate to HS⁻ and H⁺. Therefore water is necessary. Further information can be found in literature.²⁹⁶

The last possibility to intercept hydrogen sulfide is the reaction with an organic compound. An often used molecule in H₂S removal is triazin.^{269 272 297} Triazin is a six-membered ring including three nitrogen atoms, each with a 2-hydroxyethyl side chain (fig. 5.3). The main product after the reaction with two hydrogen sulfide molecules was assumed to be 5-(2-hydroxyethyl) hexahydro-1,3,5-dithiazine. A nucleophilic substitution of sulfur into the ring occurs. The reactivity decreases from compound **1** to **3**. The substitution with sulfur always competes with the hydrolysis reaction²⁷¹ and is dependent on the pH of the medium²⁷². The likely reason for the pH dependency is the activation of the triazine ring by protonation of an nitrogen atom. Therefore a high pH is necessary, which although result in HS⁻ as the main species of the H₂S system.²⁷⁹ Due to the hydrophilic character of triazine, induced by the three hydroxy groups, the preparation of a dispersion with Hyflon AD 60 was not possible. Even the use of a triazine/ethyl cellulose-dispersion was problematic in terms of knife coating. It was not possible to produce a homogeneous layer. To overcome this problem, triazine was adsorbt at particles like Trisopor[®] (granular porous glass material) and Kieselgur (amorphous silicone dioxide). Thereupon the particles were suspended in Hyflon AD 60.

**Figure 5.3:** Proposed reaction of triazine with two molecules hydrogen sulfide.²⁷¹

A compilation of all the used scavengers can be found in table 5.3. The experiments were done in the gas phase with and without the presence of oxygen. The change in color due to the poisoning process can be seen with the naked eye. A selection of pictures of all experiment numbers can be found in Appendix A. The suspension of the scavenger particles was not a problem, as well as knife coating.

Table 5.3: Overview tested hydrogen sulfide scavenger in the gasphase. Shown are the ratio between particles and Hyflon[®] AD 60, the possible use of the plasticizer Fomblin[®] Y, the experiment number with photographic images in Appendix A. * experiment with and without oxygen; ** embedded in Trisopor and Kieselgur; *** milled.

particles	ratio (w:w)	plasticizer use	exp.- no.	scavenger potential
charcoal	1:4	X	1	red
copper(I)oxide (Cu ₂ O)	1:3.9	X	1	yellow
copper(II)oxide (CuO)	1:3.9	X	3	yellow
zinc oxide (ZnO)	1:4	X	1	green
silver(I)oxide (Ag ₂ O)	1:2.5	X	1,2,3	yellow
dicopper carbonate dihydroxide (CuCO ₃ · Cu(OH) ₂)	1:1.4	X	1,2,3	yellow
Triazinane (C ₉ H ₂₁ N ₃ O ₃)	1:1.4	X	2,3*	yellow**
manganese oxide (MnO ₂)	1:3.7	X	3	red
silver(I)oxide (Ag ₂ O)	1:1	✓	4,5	yellow
dicopper carbonate dihydroxide (CuCO ₃ · Cu(OH) ₂) ***	1:1	✓	4	yellow
silver nanoparticles (Ag)	1:1.7	✓	4	yellow
iron(III)oxide (Fe ₂ O ₃)	1:1.7	✓	4	red
zinc oxide (ZnO)	1:1	✓	5	green
lead(II)oxide (PbO)	1:1	✓	5	red
lead(IV)oxide (PbO ₂)	1:1	✓	5	yellow
silver triflate	1:1	✓	5	red

Charcoal, possibly the easiest approach, showed no significant improvement in long-term stability in a hydrogen sulfide containing atmosphere. The surface of the particles was potentially covered with the matrix-polymer, so no active surface space was left for adsorption. All organic compounds seemed not to work as a scavenger for hydrogen sulfide when they are embedded in a polymer matrix. A likely reason is the dramatically reduced mobility in the rigid matrix. Manganese dioxide did not react with hydrogen sulfide either. The lack of water in the layer and a low temperature might be the cause. A wide variety of metal oxides were tested as well, additionally a dicopper carbonate dihydroxide. After preliminary tests dicopper carbonate dihydroxide, silver oxide and zinc oxide were promising candidates to provide a long-term protection against hydrogen sulfide. After the last experiment (exp.-no.5) zinc oxide was chosen as the compound for further investigations. This metal oxide showed a significantly slower

and later starting poisoning process induced by H₂S compared to a scavenger-free sensor foil. Besides the particle composition, the particle size and the specific surface area has a significant impact on the ability of the particle to react with hydrogen sulfide.

5.3.3 Particle size dependency – Zinc oxide

Zinc oxide is an often used compound for the removal of hydrogen sulfide from fluids²⁹⁸ or gas streams^{299 300 301}. It is non-toxic and used in personal care products. Elsevier and Verelst (1999) investigated transition metal oxides for desulphuration of hot gases (400 °C-700 °C) and revealed zinc oxide as the best candidate. It was possible to reduce the H₂S level from initially 3250 ppm to 0.03 ppm at 400 °C.³⁰¹ Sun et al. (2007) investigated the kinetics of the zinc oxide sulfidation reaction in the gas phase. The study presented a three step reaction: 1) adsorption and dissociation of H₂S at two active sites; 2) reaction of HS⁻ with ZnO; 3) waterformation. An ion migration into the particle is described although.



It is assumed, that the adsorption and dissociation is the rate-limiting step. Additionally zinc oxide is relatively stable and not reduced by H₂S (T: 150 °C-450 °C).³⁰² The study of Sayyadnejad et al. (2008) dealt with the removal efficiency of hydrogen sulfide from drilling fluids as a function of the surface area of ZnO particles. They compared bulk ZnO with ZnO nanoparticles. The dramatically increase in the surface areas resulted in a faster and more efficient removal.

Keeping these studies in mind, we investigated the protection potential depending on the ZnO particle size in a polymer layer. Three different particle sizes were purchased and investigated: <300 nm, <100 nm (surface area: 15-25 m²/g, value given by producer) and <50 nm (surface area: >10.8 m²/g, value given by producer). The particles were homogenously suspended in Hyflon AD 60 with a polymer:particle ratio of 1:1. To evaluate the real protection potential a sensor foil without any particles was integrated in the experiment. It is clearly visible, the pure Hyflon sensor foil was completely poisoned after 23 hours of hydrogen sulfide exposure. Like expected the sensor foil with ZnO particles <300 nm showed less protection potential than ZnO <100 nm and ZnO <50 nm. The difference between the last two was visible after 76 hours of exposure. The sensor foil with ZnO particles less than 100 nm and a surface area of 15-25 m²/g showed the slowest poisoning process (fig. 5.4). The observations correlated perfectly with the surface areas given by the producer for the used ZnO particles. Further development steps are based on ZnO scavenger particles with a particle size of <100 nm and a surface area of 15-25 m²/g.


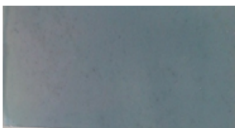


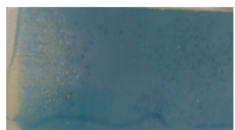


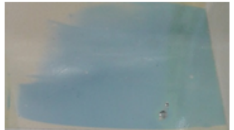
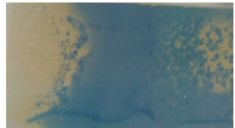



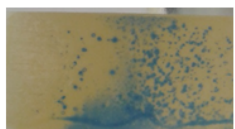


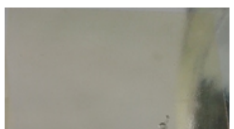
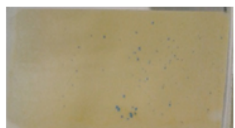


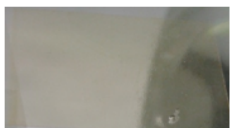
time [h]	ZnO <300 nm	ZnO <100 nm	ZnO <50nm	Hyflon (reference)
0				
10				
23				
35				
76				

Figure 5.4: Photographic images of H₂S poisoning experiment in gaseous phase consisting of 0.1% hydrogen sulfide and room air at room temperature. Plasticizer was used during foil production. Black marked area was not considered. Used scavenger: ZnO (particles <300nm), ZnO (particles <100 nm, SA=15-25 m²/g), ZnO (particles <50 nm, SA>10.8 m²/g) and pure Hyflon (reference). Order: Hyflon (pure)<ZnO (<300 nm)<ZnO(<50 nm)<ZnO(<100 nm).

5.3.4 Sensor structure optimization

The focus during the last development step was set to the extension of time the sensing chemistry is protected against hydrogen sulfide. Therefore we rethought the layer structure of the sensor foil. The material for the scavenger particles containing layer was Hyflon AD 60 at the beginning. The thicker the layer the more particles are present and the higher the protection potential. At the same time the response time increases exponentially. Silicone rubber was expected to be the better choice for the scavenger particle containing layer. The permeability for carbon dioxide and hydrogen sulfide is significantly higher than of Hyflon AD 60 (tab. 5.1). By the use of silicone rubber a thicker layer with a higher content of scavenger particles can be used by keeping the response time constant. As a result a longer time of protection against hydrogen sulfide is expected. An important point is the ratio between vinyl dimethyl siloxy-terminated polydimethylsiloxane (main component silicone rubber mixture) and ZnO particles, called particle load. We tested silicone rubber mixtures with a particle load between 48% and 171%. The higher the content of particles, the more past-like is the 'cocktail' and the more difficult is the handling. The high content of zinc oxide particles was expected to adsorb a part of the catalyst. To ensure a solid silicone rubber layer, the catalyst content was increased with the particle load

from 0.008% to 0.012%. Furthermore the content of solvent, which had to be added to obtain an appropriate silicone cocktail, had to be increased. A higher solvent content resulted in a less concentrated cocktail and a reduced layer thickness compared to a cocktail with a lower particle load. Finally a particle load of around 100% was chosen for further experiments.

Moreover the CO₂-sensitive layer and the H₂S scavenger layer were covered with a diffusion barrier. The barrier was made of Hyflon AD 60, known for its low permeability for hydrogen sulfide (fig. 5.1). Diffusion barriers are often used to tune the sensor performance.^{303 304 305} In the case of our investigation such a diffusion barrier reduces the amount of hydrogen sulfide entering the sensor, before the gas molecules reach the scavenger reservoir (silicon rubber + ZnO particles) and get intercepted. Omitting the diffusion barrier would result in a fast consumption of zinc oxide. The poisoning process of the indicator/base pair (CO₂-sensitive layer) starts when the reservoir is 'empty' and the hydrogen sulfide molecules break through the second barrier. A cross section of the new sensor foil structure is shown in figure 5.5.

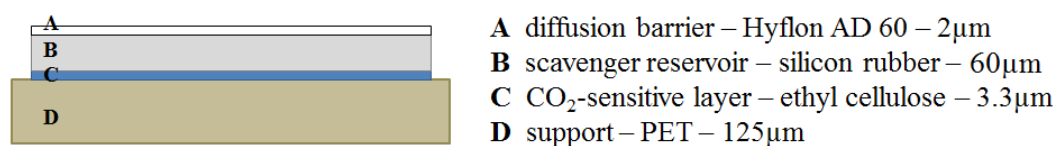


Figure 5.5: Schematic image of the final layer structure including H₂S scavenger layer.

Besides the above shown layer structure (fig. 5.5), other alternatives to realize H₂S protection are possible. To enhance the protection potential a second diffusion barrier can be inserted right on top of the CO₂-sensitive layer. This additional layer would increase the response time. Embedding zinc oxide particles in a reference layer can enhance the signal intensity, due to the white color (stray light), but although can negatively affect the sensor performance. It has to be considered if hydrogen sulfide react with other parts of the sensing chemistry besides the indicator/base pair, like reference particles. So mixing the reference particles with the scavenger particles is not recommended.

During the production a critical point was noticed. The hydrophobicity of silicone rubber and Hyflon AD 60 are different. So the connection between the silicone rubber based scavenger layer and the Hyflon AD 60 based diffusion barrier is poor. After knife coating the Hyflon solution tended to tighten. The use of plasticizer (Fomblin Y) intensified the effect. Therefore a pure Hyflon solution was used for the diffusion barrier. Moreover the whole silicone rubber layer should be covered with the diffusion barrier, otherwise the scavenger layer can be scratched off easily.

In the next experiment the new developed sensor structure was tested in a gaseous H₂S-containing atmosphere (H₂S mixed with room air). Additionally a sensor foil completely based on Hyflon AD 60 was inserted. The layer thickness of the silicone rubber was set to ~25 μm and ~60 μm, covered with a diffusion barrier of roughly equal thickness compared to the diffusion barrier of the Hyflon based sensor foil. With this experiment the matrix effect of the scavenger layer was investigated. A zinc oxide free sensor foil with the same layer structure was

prepared as well, to evaluate the effect of the scavenger particles. Because of the good protection characteristics of Hyflon AD 60 and zinc oxide, the atmosphere in the dessicator, used for the experiment, had to be renewed at the second day of the experiment. The complete investigation took 6 days with a hydrogen sulfide concentration of 0.15% in air. No complete poisoning was reached after 10 days for the silicone rubber 3 Mil ZnO.

time [h]	silicone rubber 1Mil reference	silicone rubber 1 Mil ZnO	silicone rubber 3 Mil reference	silicone rubber 3 Mil ZnO	Hyflon AD 60 reference	Hyflon AD 60 ZnO
0						
3						
7						
34						
49						
96						

Figure 5.6: Photographic images of H₂S poisoning experiment in gas phase consisting of 0.15% hydrogen sulfide and room air at room temperature in darkness. Zinc oxide was used as a scavenger for hydrogen sulfide. The scavenger was suspended in Hyflon AD 60 and silicone rubber with a particle load of 100% in respect to the polymer in each case. Zinc oxide free reference sensor foils were inserted as well.

The experiment shown in figure 5.6 reveal two main things. First, if we just consider the reference sensor foils (fig. 5.6 column 2,4,6) silicone rubber itself do not provide protection against hydrogen sulfide independent on the layer thickness. Hyflon AD 60 instead is an effective diffusion barrier against poisoning gases. This result was expected considering the permeability for H₂S of both polymers (tab. 5.1). Second, the protection potential of the Hyflon AD 60 based sensor foil with ZnO and the silicone rubber based sensor foil (thick ZnO layer) were similar. The particle to polymer ratio was equal in both sensor foils. The first signs of dye protonation (yellow color) were observable after 25 hours looking at the sensor foil with a thin silicone rubber scavenger layer. A complete protonation was observable after 49 hours. Comparing the 'silicone rubber 3 Mil ZnO' sensor foil with the 'Hyflon AD 60 ZnO' sensor foil visible poisoning was observed first at the silicone rubber after 34 hours. After 96 hours both sensor foils showed a similar level of protonation/poisoning. The likely reason for the similar protection potential is

the proportion of protection provided by the polymer itself and the zinc oxide particles. In the case of the Hyflon AD 60 sensor foil the proportion of the polymer is rather high. The protection provided by the silicone rubber scavenger layer is almost completely based on the reaction of H₂S with zinc oxide. Due to the thickness of the scavenger layer a high amount of zinc oxide particles were implemented in the sensor foil. Previous experiments (see section 4) revealed no response time increase with a higher silicone rubber layer thickness. Only the recovery time increased, but is still several times faster than for Hyflon AD 60. Using this phenomenon the thickness of the scavenger layer/ amount of scavenger particles can be increased, resulting in a longer protection against hydrogen sulfide. Therefore silicone rubber seems to be the best choice in combination with zinc oxide for hydrogen sulfide protection.

5.4 H₂S-protected carbon dioxide sensor

Based on the previous described experiments and results, an established carbon dioxide sensor (described in section 2) was restructured to insert a silicone rubber based scavenger layer for enhanced hydrogen sulfide protection. The established sensor was completely based on Hyflon AD 60 in combination with ethyl cellulose (fig. 5.7). To reduce the response and recovery time, as well as implementing zinc oxide particles, the material of the inert light emitting layer was changed to silicone rubber. Two different layer structures of the new sensor foil were tested in the lab; The first included two separate silicone rubber layer one with the light emitting particles and one with zinc oxide. The second approach was to mix all three types of particles in one silicone 'cocktail' (fig. 5.7). They were tested in terms of signal intensity, response and recovery time. The production procedure of the protected sensor foil was less time consuming and more reproducible than for the established carbon dioxide sensor. No precutting of the support and no pipetting was necessary. Moreover the use of just one silicone rubber layer containing the light emitting particles and zinc oxide shorten the time for production.

The new structured sensor foils were tested in terms of signal intensity, response and recovery times. The signal intensity was around 5 times higher compared to the established CO₂ sensor, whereas the signal intensity of the sensor foil with separate silicone rubber layer were even slightly higher. The silicone rubber layer thicknesses are equal. The response and recovery times were determined at 20 °C in a 0.1 M phosphate buffer (pH 8.04) with 10 μM and 40 μM dissolved carbon dioxide adjusted by using sodium bicarbonate. The response and recovery times are very similar, which was expected according to the same layer thicknesses. The recovery time is 1.7 times higher than the response time, which correspond well with the observations described in section 4. Overall the response time is roughly 13 times faster than for the established Hyflon AD 60 based CO₂ sensor (tab. 5.4).

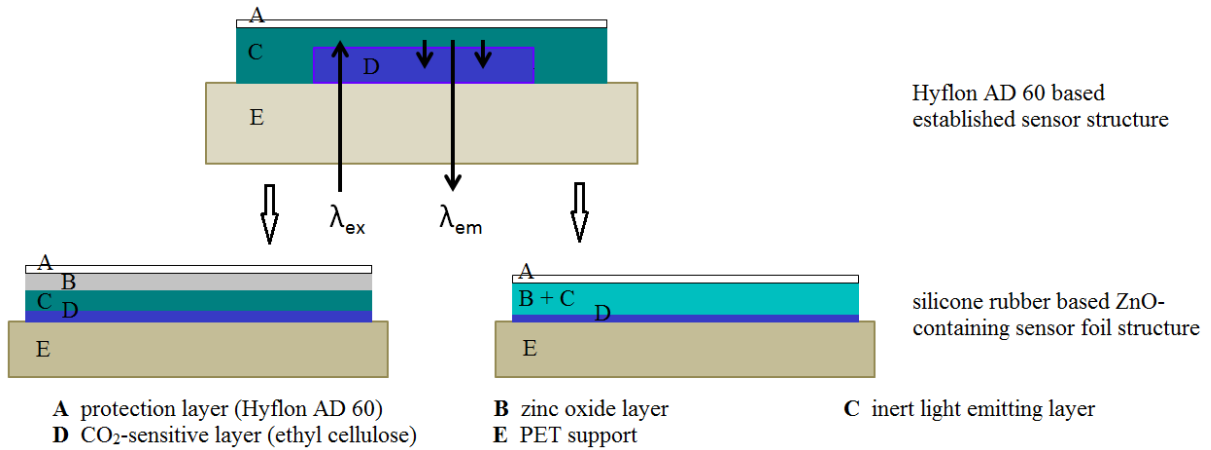


Figure 5.7: Sensor foil structures of an established carbon dioxide sensor based on Hyflon AD 60 and new layer structures inserting a zinc oxide containing layer for enhanced hydrogen sulfide protection.

Table 5.4: Signal intensity, layer thicknesses, response and recovery time of the protected silicone rubber based carbon dioxide sensor foils with separate silicone rubber layer and one mixed silicone rubber layer (fig. 5.7).

	separate	mixed
layer thickness [μm]	inert light emitting: 25 ZnO : 35	60
signal intensity	833	637
response time [s]	327 ± 45.3	324 ± 32.9
recovery time [s]	527 ± 5.9	569 ± 31.4

It is further estimated that the long-term stability do not or just slightly decrease because of the use of silicone rubber. The low permeability for acidic gases of Hyflon AD 60 is still beneficial for the protection layer/diffusion barrier. Furthermore the high amount of zinc oxide contributes to a long shelf life and long-term stability as well.

An additional poisoning experiment in 0.1 M phosphate buffer was done under lab conditions at roomtemperature ($T = 22.5 - 23.4 \text{ }^\circ\text{C}$). Two sensor spots, one of each kind (separate and mixed), were inserted in a completely closable, constantly-stirred vessel with 120 mL phosphate buffer (pH 8.04), 6.6 mg sodium hydrosulfide ($\text{NaHS} \cdot x\text{H}_2\text{O}$) were added and complete poisoning occurred (fig. 5.8). The level of hydrogen sulfide in the buffer was set relatively high to see a full poisoning process within one week. The chosen level was 1.620 mM (total sulfide), which represent eight times the hydrogen sulfide level found in the Baltic Sea after a long period of stagnation¹⁸⁰. A reference spot based on silicone rubber was expected to get completely poisoned within a very short time and therefore was not inserted in the experiment (fig. 5.6).

A clearly visible poisoning process occurred over time. It started roughly two hours after generating hydrogen sulfide. The process had a linear correlation in a time range from 2 to 20 hours. The increase of the phase angle was 0.032 units/h and 0.034 units/h for the separate and mixed

layer structure, respectively. The change in the phase angle are equal to a change in calculated carbon dioxide concentration of 0.6 $\mu\text{M}/\text{h}$ (separate) and 0.5 $\mu\text{M}/\text{h}$ (mixed). Almost 90% of the poisoning process happend between 20 and 78 hours with a significant higher slope than in the first 20 hours. Complete poisoning was indicated by a not changing phase angle and was visible after ~ 78 hours for both sensors. Overall both poisoning processes were very similar. A slower poisoning is expected in natural waters with a lower content of hydrogen sulfide and a potentially lower temperature. The sensor are at this point suitable for measurements in hydrogen sulfide containing environments for at least 3 hours. Moreover a potential shift in the calibration should be considered.

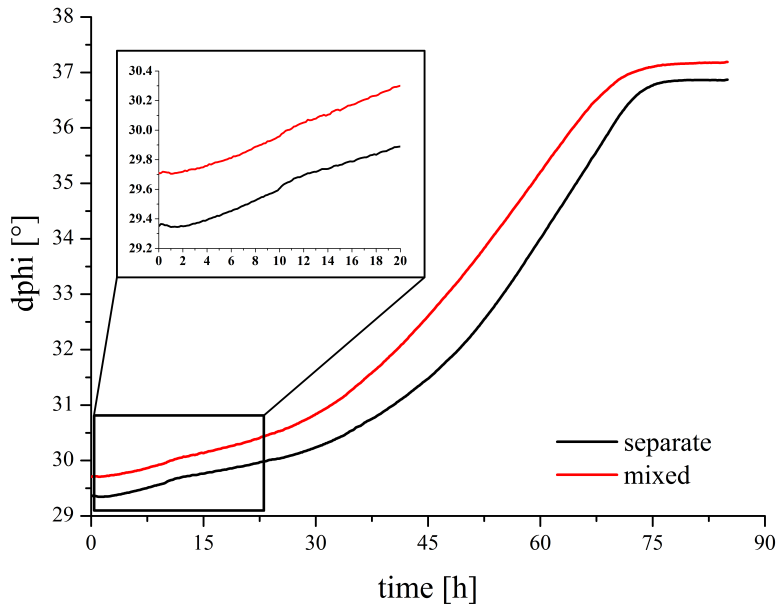


Figure 5.8: Poisoning experiment of new developed protected sensor spots with separate and mixed layer structure in H₂S-containing, constantly-stirred phosphate buffer at room temperature.

Future work

The performed test was a rough preliminary experiment. A more detailed investigation on the implementation of the scavenger layer containing ZnO should be done. The effect of the reference layer matrix should be examined in terms of protection potential and response time changes. The temperature dependency of the poisoning should be characterized, as well as a possible shift in the calibration of the sensor spot. Moreover the new developed and protected sensor spot has to be compared with the established carbon dioxide sensor.

5.5 Conclusion

Carbon dioxide optodes often show a hydrogen sulfide cross sensitivity. Hydrogen sulfide appears for example in oxygen minimum zones. To enable measurements in such water masses an effective protection has to be developed. We investigated a wide range of so called scavenger particles to irreversible react with H₂S molecules. Chosen scavenger included inorganic metal oxides and

organic molecules. Finally zinc oxide was indentified to be the best candidate for a sufficient protection against hydrogen sulfide. Furthermore the effect of different zinc oxide particle size was investigated. Experiments revealed, that the particles with the highest specific surface are the best. Afterwards an established and in section 2 described carbon dioxide optode was restructured to implement a zinc oxide containing layer for protection purposes. Two different new layer structures of the optode were tested in terms of signal intensity, response time, recovery time and protection potential. The signal intensities for both new developed sensor foils were significantly higher in comparison with the established optode. Although the response and recovery times were 13 times faster and around 6 minutes (response time) and 10 minutes (recovery time).

Conclusion and Outlook

The work was dedicated to the development of an long-term stable and robust carbon dioxide optode and their application in marine environments. Moreover optimizations of the optode structure were made to enable the use of the sensor in oxygen minimum zones and profiling applications.

In Chapter one a long-term stable carbon dioxide optode was presented. The main reason for the enhanced chemical stability is the use of Hyflon AD 60, a perfluorinated polymer. It is characterized by a low permeability for carbon dioxide, a high selectivity over hydrogen sulfide and a very high hydrophobicity. The perfluorinated polymer was used to realize an optode based on aza-BODIPY indicator dyes and the inner filter effect. The indicator dye is embedded with a lipophilic ammonium base in ethyl cellulose (EC). The combination of EC and Hyflon requires a special production procedure, due to a different hydrophobicity and thermal expansion. The production process was varied to obtain a mechanical stable sensor spot. Methods like laser cutting, dip coating and pipetting were used. Furthermore the response time was determined depending on the temperature. The response and recovery time for a carbon dioxide concentration between 14 and 28 μM was up to 180 minutes at 5°C and 40 minutes at 35°C. An optode calibration was although characterized. Finally the carbon dioxide optode was used to measure a stepwise depth profile in the Gotland Basin, Baltic Sea down to 225 m and the Gulf of Finland down to 70 m. The highest gradient was measured between 40 and 100 m.

In the second chapter an extensive evaluation and comparison study was performed. Used optodes in this study measured dissolved oxygen, pH and dissolved carbon dioxide. The developed carbon dioxide optode (first chapter) was used in an aquarium with an almost stable temperature, an aquaculture facility in the monitoring system and a breeding tank (direct sunlight and high amount of algae) and at a mooring buoy in an estuary. Estuaries are mostly influenced by the tidal cycle, resulting in a highly changing environment. The dissolved oxygen and the pH sensor were integrated in a profiling float, measuring depth profiles every 6 hours till 100 m water depth. The oxygen sensor was although integrated in an AUV for a 24 hour-deployment in the Monterey Bay, California. For each analyte commercially available sensor systems were implemented in the deployments as well. Producers were Aanderaa Data Instruments, Sea-Bird Scientific and OxyGuard[®] for dissolved oxygen, Satlantic and Hach[®] for pH and Turner Designs for carbon dioxide. The comparison revealed a good agreement between the data sets. A long-term deployment was done with the pH optode. The comparison with reference samples were investigated as well. Biofouling prevention was realized by using copper guards.

The application of the carbon dioxide optode at the profiling float was not possible, due to a too long response time (t_{90}). Chapter three dealt with a response and recovery time optimization of the carbon dioxide and pH optode. It was realized by using different materials and reducing the layer thickness. The response time of the pH optode was reduced from 14 s to 4 s at 4°C by reducing the layer thickness. For the carbon dioxide optode silicone rubber was used to embed necessary reference particles. Silicone rubber has a significantly higher permeability

for carbon dioxide and other gases. Moreover the layer thickness of the ethyl cellulose layer and the silicone rubber layer was reduced. It was possible to decrease the response time of the carbon dioxide optode from 70 min to 100 s at 20 °C. At the same time the long-term stability was reduced dramatically. Furthermore a detailed calibration for both optodes were measured in the lab. These two fast-responding optodes were used for profiling applications. Due to the response time of the carbon dioxide optode a stepwise measurement was still necessary with a waiting times of 90 s. Additionally reference samples were taken at each depth. The data obtained with the optodes agreed very good with the reference values.

In the last chapter a protection against hydrogen sulfide was investigated. The combination of a perfluorinated polymer and an efficient scavenger was considered to be the best option for a time-limited protection. At the beginning a wide variety of scavenger particles were analysed in the gas phase using a sensor foil based on *m*-cresol purple. Compounds like metal oxides or organic compounds were chosen. These particles irreversibly form metal sulfides, when reacting with hydrogen sulfide. Zinc oxide with a high specific surface area showed the most-promising protection potential. A mixture of silicone rubber and zinc oxide particles revealed similar protection than Hyflon AD 60 with zinc oxide particles, but has a significantly faster response and recovery time.

Future work should include further deployments in marine environments over a longer period (>6 months) to evaluate potential long-term drifts, leaching effects and biofouling issues. Additionally the production procedure for the carbon dioxide optodes should be improved in terms of reproducibility and time-consumption. The hydrogen sulfide protection should be adequately implemented in the carbon dioxide optode, considering a sufficient response time and protection potential. Furthermore these optodes should be tested in the lab in a H₂S-containing environment in comparison to a H₂S free system. Afterwards field deployments in an oxygen minimum zone are necessary to fully evaluate the sensor performance.

The response time of the Hyflon AD 60 based CO₂ optode and the time-consuming production procedure are the major issues. The main reason is the sensor foil structure, which is required for a ratiometric read out via phase fluorometry. An internal-referenced fluorescent-based carbon dioxide optode would be a promising alternative.

References

- [1] S. C. Doney, V. Fabry, R. A. Feely, and J. A. Kleypas. Ocean acidification: the other CO₂ problem. *Annu. Rev. Mater. Sci.*, 1:169–192, 2009. doi: 10.1146/annurev.marine.010908.163834.
- [2] R. F. Weiss. Carbon dioxide in water and seawater: The solubility of a non-ideal gas. *Mar. Chem.*, 2:203–215, 1974. doi: 10.1016/0304-4203(74)90015-2.
- [3] F. J. Millero. Thermodynamics of the carbon dioxide system in the oceans. *Geochim. Cosmochim. Acta*, 59:661–677, 1995. doi: 10.1016/0016-7037(94)00354-O.
- [4] R. N. Roy, L. N. Roy, K. M. Vogel, C. Porter-Moore, T. Pearson, C. E. Good, F. J. Millero, and D. M. Campbell. The dissociation constants of carbonic acid in seawater at salinities 5 to 45 and temperatures 0 to 45 °C. *Mar. Chem.*, 44:249–267, 1993. doi: 10.1016/0304-4203(93)90207-5.
- [5] F. J. Millero, D. Pierrot, K. Lee, R. Wanninkhof, R. Feely, C. L. Sabine, R. M. Key, and T. Takahashi. Dissociation constants for carbonic acid determined from field measurements. *Deep Sea Res., Part I*, 49:1705–1723, 2002. doi: 10.1016/S0967-0637(02)00093-6.
- [6] A. G. Dickson. An exact definition of total alkalinity and a procedure for the estimation of alkalinity and total inorganic carbon from titration data. *Deep Sea Res.*, 6:609–623, 1981. doi: 10.1016/0198-0149(81)90121-7.
- [7] K. Lee, F. J. Millero, R. H. Byrne, R. A. Feely, and R. Wanninkhof. The recommended dissociation constants for carbonic acid in seawater. *Geophys. Res. Lett.*, 27:229–232, 2000. doi: 10.1029/1999GL002345.
- [8] I. Hansson. A new set of pH-scales and standard buffers for sea water. *Deep Sea Res.*, 20:479–491, 1973. doi: 10.1016/0011-7471(73)90101-0.
- [9] P. K. Park. Oceanic CO₂ system: An evaluation of ten methods of investigation. *Limnol. Oceanogr.*, 14:179–186, 1969. doi: 10.4319/lo.1969.14.2.0179.
- [10] T. D. Clayton, R. H. Byrne, J. A. Breland, R. A. Feely, F. J. Millero, D. M. Campbell, P. P. Murphy, and M. F. Lamb. The role of pH measurements in modern oceanic CO₂-system characterizations: Precision and thermodynamic consistency. *Deep Sea Res., Part II*, 42, 1995.

- [11] D. J. Hydes, S. Lucaides, and T. Tyrrell. Report on a desk study to identify likely sources of error in the measurements of carbonate system parameters and related calculations, particularly with respect to coastal waters and ocean acidification experiments. *Research and Consultancy Report No. 83, National Oceanography Centre, Southampton*, 83, 2010.
- [12] S. C. Talmage and C. J. Gobler. Effects of past, present and future ocean carbon dioxide concentrations on the growth and survival of larval shellfish. *PNAS*, 107:177246–177251, 2010. doi: 10.1073/pnas.0913804107.
- [13] R. E. Zeebe and D. A. Wolf-Gladow. *CO₂ in seawater: Equilibrium, kinetics, isotopes. Elsevier Oceanography Book Series*, 2001.
- [14] C. B. Andersen. Understanding carbonate equilibria by measuring alkalinity in experimental and natural systems. *Journal of Geoscience Education*, 50:389–403, 2002. doi: 10.5408/1089-9995-50.4.389.
- [15] T. J. Lueker, A. G. Dickson, and C. D. Keeling. Ocean pco₂ calculated from dissolved inorganic carbon, alkalinity and equations for k₁ and k₂: validation based on laboratory measurements of co₂ in gas and seawater at equilibrium. *Mar. Chem.*, 70:105–119, 2000. doi: 10.1016/S0304-4203(00)00022-0.
- [16] C. J. M. Hoppe, G. Langer, S. D. Rokitta, D. A. Wolf-Gladow, and B. Rost. Implications of observed inconsistencies in carbonate chemistry measurements for ocean acidification studies. *Biogeoscience*, 9:2401–2405, 2012. doi: 10.5194/bg-9-2401-2012.
- [17] U. Riebesell, V. J. Fabry, L. Hansson, and J.-P. Gattuso. Guide for best practices in ocean acidification research and data reporting. *Office for Official Publications of the European Union, Luxembourg*, 2011.
- [18] S. McElligott, R. H. Byrne, K. Lee, R. Wanninkhof, F. J. Millero, and R. A. Feely. Discrete water column measurements of co₂ fugacity and ph_t seawater: A comparison of direct measurements and thermodynamic calculations. *Mar. Chem.*, 60:63–73, 1998. doi: 10.1016/S0304-4203(97)00080-7.
- [19] R. A. Feely, C. L. Sabine, J. M. Hernandez-Ayon, D. Ianson, and B. Hales. Evidence for upwelling of corrosive 'acidified' water onto the continental shelf. *Science*, 320:1490–1492, 2008. doi: 10.1126/science.1155676.
- [20] K. E. Fabricius, C. Langdon, S. Uthicke, C. Humphrey, S. Noonan, G. Death, R. Okazaki, N. Muehllehner, M. S. Glas, and J. M. Lough. Losers and winners in coral reefs acclimatized to elevated carbon dioxide concentrations. *Nat. Clim. Change*, 1:165–169, 2011. doi: 10.1038/NCLIMATE1122.
- [21] E. Lewis and D. Wallace. Program developed for co₂ system calculations. *Carbon dioxide information analysis center, Oak Ridge National Laboratory*, 1998.
- [22] L. L. Robbins, M. E. Hansen, J. A. Kleypas, and S. C. Meylan. Co2calc: A user-friendly seawater carbon calculator for windows, macos x and ios (iphone). *U.S. Geological Survey*, 2010.

- [23] H. Lavigne and J. P. Gattuso. Seacarb: seawater carbonate chemistry with r r package version 2.3.3. 2010.
- [24] K. A. Hunter. Swco2 seawater co2 equilibrium calculations. *University of Otago, New Zealand*, 2007.
- [25] W. M. Post, T.-H. Peng, W. R. Emanuel, A. W. King, V. H. Dale, and D. L. DeAngelis. The global carbon cycle. *American Scientist*, 78:310–326, 1990.
- [26] P. Falkowski, R. J. Scholes, E. Boyle, J. Canadell, D. Canfield, J. Elser, N. Gruber, K. Hibbard, P. ögberg, S. Linder, F. T. Mackenzie, B. Moore III, T. Pedersen, Y. Rosenthal, S. Seitzinger, V. Smetacek, and W. Steffen. The global carbon cycle: A test of our knowledge of earth as a system. *Science*, 290:291–295, 2000. doi: 10.1126/science.290.5490.291.
- [27] Credit by nasa earth observatory.
- [28] D. S. Schimel. Terrestrial ecosystems and the carbon cycle. *Glob. Change Biol.*, 1:77–91, 1995. doi: 10.1111/j.1365-2486.1995.tb00008.x.
- [29] T. J. Battin, S. Luyssaert, L. A. Kaplan, A. K. Aufdenkampe, A. Richter, and L. J. Travnik. The boundless carbon cycle. *Nature Geoscience*, 2:598–600, 2009.
- [30] W. H. Schlesinger and J. A. Andrews. Soil respiration and the global carbon cycle. *Biogeochemistry*, 48:77–91, 2000. doi: 10.1111/j.1365-2486.1995.tb00008.x.
- [31] R. Lal. Agriculture activities and the global carbon cycle. *Nutr. Cycl. Agroecosys.*, 70: 103–116, 2004.
- [32] M. Reichstein, M. Bahn, P. Ciais, D. Frank, M. D. Mahecha, S. I. Senevirante, J. Zscheischler, C. Beer, N. Buchmann, D. C. Frank, D. Papale, A. Rammig, P. Smith, K. Thonicke, M. van der Velde, S. Vicca, A. Walz, and M. Wattenbach. Climate extremes and the carbon cycle. *Nature*, 500:287–295, 2013. doi: 10.1038/nature12350.
- [33] W. Cramer, A. Bondeau, S. Schaphoff, W. Lucht, B. Smith, and S. Sitch. Tropical forests and the global carbon cycle: impacts of atmospheric carbon dioxide, climate change and rate of deforestation. *Philos. Trans. R. Soc. Lond. B Biol. Sci.*, 359, 2013. doi: 10.1098/rstb.2003.1428.
- [34] P. Tett. Light and life in the sea, chapter 4 photonic zone. *Cambridge University Press*, pages 59–65, 1990.
- [35] C. B. Field, M. J. Behrenfeld, J. T. Randerson, and P. Falkowski. Primary production of the biosphere: Integrating terrestrial and oceanic components. *Science*, 281:237–240, 1998. doi: 10.1126/science.281.5374.237.
- [36] P. G. Falkowski, R. T. Barber, and V. Smetacek. Biogeochemical controls and feedbacks on ocean primary production. *Science*, 281:200–206, 1998. doi: 10.1126/science.281.5374.200.

- [37] J. W. Morse, R. S. Arvidson, and A. Lüttge. Calcium carbonate formation and dissolution. *Chem. Rev.*, 107:342–381, 2007. doi: 10.1021/cr050358j.
- [38] V. J. Fabry, B. A. Seibel, R. A. Feely, and J. C. Orr. Impacts of ocean acidification on marine fauna and ecosystem processes. *ICES J. Mar. Sci.*, 65:414–432, 2008. doi: 10.1093/icesjms/fsn048.
- [39] G. Falini, S. Albeck, S. Weiner, and L. Addadi. Control of aragonite or calcite polymorphism by mollusk shell macromolecules. *Science*, 271:67–69, 1996.
- [40] R. A. Feely, C. L. Sabine, K. Lee, W. Berelson, J. Kleypas, V. J. Fabry, and F. J. Millero. Impact of anthropogenic CO_2 on the CaCO_3 system in the oceans. *Science*, 305:362–366, 2004. doi: 10.1126/science.1097329.
- [41] R. B. Rivkin and L. Legendre. Biogenic carbon cycling in the upper ocean: Effects of microbial respiration. *Science*, 291:2398–2400, 2001. doi: 10.1126/science.291.5512.2398.
- [42] S. A. Hensen, R. Sanders, and E. Madsen. Global patterns in efficiency of particulate organic carbon export and transfer to the deep ocean. *Global Biochem. Cy.*, 26:1–14, 2012. doi: 10.1029/2011GB004099.
- [43] E. Y. Kwon, F. Primeau, and J. L. Sarmiento. The impact of remineralization depth on the air-sea carbon balance. *Nat. Geosci.*, 2:630–635, 2009. doi: 10.1038/NGEO612.
- [44] A. E. White, K. S. Watkins-Brandt, M. A. Engle, B. Burkhardt, and A. Paytan. Characterization of the rate and temperature sensitivity of bacterial remineralization of dissolved organic phosphorus compounds by natural populations. *Front. Microbiol.*, 3:1–13, 2012. doi: 10.3389/fmicb.2012.00276.
- [45] C. D. Keeling, R. B. Bacastow, A. E. Bainbridge, C. A. Ekdahl Jr., P. R. Guenther, L. S. Waterman, and J. F. S. Chin. Atmospheric carbon dioxide variations at mauna loa observatory, hawaii. *Tellus*, 28:538–551, 1976. doi: 10.3402/tellusa.v28i6.11322.
- [46] C. L. Sabine and et al. The oceanic sink for anthropogenic CO_2 . *Science*, 305:367–371, 2004. doi: 10.1126/science.1097403.
- [47] G. P. Robertson, E. A. Paul, and R. R. Harwood. Agriculture: Contributions of individual gases to the radiative forcing of the atmosphere. *Science*, 289:1922–1925, 2000. doi: 10.1126/science.289.5486.1922.
- [48] A. Raval and V. Ramanathan. Observational determination of the greenhouse effect. *Nature*, 342:758–761, 1989.
- [49] O. Hoegh-Guldberg and J. F. Bruno. The impact of climate change on the world’s marine ecosystem. *Science*, 328:1523–1528, 2010. doi: 10.1126/Science.1189930.
- [50] J. C. Orr et al. Anthropogenic ocean acidification at the twenty-first century and its impact on calcifying organisms. *Nature*, 437:681–686, 2005. doi: 10.1038/nature04095.

- [51] K. R. N. Anthony, D. I. Kline, G. Diaz-Pulido, S. Dove, and O. Hoegh-Guldberg. Ocean acidification causes bleaching and productivity loss in coral reef builders. *Proc. Natl. Acad. Sci. USA*, 105:17442–17446, 2008. doi: 10.1073/pnas.0804478105.
- [52] F. Joos, G.-K. Plattner, T. F. Stocker, A. Körtzinger, and D. W. R. Wallace. Trends in marine dissolved oxygen: Implications for ocean circulation changes and the carbon budget. *EOS*, 84:197–201, 2003. doi: 10.1029/2003EO210001.
- [53] T. Moutin and P. Raimbault. Primary production, carbon export and nutrients availability in western and eastern mediterranean sea in early summer 1996 (minos cruise). *J. Marine Syst.*, 33-34:273–288, 2002. doi: 10.1016/S0924-7963(02)00062-3.
- [54] M. A. Charette and W. H. F. Smith. The volume of earth’s ocean. *Oceanography*, 23: 112–114, 2010.
- [55] C. Kato, L. Li, Y. Nogi, Y. Nakamura, J. Tamaoka, and K. Horikoshi. Extremely barophilic bacteria isolated from the mariana trench, challenger deep, at a depth of 11,000 meters. *Appl. Environ. Microbiol.*, 64:1510–1513, 1998.
- [56] World ocean review 1 2010. *maribus in cooperation with 'ocean of the future'*, 2010. doi: ISBN978-86648-000-1.
- [57] P. U. Clark, N. G. Pias, T. F. Stocker, and A. J. Weaver. The role of the thermohaline circulation in abrupt climate change. *Nature*, 415:863–869, 2002. doi: 10.1038/415863.
- [58] R. J. Stouffer, J. Yin, J. M. Gregory, and et al. Investigating the causes of the response of the thermohaline circulation to past and future climate changes. *J. Clim.*, 19:1365–1387, 2006. doi: 10.1175/JCLI3689.1.
- [59] R. Zhang and T. L. Delworth. Simulated tropical response to a substantial weakening of the atlantic thermohaline circulation. *Nature*, 18:1853–1860, 2005. doi: 10.1175/JCLI3460.1.
- [60] C. de Boyer Montégut, G. Madec, A. S. Fischer, A. Lazar, and D. Iudicone. Mixed layer depth over the global ocean: an examination of profile data and a profile-based climatology. *J. Geophys. Res.*, 109:C12003, 2004. doi: 10.1029/2004JC002378.
- [61] <http://www.seasky.org/deep-sea/ocean-layers.html>. 2017.
- [62] C. Robinson, D. K. Steinberg, T. R. Anderson, J. Aristegui, and C. A. Carlson et al. Mesopelagic zone ecology and biogeochemistry - a synthesis. *Deep Sea Res., Part II*, 57: 1504–1518, 2010. doi: 10.1016/j.dsr2.2010.018.
- [63] G. Badin, A. Tandon, and A. Mahadevan. Lateral mixing in the pycnocline by baroclinic mixed layer eddies. *J. Phys. Oceanogr.*, 41:2080–2101, 2011. doi: 10.1175/JPO-D-11-05.1.
- [64] A. R. Longhurst, A. W. Bedo, W. G. Harrison, E. J. H. Head, and D. D. Sameoto. Vertical flux of respiratory carbon by oceanic diel migrant biota. *Deep Sea Res.*, 37:685–694, 1990.

- [65] P. C. Fiedler and L. D. Talley. Hydrography of the eastern tropical pacific: A review. *Prog. Oceanogr.*, 69:143–180, 2006. doi: 10.1016/j.pocean.2006.03.008.
- [66] C. Tamburini, M. Canals, X. D. de Madron, L. Houpert, D. Lefèvre, S. Martini, F. D’Ortenzio, A. Robert, P. Testor, J. A. Aguilar, I. Al Samarai, A. Albert, and M. André et al. Deep-sea bioluminescence blooms after dense water formation at the ocean surface. *PLoS one*, 8:1–10, 2013. doi: 10.1371/journal.pone.0067523.
- [67] K. L. Smith Jr., H. A. Ruhl, B. J. Bett, D. S. Billett, R. S. Lampitt, and R. S. Kaufmann. Climate, carbon cycling and deep-ocean ecosystems. *PNAS*, 106:19211–19218, 2009. doi: 10.1073/pnas.0908322106.
- [68] R. J. Diaz and R. Rosenberg. Spreading dead zones and consequences for marine ecosystems. *Science*, 321:926–929, 2008. doi: 10.1126/science.1156401.
- [69] J. J. Childress and B. A. Seibel. Life at stable low oxygen levels: adaptations of animals to oceanic oxygen minimum layers. *J. Exp. Biol.*, 201:1223–1232, 1998.
- [70] A. Paulmier and D. Ruiz-Pino. Oxygen minimum zones (omz) in the modern ocean. *Progress in Oceanography*, 80:113–128, 2009. doi: 10.1016/j.pocean.2008.08.001.
- [71] S. Kröger and R. J. Law. Biosensors for marine applications we all need the sea, but does the sea need biosensors. *Biosens. Bioelectron.*, 20:1903–1913, 2005. doi: 10.1016/j.bios.2004.08.036.
- [72] U. Schuster, A. Hannides, L. Mintrop, and A. Körtzinger. Sensors and instruments for oceanic dissolved carbon measurements. *Ocean Sci.*, 5:547–558, 2009. doi: 10.5194/os-5-547-2009.
- [73] K. Daly, R. H. Byrne, A. G. Dickson, S. M. Gallagher, M. J. Perry, and M. K. Twey. Chemical and biological sensors for time-series research: Current status and new directions. *Mar. Technol. Sci. J.*, 38:121–143, 2004. doi: 10.4031/002533204787522767.
- [74] D. S. Simbeye and S. F. Yang. Water quality monitoring and control for aquaculture based on wireless sensor networks. *Journal of Networks*, 9:840–849, 2014. doi: 10.4304/jnw.9.4.840-849.
- [75] P. J. Thomas, D. Atamanchuk, J. Hovdenes, and A. Tengberg. The use of novel optode sensor technology for monitoring dissolved carbon dioxide and ammonia concentrations under live haul conditions. *Aquacult. Eng.*, 77:89–96, 2017. doi: 10.1016/j.aquaeng.2017.02.004.
- [76] M. Elliott and D. S. McLusky. The need for definitions in understanding estuaries. *Estuar. Coast Shelf Sci.*, 55:815–827, 2002. doi: 10.1006/ecss.2002.1031.
- [77] K. Taira, D. Yanagimoto, and S. Kitagawa. Deep ctd casts in the challenger deep, mariana trench. *J. Oceanogr.*, 61:447–454, 2005.

- [78] R. D. Prien and D. E. Schulz-Bull. Technical note: Godess – a profiling mooring in the gotland basin. *Ocean Sci.*, 12:899–907, 2016. doi: 10.5194/os-12-899-2016.
- [79] J. Manley and Scott Willcox. The wave glider: A persistent platform for oceanic science. *OCEANS 2010 IEEE*, 2010. doi: 10.1109/OCEANSSYD.2010.5603614.
- [80] R. Hine, S. Willcox, G. Hine, and T. Richardson. The wave glider: A wave-powered autonomous marine vehicle. *OCEANS 2009 IEEE*, 2009. doi: 10.23919/OCEANS.2009.5422129.
- [81] J. Gould, D. Roemmich, and S. Wuffels et al. Argo profiling float bring new era of in situ ocean observations. *EOS*, 85:179–190, 2004.
- [82] United Nations Educational. Global ocean science report – the current status of ocean science around the world. *UNESCO*, Executive Summary, 2017.
- [83] R. B. Wynn et al. Autonomous underwater vehicles (auvs): Their past, present and future contributions to the advancement of marine geoscience. *Mar. Geol.*, 352:451–468, 2014. doi: 10.1016/j.margeo.2014.03.012.
- [84] C. C. Eriksen, J. T. Osse, R. D. Light, T. Wen, T. W. Lehman, P. L. Sabin, J. W. Ballard, and A. M. Chiodi. Seaglider: A long-range autonomous underwater vehicle for oceanographic research. *IEEE J. Ocean. Eng.*, 26:424–436, 2001. doi: 10.1109/OCEANS.2007.4449125.
- [85] T. J. Osse and C. C. Eriksen. The deepglider: A full ocean depth glider for oceanographic research. *OCEANS2007*, 2007. doi: 10.1109/OCEANS.2007.4449125.
- [86] from left: www.uvs.com.au/products/wave-glider ; www.seabird.com/navis-autonomous-profiling-float; www.unmannedsystemstechnology.com/category; www.bridges-h2020.eu/. sept. 2017.
- [87] J. W. Severinghaus and A. F. Bradley. Electrodes for blood po_2 and pcO_2 determination. *J. Appl. Physiol.*, 13:515–520, 1958.
- [88] V. Vojinović, J. M. S. Cabral, and L. P. Fonseca. Real-time bioprocess monitoring part i: In situ sensors. *Sens. Actuators B*, 114:1083–1091, 2006. doi: 10.1016/j.snb.2005.07.059.
- [89] J. S. Clarke, E. P. Achterberg, D. P. Connelly, U. Schuster, and M. C. Mowlem. Developments in marine pcO_2 measurement technology; towards sustained in situ observations. *Trends Anal. Chem.*, 88:53–61, 2017. doi: 10.1016/j.trac.2016.12.008.
- [90] J. H. Shin, H. J. Lee, C. Y. Kim, B.K. Oh, K. L. Rho, H. Nam, and G. S. Cha. Isfet-based differential pcO_2 sensors employing a low-resistance gas-permeable membrane. *Anal. Chem.*, 68:3166–3172, 1996. doi: 10.1021/ac960473h.
- [91] P. Fietzek, B. Fiedler, T. Steinhoff, and A. Kötzing. In situ quality assessment of a novel underwater pcO_2 sensor based on membrane equilibration and ndir spectrometry. *J. Atmos. Oceanic Techn.*, 31:181–196, 2014. doi: 10.1175/JTECH-D-13-00083.1.

- [92] Ir spectra of carbon dioxide from coblenz - society's evaluated infrared reference spectra collection. 2009.
- [93] E. R. Crosson. A cavity ring-down analyzer for measuring atmospheric levels of methane, carbon dioxide and water vapor. *Appl. Phys. B*, 92:403–408, 2008. doi: 10.1007/s00340-008-3135-y.
- [94] N. Lefèvre, J. P. Ciabrini, G. Michard, B. Brient, M. DuChaffaut, and L. Merlivat. A new optical sensor for p_{CO_2} measurements in seawater. *Mar. Chem.*, 3-4:189–198, 1993. doi: 10.1016/0304-4203(93)90011-C.
- [95] E. M. Hood, L. Merlivat, and T. Johannessen. Variations of f_{CO_2} and air-sea flux of CO_2 in the greenland sea gyre using high-frequency time series data from carioaca drift buoys. *J. Geophys. Res.*, 104:20571–20583, 1999. doi: 10.1029/1999JC900130.
- [96] M. D. DeGrandpre, T. R. Hammar, S. P. Smith, and F. L. Sayles. In situ measurements of seawater p_{CO_2} . *Limnol. Oceanogr.*, 40:969–975, 1995. doi: 10.4319/lo.1995.40.5.0969.
- [97] X. Ge, Y. Kostov, R. Hendersen, N. Selock, and G. Rao. A low-cost fluorescent sensor for p_{CO_2} measurements. *Chemosensors*, 2:108–120, 2014. doi: 10.3390/chemosensors2020108.
- [98] Y. Liu, Y. Tang, N. N. Barashkow, I. S. Irgibaeva, J. W. Y. Lam, R. Hu, D. Birimzhanova, Y. Yu, and B. Z. Tang. Fluorescent chemosensor for detection and quantification of carbon dioxide gas. *JACS*, 132:13951–13953, 2010. doi: 10.1021/ja103947j.
- [99] T. Seiyama, A. Kato, and M. Nagatani. A new detector for gaseous components using semiconductive thin films. *Anal. Chem.*, 34:1502–1503, 1962.
- [100] H. J. Yoon, D. H. Jun, J. H. Yang, Z. Zhou, S. S. Yang, and M. Ming-Cheng Cheng. Carbon dioxide gas sensor using a graphene sheet. *Sens. Actuators B*, 157:310–313, 2011. doi: 10.1016/j.snb.2011.03.035.
- [101] S. A. Waghuley, S. M. Yenorkar, S. S. Yamale, and S. P. Yawale. Application of chemically synthesized conducting polymer-polypyrrole as a carbon dioxide gas sensor. *Sens. Actuators B*, 128:366–373, 2008. doi: 10.1016/j.snb.2007.06.023.
- [102] J. W. Fergus. A review of electrolyte and electrode materials for high temperature electrochemical CO_2 and SO_2 gas sensors. *Sens. Actuators B*, 134:1034–1041, 2008. doi: 10.1016/j.snb.2008.07.005.
- [103] K. Shitashima. Evolution of compact electrochemical in-situ $pH-p_{CO_2}$ sensor using isfet- pH electrode. *OCEANS2010*, pages 1–4, 2010. doi: 10.1109/OCEANS.2010.5663782.
- [104] W.-J. Cai, P. Zhao, and Y. Wang. pH and p_{CO_2} microelectrode measurements and the diffusive behaviour of carbon dioxide species in coastal marine sediments. *Mar. Chem.*, 70:133–148, 2000. doi: 10.1016/S0304-4203(00)00017-7.
- [105] P. Zhao and W.-J. Cai. An improved potentiometric p_{CO_2} microelectrode. *Anal. Chem.*, 69:5052–5058, 1997. doi: 10.1021/ac970747g.

- [106] M. Molari, S. Meyer, M. Weber, K. Guilini, L. Vielstädte, N. Bigalke, S. Schutting, C. Howe, M. Kreuzburg, B. Unger, M. Schneider, H. Kuhfuss, A. Eich, F. Wenzhöfer, D. de Beer, A. Ramette, C. Lott, A. Vanreusel, and A. Boetius. Cruise report eco2-8 (panarea island, italy). 2013.
- [107] D. Atamanchuk, A. Tengberg, P. J. Thomas, J. Hovdenes, A. Apostolidis, C. Huber, and P. O. J. Hall. Performance of a lifetime-based optode for measuring partial pressure of carbon dioxide in natural waters. *Limnol. Oceanogr.: Methods*, 12:63–73, 2014. doi: 10.4319/lom.2014.12.63.
- [108] E. Fritzsche, P. Gruber, S. Schutting, J. P. Fischer, M. Strobl, J. D. Müller, S. M. Borisov, and I. Klimant.
- [109] C. R. Schröder, G. Neuraüter, and I. Klimant. Luminescent dual sensor for time-resolved imaging of $p\text{CO}_2$ and $p\text{O}_2$ in aquatic systems. *Micrichim Acta*, 158:205–218, 2007. doi: 10.1007/s00604-006-0696-5.
- [110] Y Nakano and H. Yoshida. Development of in situ CO_2 and pH sensor (hybrid CO_2 -pH-sensor: Hcs) for auv. *IEEE 2011*, 2011. doi: 10.1109/UT.2011.5774126.
- [111] <http://www.senseocean.eu/>. hosted by National Oceanography Centre, 2017.
- [112] <http://www.senseocean.eu/senseocean/sites/senseocean/files/documents/senseocean%20brochure%20-%20e.pdf>. 2017.
- [113] Sunburst sensors, sami CO_2 ocean CO_2 sensor, www.sunburstsensors.com/products/oceanographic-carbon-dioxide-sensor. Sept. 2017.
- [114] Kongsberg maritime contros gmbh, contros hydroc CO_2 highly accurate underwater $p\text{CO}_2$ sensor, www.km.kongsberg.com/ks/web/nokbg0240.nsf/all-web/537648638d3f59aac1257edc0040495f?opendocument. 2016.
- [115] Battelle seaology [®] $p\text{CO}_2$ monitoring system, system manual 635108h1010. Sept. 2017.
- [116] A. J. Sutton, C. L. Sabine, S. Maenner-Jones, N. Lawrence-Slavas, C. Meinig, R. A. Feely, J. T. Mathis, S. Musielewicz, R. Bott, P. D. McLain, H. J. Fought, and A. Kozyr. A high-frequency atmospheric and seawater $p\text{CO}_2$ data set from 14 open-ocean sites using a moored autonomous system. *Earth Syst. Sci Data*, 6:353–366, 2014.
- [117] Pro-oceanus systems inc., CO_2 -pro cvTM submersible $p\text{CO}_2$ sensor, www.pro-oceanus.com/co2-pro-cv. Sept. 2017.
- [118] Picarro inc., picarro g2201-i analyzer, www.picarro.com/products_solutions/isotope_analyzers/13c_for_ch4_co2. Sept. 2017.
- [119] M. Becker, N. Andersen, B. Fiedler, A. Körtzinger, T. Steinhoff, and G. Friedrichs. Using cavity ringdown spectroscopy for continuous monitoring of $\Delta^{13}\text{C}(\text{CO}_2)$ and $f\text{CO}_2$ in the surface ocean. *Limnol. Ocenogr. Methods*, 10:752–766, 2012. doi: 10.4319/lom.2012.10.752.

- [120] D. Turk, V. Malačič, M. D. DeGrandpre, and W. R. McGillis. Carbon dioxide variability and air-sea fluxes in the northern adriatic sea. *J. Geophys. Res.*, 115:1–12, 2010. doi: 10.1029/2009JC006034.
- [121] E. Podgrajsek, E. Sahlé, and A. Rutgersson. Enhanced nighttime gas emissions from a lake. *IOP Conference Series: Earth and Environmental Science*, 35:1–4, 2016. doi: 10.1088/1755-1315/35/1/012014.
- [122] B. Fiedler, P. Fietzek, N. Vieira, P. Silva, H. C. Bittig, and A. Körtzinger. In situ CO_2 and O_2 measurements on a profiling float. *J. Atmos. Oceanic. Technol.*, 30:112–126, 2012. doi: 10.1175/JTECH-D-12-00043.1.
- [123] R. B. Wallace, H. Baumann, J. S. Grear, R. C. Aller, and C. J. Gobler. Coastal ocean acidification: the other eutrophication problem. *Estuar. Coast. Shelf. Sci.*, 148:1–13, 2014. doi: 10.1016/j.ecss.2014.05.027.
- [124] <https://www.pmel.noaa.gov/co2/story/buoys+and+autonomous+systems>. 2017.
- [125] S. E. Hartman, Z.-P. Jiang, D. Turk, R. S. Lampitt, H. Frigstad, C. Ostle, and U. Schuster. Biogeochemical variations at the porcupine abyssal plain sustained observatory in the northeast atlantic ocean, from weekly to inter-annual timescales. *Biogeoscience*, 12:845–853, 2015. doi: 10.5194/bg-12-845-2015.
- [126] J. W. Pohlmann, J. Greinert, C. Ruppel, A. Silyakova, L. Vielstädte, M. Casso, J. Mienert, and S. Bünz. Enhanced CO_2 uptake at a shallow arctic ocean seep field overwhelms the positive warming potential of emitted methane. *PNAS*, 114:5355–5360, 2017. doi: 10.1073/pnas.1618926114.
- [127] picture provided from ocean observatories initiative/sensors, sept. 2017.
- [128] M. D. DeGrandpre and M. M. Baehr. Calibration-free optical chemical sensors. *Anal. Chem.*, 71:1152–1159, 1999. doi: 10.1021/ac9805955.
- [129] D. Turk, J. M. Bedard, W. J. Burt, S. Vagle, H. Thomas, K. Azetsu-Scott, W. R. McGillis, S. J. Iversen, and D. W. R. Wallace. Inorganic carbon in a high latitude estuary-fjord system in canada’s eastern arctic. *Estuar. Coast Shelf Sci.*, 178:137–147, 2016. doi: 10.1016/j.ecss.2016.06.006.
- [130] Z.-P. Jiang, D. J. Hydes, S. E. Hartman, M. C. Hartman, J. M. Campbell, B. D. Johnson, B. Schofield, D. Turk, D. Wallace, W. J. Burt, H. Thomas, C. Cosca, and R. Feely. Application and assessment of a membrane-based pCO_2 sensor under field and laboratory conditions. *Limnol. Oceanogr.: Methods*, 12:264–280, 2014. doi: 10.4319/lom.2014.12.264.
- [131] Turner-designs, c-senseTM in situ pCO_2 sensor, www.turnerdesigns.com/products/submersible-fluorometer/c-sense-in-situ-pco2-sensors. 2014.
- [132] A. Mills and Q. Chang. Fluorescence plastic thin-film sensor for carbon dioxide. *Analyst*, 118:839–843, 1993.

- [133] O. S. Wolfbeis, B. Kovács, K. Goswami, and S. M. Klainer. Fiber-optic fluorescence carbon dioxide sensor for environmental monitoring. *Mikrochim. Acta*, 129:181–188, 1998. doi: 10.1007/bf01244739.
- [134] O. Oter, K. Ertekin, D. Topkaya, and S. Alp. Emission-based optical carbon dioxide sensing with hpts in green chemistry reagents: room temperature ionic liquid. *Anal. Bioanal. Chem.*, 386:1225–1234, 2006. doi: 10.1007/s00216-006-0659-z.
- [135] C. S. Burke, A. Markey, R. I. Nooney, P. Byrne, and C. McDonagh. Development of an optical sensor probe for the detection of dissolved carbon dioxide. *Sens. Actuators, B*, 119:288–294, 2006. doi: 10.1016/j.snb.2005.12.022.
- [136] D. Aigner, B. Ungerböck, T. Mayr, R. Saf, I. Klimant, and S. M. Borisov. Fluorescent materials for ph sensing and imaging based on novel 1,4-diketopyrrolo-[3,4-c]pyrrole dyes. *J. Mater. Chem. C*, 1:5685–5693, 2013. doi: 10.1039/c3tc31130a.
- [137] S. Schutting, S. M. Borisov, and I. Klimant. Diketo-pyrrolo-pyrrole dyes as new colorimetric and fluorescent ph indicators for optical carbon dioxide sensors. *Anal. Chem.*, 85: 3271–3279, 2013. doi: 10.1021/ac303595v.
- [138] A. Mills and Q. Chang. Tuning colourimetric and fluorimetric gas sensors for carbon dioxide. *Anal. Chim. Acta*, 285:113–123, 1994. doi: 10.1016/0003-2670(94)85015-1.
- [139] S. Schutting, T. Jokic, M. Strobl, S. M. Borisov, D. de Beer, and I. Klimant. Nir optical carbon dioxide sensors based on highly photostable dihydroxy-aza-bodipy dyes. *J. Mater. Chem.*, 3:5474–5783, 2015. doi: 10.1039/c5tc00346f.
- [140] R. Rebane, I. Leito, S. Yurchenko, and K. Herodes. A review of analytical techniques for determination of sudan i-iv dyes in food matrixes. *J. Chrom. A*, 1217:2747–2757, 2010. doi: 10.1016/j.chroma.2010.02.038.
- [141] C. von Bültzingslöwen, K. McEvoy, C. McDonagh, B. D. MacCraith, I. Klimant, C. Krause, and O. S. Wolfbeis. Sol-gel based optical carbon dioxide sensor employing dual luminophore referencing for application in food packaging technology. *Analyst*, 127: 1478–1483, 2002. doi: 10.1039/b207438a.
- [142] S. Blümel, H.-J. Knackmuss, and A. Stolz. Molecular cloning and characterization of the gene coding for the aerobic azoreductase from *Xenophilus azovorans* kf46f. *Appl. Environ. Microbiol.*, 68:3948–3955, 2002. doi: 10.1128/AEM.68.8.3948-3955.2002.
- [143] M. Cajlaković, A. Bizzarri, and V. Ribitsch. Luminescence lifetime-based carbon dioxide optical sensor for clinical applications. *Anal. Chim. Acta*, 573-574:57–64, 2006. doi: 10.1016/j.aca.2006.05.085.
- [144] I. Klimant, C. Huber, G. Liebsch, G. Neurauther, A. Stangel-Mayer, and O. S. Wolfbeis. New trends in fluorescence spectroscopy: Application to chemical and life science. *Springer Verlag*, Chapter 13:57–274, 2001.

- [145] S. M. Borisov and I. Klimant. A versatile approach for ratiometric time-resolved read-out of colorimetric chemosensors using broadband phosphors as second emitters. *Anal. Chim. Acta*, 787:219–225, 2013. doi: 10.1016/j.aca.2013.05.032.
- [146] I. M. Pérez de Vargas-Sansalvador, M. A. Carvajal, O. M. Roldán-Muñoz, J. Banqueri, M. D. Fernández-Ramos, and L. F. Capitán-Valley. Phosphorescent sensing of carbon dioxide based on secondary inner-filter quenching. *Anal. Chim. Acta*, 655:66–74, 2009. doi: 10.1016/j.aca.2009.09.037.
- [147] A. Mills, Q. Chang, and N. McMurray. Equilibrium studies on colorimetric plastic film sensors for carbon dioxide. 64:1383–1389, 1992. doi: 10.1021/ac00037a015.
- [148] C. R. Schröder and I. Klimant. The influence of the lipophilic base in solid state optical pco₂ sensors. *Sens. Actuators B*, 107:572–579, 2005. doi: 10.1016/j.snb.2004.11.019.
- [149] C. Staudinger et al. A versatile optode system for oxygen, carbon dioxide and ph measurements in seawater with integrated battery and logger. *Limnol. Oceanogr. Methods*, submitted, 2017.
- [150] G. Neurauter, I. Klimant, and O. S. Wolfbeis. Fiber-optic microsensor for high resolution pco₂ sensing in marine environment. *Fresenius J. Anal. Chem.*, 366:481–487, 2000. doi: 10.1007/s002160050097.
- [151] A. Mills, A. Lepre, and L. Wild. Breath-by-breath measurement of carbon dioxide using plastic film optical sensor. *Sens. Actuators B*, 39:419–425, 1997. doi: 10.1016/S0925-4005(96)02116-8.
- [152] M. D. DeGrandpre. Measurement of seawater pco₂ using a renewable-reagent fiber optic sensor with colorimetric detection. *Anal. Chem.*, 65:331–337, 1993. doi: 10.1021/ac00052a005.
- [153] R. Ali, T. Lang, S. M. Saleh, R. J. Meier, and O. S. Wolfbeis. Optical sensing scheme for carbon dioxide using a solvatochromic probe. *Anal. Chem.*, 83:2846–2851, 2011. doi: 10.1021/ac200298j.
- [154] S. Pandey, S. N. Baker, S. Pandey, and G. A. Baker. Optically responsive switchable ionic liquid for internally-referenced fluorescence monitoring and visual determination of carbon dioxide. *Chem. Commun.*, 48:7043–7045, 2012. doi: 10.1039/c2cc32164e.
- [155] L. Chen, D. Huang, S. Ren, Y. Chi, and G. Chen. Carbon dioxide gas sensor based on ionic liquid-induced electrochemiluminescence. *Anal. Chem.*, 83:6862–6867, 2011. doi: 10.1021/ac201067u.
- [156] Y. Kawabata, T. Kamichika, T. Imasaka, and N. Ishibashi. Fiber-optic sensor for carbon dioxide with a ph indicator dispersed in a poly(ethylene glycol) membrane. *Anal. Chim. Acta*, 219:223–229, 1989. doi: 10.1016/s0003-2670(00)80353-0.
- [157] O. Oter, K. Ertekin, and S. Derinkuyu. Ratiometric sensing of co₂ in ionic liquid modified ethyl cellulose matrix. *Talanta*, 76:557–563, 2008. doi: 10.1016/j.talanta.2008.03.047.

- [158] R. N. Dansby-Sparks, J. Jin, S. J. Mechery, U. Sampathkumaran, T. W. Owen, B. D. Yu, K. Goswami, K. Hong, J. Grant, and Z.-L. Xue. Fluorescent-dye-doped sol-gel sensor for highly sensitive carbon dioxide gas detection below atmospheric concentrations. *Anal. Chem.*, 82:593–600, 2010. doi: 10.1021/ac901890r.
- [159] A. Mills and G. A. Skinner. Water-based colourimetric optical indicators for the detection of carbon dioxide. *Analyst*, 135:1912–1917, 2010. doi: 10.1039/c000688b.
- [160] G. Liebsch, I. Klimant, C. Krause, and O. S. Wolfbeis. Fluorescent imaging of ph with optical sensors using time domain dual lifetime referencing. *Anal. Chem.*, 73:4354–4363, 2001. doi: 10.1021/ac0100852.
- [161] M. Uttamlal and D. R. Walt. A fiber-optic carbon dioxide sensor for fermentation monitoring. *Nat. Biotechnol.*, 13:597–601, 1995. doi: 10.1038/nbt0695-597.
- [162] C.-S. Chu and Y.-L. Lo. Fiber-optic carbon dioxide sensor based on fluorinated xerogels doped with hpts. *Sens. Actuators, B*, 129:120–125, 2008. doi: 10.1016/j.snb.2007.07.082.
- [163] A. Loudet, R. Bandichhor, K. Burgess, A. Palma, S. O. McDonell, M. J. Hall, and D. F. O’Shea. B,o-chelated azadipyrromethenes as near-ir probes. *Org. Lett.*, 10:4771–4774, 2008. doi: 10.1021/ol8018506.
- [164] T. Jokic, S. M. Borisov, R. Saf, D. A. Nielsen, M. Kühl, and I. Klimant. Highly photostable near-infrared fluorescent ph indicators and sensors based on bf₂-chelated tetraarylazadipyrromethenes dyes. *Anal. Chem.*, 84:6723–6730, 2012. doi: 10.1021/ac3011796.
- [165] L. M. Mosley, S. L. G. Husheer, and K. A. Hunter. Spectrophotometric ph measurement in estuaries using thymol blue and m-cresol purple. *Mar. Chem.*, 91:175–186, 2004. doi: 10.1016/j.marchem.2004.06.008.
- [166] A. G. Dickson, C. L. Sabine, and J. R. Christian. Guide to best practices for ocean co₂ measurements. *North Pacific Marine Science Organisation*, 2007.
- [167] J. B. Brolly, D. I. Bower, and I. M. Ward. Diffusion and sorption of co₂ in poly(ethylene terephthalate) and poly(ethylene naphthalate). *J. Polym. Sci., Part B: Polym. Phys.*, 34:769–780, 1996. doi: 10.1002/(sici)1099-0488(199603)34:4.
- [168] B. H. Weigl and O. S. Wolfbeis. New hydrophobic materials for optical carbon dioxide sensors based on ion pairing. *Anal. Chim. Acta*, 302:249–254, 1995. doi: 10.1016/0003-2670(94)00473-y.
- [169] L. M. Mosley, S. L. G. Husheer, and K. A. Hunter. A novel planar optical sensor for simultaneous monitoring of oxygen, carbon dioxide, ph and temperature. *Anal. Bioanal. Chem.*, 400:2463–2474, 2011. doi: 10.1007/s00216-010-4617-4.
- [170] J. C. Lötters, W. Olthuis, P. H. Veltink, and P. Bergveld. The mechanical properties of the rubber elastic polymer polydimethylsiloxane for sensor applications. *J. Microchem. Microeng.*, 7:145–147, 1997.

- [171] L. M. Robeson. The upper bound revisited. *J. Membr. Sci.*, 320:390–400, 2008. doi: 10.1016/j.memsci.2008.04.030.
- [172] P. Bernardo, E. Drioli, and G. Golemme. Membrane gas separation: a review/state of the art. *Ind. Eng. Chem. Res.*, 48:4638–4663, 2009. doi: 10.1021/ie8019032.
- [173] P. M. Budd and N. B. McKeown. Highly permeable polymers for gas separation membranes. *Polym. Chem.*, 1:63–68, 2010. doi: 10.1039/b9py00319c.
- [174] C. A. Scholes, G. W. Stevens, and S. E. Kentish. Membrane gas separation applications in natural gas processing. *Fuel*, 96:15–28, 2012. doi: 10.1016/j.fuel.2011.12.074.
- [175] Y. Okamoto, H. Zhang, F. Mikes, Y. Koike, Z. He, and T. C. Merkel. New perfluoro-dioxolane-based membranes for gas separations. *J. Membr. Sci.*, 471:412–419, 2014. doi: 10.1016/j.memsci.2014.07.074.
- [176] T. Graunke, K. Schmitt, S. Raible, and J. Wöllenstein. Towards enhanced gas sensor performance with fluoropolymer membranes. *Sensors*, 16:1605, 2016. doi: 10.3390/s16101605.
- [177] S. Z. Baykara, E. H. Figen, A. Kale, and T. Nejat Veziroglu. Hydrogen from hydrogen sulphide in black sea. *Int. J. Hydrogen Energy*, pages 1246–1250, 2007. doi: 10.1016/j.ijhydene.2006.07.021.
- [178] M. Naumann and G. Nausch. Die ostsee atmet auf. *Chem. Unsere Zeit*, 49:76–80, 2015. doi: 10.1002/ciuz.201400695.
- [179] T. C. Merkel and L. G. Toy. Comparison of hydrogen sulfide transport properties in fluorinated and nonfluorinated polymers. *Macromolecules*, 39:7591–7600, 2006. doi: 10.1021/ma061072z.
- [180] E. Gustafsson, T. Wällstedt, C. Humborg, C.-M. Mörth, and B. G. Gustafsson. External total alkalinity loads versus internal generation: The influence of nonriverine alkalinity sources in the baltic sea. *Global Biogeochem. Cycles*, 28:1358–1370, 2014. doi: 10.1002/2014gb004888.
- [181] S. A. Stern. Polymers for gas separations: the next decade. *J. Membr. Sci.*, 94:1–65, 1994. doi: 10.1016/0376-7388(94)00141-3.
- [182] V. Arcella, A. Ghielmi, and G. Tommasi. High performance perfluoropolymer films and membranes. *Ann. N. Y. Acad. Sci.*, 984:226–244, 2003. doi: 10.1111/j.1749-6632.2003.tb06002.x.
- [183] C. Makhloufi, D. Roizard, and E. Favre. Reverse selective nh₃/co₂ permeation in fluorinated polymers using membranes gas separation. *J. Membr. Sci.*, 441:63–72, 2013. doi: 10.1016/j.memsci.2013.03.048.
- [184] V. Arcella, P. Colaianna, P. Maccone, A. Sanguineti, A. Gordano, G. Clarizia, and E. Drioli. A study on a perfluoropolymer purification and its application to membrane formation. *J. Membr. Sci.*, 163:203–209, 1999. doi: 10.1016/s0376-7388(99)00184-2.

- [185] T. D. Clayton and R. H. Byrne. Spectrophotometric seawater ph measurements: total hydrogen ion concentration scale calibration of m-cresol purple and at-sea results. *Deep Sea Res., Part I*, 40:2115–2129, 1993. doi: 10.1016/0967-0637(93)90048-8.
- [186] M. Chierici, A. Anderson, A. Fransson, and L. G. Anderson. Influence of m-cresol purple indicator additions on the ph of seawater samples: correction factors evaluated from a chemical speciation model. *Mar. Chem.*, 65:281–290, 1999. doi: 10.1016/S0304-4203(99)00020-1.
- [187] M. P. Seidel, M.D. DeGrandpre, and A. G. Dickson. A sensor for in situ indicator-based measurements of seawater ph. *Mar. Chem.*, 109:18–28, 2008. doi: 10.1016/j.marchem.2007.11.013.
- [188] X. Liu, M. C. Patsavas, and R. H. Byrne. Purification and characterization of meta-cresol purple for spectrophotometric seawater ph measurements. *Environ. Sci. Technol.*, 45:4862–4868, 2011. doi: 10.1021/es200665d.
- [189] J. C. Jansen, F. Taselli, E. Tocci, and E. Drioli. High-flux composite perfluorinated gas separation membranes of hyflon ad on a hollow fibre ultrafiltration membrane support. *Desalination*, 192:207–213, 2005. doi: 10.1016/j.desal.2005.04.134.
- [190] M. Yarrow, V. H. Marin, M. Finlayson, A. Tironi, L. E. Delgado, and F. Fischer. The ecology of egeria densa planchon (liliopsida: Alismatales): A wetland ecosystem engineer? *Rev. Chil. Hist. Nat.*, 82:299–313, 2009. doi: 10.1021/ma061072z.
- [191] M. Samuelsson. Interannual salinity variations in the baltic sea during the period 1954–1990. *Cont. Shelf Res*, 16:1463–1477, 1996. doi: 10.1016/0278-4343(95)00082-8.
- [192] H. E. M. Meier. Modeling the pathways and ages of inflowing salt- and freshwater in the baltic sea. *Estuarine, Coastal Shelf Sci.*, 74:610–627, 2007. doi: 10.1016/j.ecss.2007.05.019.
- [193] U. Gräwe, M. Naumann, V. Mohrholz, and H. Burchard. Anatomizing one of the largest saltwater inflows into the baltic sea in december 2014. *J. Geophys. Res.: Oceans*, 120:7676–7697, 2015. doi: 10.1002/2015jc011269.
- [194] S. C. Doney, M. Ruckelshaus, J. E. Duffy, J. P. Barry, F. Chan, C. A. English, H. M. Galindo, J. M. Grebmeier, A. B. Hollowed, N. Knowlton, J. Polovina, N. N. Rabalais, W. J. Sydeman, and L. D. Talley. Climate change impacts on marine ecosystems. *Ann. Rev. Mar. Sci.*, 4:11–37, 2011. doi: 10.1146/annurev-marine-041911-111611.
- [195] L. Stramma, G. C. Johnson, J. Sprintall, and V. Mohrholz. Expanding oxygen-minimum zones in the tropical oceans. *Science*, 320:655–658, 2008. doi: 10.1126/science.1153847.
- [196] T. D. Dickey, E. C. Itsweire, M. A. Moline, and J. M. Perry. Introduction to the limnology and oceanography special issue on autonomous and lagrangian platforms and sensors (alps). *Limnol. Oceanogr.*, 53:2057–2061, 2008. doi: 10.4319/lo.2008.53.5_part.2.2057.
- [197] G. Mills and G. A. Fones. A review of in situ methods and sensors for monitoring the marine environment. *Sensor Review*, 32:17–28, 2012. doi: 10.1108/02602281211197116.

- [198] R. H. Byrne. Measuring ocean acidification: New technology for a new era of ocean chemistry. *Environ. Sci. Technol.*, 48:5352–5360, 2014. doi: 10.1021/es405819p.
- [199] N. P. Revsbach, L. H. Larsen, J. Gunderson, T. Dalsgaard, O. Ulloa, and B. Thamdrup. Determination of ultra-low oxygen concentrations in oxygen minimum zones by the stox sensor. *Science*, 7:371–381, 2009. doi: 10.4319/lom.2009.7.371.
- [200] M. Sosna, G. Denault, R. W. Pascal, R. D. Prien, and M. Mowlem. Development of a reliable microelectrode dissolved oxygen sensor. *Sens. Actuators B*, 123:344–351, 2006. doi: 10.1016/j.snb.2006.08.033.
- [201] H. Hasumoto, T. Imazu, T. Miura, and K. Kogure. Use of an optical oxygen sensor to measure dissolved oxygen in seawater. *J. Oceanogr.*, 62:99–103, 2006.
- [202] B. J. Müller, T. Burger, S. M. Borisov, and I. Klimant. High performance optical trace oxygen sensors based on nir-emitting benzoporphyrins covalently coupled to silicone matrices. *Sens. Actuators B*, 216:527–534, 2015. doi: 10.1016/j.snb.2015.04.067.
- [203] T. R. Martz, J. G. Connery, and K. S. Johnson. Testing the honeywell durafet[®] for seawater ph applications. *Limnol. Oceanogr. Methods*, 8:172–184, 2010. doi: 10.4319/lom.2010.8.172.
- [204] K. Shitashima, M. Kyo, Y. Koike, and H. Henmi. Development of in situ ph sensor using isfet. *J. Underw. Technol.*, pages 106–108, 2002. doi: 10.1109/UT.2002.1002403.
- [205] R. G. Bellerby, A. Olsen, T. Johannessen, and P. Croot. A high precision spectrophotometric method for online shipboard seawater ph measurements: the automated marine ph sensor (amps). *Talanta*, 56:61–69, 2002. doi: 10.1016/S0039-9140(01)00541-0.
- [206] H. Stahl, A. Glud, C. R. Schröder, I. Klimant, A. Tengberg, and R. N. Glud. Time-resolved ph imaging in marine sediments with a luminescent planar optode. *Limnol. Oceanogr. Methods*, 4:336–345, 2006. doi: 10.4319/lom.2006.4.336.
- [207] G. E. Friederich, P. G. Brewer, R. Herlien, and F. P. Chavez. Measurement of sea surface partial pressure of CO_2 from a moored buoy. *Deep Sea Res.*, 42:1175–1186, 1995. doi: 10.1016/0967-0637(95)00044-7.
- [208] X. Xie and E. Bakker. Non-severinghaus potentiometric dissolved CO_2 sensor with improved characteristics. *Anal. Chem.*, 85:1332–1336, 2013. doi: 10.1021/ac303534v.
- [209] S. C. Riser and K. S. Johnson. Net production of oxygen in the subtropical ocean. *Nature Letters*, 451:323–326, 2008. doi: 10.1038/nature06441.
- [210] R. Czeschel, L. Stramma, R. A. Weller, and T. Fischer. Circulation, eddies, oxygen and nutrient changes in the eastern tropical south pacific ocean. *Ocean Sci.*, 11:455–470, 2015. doi: 10.5194/os-11-455-2015.
- [211] C. E. Reimers. Applications of microelectrodes to problems in chemical oceanography. *Chem. Rev.*, 107:590–600, 2007. doi: 10.1021/cr050363n.

- [212] J. Carlson. Development of an optimized dissolved oxygen sensor for oceanographic profiling. *Int. Ocean Syst.*, 6:20–21, 2002.
- [213] M. Martini, B. Butman, and M. J. Mickelson. Long-term performance of aanderaa optodes and sea-bird sbe 43 dissolved-oxygen sensors bottom mounted at 32 m in massachusetts bay. *J. Atmos. Oceanic Technol.*, 24:1924–1935, 2007. doi: 10.1175/JTECH2078.1.
- [214] Oxyguard[®], oxyguard 840 oxygen probe. 2017.
- [215] A. Tengberg, J. Hovdenes, H. J. Andersson, O. Brocandel, R. Diaz, D. Hebert, T. Arnerich, C. Huber, A. Kötzing, A. Khripounoff, F. Rey, C. Rønning, J. Schimanski, S. Sommer, and A. Stangelmayer. Evaluation of a lifetime-based optode to measure oxygen in aquatic systems. *Limnol. Oceanogr. Methods*, 4:7–17, 2006. doi: 10.4319/lom.2006.4.7.
- [216] Sea and Sun Marine Tech. Fast optical oxygen sensor, http://www.sea-sun-tech.com/fileadmin/img/pdf_sea/sst_do.pdf. Sept. 2017.
- [217] Hach[®], gli encapsulated lcp (liquid crystal polymer) differential ph sensor with internal preamplifier, glass electrode, 5-wire, 30 ft cable. Sept. 2017.
- [218] Sea-bird scientific, seafetTM ocean ph sensor, www.seabird.com/seafet. Sept. 2017.
- [219] Ocean networks canada innovation: Bosma, j., atlantic seafetTM ocean ph sensor verification report 2015, project #3021.
- [220] K. S. Johnson, H. W. Jannasch, L. J. Coletti, V. A. Elrod, T. R. Martz, Y. Takeshita, R. J. Carlson, and J. G. Connery. Deep-sea durafet: A pressure tolerant ph sensor designed for global sensor networks. *Anal. Chem.*, 88:3249–3256, 2016. doi: 10.1021/acs.analchem.5b04653.
- [221] Z. A. Wang, F. N. Sonnichsen, A. M. Bradley, K. A. Hoering, T. M. Lanagan, S. N. Chu, T. R. Hammar, and R. Camilli. In situ sensor technology for simultaneous spectrophotometric measurements of seawater total dissolved inorganic carbon and ph. *Environ. Sci. Technol.*, 49:4441–4449, 2015. doi: 10.1021/es504893n.
- [222] S. Loucaides, V. M. C. Rerolle, S. Papadimitriou, H. Kennedy, M. C. Mowlem, A. G. Dickson, M. Gledhill, and E. P. Achterberg. Characterization of meta-cresol purple for spectrophotometric ph measurements in saline and hypersaline media at sub-zero temperatures. *Sci. Rep.*, 7:2481, 2017. doi: 10.1038/s41598-017-02624-0.
- [223] J. S. Clarke, E. P. Achterberg, V. M. C. Rerolle, S. A. K. Bey, C. F. A. Floquet, and M. C. Mowlem. Characterization and deployment of an immobilised ph sensor spot towards surface ocean ph measurements. *Anal. Chem. Acta*, 897:69–80, 2015. doi: 10.1016/j.aca.2015.09.026.
- [224] M. D. Stokes and G. N. Somero. An optical oxygen sensor and reaction vessel for high-pressure applications. *Limnol. Oceanogr.*, 44:189–195, 1999. doi: 10.4319/lo.1999.44.1.0189.

- [225] S. M. Borisov, G. Nuss, and I. Klimant. Red light-excitable oxygen sensing materials based on platinum(ii) and palladium (ii) benzoporphyrins. *Anal. Chem.*, 80:9435–9442, 2008. doi: 10.1016/j.jphotochem.2009.05.018.
- [226] L. H. Hutter, B. J. Müller, K. Koren, S. M. Borisov, and I. Klimant. Robust optical oxygen sensors based on polymer-bound nir-emitting platinum(ii)-benzoporphyrins. *J. Mater. Chem. C*, 2:7589–7598, 2014. doi: 10.1039/C4TC00983E.
- [227] M. Strobl, T. Rappitsch, S. M. Borisov, T. Mayr, and I. Klimant. Nir-emitting aza-bodipy dyes - new building blocks for broad-range optical ph sensors. *Analyt.*, 140:7150–7153, 2015. doi: 10.1039/C5AN01389E.
- [228] R. G. Perkin and E. L. Lewis. The practical salinity scale 1978: Fitting the data. *IEEE J. Ocean. Eng.*, 5:9–16, 1980. doi: 10.1109/JOE.1980.1145441.
- [229] H. Jannasch, L. J. Coletti, K. S. Johnson, S. E. Fitzwater, J. A. Needoba, and J. N. Plant. The land/ocean biogeochemical observatory: A robust networked mooring system for continuously monitoring complex biogeochemical cycle in estuaries. *Limnol. Oceanogr. Methods*, 6:263–276, 2008. doi: 10.4319/lom.2008.6.263.
- [230] Li-cor gmbh, measuring small volumes of co₂ with the li-7000, www.licor.com/documents/iz1drf5m77c93geim8hw. 2014.
- [231] E. R. Carraway, J. N. Demas, B. A. DeGraff, and J. R. Bacon. Photophysics and photochemistry of oxygen sensors based on luminescent transition-metal complexes. *Anal. Chem.*, 63:337–342, 1991.
- [232] Y. Takeshita, T. R. Martz, K. S. Johnson, and A. G. Dickson. Characterization of an ion selective field effect transistor and chloride ion selective electrodes for ph measurements in seawater. *Anal. Chem.*, 86:11189–11195, 2014. doi: 10.1021/ac502631z.
- [233] P. J. Bresnahan Jr., T. R. Martz, Y. Takeshita, K. S. Johnson, and M. LaShomb. Best practices for autonomous measurement of seawater ph with the honeywell durafet. *Methods in Oceanography*, 9:44–60, 2014. doi: 10.1016/j.mio.2014.08.003.
- [234] K. S. Johnson. Developing chemical sensors to observe the health of the global ocean. *TRANSDUCER*, pages 10–15, 2017. doi: 10.1109/TRANSDUCER.2017.7993975.
- [235] Pyro science gmbh, robust oxygen probe, www.pyro-science.com/optical_oxygen_meter_firering_o2. Sept. 2017.
- [236] K. Wasson, R. Jeppesen, C. Endris, D. C. Perry, A. Woolfolk, K. Beheshti, M. Rodriguez, R. Eby, E. B. Watson, F. Rahman, J. Haskins, and B. B. Hughes. Eutrophication decreases salt marsh resilience through proliferation of algae mats. *Biol. Conserv.*, 212:1–11, 2017. doi: 10.1016/j.biocon.2017.05.019.
- [237] weather data obtained from: <http://www.accuweather.com/en/us/moss-landing-ca/95039/february-weather/2167232?monyr=2/1/2017&view=table>.

- [238] J. T. Wootton, C. A. Pfister, and J. D. Forester. Dynamic patterns and ecological impacts of declining ocean pH in a high-resolution multi-year dataset. *PNAS*, 105:18848–18853, 2008. doi: 10.1073/pnas.0810079105.
- [239] T. R. Martz, J. J. Carr, C. R. French, and M. D. DeGrandpre. A submersible autonomous sensor for spectrophotometric pH measurements of natural waters. *Anal. Chem.*, 75:1844–1850, 2003. doi: 10.1021/ac0205681.
- [240] C. H. Bittig, B. Fiedler, R. Scholz, G. Krahlmann, and A. Körtzinger. Time response of oxygen optodes on profiling platforms and its dependence on flow speed and temperature. *Limnol. Oceanogr.: Methods*, 12:617–636, 2014. doi: 10.4319/lom.2014.12.617.
- [241] H. Uchida and K. E. McTaggart G. C. Johnson. Ctd oxygen sensor calibration procedure. *The GO-SHIP Repeat Hydrography Manual*, IOCCP Report No. 14, 2010.
- [242] D. Donis and et al. An assessment of the precision and confidence of aquatic eddy correlation measurements. *J. Atmos. Oceanic Technol.*, 32:642–655, 2015. doi: 10.1175/JTECH-D-14-00089.1.
- [243] E. Fritzsche, C. Staudinger, J. P. Fischer, R. Thar, H. W. Jannasch, and et al. A validation and comparison study of new, compact, versatile optode for oxygen, pH and carbon dioxide in marine environments. *submission to Environ. Sci. Technol.*, 2017.
- [244] Ocean Networks Canada Innovation: J. Bosma. Satlantic seafetTM ocean pH sensor verification report 2015, project# 3021.
- [245] X. Liu, Z. A. Wang and R. H. Byrne, E. A. Kaltenbacher, and R. E. Bernstein. Spectrophotometric measurements of pH in-situ: Laboratory and field evaluations of instrumental performance. *Environ. Sci. Technol.*, 40:5036–5044, 2006. doi: 10.1021/es0601843.
- [246] M. C. Rérolle, C. F. A. Floquet, M. C. Mowlem, D. P. Connelly, and R. R. G. J. Bellerby E. P. Achterberg. Seawater-pH measurements for ocean-acidification observations. *Trends Anal. Chem.*, 40:146–157, 2012. doi: 10.1016/j.trac.2012.07.016.
- [247] D. de Beer, A. Glud, E. Epping, and M. Kühl. A fast responding CO₂ microelectrode for profiling sediments, microbial mats and biofilms. *Limnol. Oceanogr.*, 41:1790–1800, 1997. doi: 10.4319/lo.1997.42.7.1590.
- [248] W.-J. Cai and C. E. Reimers. The development of pH and pCO₂ micro-electrodes for studying the carbonate chemistry of porewater near the sediment-water interface. *Limnol. Oceanogr.*, 38:157–161, 1993. doi: 10.1021/ac980513c.
- [249] R. A. Easley and R. H. Byrne. Spectrophotometric calibration of pH electrodes in seawater using purified *m*-cresol purple. *Environ. Sci. Technol.*, 46:5018–5024, 2012. doi: 10.1021/es300491s.
- [250] K. Ertekin, I. Klimant, G. Neuraüter, and O. S. Wolfbeis. Characterization of a reservoir-type capillary optical microsensors for pCO₂ measurements. *Talanta*, 59:261–267, 2003. doi: 10.1016/S0039-9140(02)00495-2.

- [251] S. R. Ricketts and P. Douglas. A simple colorimetric luminescent oxygen sensor using a green led with pt octaethylporphyrin in ethyl cellulose as the oxygen-responsive element. *Sens. Actuators B*, 135:46–51, 2008. doi: 10.1016/j.snb.2008.07.017.
- [252] D. E. Achatz, R. J. Meier, L. H. Fischer, and O. S. Wolfbeis. Luminescent sensing of oxygen using a quenchable probe and upconverting nanoparticles. *Angew. Chem. Int. Ed.*, 50:260–263, 2011. doi: 10.1002/anie.201004902.
- [253] X.-M. Li, F.-C. Ruan, and K.-Y. Wong. Optical characteristics of a ruthenium(ii) complex immobilized in a silicone rubber film for oxygen measurement. *Analyst*, 118:289–292, 1993. doi: 10.1039/AN9931800289.
- [254] L. Lochmann, P. Zimcik, I. Klimant, V. Novakova, and S. M. Borisov. Red-emitting CO₂ sensors with tunable dynamic range based on pH-sensitive azathalocyanine indicators. *Sens. Actuators B*, 246:1100–1107, 2017. doi: 10.1016/j.snb.2016.10.135.
- [255] V. Bhardwaj, R. K. Gangwar, and V. K. Singh. Silicone rubber-coated highly sensitive optical fiber sensor for temperature measurement. *Opt. Eng.*, 55:126107, 2016. doi: 10.1117/1.OE.55.12.126107.
- [256] P. Y. Hsieh. Diffusibility and solubility of gases in ethyl cellulose and nitrocellulose. *J. Appl. Polym. Sci.*, 7:1743–1756, 1963. doi: 10.1002/app.1963.070070515.
- [257] K. Adamczyk, M. Prémont-Schwarz, Dina Pines, E. Pines, and E. T. J. Nibbering. Real-time observation of carbonic acid formation in aqueous solution. *Science*, 326:1690–1694, 2009. doi: 10.1126/science.1180060.
- [258] D. J. Conley, J. Carstensen, J. Aigars, P. Axe, E. Bonsdorff, T. Eremina, B.-M. Haahti, C. Humborg, P. Jonsson, J. Kotta, C. Lännegren, U. Larsson, A. Maximov, M. R. Medina, E. Lysiak-Pastuszek, N. Remeikaite-Nikiene, J. Walve, S. Wilhelms, and L. Zillen. Hypoxia is increasing in the coastal zone of the baltic sea. *Environ. Sci. Technol.*, 45: 6777–6783, 2011. doi: 10.1021/es201212r.
- [259] J. J. Wright, K. M. Konwar, and S. J. Hallam. Microbial ecology of expanding oxygen minimum zones. *Nature Reviews*, 10:381–394, 2012. doi: 10.1038/nrmicro2778.
- [260] J. P. McCreary Jr., Z. Yu, R. R. Hood, P. N. Vinaychandran, R. Furue, A. Ishida, and K. J. Richards. Dynamics of the indian-ocean oxygen minimum zones. *Progress in Oceanography*, 112-113:15–37, 2013. doi: 10.1016/j.pocean.2013.03.002.
- [261] D. Wobken, P. Lam, M. M. M. Kuypers, W. A. Naqvi, B. Kartal, M. Strous, M. S. M. Jetten, B. M. Fuchs, and R. Amann. A microdiversity study of anammox bacteria reveals novel candidatus scalindua phylotype in marine oxygen minimum zones. *Environ. Microbiol.*, 11:3106–3119, 2008. doi: 10.1111/j.1462-2920.2008.01640.x.
- [262] N. N. Rabalais, R. E. Turner, and W. J. Wiseman Jr. Gulf of Mexico hypoxia, a.k.a. "the dead zone". *Annu. Rev. Ecol. Syst.*, 33:235–263, 2002. doi: 10.1146/annurev.ecolsys.33.010802.150513.

- [263] B. B. Jørgensen. Sulphur bacteria-ecology of the bacteria of the sulphur cycle with spatial reference to anoxic-oxic interface environments. *Philos. Trans. R. Soc. Lond. B*, 1093:543–561, 1982. doi: 10.1098/rstb.1982.0096.
- [264] H. Schunck, G. Lavik, D. K. Desai, T. Grosskopf, T. Kalvelage, C. R. Löscher, A. Paulmier, S. Contreras, H. Siegel, M. Holtappels, P. Rosenstiel, M. B. Schilhabel, M. Graco, R. A. Schmitz, M. M. M. Kuypers, and J. LaRoche. Giant hydrogen sulfide plume in the oxygen minimum zone off peru supports chemolithoautotrophy. *PLoS ONE*, 8:1–18, 2013. doi: 10.1371/journal.pone.0068661.
- [265] V. Brücker, B. B. Jørgensen, K. Neumann, D. Riechmann, M. Schlösser, and H. Schulz. Regulation of bacterial sulfate reduction and hydrogen sulfide fluxes in the central namibian coastal upwelling zone. *Geochim. Cosmochim. Acta*, 67:4505–4518, 2003. doi: 10.1098/rstb.1982.0096.
- [266] B. Thamdrup, T. Dalsgaard, and N. P. Revsback. Widespread functional anoxia in the oxygen minimum zone of the eastern south pacific. *Deep Sea Res., Part I*, 65:36–45, 2012. doi: 10.1016/j.dsr.2012.03.001.
- [267] M. Larsen, P. Lehner, S. M. Borisov, I. Klimant, J. P. Fischer, F. J. Stewart, D. E. Canfield, and R. N. Glud. In situ quantification of ultra-low O_2 concentrations in oxygen minimum zones: Application of novel optodes. *Limnol. Oceanogr. Methods*, 14:784–800, 2016. doi: 10.1002/lom3.10126.
- [268] R. L. Garrett, R. K. Clark, L. L. Carney, and C. K. Grantham Sr. Chemical scavenger for sulfides in water-base drilling fluids. *SPE Paper, Annual Mtg., Houston*, pages 787–794, 1979. doi: 10.2118/7499-PA.
- [269] M. K. Amosa, I. A. Mohammed, and S. A. Yaro. Sulphide scavengers in oil and gas industry- a review. *NAFTA*, 61:85–92, 2010.
- [270] I. Rosso, C. Galletti, M. Bizzi, G. Saracco, and V. Specchia. Zinc oxide sorbents for the removal of hydrogen sulfide from syngases. *Ind. Eng. Chem. Res.*, 42:1688–1697, 2003. doi: 10.1021/ie0208467.
- [271] J. M. Bakke, J. Buhaug, and J. Riha. Hydrolysis of 1,3,5-tris(2-hydroxyethyl)hexahydro-s-triazine and its reaction with H_2S . *Ind. Eng. Chem. Res.*, 40:6051–6054, 2001. doi: 10.1021/ie010311y.
- [272] J. M. Bakke and J. B. Buhaug. Hydrogen sulfide scavenging by 1,3,5-triazinanes. comparison of the rates of reaction. *Ind. Eng. Chem. Res.*, 9:1962–1965, 2004. doi: 10.1021/ie030510c.
- [273] L. M. Frare, M. G. A. Vieira, M. G. C. Silvy, N. C. Pereira, and M. L. Gimenes. Hydrogen sulfide removal from biogas using Fe/EDTA solution: Gas/liquid contacting and sulfur formation. *Environ. Prog. Sustain. Energy*, 29:34–41, 2009. doi: 10.1002/ep.10374.

- [274] P. Oyarzún, F. Arancibia, C. Canales, and G. E. Arocy. Biofiltration of high concentration of hydrogen sulfide using *Thiobacillus thioparus*. *Process Biochemistry*, 39:165–170, 2003. doi: 10.1016/S0032-9592(03)00050-5.
- [275] A. H. Wani, A. K. Lau, and R. M. R. Branion. Biofiltration control of pulping odors-hydrogen sulfide: performance, macrokinetics and coexistence effects of organo-sulfur species. *J. Chem. Technol. Biot.*, 74:9–16, 1999. doi: 10.1002/(SICI)1097-4660(199901)74:1\$(\$9::AID-JCTB981\$)\$3.0.CO;2-B.
- [276] J. M. Morgan-Sagastume and A. Noyola. Hydrogen sulfide removal by compost biofiltration: Effect of mixing the filter media on operational factors. *Bioresource Technology*, 97: 1546–1553, 2006. doi: 10.1016/j.biortech.2005.06.003.
- [277] J. Park, E. A. Evans, and T. G. Ellis. Development of a biofilter with tire-derived rubber particle media for hydrogen sulfide odor removal. *Water Air Soil Pollut.*, 215:145–153, 2010. doi: 10.1007/s11270-010-0466-1.
- [278] M. Syed, G. Soreanu, P. Faletta, and M. Beland. Removal of hydrogen sulfide from gas streams using biological processes – a review. *Can. Biosyst. Eng.*, 48:1–14, 2006.
- [279] J. B. Buhaug. Investigation of the chemistry of liquid h₂s scavengers. *PhD, Norwegian University of Science and Technology*, page 103, 2002.
- [280] P. Hartmann, M. J. P Leiner, and M. E. Lippitsch. Luminescence quenching behavior of an oxygen sensor based on a ru(ii) complex dissolved in polystyrene. *Anal. Chem.*, 67: 88–93, 1995.
- [281] L. Zhang, M. E. Langmuir, M. Bai, and W. R. Seitz. A sensor for ph based on an optical reflective device coupled to the swelling of an aminated polystyrene membrane. *Talanta*, 44:1691–1698, 1997. doi: 10.1016/S0039-9140(97)00080-5.
- [282] S. M. Borisov, A. S. Vasylevska, C. Krause, and O. S. Wolfbeis. Composite luminescent material for dual sensing of oxygen and temperature. *Adv. Funct. Mater.*, 16:1536–1542, 2006. doi: 10.1002/adfm.200500778.
- [283] A. C. Puleo, N. Muruganandam, and D. R. Paul. Gas sorption and transport in substituted polystyrene. *J. Polym. Sci. Pol. Phys.*, 11:2385–2406, 1989. doi: 10.1002/polb.1989.090271116.
- [284] W. Heilman, V. Tammela, J.A. Meyer, V. Stannett, and M. Szwarc. Permeability of polymer films to hydrogen sulfide gas. *Ibid.*, 48:821–824, 1956.
- [285] W. D. Decker, H. F. Combs, and D. G. Corby. Adsorption of drugs and poisons by activated charcoal. *Toxicol. Appl. Pharmacol.*, 13:454–460, 1968. doi: 10.1002/polb.1989.090271116.
- [286] P. J. Neuvonen and K. T. Olkkola. Oral activated charcoal in the treatment of intoxications. *Med. Toxicol. Adverse Drug Exp.*, 3:33–58, 1988.

- [287] A. S. Shalkham, B. M. Kirrane, R. S. Hoffman, D. S. Goldfarb, and L. S. Nelson. The availability and use of charcoal hemoperfusion in the treatment of poisoned patients. *Am. J. Kidney Dis.*, 48:239–241, 2006. doi: 10.1053/j.ajkd.2006.04.080.
- [288] D. Bergis, M. Friedrich-Rust, S. Zeuzem, C. Betz, C. Sarrazin, and J. Bojunga. Treatment of amanita phalloides intoxication by fractionated plasma separation and adsorption (prometheus[®]). *J. Gastrointestin. Liver Dis.*, 21:171–176, 2012.
- [289] J. Diaz-Teran, D. M. Nevskaja, A. J. Lopez-Peinado, and A. Jerez. Porosity and adsorption properties of an activated charcoal. *Colloids and Surface A: Physicochem. Eng. Aspects*, 187-188:167–175, 2001. doi: 10.1016/S0927-7757(01)00622-7.
- [290] M. P. Cal, B. W. Strickler, A. A. Lizzio, and S. K. Gangwal. High temperature hydrogen sulfide adsorption on activated carbon: II. effects of gas temperature, gas pressure and sorbent regeneration. *Carbon*, 38:1767–1774, 2000. doi: 10.1016/S0008-6223(00)00011-7.
- [291] W. Feng, S. Kwon, E. Borguet, and R. Vidic. Adsorption of hydrogen sulfide onto activated carbon fibers: Effect of pore structure and surface chemistry. *Environ. Sci. Technol.*, 39:9744–9746, 2005. doi: 10.1021/es0507158.
- [292] Y. Xiao, S. Wang, D. Wu, and Q. Yuan. Experimental and simulation study of hydrogen sulfide adsorption on impregnated activated carbon under anaerobic conditions. *J. Hazard. Mater.*, 153:1193–1200, 2008. doi: 10.1016/j.jhazmat.2007.09.081.
- [293] L. M. Le Leuch, A. Subrenat, and P. Le Cloirec. Hydrogen sulfide adsorption and oxidation onto activated carbon cloths: Applications to odorous gaseous emission treatments. *Langmuir*, 26:10869–10877, 2003. doi: 10.1021/la035163q.
- [294] R. J. Highet and W. C. Wildman. Solid manganese dioxide as an oxidizing agent. *J. Am. Chem. Soc.*, 77:4399–4401, 1955.
- [295] R. J. K. Taylor, M. Reid, J. Foot, and S. A. Raw. Tandem oxidation processes using manganese dioxide: Discovery, applications and current status. *Acc. Chem. Res.*, 38: 851–869, 2005. doi: 10.1021/ar050113t.
- [296] J. Herszage and M. dos Santos Afonso. Mechanism of hydrogen sulfide oxidation by manganese(IV)oxide in aqueous solutions. *Langmuir*, 19:9684–9692, 2003. doi: 10.1021/la034016p.
- [297] K. Rajagopal, R. Lacerda, I. Slobodnicov, and E. Campagnolo. Modeling and simulation of hydrogen sulfide removal from petroleum production lines by chemical scavenger. *Chem. Eng. Commun.*, 10:1237–1248, 2009. doi: 10.1080/00986440902832100.
- [298] M. A. Sayyadnejad, H. R. Ghaffarian, and M. Saeidi. Removal of hydrogen sulfide by zinc oxide nanoparticles in drilling fluids. *Int. J. Environ. Sci. Tech.*, 4:565–569, 2008.
- [299] I. I. Novochinskii, C. Song, X. Ma, X. Liu, L. Shore, J. Lampert, and R. J. Farrauto. Low-temperature h₂s removal from steam-containing gas mixtures with zno for fuel cell applications. 1. zno particles and extrudates. *Energy and Fuels*, 18:576–583, 2004.

- [300] T.-H. Ko, H. Chu, and L.-K. Chaung. The sorption of hydrogen sulfide from hot syngas by metal oxides over supports. *Chemosphere*, 58:467–474, 2005. doi: 10.1016/j.chemosphere.2004.09.029.
- [301] W. F. Elseviers and H. Verelst. Transition metal oxides for hot gas desulphurisation. *Fuel*, 78:601–612, 1999. doi: 10.1016/S0016-2361(98)00185-9.
- [302] J. Sun, S. Modi, K.Liu, R. Lesieur, and J. Buglass. Kinetics of zinc oxide sulfidation for packed-bed desulfurizer modeling. *Energy and Fuels*, 21:1863–1871, 2007. doi: 10.1021/ef060521t.
- [303] A. Poghossian, M. Thust, M. J. Schöning, M. Müller-Veggian, P. Kordos, and H. Lüth. Cross-sensitivity of a capacitive penicilin sensor combined with a diffusion barrier. *Sens. Actuators B*, 68:260–265, 2000. doi: 10.1016/S0925-4005(00)00442-1.
- [304] F. Garzona, I. Raistricka, E. Broshaa, R. Houltona, and B. W. Chungb. Dense diffusion barrier limiting current oxygen sensors. *Sens. Actuators B*, 50:125–130, 1998. doi: 10.1016/S0925-4005(98)00169-5.
- [305] U. Bilitewski, P. Rüdiger, and R. D. Schmid. Glucose biosensors based on thick film technology. *Biosens. Bioelectron.*, 6:369–373, 1991. doi: 10.1016/0956-5663(91)85024-Q.

Appendix A - Photographic images hydrogen sulphide experiments

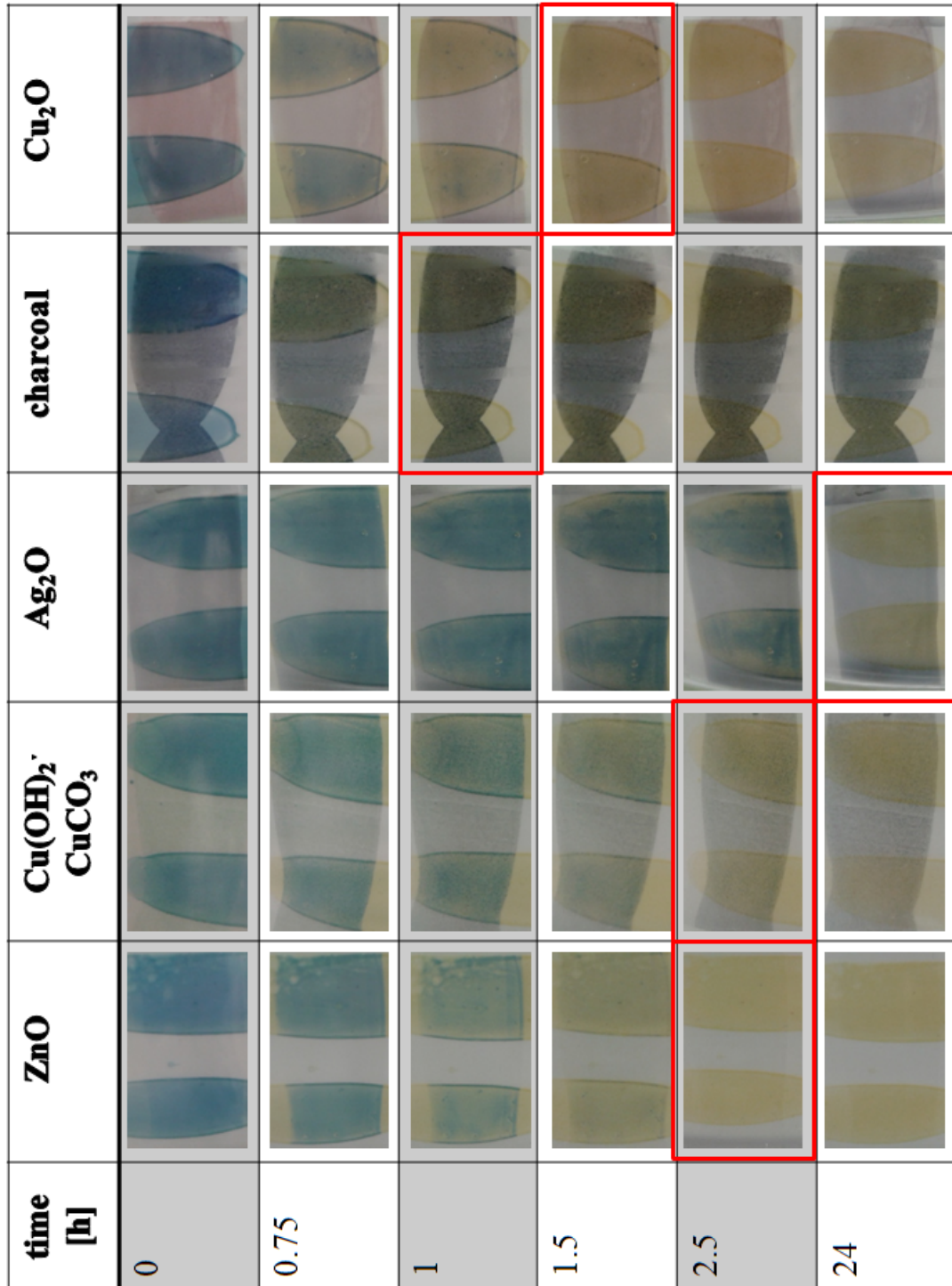


Figure 5.9: Photographic images of H₂S poisoning experiment **1a** in gaseous phase consisting of 1% hydrogen sulfide and room air at room temperature. Used scavenger: ZnO, Cu(OH)₂ · CuCO₃, charcoal, Ag₂O, Cu₂O. Order: charcoal < Cu₂O < Cu(OH)₂ · CuCO₃ = ZnO < Ag₂O.

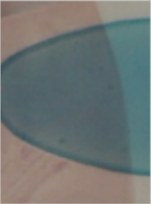



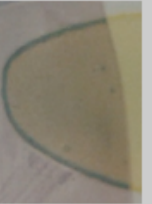











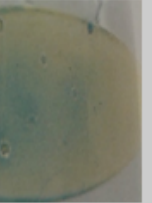













Cu₂O						
charcoal						
Ag₂O						
Cu(OH)₂ · CuCO₃						
ZnO						
time [h]	0	0.75	1	1.25	1.5	3.25

Figure 5.10: Photographic images of H₂S poisoning experiment **1b** in gaseous phase consisting of 1% hydrogen sulfide and nitrogen at room temperature. Used scavenger: ZnO, Cu(OH)₂ · CuCO₃, charcoal, Ag₂O, Cu₂O. Order: charcoal < Cu₂O = ZnO < Cu(OH)₂ · CuCO₃ < Ag₂O.






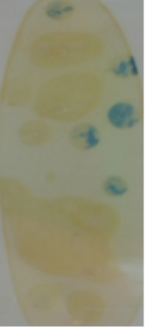




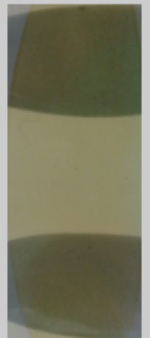
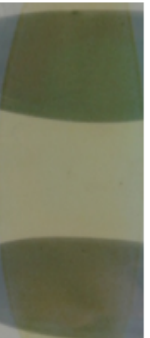

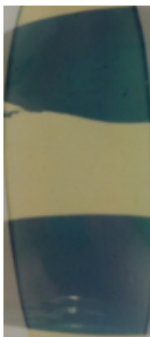
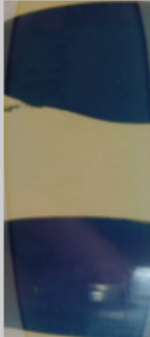

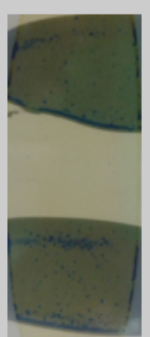

Triazinane						
Ag₂O						
Cu(OH)₂ · CuCO₃						
time [h]	0	1	25.25	49	92	147

Figure 5.11: Photographic images of H₂S poisoning experiment **2** in gaseous phase consisting of 1% hydrogen sulfide and room air at room temperature. Used scavenger: Cu(OH)₂ · CuCO₃, Ag₂O, Triazinane. Order: Ag₂O < Cu(OH)₂ · CuCO₃ = Triazinane (very thick layer).


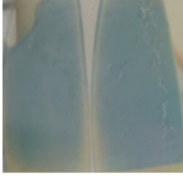






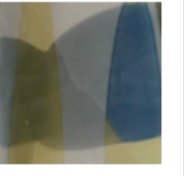
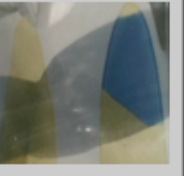

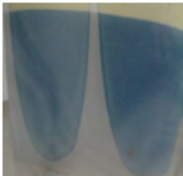

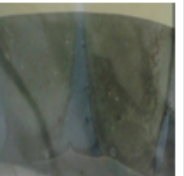

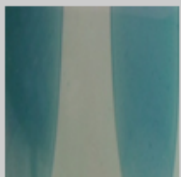



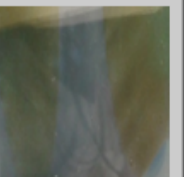
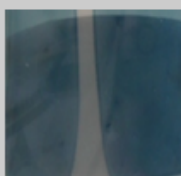


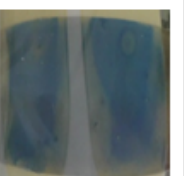
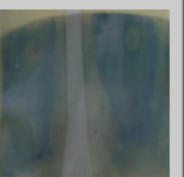
Hyflon (reference)					
CuO					
Ag₂O					
Cu(OH)₂ · CuCO₃					
MnO₂					
time [h]	0	7	19.5	66.75	98

Figure 5.12: Photographic images of H₂S poisoning experiment **3a** in gaseous phase consisting of 1% hydrogen sulfide and room air at room temperature. Used scavenger: Cu(OH)₂ · CuCO₃, Ag₂O, CuO, MnO₂ and pure Hyflon (reference). Order: Hyflon (pure) < others. Blue box mark detached scavenger layer, therefore no evaluation possible.

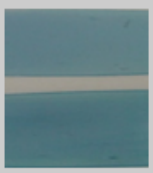

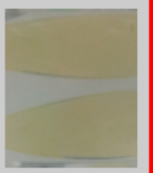



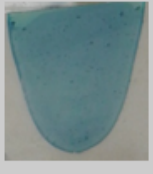
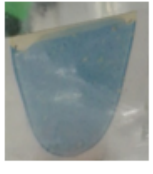


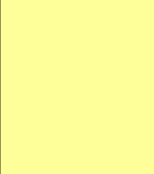
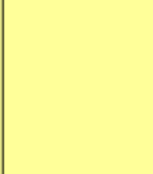
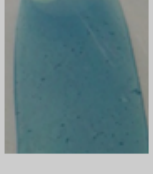
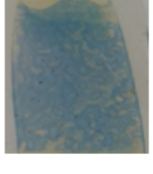


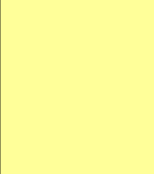
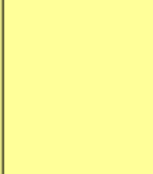
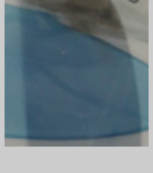

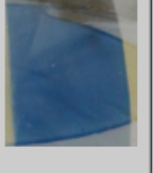
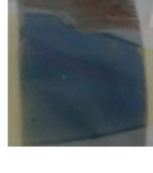
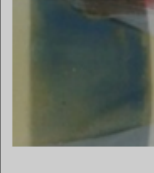
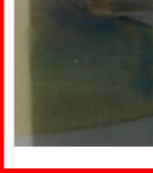
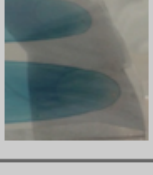

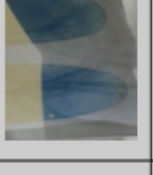
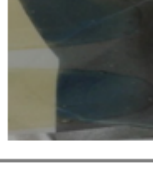
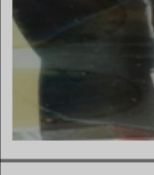
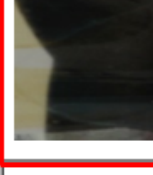
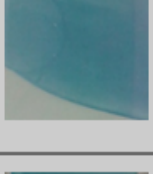
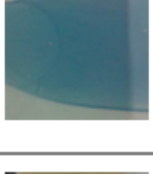
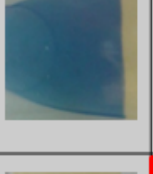
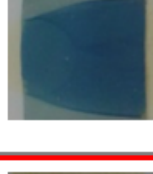
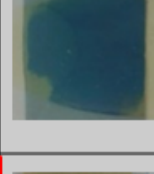
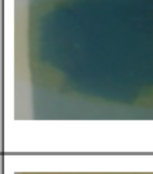
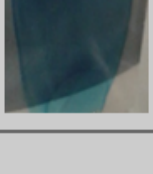
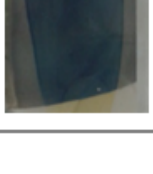
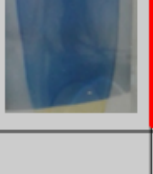
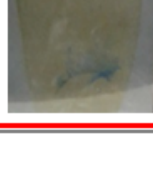
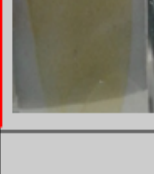

Hyflon (reference)						
Triazinane Kieselgur						
Triazinane Trisopor						
CuO						
Ag₂O						
Cu(OH)₂ · CuCO₃						
MnO₂						
time [d]	0	1	2	7	13	18

Figure 5.13: Photographic images of H₂S poisoning experiment **3b** in gaseous phase consisting of 0.1% hydrogen sulfide and nitrogen at room temperature. Used scavenger: MnO₂, Cu(OH)₂ · CuCO₃, Ag₂O, CuO, Triazinane in Trisopor[®] particles, Triazinane in Kieselgur[®] particles and pure Hyflon (reference). Order: Triazinane in Trisopor[®] particles=Triazinane in Kieselgur[®] particles=Hyflon (pure) < MnO₂ < Ag₂O < CuO < Cu(OH)₂ · CuCO₃.


























Hyflon (reference)					
Fe₂O₃					
Ag₂O					
Cu(OH)₂ · CuCO₃ (milled)					
Ag (nano)					
time [h]	0	2	4.5	6.5	7.5

Figure 5.14: Photographic images of H₂S poisoning experiment 4 in gaseous phase consisting of 0.1% hydrogen sulfide and room air at room temperature. Plasticizer was used during foil production. Used scavenger: Ag (nanoparticles), Cu(OH)₂ · CuCO₃, Ag₂O, Fe₂O₃ and pure Hyflon (reference). Order: Hyflon (pure) = Cu₂O < Cu(OH)₂ · CuCO₃ < Ag (nano) = Fe₂O₃ < Ag₂O.


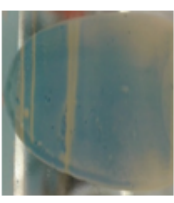
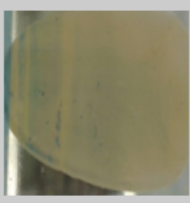

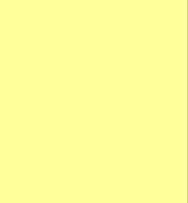




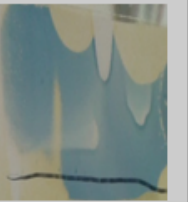




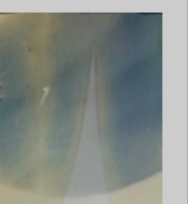
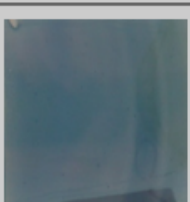
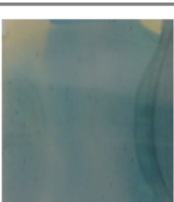
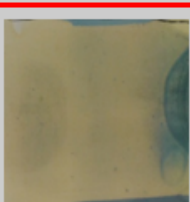
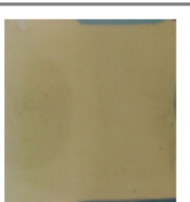
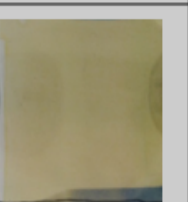





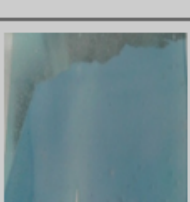

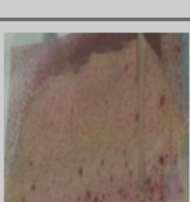


Hyflon (reference)					
ZnO					
Ag₂O					
PbO					
PbO₂					
Ag-triflate					
time [h]	0	3.5	6.5	9.5	over night

Figure 5.15: Photographic images of H₂S poisoning experiment 5 in gaseous phase consisting of 0.1% hydrogen sulfide and room air at room temperature. Plasticizer was used during foil production. Used scavenger: silver-triflate, PbO₂, PbO, Ag₂O, ZnO and pure Hyflon (reference). Order: Ag-triflate < Hyflon (pure) < PbO < PbO₂ < Ag₂O = ZnO.

Appendix B - Curriculum Vitae

Eva Fritzsche

Date and Place of Birth: 14.01.1990, Werdau, Germany

Nationality: Germany

Marital Status: unmarried

Current address:	Brucknerstrasse 86/17	Permanent address:	Dorfstrasse 23
	8010 Graz		08459 Neukirchen
	Austria		Germany

Special Skills:

Languages:	German (native), Englisch (fluent)
Driving Licence	A1, B
Management:	Operational Economics (basic) Marketing Management (basic) Project Management (basic)
Computing:	MS Word, MS Excel, MS Powerpoint, OriginLab, Latex
Soft Skills	Competence Training for Student Assistents, DGSS-Rhetoric certificate

Educational Background:

09/2002 - 06/2008	Gymnasium 'Julius Motteler' Crimmitschau Allgemeine Hochschulreife (A-Levels)
10/2008 - 09/2011	University of Technology Chemnitz, Department of Chemistry Bachelor of Science Chemistry Bachelor Thesis (Nucleophilic Substitution of Cyclopropane)
10/2011 - 10/2013	University of Technology Chemnitz, Department of Chemistry Master of Science Chemistry
05/2013 - 10/2013	IOW - Leibniz Institute for Baltic Sea Research Warnemünde, Department of Marine Chemistry Master Thesis Determination of Organic Contaminants in the Baltic Sea via Modern Mass Spectrometric Methods
07/2014 - ongoing	Graz University of Technology, Institute for Analytical Chemistry and Food Chemistry PhD studies Development of Optical CO ₂ Sensors for Marine Applications (EU-project 'SenseOCEAN'), oral exam expected Dec. 2017
07/2015	9th ASCOS Summer School Porto, Portugal - Advanced School on Chemical Optical Sensors Focus on 'Nanotechnology for (bio) chemical sensors'

Practical Experience and non-profit Activities:

- 05/2005 - ongoing **German Red Cross** local chapter Zwickauer Land e.V.
Lifeguard and Emergency Responder
- 01/2010 - 03/2011 **University of Technology Chemnitz**
Student representative Chemistry
- 11/2011-02/2012, **University of Technology Chemnitz, Institute of Chemistry**
04/2012-05/2012, student assistant Organic Chemistry
11/2012-12/2012,
01/2013-02/2013
- 09/2012 **DAW AEROCIT Schmiertechnik GmbH, Werdau**
trainee R& D department
- 02/2017 - 04/2017 **Monterey Bay Aquarium Research Institute, Moss Landing, USA**
Guest researcher, Kenneth Johnson lab - Sensor group
- 07/2014 - 09/2017 **Graz University of Technology, Institute for Analytical Chemistry and Food Chemistry**
PhD studies Development of Optical CO₂ Sensors for Marine Applications (EU-project 'SenseOCEAN')

Poster Presentations:

- 2015 Fritzsche, E.; Schutting, S.; Jokic, T.; Strobl, M.; Borisov, S. M.; Klimant, I. **New High Performance Optical pCO₂ Sensors Based on BF₂-Chelates of Dihydroxy-aza-Dipyrromethene.** Aquatic Science Meeting, Granada, Spain, Poster Presentation
- Fritzsche, E.; Schutting, S.; Jokic, T.; Strobl, M.; Borisov, S. M.; Klimant, I. **Neuartige optische pCO₂-Sensoren basierend auf BF₂-Chelatverbindungen von Dihydroxy-aza-Dipyrromethenen.** ANAKON, Graz, Austria, Poster Presentation
- 2016 Fritzsche, E.; Gruber, P.; Schutting, S.; Fischer, J. P.; Müller, J.; Borisov, S. M.; Klimant, I. **New Robust, Long-term Stable Optical Carbon Dioxide Sensor Based on Dihydroxy-aza-BODIPY Dyes.** XIII Europt(r)ode, Graz, Austria, Poster Presentation

Articles:

- 2017 Fritzsche, E.; Gruber, P.; Schutting, S.; Fischer, J. P.; Strobl, M.; Müller, J. D.; Borisov, S. M.; Klimant, I., Highly sensitive poisoning-resistant optical carbon dioxide sensors for environmental monitoring, *Analytical Methods*, **2017**, *9*, 55-65, doi: 10.1039/c6ay02949c.
- Fritzsche, E., Staudinger, C., Fischer, J. P., Thar, R., Jannasch, H. W., Plant, J. N., Blum, M., Massion, G., Thomas, H., Hoech, J., Johnson, K. S., Borisov, S. M., Klimant, I., A validation and comparison study of new, compact, versatile optode for oxygen, pH and carbon dioxide in marine environments, submission to *Environ. Sci. Techn.*, 2017.

Oral Presentations:

- 2016 Fritzsche, E.; Staudinger, C.; Strobl, M.; Fischer, J. P.; Müller, J.; Borisov, S. M.; Klimant, I. **A Small Autonomous Optode for Oceanographic pH, CO₂ and Oxygen Measurements.** XIII Europt(r)ode, Graz, Austria
- Fritzsche, E.; Staudinger, C.; Strobl, M.; Fischer, J. P.; Müller, J.; Borisov, S. M.; Klimant, I. , **A Small Autonomous Optode for Oceanographic pH, CO₂ and Oxygen Measurements.** ASAC Junganalytikerforum, Graz, Austria